LILIANA RAQUEL FERNANDES PIRES

PhD Thesis

Bridging the Lesion – Engineering a Permissive Substrate Towards Nerve Regeneration

Dissertação submetida à Faculdade de Engenharia da Universidade do Porto para obtenção do grau de Doutor em Engenharia Biomédica

Faculdade de Engenharia
Universidade do Porto
2014

This thesis was supervised by:

Doctor Ana Paula Pêgo (supervisor)
INEB – Instituto de Engenharia Biomédica

Doctor Luigi Ambrosio (co-supervisor)
ICBM – Institute of Composite and Biomedical Materials,
University of Naples “Frederico II”, Italy

The work described in this thesis was performed in:

INEB - Instituto de Engenharia Biomédica, Divisão de Biomateriais, Universidade do Porto, Portugal;

and

ICBM - Institute of Composite and Biomedical Materials, University “Frederico II”, Naples, Italy.

The research described in this thesis was financed by:

Fundação para a Ciência e a Tecnologia (FCT)
- PhD grant: SFRH/BD/46015/2008;
- Projects: POCI/SAU-BMA/58170/2004, PTDC/CTM-NAN/115124/2009, and PEst-C/SAU/LA0002/2011 and PEst-C/SAU/LA0002/2013-14.

FEDER funds through the *Programa Operacional Factores de Competitividade* – COMPETE.

“So many of our dreams at first seem impossible, then they seem improbable, and then, when we summon the will, they soon become inevitable.”

Christopher Reeve

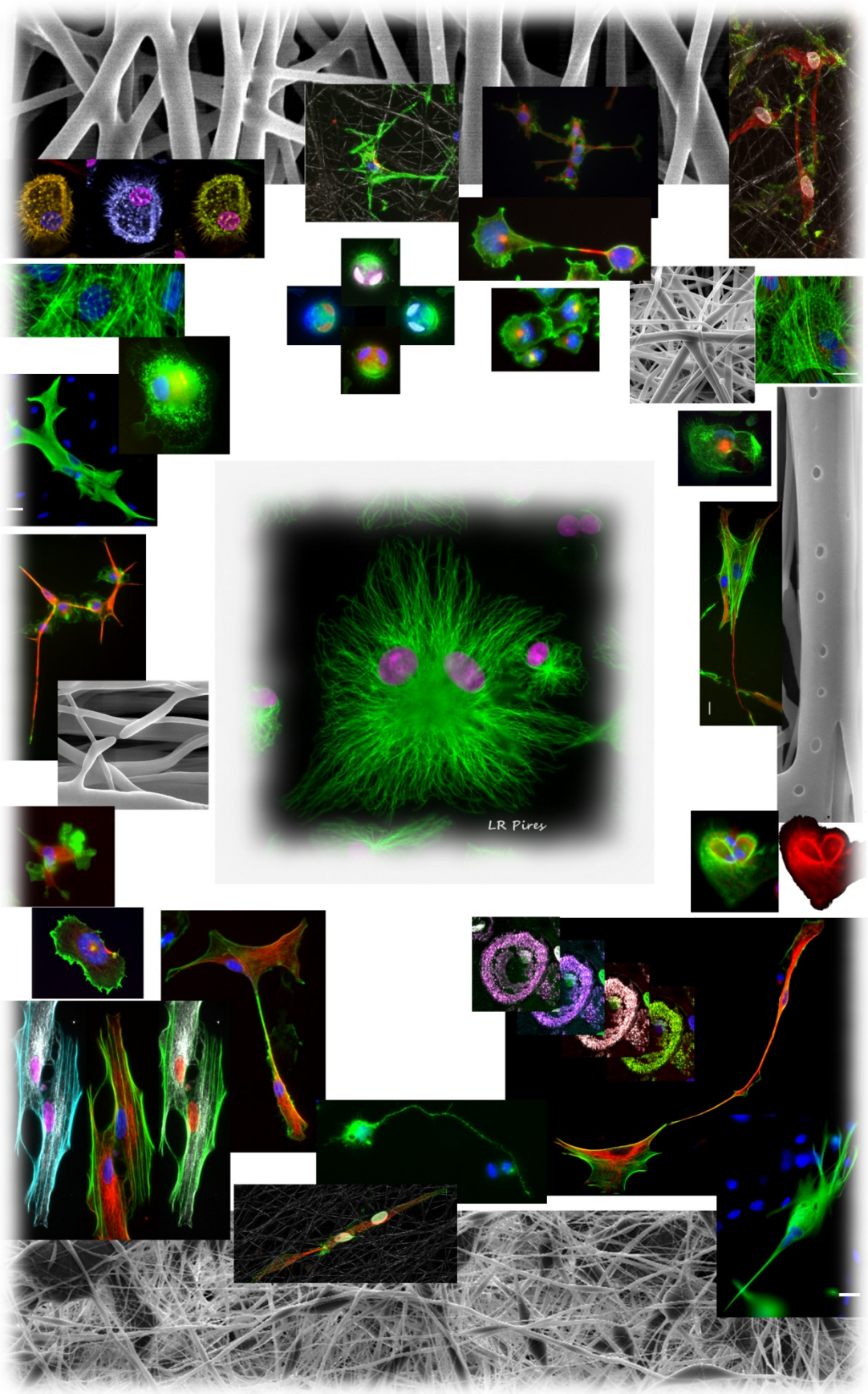

A (multiple) kind of magic!

ACKNOWLEDGEMENTS

Quando escrevi a minha tese de Mestrado usei como “frase inspiradora” um excerto de Fernando Pessoa onde se lê: “Pedras no caminho? Guardo todas. Um dia vou construir um castelo.”. Penso que desde dessa altura sonhei que a minha tese de Doutoramento seria o meu castelo. E cá está ele! Construi-o com algumas pedras que apanhei durante o Mestrado (algumas basilares) e com outras novas que encontrei durante Doutoramento. Algumas foram-me oferecidas, da experiência de outros, outras encontrei-as enquanto escavava com outros a meu lado. Depois foi (só) encaixá-las… Para tudo isto contribuíram muitas pessoas, de muitas formas. A todos os engenheiros, picheleiros e decoradores deste castelo, o meu muito obrigada!

O meu primeiro e maior agradecimento é dirigido à minha orientadora, uma das pedras basilares do meu castelo. Obrigada Ana Paula pela oportunidade que me deu de seguir para Doutoramento, obrigada pela orientação, pela partilha, pela confiança e por aquela cumplicidade… Obrigada por todas as pedras que me deu para o meu castelo e pelas que me mostrou o caminho para encontrar. As janelas do meu castelo são suas, porque é daí que vem o $^{+++}$brilho^{+++} deste trabalho!

I also would like to express my gratitude to Professor Luigi Ambrosio for accepting to co-supervise this thesis and, particularly, for welcoming me in his lab at Napoli and for the great discussions we shared.

O meu agradecimento ao Professor Mário pela oportunidade de fazer o meu Doutoramento no INEB e pelas discussões que partilhámos durante estes anos.

Gostaria de demonstrar a minha gratidão por aqueles que estiveram diretamente envolvidos em trabalhos incluídos nesta tese, os meus co-autores. De A a S: António José Pereira, Cristina Barrias, Cristina Ribeiro, Daniela Rocha, Hélder Maiato, Maria José Oliveira, Mónica Sousa, Paula Sampaio, Sérgio Simões.

I spent 6 months from my PhD at Napoli and some people managed to provide logistic and scientific assistance during my stay. My most sincere thanks to Vincenzo Guarino, who introduce me to the electrospinning world. Thanks to Valentina Cirillo and Marco Alvarez for the endless conversations about tricks to solve electrospinning issues. Thanks also to Maria Grazia Raucci for the kindness and to my dear friend Mariagemiliana Dessi, who was “volunteered” to share desk, space and internet cable with me, but shared also friendship and amazing touristic journeys.

O meu sincero agradecimento à Sofia Santos, João Relvas, Renato Sodocato, Ana Marques, Marlene Morgado e Joana Faria, do IBMC, pelo apoio, discussões científicas e pelo apoio experimental.

O meu muito obrigada ao Sr Carlos pela preciosa ajuda na montagem do *electrospinning* no INEB.

Gostaria de agradecer ao Sérgio Simões, por ser sempre tão disponível para nos ajudar e por me ter dado a oportunidade de passar alguns dias na Bluepharma, num contexto empresarial, que eu nunca tinha experienciado. Obrigada pela assistência e acompanhamento à Yara Roque, Isabel Lapa e Sónia Alfar.

Quem faz *electrospinning* precisa muito de um SEM, por isso o meu agradecimento ao Engº Carlos Sá por me ter permitido usar o equipamento do CEMUP. Obrigada ao Rui não só pelas "melhores imagens de SEM de sempre", mas pela simpatia e disponibilidade para me encaixar num qualquer furinho na agenda. Obrigada à Liliana pela assistência nas minhas inúmeras visitas.

Faço parte desta casa há muitos anos e há dias em que o céu continua a ser mais azul no INEB! Cresci, vi crescer. Vi chegar e vi partir. Como numa família, de alguma forma, todos fazem parte do meu percurso e deste trabalho.

Em primeiro lugar, gostava de agradecer aos INEBianos que, não sendo co-autores, contribuíram diretamente para esta tese com algum trabalho experimental. Um simpático obrigada à Cátia, Aida, Marta Pinto, Daniela Salvador, Vicky, Patrick e Ana Pinto.

No INEB existe um núcleo duro, coeso, que nos torna a todos muito mais fortes. O meu doce obrigada *for being so inspiring* à Barrias, Martins, Maria, Perpétua, Pedro, Professor Fernando Jorge; e um amistoso obrigada *for being there for me* à Meriem, Isabel, Ana Paula Filipe, Dulce, Eliana, Virgínia e Ricardini (*roses are red, violets are blue*... ha!ha! quem haveria de usar rolhas de champagne como rodas :).

Pela partilha da experiência, pelas discussões (mais ou menos) científicas, pela amizade e pelos *expert advices*, o meu agradecimento repenicado à Raquel Gonçalves, Inês Gonçalves, Catarina Almeida, Marta Oliveira, Daniela Sousa, Diana Nascimento, Juliana Alves, Susana Santos.

À malta jovem Boa-Onda que não se esqueceu de mandar uma piada quando eu andava às escuras em busca da "banda perdida"; o meu obrigada malandrinho à Estrelaça, Ritusca, Filipa, Ana Freire, Catarina Pereira, Mariana Valente, Luísa (às vezes Sofia :s), Daniela Vasconcelos, Ana Silva, Andreia Silva, David, Bianca, Maria Molinos, Tiago Laúndos, Tiago Santos.

Quando nos sentimos parte de uma família, temos de agradecer a todos os que dela fazem parte. Um simpático obrigada para a Ana Sadio, Catarina Seabra, Carla Gomes, Carla Cunha, Cláudia Monteiro, Daniel Vasconcelos, Daniela Azevedo, Diana Leite, Fabíola Moutinho, Inês Alencastre, Joana Antunes, Joana Silva, João Cortez, Manuela Brás, Miguel Xavier, Nilza Ribeiro, Pedro Moreno, Raquel Maia, Rita Bento, Susana Carrilho, Tatiana Resende, ...

O meu agradecimento àqueles que sendo parte da família seguiram o seu caminho para outros laboratórios (outros países, outras vidas), mas que de uma qualquer forma contribuíram na edificação deste castelo. Um saudoso obrigada para a Sandrinha, Maritie Grellier, Alejo, Ana Lopes, Sidónio, Keila, Paula Parreira, Joana Maciel.

Aos meus amigos com quem comecei a procura de pedras basilares para construir castelos. Um refrescante obrigada à Carla. *Continuo a encontrar-te em coisas que faço e por isso, apesar do tempo que já passou, és parte integrante deste meu castelo*.
Hugo, para ti um carinhoso "obrigadinha", por me teres deixado uma enorme herança de reagentes, amostras, *logbooks* codificados e protocolos por escrever (:p)! Obrigada por teres partilhado comigo toda a tua genialidade e sentido crítico – ainda os trago comigo. Deixaste-me na ingrata posição de ser depois de ti … e por isso sentir sempre a tua falta!

Para a Sívlia (☼), Pat e Suse o meu obrigada muito apertadinho pela amizade, por me compreenderem, ouvirem e apoiarem. Nem sabem a falta que me fazem!

Um arrebatado obrigada para os meus amigos "não-INEBianos", que entendendo melhor ou pior naquilo em que eu me tinha metido foram dando o seu apoio, arrastando-me de casa ou do lab e desafiando-me para programas sociais.

Não há palavras que compreendam o agradecimento a uma Família.
Prrriiiiiiiimmmmaaaasss e Tiiiiiiiiaaaaaaaasssssssssss, para vós um divertido obrigada pelo carinho, pelo vosso apoio e boa disposição! Talentoso obrigada para a minha avó por me ensinar que a melhor forma de "superar" as nossas fragilidades é sermos capazes de nos rirmos de nós próprios. *Nem fazes ideia de quanto esse ensinamento encaixa num Doutoramento!*

Obrigada (com ternura) para a minha querida sobrinha por me vir "desorientar" na reta final com tamanha alegria que trouxe para a nossa casa.

Maninha, uma tese não se escreve de pés frios, nem de coração vazio. Tu cuidas-te dos dois. Um obrigada simbiótico para ti!

Obrigada poético para ti Toni, por não teres desistido.

Um emocionado obrigada aos meus pais, pelo apoio incondicional, pela motivação e pelo orgulho. Obrigada pela compreensão sem explicação, pelos mimos, pelos bifes e pelas "mouladinhas". Este é em Engenharia Biomédica, mas ainda hei-de ter um Doutoramento como o vosso, em Generosidade.

ABSTRACT

Injury to the spinal cord is marked by the disruption of ascending and descending axonal pathways, interrupting the communication between the brain and other parts of the body. The primary lesion, which essentially leads to cell death, is followed by a cascade of secondary events that include inflammation, activation of myelin associated-inhibitory pathways, and glutamate excitotoxicity. In this inhibitory environment regeneration fails to occur and the process ends up with the formation of a cavity delimited by a glial scar. Developing a therapeutic strategy to address a spinal cord lesion demands a multi-target approach that can counteract the inhibitory signalling process that is triggered upon injury and also bridge the interrupted connectivity.

The main aim of this thesis was to design a scaffold that combines multiple cues to assist and enhance nerve regeneration in the context of the spinal cord, providing physical support, guidance and the delivery of therapeutic molecules constituting, ultimately, a permissive substrate for axonal regrowth.

In the present work, poly(trimethylene carbonate-co-ε-caprolactone) [P(TMC-CL)] was applied as starting material for building up such a structure. The preparation of fibrous structures based on this polymer by electrospinning is described. Taking into consideration that microglia is in the front line of the central nervous system (CNS) response to injury, we investigated the effect of the fibrous topography on the behaviour of primary microglia, in comparison to P(TMC-CL) solvent cast films. Microglia was found to organize their cytoskeleton according to the topography of the substrate, being an elongated shape favoured when cells are cultured on P(TMC-CL) fibres, where an increased release of the pro-inflammatory cytokine tumour necrosis factor-α (TNFα) was also observed. This study highlighted the importance of specifically address microglia response in the context of tissue engineering for CNS regeneration. Moreover, we showed that microglia cultured on P(TMC-CL) surfaces can actively contribute for myelin phagocytosis and conditioned medium from microglia cultured on these substrates does not trigger astrogliosis markers in astrocytes. These results suggest that P(TMC-CL) scaffolds can actively contribute to modulate microglia towards a pro-regenerative phenotype.

An alternative to modulate cellular response at the lesion site is to combine the scaffolds with the delivery of an anti-inflammatory drug. We tested the incorporation of ibuprofen (a non-steroidal anti-inflammatory drug) in P(TMC-CL) fibres by single solution electrospinning. Ibuprofen-loaded fibres were successfully prepared and, by changing the solvent composition, we showed that fibres of different diameter could be obtained. When the loaded fibres were incubated in physiological medium in sink conditions, the drug was released in 24 hrs. The secretion of prostaglandin E_2 by human monocyte-derived macrophages was found to be reduced when cells were in the presence of ibuprofen-loaded fibres, confirming the bioactivity of the released drug.

Apart from its anti-inflammatory properties, the selection of ibuprofen to load on P(TMC-CL) scaffolds relied also on the recent evidence that this drug can inhibit Ras homolog gene family, member A (RhoA) activation, a convergence effector to several inhibitory pathways triggered after a lesion in the CNS. Envisaging an application *in vivo*, in a spinal cord injury scenario, a bilayer P(TMC-CL) scaffold was prepared. A solvent cast film was used as outer layer and preferentially longitudinally aligned fibres composed the inner layer. Both layers were loaded with ibuprofen. It was demonstrated that the drug released from the scaffolds limits RhoA activation in ND7/23 cells (a neuronal cell line) when these are stimulated with lysophosphatidic acid. Additionally, the scaffolds were tested *in vivo*, in a dorsal hemisection model of spinal cord injury. The preliminary results showed that the scaffold can be implanted at the lesion site and the implantation of ibuprofen-loaded scaffolds had no impact on animal survival.

An alternative to provide scaffolds with biochemical cues is to combine gene therapy approaches that can assure the *in situ* expression of proteins of interest. Chitosan has been under investigation as a promising alternative non-viral gene delivery vector due to its biodegradability and biocompatibility. In order to understand how chitosan-mediated gene delivery can be modulated, an *in vitro* study on transfection, intracellular trafficking and degradation was firstly conducted. Chitosan-based vectors were found to be able to mediate a long-term gene expression that can be tuned by adjusting the polymer degradation rate. In order to translate this knowledge into a 3D scaffold, chitosan-based nanoparticles were mixed with P(TMC-CL) solutions prior to electrospinning. Following this approach it was not possible to obtain a homogeneous mixture that one would be able to electrospun. Due to the better solubility and nanoparticle stability of trimethylated-chitosan, the use of quaternized chitosan was explored. By freeze-drying and subsequent resuspension in organic solvents, the nanoparticles based on trimethyl-chitosan were electrospun along with a P(TMC-CL) solution. In this manner, fibres with a homogeneous morphology were prepared opening new avenues for the design of a scaffold combining electrospun fibres and nanoparticle-based gene delivery.

Overall, the results presented in this thesis point out P(TMC-CL)-based scaffolds as a promising platform for building up a multi-target strategy, combining different cues that, as a whole, can contribute for nerve regeneration after SCI.

RESUMO

Uma lesão na medula espinhal caracteriza-se pela interrupção de tratos axonais ascendentes e descendentes, suspendendo a comunicação entre o cérebro e as outras partes do corpo. A lesão primária, que leva essencialmente a morte celular, é seguida por uma cascata de eventos secundários que incluem inflamação, ativação de mecanismos inibidores associados à mielina e excitotoxicidade mediada pelo glutamato. Neste ambiente inibitório, a regeneração falha e o processo culmina com a formação de uma cavidade delimitada por uma cicatriz glial. Para desenvolver uma estratégia adequada ao tratamento de uma lesão na medula espinhal é necessária uma terapêutica multi-direcionada que consiga contrariar o processo inibitório ativado pela lesão, ao mesmo tempo que reestabelece a conectividade interrompida.

O objetivo do trabalho desta tese foi desenvolver uma estrutura tridimensional (3D) que combinasse múltiplos sinais com vista a assegurar e favorecer a regeneração nervosa no contexto da medula espinhal, fornecendo suporte físico, orientação espacial e entrega de moléculas terapêuticas, e constituindo, como um todo, um substrato permissivo para o crescimento axonal.

Neste trabalho, o poli(carbonato de trimetileno-co-ε-caprolactona) [P(TMC-CL)] foi usado como material inicial para desenvolver essa estrutura, e a técnica de *electrospinning* foi utilizada para o processar sobre a forma de micro/nanofibras. Tendo em consideração que a microglia está na linha da frente da resposta do sistema nervoso central (CNS) à injúria, foi investigado o efeito da topografia de substratos fibrosos no comportamento de culturas primárias de microglia, em comparação com filmes de P(TMC-CL) obtidos por evaporação do solvente. Observou-se que a microglia organiza o seu citoesqueleto de acordo com a topografia do substrato, sendo a forma alongada favorecida quando as células são cultivadas sobre fibras de P(TMC-CL), onde se verifica também um aumento da libertação de uma citoquina pro-inflamatória, o fator de necrose tumoral-α (TNFα). Este estudo realça a importância de estudar especificamente a resposta da microglia no contexto da engenharia de tecidos para o CNS. Adicionalmente, foi demonstrado que microglia cultivada sobre superfícies de P(TMC-CL) pode contribuir ativamente para a fagocitose da mielina e que os meios condicionados de microglia cultivada nestes substratos não induzem um aumento de marcadores de astrogliose em astrócitos. Estes resultados sugerem que as estruturas 3D à base de P(TMC-CL) podem contribuir ativamente para modular a reposta da microglia, direcionando-a para um fenótipo de pro-regeneração.

Uma alternativa para modular a resposta celular no local da lesão é combinar as estruturas 3D com a libertação de um fármaco anti-inflamatório. Neste trabalho, foi testada a incorporação de ibuprofeno (um fármaco anti-inflamatório não esteroide) nas fibras de P(TMC-CL) por *electrospinning* a partir de uma solução única. Fibras com diferentes diâmetros podem ser

obtidas, ajustando a composição do solvente. Quando as fibras com ibuprofeno são incubadas em meio fisiológico (condições "sink"), o fármaco é libertado em 24 hrs. A secreção de prostaglandina E_2 mediada por macrófagos derivados de monócitos humanos diminuiu quando as células foram incubadas com fibras de P(TMC-CL) contendo ibuprofeno, confirmando a atividade biológica do fármaco.

Além das suas propriedades anti-inflamatórias, foi recentemente descrito que o iburpofeno está envolvido na inibição da via de sinalização do RhoA (*Ras homolog gene family, member A*), uma molécula de convergência de vários mecanismos inibitórios despoletados pela lesão medular. Com vista a uma aplicação *in vivo*, num cenário de lesão, foi criada uma estrutura tridimensional de P(TMC-CL) com ibuprofeno constituída por duas camadas. Um filme preparado por evaporação do solvente foi usado para constituir a camada externa, sendo a camada interna composta por fibras longitudinalmente alinhadas. Demonstrou-se que o fármaco libertado da estrutura 3D de P(TMC-CL) reduz a ativação do RhoA em células neuronais (ND7/23) quando estas são estimuladas com ácido lisofosfatídico. As estruturas 3D foram testadas *in vivo* num modelo de lesão da medula espinhal, a hemi-secção dorsal sendo que foi demonstrado que a estrutura 3D desenvolvida pode ser implantada no local da lesão e que a implantação destas estruturas com ibuprofeno não afeta a sobrevivência dos animais operados.

Uma forma para prover as estruturas 3D com sinais bioquímicos é combinar estratégias de terapia génica que possam garantir uma expressão prolongada de proteínas de interesse no local da lesão da medula espinhal. O quitosano tem sido investigado como uma alternativa promissora na mediação não-viral de genes devido à sua biodegradabilidade e biocompatibilidade. De forma a compreender como é que sistemas de entrega de genes à base de nanopartículas de quitosano podem ser modulados, foi elaborado um estudo *in vitro* abordando a transfeção, o tráfego intracelular e a degradação. Foi detetada uma expressão prologada do gene de interesse, sendo que esta pode ser modulada ajustando a taxa de degradação do quitosano. Com o objetivo de traduzir esse conhecimento para uma estrutura 3D, foi testada a possibilidade de incorporar as nanopartículas de quitosano nas fibras através da sua mistura com soluções de P(TMC-CL) antes do processo *electrospinning*. No entanto, este método não permitiu obter uma mistura homogénea nem a formação de fibras. A aplicabilidade de nanopartículas à base de quitosano trimetilado foi alternativamente investigada, uma vez que estas apresentam maior solubilidade e estabilidade. Após liofilização e posterior re-suspensão em solventes orgânicos, as nanopartículas de quitosano quaternizado foram processadas por *electrospinning* juntamente com uma solução de P(TMC-CL). Desta forma foram preparadas fibras de morfologia homogénea, abrindo caminho para o desenvolvimento de uma estrutura 3D que combine fibras obtidas por *electrospinning* e sistemas de entrega de genes baseados em nanopartículas.

Em resumo, os resultados apresentados nesta tese apontam as estruturas tridimensionais baseadas em P(TMC-CL) como promissoras para o desenvolvimento de estratégias multi-direcionadas, combinando diferentes sinais que, como um todo, podem contribuir para a regeneração nervosa depois de uma lesão na medula espinhal.

TABLE OF CONTENTS

Acknowledgments . . . . . **ix**

Abstract. . . . . **xiii**

Resumo. . . . . **xv**

Table of contents. . . . . **xvii**

List of abbreviations. . . . . **xix**

Chapter I – Aim and structure of the thesis **1**

Chapter II – State of the art: Current strategies for spinal cord injury. . . . **9**

1. Pathophysiology of spinal cord injury **11**

2. Inhibitory signals **12**

2.1. Inflammation **12**

2.2. The glial scar **14**

2.3. Myelin-associated inhibition **15**

3. Therapeutic approaches **17**

3.1. Promoting neuroprotection **18**

3.2. Targeting inflammatory cells **19**

3.3. Digesting chondroitin sulfate proteoglicans **20**

3.4. Blocking myelin-associated signaling **20**

3.5. Cell-based therapies **22**

3.6. Other therapeutic strategies **23**

4. The biomaterials-based approach for spinal cord injury **23**

4.1. Scaffold materials **24**

4.2. Scaffold design **28**

4.2.1. Electrospun scaffolds **29**

4.3. Combinatorial strategies **33**

4.3.1. Drug releasing bridges **33**

4.3.2. Drug releasing bridges with cells **34**

5. References **37**

Chapter III – Effect of surface topography on microglia - implications for central nervous tissue engineering **51**

Chapter IV – Ibuprofen-loaded poly(trimethylene carbonate – co – ε-caprolactone) electrospun fibres for nerve regeneration **75**

Chapter V – Ibuprofen-loaded scaffolds for spinal cord injury regeneration – targeting RhoA at the lesion site **105**

Chapter VI – Imidazole-grafted chitosan mediated gene delivery: *in vitro* study on transfection, intracellular trafficking, and degradation **125**

Appendix I – Preliminary results on the incorporation of chitosan-based nanoparticles in poly(trimethylene carbonate – co – ε-caprolactone) electrospun fibres **159**

Chapter VII – Concluding Remarks and Future Perspectives. **177**

LIST OF ABBREVIATIONS

ASIA	American Spinal Cord Injury Association
ATR	Attenuated Total Reflectance
BBB	Blood Brain Barrier
BDNF	Brain Derived Growth Factor
BSA	Bovine Serum Albumin
cAMP	Cyclic Adenosine Monophosphate
CH	Chitosan
CHimi	Imidazole-grafted chitosan
CL	ε-Caprolactone
CLSM	Confocal laser scanning microscopy
CNS	Central Nervous System
COX	Ciclooxygenase
CSPG	Chondroitin Sulfate Proteoglycan
DA	Degree N-acetylation
DAPI	4',6-diamidino-2-phenylindole
DCM	Dichloromethane
DDA	Degree of deacetylation
DMEM	Dulbecco's modified Eagle medium
DMF	Dimethylformamide
DOTMA	bis[oleyl]oxipropyltrimethylammonium chloride
DQ	Degree of quaternization
EDTA	Ethylenediamine Tetraacetic Acid
EGFR	Epidermal Growth Factor Receptor
ELISA	Enzyme-Linked Immunosorbent Assay
FACS	Fluorescence activated cell sorting
FBS	Foetal Bovine Serum
FTIR	Fourier Transform Infrared Spectroscopy
GDNF	Glial Derived Growth Factor
GFAP	Glial Fibrillar Acidic Protein
GFP	Green fluorescence Protein
HEK	Human Embrionic Kidney
HPLC	High Pressure Liquid Chromatography
IBU	Ibuprofen
IGF-1	Insulin-like Growth Factor
IL	Interleukin
LPA	Lysophosphatidic acid
LPS	Lipopolysaccharide
MAG	Myelin-associated glycoprotein
MBP	Myelin Binding Protein

MGC	Multinucleated Giant Cells
MP	Methylprednisolone
Mw	Molecular weight
N/P	Primary amines to phosphate group molar ratio
NGF	Nerve Growth Factor
NgR	Nogo-66 receptor
NMR	Nuclear Magnetic Resonance
NT-3	Neurotrophin-3
OCT	Optimum Cutting Medium
OMgp	Oligodendrocyte-myelin glycoprotein
P(HEMA)	Poly(2-hydroxyehtyl methacrylate)
P(HPMA)	Poly(N-2-hydroxypropyl methacrylate)
P(TMC-CL)	Poly(trimethylene carbonate-co-ε-caprolactone)
P/S	Penicillin/Streptomycin
PBS	Phosphate Buffered Saline
PCL	Poly(ε-caprolactone)
PDI	Polydispersity Index
PDL	Poly(D-lysine)
PEI	Poly(ethylene imine)
PGA	Poly(glycolide)
PGE	Prostaglandin
PLA	Poly(lactide)
PLGA	Poly(lactide-co-glycolide)
PPAR γ	Peroxisome Proliferator-Activated Receptor γ
RhoA	Ras homolog gene family, member A
ROCK	RhoA-associated kinase
ROX	5(6)-Carboxy-X-rhodamine N-succinimidyl ester
SCI	Spinal Cord Injury
SEC	Size Exclusion Chromatography
SEM	Scanning Electron Microscopy
TMC	Trimethylene carbonate
TNFα	Tumour Necrosis Factor α
TriM-CH	Trimethylated Chitosan
TTR	Transthyretin
UV/Vis	Ultraviolet/Visible spectroscopy
VIM	Vimentin
β-gal	β-galactosidase

CHAPTER I

Aim and structure of the thesis

It is estimated that lesions in the spinal cord affect around 2.5 million people worldwide, being the annual incidence in the order of 22 per million [1, 2]. Spinal cord injury (SCI) is characterized by the loss of sensorial, motor and involuntary functions below the site of lesion, resulting in severe psychological, social and economic burdens for patients [3]. Furthermore, the majority of SCI patients require lifelong medical care and physical therapy, representing high costs for the health systems, particularly because SCI affects more frequently individuals before the age of 40 [3]. Notwithstanding the need, currently there is no treatment for SCI.

The development of therapies for this multi-faced condition resulted to be a tremendous challenge. SCI is frequently caused by a mechanical impact on the spinal cord that leads to cellular damage and death. However, the injury is not limited to the loss of cells. The physical support for axonal growth is also interrupted and a number of inhibitory mechanisms are triggered, turning the lesion site into a hostile environment for axonal regrowth. These mechanisms constitute the secondary injury and include the recruitment of inflammatory cells, cytokine release, activation of myelin-associated inhibitory pathways and release of inhibitory molecules. This process ends up with the formation of a glial scar that constitutes, ultimately, a physical barrier thwarting the re-wiring of the central nervous system (CNS) [4].

The ultimate goal of the work described in this thesis is to design a scaffold that gathers physical and chemical cues, providing a permissive substrate for nerve regeneration after a lesion in the spinal cord.

Significant progress was achieved in the last few years in the understanding of the mechanisms associated with the secondary injury and identifying potential targets for new therapies. This knowledge constitutes the basis for a number of strategies presently being investigated for promoting regeneration in the aftermath of SCI. These are reviewed in Chapter II, giving particular emphasis to the most recent innovations on biomaterials-based regenerative therapies for SCI.

There is agreement in the current field supporting the need of a multi-target approach in order to create a therapeutic strategy that can support regeneration after SCI [5]. This should assure physical support for axonal re-growth, and also physical/chemical signals that can counteract the inhibitory environment. Taking this into account, the work presented in this thesis focused on the design of a scaffold that provides physical cues to support and guide axonal regrowth, while modulating cells present at the lesion site into a pro-regenerative activity and serving as platform for the *in situ* delivery of molecules known to contribute to the nerve regeneration process.

Previous studies using poly(trimethylene carbonate-co-ε-caprolactone) [P(TMC-CL)] showed that this synthetic copolymer owns appropriate properties to serve as nerve conduit [6, 7], being able to support peripheral nerve regeneration *in vivo* [8]. In the context of the CNS, P(TMC-CL) showed to stimulate cortical neuron polarization and promote axonal elongation. Moreover, even in the presence of myelin, cortical neurons cultured on P(TMC-CL) films were found to extend more

neurites, showing P(TMC-CL)'s ability to tame myelin inhibition in a CNS lesion scenario [9]. These results motivated the use of this polymer as the starting material for building up a scaffold to promote regeneration at the spinal cord.

Electrospinning has been attracting an ample interest in the tissue-engineering field for the preparation of scaffolds, as fibrous structures can be obtained at the nano/micrometer scale, emulating the structure of the extracellular matrix [10, 11]. The topographic signals provided by electrospun fibres have previously showed to promote axonal guidance and growth [12-14] and stem cell differentiation into the neuronal lineage [15, 16], as well as to modulate astrocytic cell phenotype [17].

In view of an application in the CNS regeneration, we investigated the impact of the topography of P(TMC-CL) fibres on microglia cells. Microglia are the immune cells from the CNS and they are in the front line of the response to an injury. Even so, studies concerning microglia-biomaterials interaction are still very limited, being the effect of electrospun fibres on microglia behaviour described for the first time in this thesis. In the Chapter III, it is reported the effect of P(TMC-CL) fibrous surface on primary microglia cells in comparison to solvent cast (flat) films. This study was conducted in view of the impact of topography on key processes that occur at the lesion site and involving microglia, namely assessing myelin phagocytosis by microglia and evaluating the effect of these cells on astrogliosis. This study shows that P(TMC-CL) surfaces can favour the activation of a pro-regenerative program on microglia, putting forward these structures for an application in a SCI scenario.

To combine topographic cues with the delivery of a molecule with a role on the nerve regeneration process, we pursued to the preparation of P(TMC-CL) electrospun fibres loaded with ibuprofen, a non-steroidal anti-inflammatory drug used worldwide. The anti-inflammatory effect of ibuprofen has been attributed to the inhibition of the cyclooxygenases (COX), enzymes responsible for the formation of prostaglandins, associated with fever and pain [18, 19]. Recently, it has been highlighted that ibuprofen can also inhibit RhoA [20, 21]. RhoA is a small GTPase protein, and its activation has been associated with regeneration failure after SCI, since it leads to actin depolymerisation and growth cone collapse, hindering axonal outgrowth [22, 23].

In Chapter IV, the incorporation of ibuprofen on P(TMC-CL) fibres during the electrospinning process is described. The preparation of the fibres was optimized and we show that the drug released from the fibres was able to reduce the amount of prostaglandin E_2 produced by human monocyte-derived macrophages. This result indicates that ibuprofen remains bioactive and the preparation of P(TMC-CL) fibres with anti-inflammatory properties was achieved.

As the use of ibuprofen-loaded P(TMC-CL) fibres envisaged a double target strategy, the subsequent step was to evaluate the impact of ibuprofen released from the fibres on the RhoA pathway. A bilayer ibuprofen-loaded scaffold has been developed foreseeing its implantation in a SCI animal model. The scaffold was composed by an outer layer based on a P(TMC-CL) solvent cast film, and, taking advantage of the electrospinning technique, the inner layer was made up of

longitudinally aligned fibres. In Chapter V it is reported the characterization of the bilayer scaffolds, loaded- or non-loaded with ibuprofen, as well as their performance *in vitro* and *in vivo*. It is demonstrated that the released ibuprofen can limit RhoA activation in a neuronal cell line, confirming the drug bioactivity. In this chapter the preliminary results of the *in vivo* assessment conducted with the developed scaffolds in a dorsal hemisection SCI animal model (rat) is also reported. So far, no harmful effect on animal survival was observed, but further analysis is needed to evaluate whether this strategy is influencing the RhoA pathway.

To combine gene delivery with the proposed drug loaded scaffolds would constitute a step forward in the design of a multiple strategy to address the challenge of promoting CNS regeneration. Implantable devices have previously been explored as vehicles of nanoparticles carrying genes encoding for proteins with a therapeutic effect in the context of a SCI [24, 25]. Chitosan is a natural polymer previously investigated to serve as gene carrier. Due to its biocompatibility and biodegradability the polymer holds great promise in view of an application on tissue regeneration [26, 27]. Our group have been focused on designing new strategies to improve the vector efficiency as gene carrier [28, 29]. Here we report a detailed mechanistic study on chitosan-based nanoparticles mediated DNA delivery. The results presented in Chapter VI suggest that the expression of a delivered gene can be modulated by tuning the degradation rate of chitosan. To apply this knowledge into a 3D approach, we tested the incorporation of these nanoparticles into P(TMC-CL) fibres. However, the combination of chitosan nanoparticles and P(TMC-CL) solutions lead to the formation of large precipitates, impeding the preparation of electrospun fibres containing these nanoparticles. As alternative the use of nanoparticles based on trimethylated chitosan was investigated, and it is described in Chapter VI. Quaternization is known to increase chitosan solubility and nanoparticle stability [30]. Based on this knowledge we hypothesized that a more homogeneous electrospun solution may be obtained if the nanoparticle stability is improved. The preliminary results show that the formation of fibres can be achieved, suggesting that this approach can be applied in the design of a multi-target strategy for SCI regeneration.

In Chapter VII the overall results presented in this thesis are analyzed considering each chapter and integrating the whole results. The more striking findings are highlighted and new avenues to pursue in this line of research are proposed.

References

1. Sebastià-Alcácer V, Alcanyis-Alberola M, Giner-Pascual M, and Gomez-Pajares F (2014). "Are the characteristics of the patient with a spinal cord injury changing?". *Spinal Cord*, 52 (1): 29-33.

2. Rossignol S, Schwab M, Schwartz M, and Fehlings MG (2007). "Spinal cord injury: Time to move?". *Journal of Neuroscience*, 27 (44): 11782-11792.

3. Rowland JW, Hawryluk GW, Kwon B, and Fehlings MG (2008). "Current status of acute spinal cord injury pathophysiology and emerging therapies: promise on the horizon". *Neurosurgical focus*, 25 (5): E2.

4. Schwab JM, Brechtel K, Mueller CA, Failli V, Kaps HP, Tuli SK, and Schluesener HJ (2006). "Experimental strategies to promote spinal cord regeneration - An integrative perspective". *Progress in Neurobiology*, 78 (2): 91-116.

5. Pêgo AP, Kubinova S, Cizkova D, Vanicky I, Mar FM, Sousa MM, and Sykova E (2012). "Regenerative medicine for the treatment of spinal cord injury: More than just promises?". *Journal of Cellular and Molecular Medicine*, 16 (11): 2564-2582.

6. Pêgo AP, Poot AA, Grijpma DW, and Feijen J (2001). "Copolymers of trimethylene carbonate and epsilon-caprolactone for porous nerve guides: Synthesis and properties". *Journal of Biomaterials Science, Polymer Edition*, 12 (1): 35-53.

7. Pêgo AP, Van Luyn MJA, Brouwer LA, Van Wachem PB, Poot AA, Grijpma DW, and Feijen J (2003). "*In vivo* behavior of poly(1,3-trimethylene carbonate) and copolymers of 1,3-trimethylene carbonate with D,L-lactide or epsilon-caprolactone: Degradation and tissue response". *Journal of Biomedical Materials Research - Part A*, 67 (3): 1044-1054.

8. Vleggeert-Lankamp CLAM, Wolfs J, Pêgo AP, Van Den Berg R, Feirabend H, and Lakke E (2008). "Effect of nerve graft porosity on the refractory period of regenerating nerve fibers: Laboratory investigation". *Journal of Neurosurgery*, 109 (2): 294-305.

9. Rocha DN, Brites P, Fonseca C, and Pêgo AP (2014). "Poly(Trimethylene Carbonate-co-ε-Caprolactone) Promotes Axonal Growth". *Plos One*, 9(2): e88593**.**

10. Agarwal S, Wendorff JH, and Greiner A (2009). "Progress in the Field of Electrospinning for Tissue Engineering Applications". *Advanced Materials*, 21 (32-33): 3343-3351.

11. Greiner A and Wendorff JH (2007). "Electrospinning: A fascinating method for the preparation of ultrathin fibers". *Angewandte Chemie - International Edition*, 46 (30): 5670-5703.

12. Liu T, Houle JD, Xu J, Chan BP, and Chew SY (2012). "Nanofibrous collagen nerve conduits for spinal cord repair". *Tissue Engineering - Part A*, 18 (9-10): 1057-1066.

13. Nisbet DR, Rodda AE, Horne MK, Forsythe JS, and Finkelstein DI (2009). "Neurite infiltration and cellular response to electrospun polycaprolactone scaffolds implanted into the brain". *Biomaterials*, 30 (27): 4573-4580.

14. Yucel D, Kose GT, and Hasirci V (2010). "Polyester based nerve guidance conduit design". *Biomaterials*, 31 (7): 1596-1603.

15. Xie J, Willerth SM, Li X, Macewan MR, Rader A, Sakiyama-Elbert SE, and Xia Y (2009). "The differentiation of embryonic stem cells seeded on electrospun nanofibers into neural lineages". *Biomaterials*, 30 (3): 354-362.

16. Lim SH, Liu XY, Song H, Yarema KJ, and Mao HQ (2010). "The effect of nanofiber-guided cell alignment on the preferential differentiation of neural stem cells". *Biomaterials*, 31 (34): 9031-9039.

17. Zuidema JM, Hyzinski-García MC, Van Vlasselaer K, Zaccor NW, Plopper GE, Mongin AA, and Gilbert RJ (2014). "Enhanced GLT-1 mediated glutamate uptake and migration of primary astrocytes directed by fibronectin-coated electrospun poly-l-lactic acid fibers". *Biomaterials*, 35 (5): 1439-1449.

18. Mitchell JA, Akarasereenont P, Thiemermann C, Flower RJ, and Vane JR (1993). "Selectivity of nonsteroidal antiinflammatory drugs as inhibitors of constitutive and inducible cyclooxygenase". *Proceedings of the National Academy of Sciences of the United States of America*, 90 (24): 11693-11697.

19. Rainsford KD (2009). "Ibuprofen: pharmacology, efficacy and safety". *Inflammopharmacology*, 17 (6): 275-342.

20. Dill J, Patel AR, Yang XL, Bachoo R, Powell CM, and Li S (2010). "A molecular mechanism for ibuprofen-mediated RhoA inhibition in neurons". *Journal of Neuroscience*, 30 (3): 963-972.

21. Fu Q, Hue J, and Li S (2007). "Nonsteroidal anti-inflammatory drugs promote axon regeneration via RhoA inhibition". *Journal of Neuroscience*, 27 (15): 4154-4164.

22. Dubreuil CI, Winton MJ, and McKerracher L (2003). "Rho activation patterns after spinal cord injury and the role of activated Rho in apoptosis in the central nervous system". *Journal of Cell Biology*, 162 (2): 233-243.

23. Niederast B, Oertle T, Fritsche J, McKinney RA, and Bandtlow CE (2002). "Nogo-A and myelin-associated glycoprotein mediate neurite growth inhibition by antagonistic regulation of RhoA and Rac1". *Journal of Neuroscience*, 22 (23): 10368-10376.

24. Martins A, Reis RL, and Neves NM (2008). "Electrospinning: Processing technique for tissue engineering scaffolding". *International Materials Reviews*, 53 (5): 257-274.

25. He S, Xia T, Wang H, Wei L, Luo X, and Li X (2012). "Multiple release of polyplexes of plasmids VEGF and bFGF from electrospun fibrous scaffolds towards regeneration of mature blood vessels". *Acta Biomaterialia*, 8 (7): 2659-2669.

26. Mao SR, Sun W, and Kissel T (2010). "Chitosan-based formulations for delivery of DNA and siRNA". *Advanced Drug Delivery Reviews*, 62 (1): 12-27.

27. Gomes CP, Ferreira Lopes CD, Duarte Moreno PM, Varela-Moreira A, Alonso MJ, and Pêgo AP (2014). "Translating chitosan to clinical delivery of nucleic acid-based drugs". *MRS Bulletin*, 39 (1): 60-70.

28. Moreira C, Oliveira H, Pires LR, Simões S, Barbosa MA, and Pêgo AP (2009). "Improving chitosan-mediated gene transfer by the introduction of intracellular buffering moieties into the chitosan backbone". *Acta Biomaterialia*, 5 (8): 2995-3006.

29. Oliveira H, Pires LR, Fernandez R, Martins MCL, Simões S, and Pêgo AP (2010). "Chitosan-based gene delivery vectors targeted to the peripheral nervous system". *Journal of Biomedical Materials Research - Part A*, 95 (3 A): 801-810.

30. Mao Z, Lie M, Jiang Y, Yan M, Gao C, and Shen J (2007). "N,N,N-trimethylchitosan chloride as a gene vector: Synthesis and application". *Macromolecular Bioscience*, 7 (6): 855-863.

CHAPTER II

State of the art:
Current strategies for spinal cord injury

1. Spinal cord injury – overview

Spinal cord injury (SCI) can be caused by compression, contusion, penetration or maceration of the spinal cord tissue, being very heterogeneous in cause as well as in the outcome. A lesion inflicted to the spinal cord leads to the interruption of motor and sensory neuronal pathways, resulting in the loss of motor, sensory and involuntary functions below the point of injury. Depending on the severity and location of trauma, SCI can be complete or incomplete, leading to different degrees of functional impairment. The primary injury triggers widespread cell death, including neurons, oligodendrocytes, astrocytes or precursor cells. In parallel, edema, ischemia and haemorrhage take place, resulting in the enlargement of the damaged area and creating, ultimately, a fluid-filled cyst (see Figure 1). Subsequently, in the sub-acute phase of SCI, a cascade of events that constitute the secondary damage begins with oligodendrocyte apoptosis and loss of myelin, glutamate excitotoxicity, increase of free radicals and inflammation. These secondary injury results in a protracted period of tissue destruction. In the chronic phase, a glial scar is formed and the lesion site turn out to be a particularly hostile scenery for axonal regeneration (see [1-4] for a review).

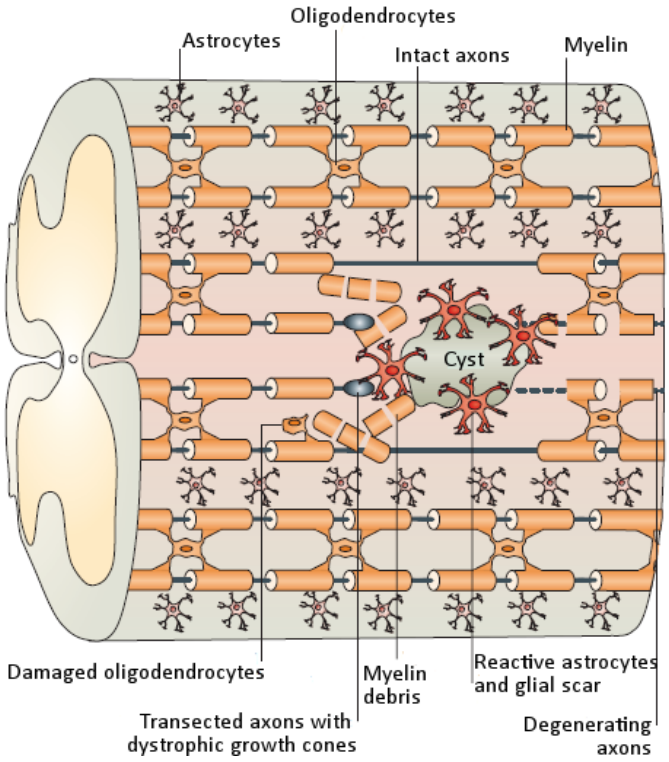

Figure 1. Scheme of spinal cord lesion site. Reproduced with permission from [5]; Macmillan Publishers Ltd., copyright 2006.

For a long time, it was considered that neurons from the central nervous system (CNS) could not regenerate and the field of research on regeneration on the follow up of a SCI was quiescent.

About three decades ago the first indications that regeneration can occur in the CNS was obtained using peripheral nerve grafts in the CNS [6, 7]. More recently, it was demonstrated that, although

for short distances, axonal sprouting occurs after lesion, contributing to compensatory recovery and to the formation of new pathways that bypass the lesion [8]. Despite this regenerative potential, the fact is that after SCI the interrupted neuronal connections are not rewired and the impaired functions cannot be completely restored. This failure is mainly attributed to the establishment of an inhibitory environment for regeneration. Several inhibitory pathways are activated and the formation of a cavity withdraws the physical support for regrowth. Additionally, the formation of a scar tissue constitutes a real physical hurdle for regeneration (see [9-11] for a revision on this subject).

The last thirty years of research brought important findings both at the cellular and molecular level on the mechanisms underlying regrowth inhibition after SCI. Although these knowledge still did not succeed being translated into the clinical setting, it formed a solid ground for the current view in the field that considers that to address such a multi-faced inhibitory environment a combination of therapies is required [4].

2. Inhibitory signals

After a lesion in the spinal cord, several pathways are activated creating an inhibitory environment for regeneration. These include: the inflammatory response, the formation of the glial scar and the activation of myelin-associated inhibitory signals, which are described below in more detail.

2.1. Inflammation

The increase of the blood brain barrier (BBB) permeability is taken as a prelude to the inflammatory response elicited by CNS trauma [12]. The breach caused by the mechanical impact is maximum in the first day after the lesion and it rapidly declines thereafter [13]. The mechanical forces contribute to the initial disruption of the BBB, but the trauma also activates endothelial and glial cells, promoting the release of vasoactive molecules – oxygen species, kinins, nitric oxide, and histamines – that influence endothelial function and enhance the BBB permeability. Moreover, pro-inflammatory cytokines like tumour necrosis factor-α (TNFα) and interleukin-1β (IL-1β) are up-regulated upon injury, contributing to further increase vascular permeability [13]. These vasoactive molecules produced at the site of injury can also lead to toxic effects. Nitric oxide and oxygen species are known to produce free radicals that are involved in the oxidation of nucleic acids or lipids, as well as in the impairment of the mitochondrial function and consequent energy depletion and cell death [14]. These events result in the enlargement of the injured area and exacerbation of damage and neurotoxicity.

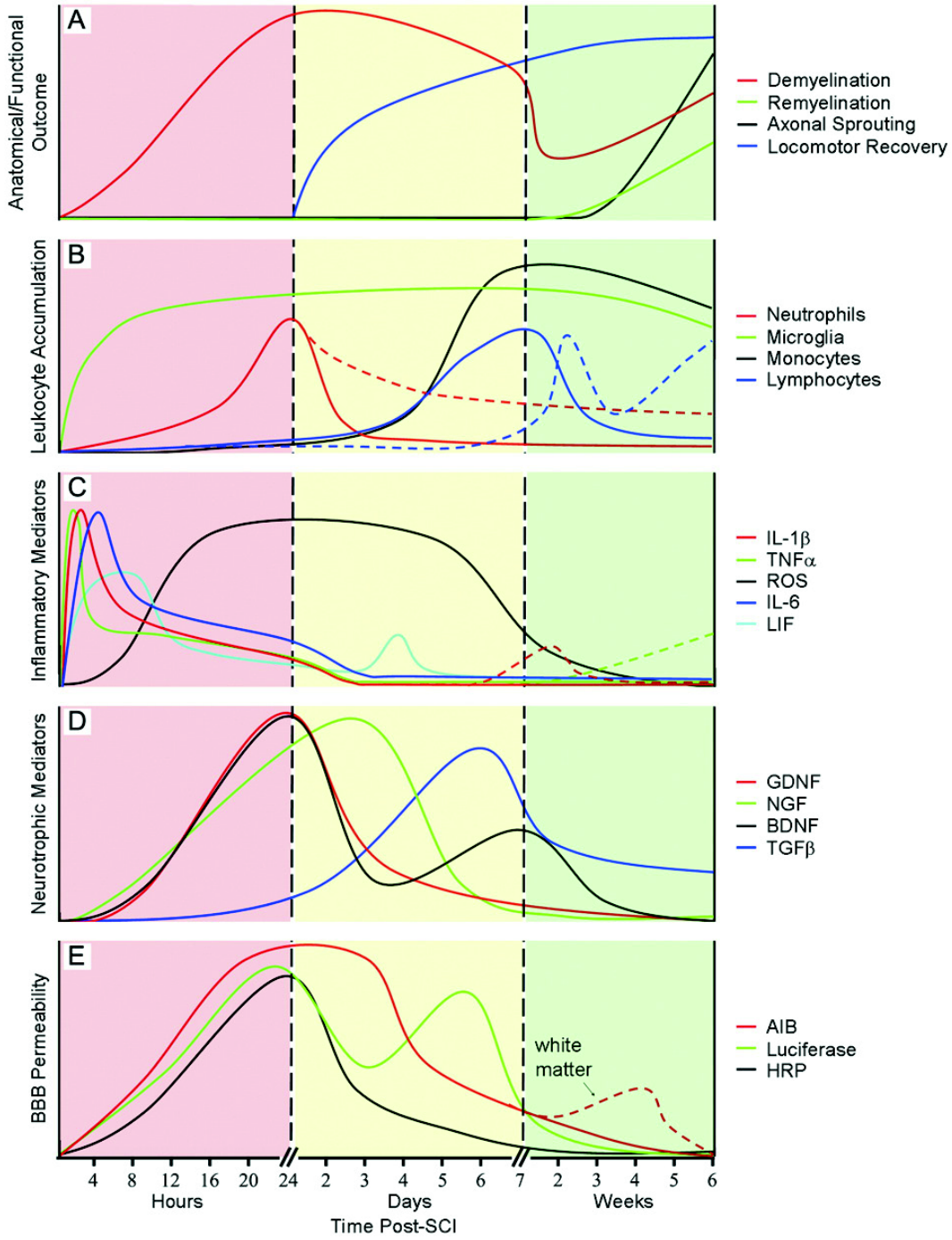

Figure 2. Temporal correlation between functional recovery, secondary neurodegenerative events and inflammatory cascades, in SCI rodents. (A) Anatomical and functional outcomes. (B) Activation of resident microglia and accumulation of leukocytes. Dashed lines depict data from SCI mice whereas solid curves indicate data from SCI rats. Solid curves before these break points are from both species. (C) Expression of pro-inflammatory cytokines and reactive oxygen species (ROS). (D) Expression of neurotrophic cytokines. (E) Blood–brain barrier permeability to α-aminoisobutyric acid (AIB; 104 Da), horseradish peroxidase (HRP; 44000 Da) and luciferase (61000 Da). Values on the vertical axis represent relative changes and are not to scale. Reproduced from [12], Copyright (2008), with permission from Elsevier.

At the cellular level, when a lesion in the spinal cord occurs, the first cells to arrive to the lesion site are the microglia – the resident immune cells of the CNS – followed by infiltrating macrophages [15] (see Figure 2). Microglia exist in the CNS in a quiescent state and, upon injury,

are activated in a graded fashion. The first stage of this process is characterized by cell proliferation, migration as well as morphological, immunophenotypical and functional changes. Only in a second stage microglia transform into phagocytic cells, also known as microglia-derived brain macrophages [16]. Then, microglia cells start to express specific cell surface molecules and releasing cytokines (IL-1β and TNFα) and chemokines (leucotrienes and prostaglandins) [17]. At this stage of activation, resident microglia cells and infiltrated blood-born macrophages express similar immunohistochemical profile. This fact make difficult to discriminate the role of each cell type in the inflammatory response after SCI [17].

Other immune cells will also populate the site of injury. Neutrophils are rapidly recruited upon injury and, as phagocytic cells, produce cytokines, oxygen reactive species and neutrophil proteases, augmenting vascular damage [18]. T-lymphocytes are also recruited after injury playing a major role recruiting other cells and producing a number of cytokines [19].

The described inflammatory reaction occurs within days after injury. However, high levels of pro-inflammatory cytokines, such as IL-2 and IL-6, are detected in patients with chronic SCI, pointing to the existence of a continuous and prolonged inflammatory process [20].

2.2. The glial scar

The glial scar formed in the site of injury is mainly an astrocytic tissue consisting of hyperfilamentous astrocytes, with processes tightly packed, with many gap and tight junctions and limited extracellular space [15]. The scar is formed to isolate the injury, reseal the BBB and prevent the damage of the spared tissue and the spreading of excitotoxicity and cytotoxic molecules [21]. The glial scar constitutes primarily a mechanical barrier for axonal regeneration, but it is also a source of chemical inhibitors for axonal re-growth. Reactive astrocytes in the scar can produce a variety of inhibitory molecules, like tenascin [22], semaphorin-3 [23], ephrin B2 [24] and chondroitin sulfate proteoglycans (CSPGs) [25].

CSPGs are mainly produced by astrocytes and constitute a large family of sulphated glycosaminoglycans including aggrecan, brevican, versican and NG2 [26]. CSPGs are the major component of the extracellular matrix in the CNS and play an important role in determining the functional responses of cells to their environment during development, cell migration, differentiation, maturation and survival, and tissue homeostasis [27]. During maturation of the nervous system, the CSPGs are involved in the “lock in” of synaptic connections, avoiding disturbances on the functional connectivity [26]. In an injury scenario, the regeneration failure has been correlated with axons contacting scar tissue rich in CSPGs [25], being axonal re-growth stopped where CSPGs are deposited [15]. Therefore, CSPGs are considered the major inhibitory species associated with the glial scar [25]. Nevertheless, the mechanism by which these molecules exert their inhibitory action is not completely understood. Some authors proposed that the action of CSPGs is mechanical, hindering axonal growth by masking adhesion molecules in the matrix, like laminin or fibronectin [28] and inactivating integrins [29]. Alternatively, other studies

associated CSPGs with specific intracellular pathways. It is accepted that CSPGs can inhibit axon outgrowth by activating Rho signalling and its downstream effector the Rho-associated kinase (ROCK) via the epidermal growth factor receptor (EGFR) (see Figure 3) [30, 31]. Significant findings have been published in the recent years describing this pathway that is also activated by myelin-associated inhibitors, as will be further discussed in the next section.

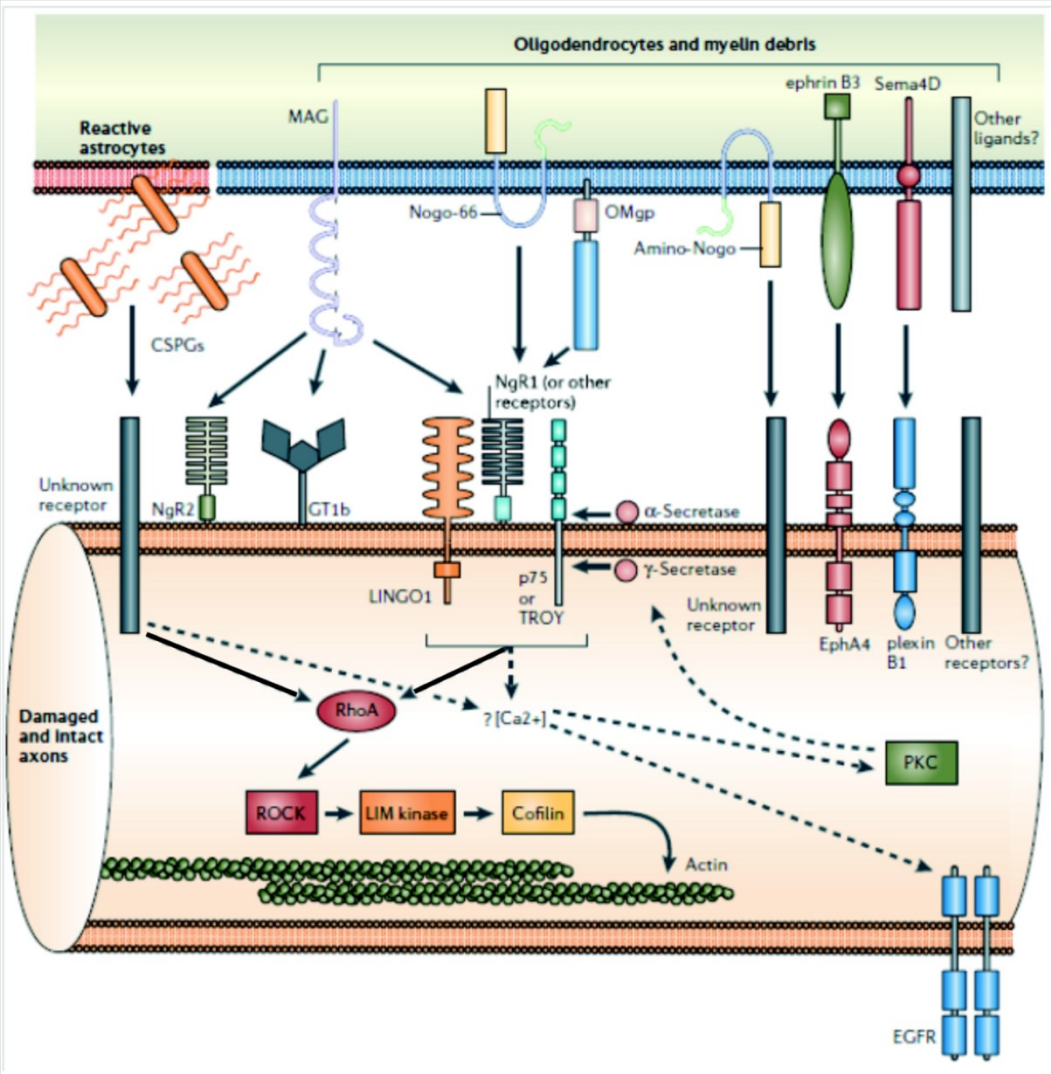

Figure 3. Glial inhibitors and intracellular signalling mechanisms. Dashed arrows show still ambiguous pathways. Adapted with permission from [5]; Macmillan Publishers Ltd., copyright 2006.

2.3. Myelin-associated inhibition

Observations by Ramón y Cajal suggested that white matter can hinder regeneration of the CNS (reviewed in [32]). These early findings were confirmed more recently and it is nowadays established that myelin and oligodendrocytes are not permissive substrates for axonal growth [33, 34] and many blockers of regeneration in the CNS are exposed when myelin is damaged [32].

After a lesion, oligodendrocyte cell death results in axon demyelinization and neuron degeneration, known as Wallerian degeneration. As in the CNS the myelin debris clearance by microglia/macrophages is very slow, it accumulates in the site of injury [15]. Some authors suggested that an inefficient ability to remove the myelin debris is one reason for the limited regeneration of the CNS [1]. This theory is based on the observation that in the peripheral nervous system, where regeneration is successful, the first event occurring upon injury is the rapid clearance of the myelin debris by macrophages [35].

Molecules already identified as inhibitors for axon growth that are present in myelin include Nogo-A, myelin-associated glycoprotein (MAG) and oligodendrocyte-myelin glycoprotein (OMgp).

Nogo-A, the first myelin-associated inhibitor described [36], is a membrane protein (~200 kDa) particularly predominant in oligodendrocytes. Nogo belongs to the reticulon family of proteins, which are mainly associated with the endoplasmic reticulum. Three isoforms were already identified – Nogo A, B, and C. The function of Nogo-B and Nogo-C in the CNS is still not fully described [37]. Nogo-B was found to be increased in hippocampus of rat receiving amyloid-β infusion and to be involved in the activation of microglia [38]. Although further research is needed, these first results suggest that Nogo isoforms, other than Nogo-A, can also be involved in the nerve regeneration process. Two inhibitory domains were identified in Nogo-A: a 66 amino acid sequence (Nogo-66), which is common to the three isoforms, and the unique amino terminal of Nogo-A (amino-Nogo). It is considered that upon injury, oligodendrocytes are damaged and both inhibitory domains would be exposed to the extracellular environment, contacting with axons that are attempting to regenerate [32]. The inhibitory ability of Nogo-A is in line with the observation that this isoform appeared late in evolution and it does not exist in fish or salamander, species with high regeneration potential [37].

Although the mechanism is still not completely understood, it has been shown that Nogo-A mediates axonal growth inhibition by activating the Nogo-66 receptor (NgR) (see Figure 3). This receptor appears to act as a major convergence point on the surface of growth cones for detecting many of the inhibitory influences of myelin. It is also activated by MAG [39] and OMgp [40]. Two homologues for NgR (NgR2 and NgR3) were identified in CNS neurons, but their function is still not fully described [41]. NgR is a glycosylphosphatidylinositol-linked protein with no transmembrane domain. For activation of a cascade of events, it likely works in a complex with transmembrane protein(s) capable of transducing inhibitory signals to neurons [42]. It was shown that p75 [43], a neurotrophin receptor, and LINGO-1, a nervous system-specific transmembrane protein, are needed to form a complex capable to transmit an inhibitory signal to axons [1], as represented in Figure 3. The activation of this ternary complex leads to Ras homolog gene family member A (RhoA) mediated stimulation of ROCK and actin-myosin contractility, which ultimately results in the inhibition of neurite outgrowth and growth cone collapse. RhoA and Rac belong to the small GTPases family and their effect on the organization of actin cytoskeleton is well characterized [44]. It has been shown that the inhibition of RhoA leads to axon growth in inhibitory substrates [40, 45]. Rac was also involved in the myelin-mediated inhibition of axonal growth [40].

Cytosolic calcium transients were proposed as downstream effectors of Nogo-A. Calcium was inversely correlated with axonal extension and can play a role in mediating this growth cone response [42]. In addition to Nogo-A, MAG and OMgp, other repulsive guidance cues with roles on axon pathfinding during development, such as ephrin B3 [46] and Semaphorin 4D [47] can also be found in myelin and are likely to be involved in the inhibition of axonal growth after injury.

3. Therapeutic approaches

For some time, the recommended pharmacological treatment for SCI was the systemic administration of high doses of methylprednisolone (MP). MP is a synthetic glucocorticoid with anti-inflammatory and antioxidant properties, thought to induce neuroprotection and reduce the secondary damage upon injury [48]. A clinical trial in 1990 indicated the bolus injection of MP (30 mg/kg) during the first 8 hrs after injury as a mean to improve neurological recovery [49]. Based on this report, MP has been prescribed worldwide for non-penetrating acute SCI. However, the use of MP has been debated and the design of that clinical trial, as well as the data analysis performed, were considered of dubious value [50, 51]. Some other studies have reported limited beneficial effect of MP and large secondary effects caused by the high dose administrated, like gastric bleeding [50, 52]. Additionally, a randomized clinical trial for head injury, demonstrated that the mortality rate increases 2% with administration of MP [53]. Still, there is recent experimental data supporting the use of MP for SCI [54, 55], and the controversy remains because negative reports are also being published [56, 57]. Consequently, the use of MP is no longer “standard of care” for acute SCI, although it is still in medical practice.

The current intervention in SCI is limited to spinal stabilization, rehabilitation, compensation of the disturbed or missing sensorimotor functions and complication-prevention [58]. However, there are a number of pre-clinical studies and clinical trials ongoing, supported by a highly active research on the neurobiology and on the neuropathophysiology of SCI that will result, hopefully, in a number of strategies being translated into the clinics in the next few years.

According to Ramer et al. [2], potential treatments for SCI can be included in one or more of five categories according to their target for intervention:
(1) *Protection* of spared neural cells;
(2) *Stimulation* of axonal growth;
(3) *Bridging* the lesion, providing a permissive substrate;
(4) *Enhancing* axonal transmission to alleviate conduction blockade;
(5) *Rehabilitation* to enhance functional plasticity.

The boundaries between these categories are subtle and, as previously mentioned, it is expected that a combinatorial approach will be needed to circumvent the action of the large variety of endogenous cells and molecules that act in concert to prevent functional connectivity after SCI. Nonetheless, this classification highlights major keywords on SCI therapeutics: *protect*, *stimulate*, *bridge*, *enhance* and *rehabilitate*. Some of the strategies currently under investigation are

described in the next sections, giving particular emphasis to the ones that are/were tested in clinical trials.

3.1. Promoting neuroprotection

A number of molecules are being studied for administration since the first hours after injury in order to promote neuroprotection; some were already tested in clinical trials. An example is a phase II clinical trial using erythropoietin [59], an hormone known for its effects in the bone marrow. It has been shown that erythropoietin can have a neuroprotective effect by reducing apoptotic cell death and decreasing the release of pro-inflammatory cytokines [60]. However, some concern arose about its use for a prolonged period, since it can increase erythrocyte volume and consequently exacerbate the injury [61]. Current research is focused on the development of erythropoietin derivatives, like carbamylated-erythropoietin, that preserves erythropoietin neuroprotective effects without increasing erythropoiesis [62]. These derivatives are considered very promising and testing in clinical trials is imperative [63].

Minocycline, an antibiotic with anti-inflammatory properties, has also been tested recently in a phase I/II clinical trial. The drug is known due to its immunomodulatory properties, being able to tune the expression of cytokines, attenuate oligodendrocyte and microglia cell death, and improve functional recovery in SCI rat models [64, 65]. In the clinical trial for acute SCI, minocycline showed to be safe and, although the functional evaluation did not accomplish statistical significance, there is a clear tendency towards improvement that encouraged the phase III clinical trial [66], currently recruiting participants [59].

Riluzole has also been tested in phase I clinical trials [59]. Riluzole is a sodium channel blocker and the rationale for its use in acute SCI is that removing sodium excess upon injury, neuronal depolarization is prevented, reducing the accumulation of glutamate and excitotoxicity. It has been shown that the administration of riluzole after SCI in rats reduces edema and improves motor recovery [67]. The clinical trial aimed at evaluating the safety of the drug administrated in 36 patients within 12 hrs after injury. Full results await publication, but a phase II/III trial is currently recruiting participants [59].

Neurotrophic factors are molecules with interest in the context of SCI as they can promote neuroprotection. Neurotrophins have been investigated due to their important role in neural development, survival and regeneration [68]. Injection of nerve growth factor (NGF) [69], brain-derived growth factor (BDNF), or neurotrophin-3 (NT-3) [70] was performed in SCI animal models with different degrees of success. Bradbury and colleagues found that NT-3 is significantly more effective than BDNF promoting the growth of injured axons in a rat dorsal crush model [70]. A large-scale animal study indicate that the topical application of BDNF can induce neuroprotection if applied at high doses and shortly after trauma [71]. Other neurotrophic factors such as glial-derived growth factor (GDNF) [70] and insulin-like growth factor (IGF-1) [71] were already proposed to treat SCI. Regardless the promising results obtained *in vitro* and in animal models, a

clinical trial using systemic delivery of growth factors for diabetic neuropathy showed limited efficacy and significant side effects [72], slowing down the progress of new clinical studies with these molecules. Currently, the use of neurotrophic factors appears to be particularly relevant when combined with drug/gene delivery strategies and/or cell-based therapies [4], as will be detailed afterwards in this chapter.

3.2. Targeting inflammatory cells

The role of inflammation and inflammatory cells after SCI has been for some time a controversial issue. Neuroinflammation is considered a dual-edged sword and both neurotoxic and neuroprotective properties are ascribed to inflammatory cells [52].

Traditionally, inflammatory cell infiltration in the CNS is regarded as pathological [73] and there are important experimental data supporting this theory. To impair macrophage function is the rationale behind the use of some neuroprotective drugs referred above, like methylprednisolone or minocycline [74], or other anti-inflammatory molecules, such as IL-10 [75, 76]. Macrophages were proposed to be the secondary damage effectors in SCI and their depletion showed to enhance axonal sprouting and improve motor function in a contusion SCI model [77]. On the other hand, some authors claim that a well-controlled innate and adaptive immune response is pivotal for repair in SCI [78]. The work of M. Schwartz group has been based on the observation that the injection of what they called “alternatively *ex vivo* activated macrophages” in a complete SCI promotes functional recovery [79]. Macrophages activated prior injection in the spinal cord by co-culturing with peripheral nerves showed increased phagocytic and proteolytic activity, and reduced pro-inflammatory bias. In the late nineties, this work was very controversial. Nowadays, macrophage polarization is well accepted (see [80, 81] for review) and to learn how to control the opposing functions that these cells can exert depending on their phenotype is a topic of interest in many different research fields.

The use of macrophages had also been inspired by the observation of the importance of these cells in mediating repair in the peripheral nervous system, by means of an effective cleaning of myelin debris [35]. The CNS is considered to have a sluggish macrophage/microglia response to injury and this has been pointed out as one of the reasons for its limited ability to regenerate [1]. A clinical trial for the injection of autologous macrophages (ProCord, Proneuron Biotechnologies, USA) was conducted and improvement was detected in 5 out of the 16 acute phase patients [73]. The trial evolved to phase II but, the published results, show no improvement on the primary outcome comparing treated and non-treated individuals [82].

A more provocative approach was also proposed by Schwartz and colleagues that championed the idea of a “protective autoimmunity”. Their assumption is that T lymphocytes, activated by the presence of myelin proteins, can trigger an advantageous response to CNS injury; however it was found to be insufficient [19]. Boosting these T-cell response at the appropriate timing, location, duration, and dosing is proposed as a mean to augment CNS repair and renewal [78]. They

showed that using therapeutic vaccines of T-lymphocytes responding to myelin antigens could contribute to CNS recovery after axonal injury [83]. Immunization can induce a local immune response that promotes migration of stem/progenitor cells to the injury site [84]. This vaccination approach is particularly exciting for application on neurodegenerative disorders like multiple sclerosis, Alzheimer and Parkinson's disease [78].

3.3. Degrading chondroitin sulfate proteoglicans

As a major constituent of the glial scar and being an inhibitory signal for axonal growth, CSPGs are an evident target for SCI therapeutics. It was demonstrated that digestion of CSPGs by chondroitinase ABC promotes axon regeneration and plasticity, leading to functional recovery of locomotor and proprioceptive behaviour after SCI [85]. Chondroitinase ABC is a bacterial enzyme that cleaves glycosaminoglican side chains from the protein core. Treatment with this enzyme is likely to be advantageous even 7 days after injury [86], making this strategy particularly interesting for non-acute spinal cord lesions. However, the origin of the enzyme (bacteria), as well as the degradation products formed, have been issue of concern due to the possibility of triggering the immune response [87]. Moreover, these degradation products can exert some inhibitory influence on the growth of spinal axons [88]. The use of lentivirus-based delivery of a modified chondroitinase gene (that encodes for a secreted form of the enzyme that can be expressed by mammalian cells) is under investigation, as a mean to circumvent some of these caveats [89]. Some authors proposed that the mechanism by which chondroitinase ABC improves functional recovery after SCI is beyond the degradation of CSPGs. The enzyme can degrade other extracellular components interfering on cell adhesion [90] and on the release of growth factors bounded to the CSPGs [87].

3.4. Blocking myelin-associated signalling

Antibodies against Nogo-A had shown to partially neutralize the myelin inhibitory activity [91]. Three different blocking antibodies have been used *in vivo* over the last 15 years [37]. The IN-1 antibody was the first to be described [36] and has been injected in the cerebrospinal fluid, leading to enhanced regenerative sprouting from injured fibres, long-distance regeneration of subpopulations of fibres, and impressive recoveries of sensorimotor functions [37, 92]. A Phase I clinical trial using an humanized anti-Nogo antibody, ATI355 produced by Novartis, is currently being finalized [59]. The anti-Nogo therapy is being tested in acute phase patients, since the time window for application of this therapy is limited, showing a progressive loss of responsiveness [93].

As referred previously, Nogo-A mediates its inhibitory function by activation of NgR receptor. This receptor is also activated by other myelin inhibitory components, such as MAG [39] or OMgp [40]. Being a convergence point to trigger inhibition, NgR emerged as a very attractive target to SCI therapeutics. A competitive antagonist based on the peptide sequence of Nogo-A was already

developed (NEP1-40). The subcutaneous application of NEP1-40 immediately or seven days after hemisection of the spinal cord of mice leads to improved axonal sprouting and locomotor recovery [94]. However, on a re-assessment study only a slight and unpredictable improvement on axonal regeneration was observed [95].

Inactivation of RhoA has been shown by several groups to overcome axonal growth inhibition by individual inhibitors and by myelin in general. Inactivation of Rho by the application at the site of injury of the toxin C3 (*Clostridium botulinum*) promotes an extensive regeneration and functional recovery in mice [96]. Hindlimb recovery was also reported after administration of the toxin or Y27632 – a specific inhibitor for ROCK [45]. These two molecules had also shown to allow growth of primary cortical neurons on inhibitory substrates, like myelin or CSPGs [31, 45]. Additionally, blocking RhoA over-activation after SCI has also showed to protect cells from apoptosis mediated by the activation of p75 neurotrophin receptor [33]. According to these data, RhoA is a convergence molecule for many inhibitors of axonal regeneration and it is, for that reason, a promising target for SCI therapeutics. Nonetheless, the use of blockers of second messenger pathways (as RhoA) encloses the risk of complex effects on other cell types and functions [73].

The first results of a phase I clinical trial using a cell-permeable Rho antagonist, called BA-210 (Cethrin®, a recombinant protein), were recently published by Alseres Pharmaceuticals [59]. Cethrin was administered by extradural application with a fibrin sealant to patients with acute cervical SCI during spinal decompression surgery conducted within 72 hrs after injury [97]. Twelve months after intervention, 5 out of 13 patients (38%) showed marked recovery of motor and sensory function after treatment, as measured by a 2-grade improvement or higher in the American Spinal Cord Injury Association (ASIA) impairment scale [98]. The results are encouraging and a multicenter, randomized, double blind, placebo-controlled, Phase IIb study sponsored by Bioaxone Biosciences is expected to start soon.

Ibuprofen is used worldwide as a non-steroidal anti-inflammatory drug. Its action has been attributed to the inhibitory effect on cyclooxygenase (COX), the enzyme responsible for the conversion of arachidonic acid in prostaglandins. Prostaglandins, like prostaglandin E_2 (PGE_2), are associated with pain, fever and acute inflammatory reaction [99, 100]. In 2007 it was described for the first time that ibuprofen can inhibit the activation of RhoA in a SCI scenario [101]. The drug prevents myelin inhibition of neurite outgrowth by reducing RhoA activation *in vitro*, and also stimulates corticospinal axonal regeneration after spinal cord transection [101]. Ibuprofen effects were observed in two different SCI rat models: when administrated immediately after spinal cord transection or seven days after spinal cord contusion [101]. Recovery of locomotion and axon growth stimulation activity was also reported by Wang and co-authors, although in this case, ibuprofen failed to support corticospinal regeneration [102]. More recently, the administration of ibuprofen showed to support peripheral nerve regeneration [103], as well as oligodendrocyte survival and axonal myelination following traumatic contusion of the spinal cord [104]. The molecular mechanism by which ibuprofen inhibits RhoA is suggested to be related with

transcription factor peroxisome proliferator-activated receptor γ (PPARγ) [105]. Even though in a recent re-assessment study the authors were able only to partially replicate the results obtained in 2007 [106], the number of publications that report positive effects of ibuprofen on nerve regeneration is significant and the use of this drug is considered very promising [107]. Due to ibuprofen widespread use, its effects are very well documented; the long-term use has a quite acceptable risk profile and the clinical application would not be meaningful in economical terms [107]. Furthermore, the release of PGE_2 was associated with neuropathic pain after SCI [108] and targeting COX_2 pathway is pointed out as a new avenue to treat this condition [109]. In fact, the effect of the chronic administration of ibuprofen after SCI has recently shown to reduce neuropathic pain, although in this study significant functional improvement were not achieved [110].

3.5. Cell-based therapies

According to clinicaltrials.gov [59,112], currently there are 14 open clinical trials for SCI using cellular therapies, representing more than 5% from all the open trials for this condition. This is a consequence of an energetic activity in the stem cell field and emerges, probably, on the outcome of the progress attained on stem cell research (see [111-114] for review). Even so, cell-based therapies have been facing important caveats when being translated into the clinic. Most of the pre-clinical studies are performed with non-human cells and the source and culture conditions of these cells vary significantly, compromising result replication. Furthermore, there is still some concern about cell survival and integration in the host tissue, what have been slowing down the progress of cell-based therapies [114].

The implantation in a spinal cord lesion of stem cells holds the promise of repopulating the injury site, promote the production of growth factors and cell plasticity. Current literature suggests that cell-based therapies will be of particular interest in acute or sub-acute phases of SCI, since transplantation in chronic patients showed to yield limited functional benefit [114]. Bone marrow stromal cells, umbilical cord blood cells and neural stem cells are stem cells currently under investigation in clinical trials. Bone marrow stromal cells present the great advantage of a minimally invasive and autologous source. However, some authors claim that the benefit of their implantation in SCI is due to immunomodulation and environment modification rather than cell differentiation onto neuronal lineage cells [112]. Neural stem cells and also umbilical cord blood cells are difficult to obtain from an autologous source; therefore, patients need to be subjected to immunosuppressive therapy. Nonetheless, a clinical trial using human-derived stem cells is ongoing, supported by Stem Cells, Inc.. The clinical use of embryonic stem/progenitor cells showed promising results in early stages [115]. The authors showed that the cells can differentiate in oligodendrocytes, astrocytes and neurons. However, its clinical use has been mainly hampered by ethical issues.

Alternative cell types studied on the context of SCI include macrophages [79] (already mentioned in this review), Schwann cells [116], and olfactory ensheathing cells [117, 118]. Schwann cells are the responsible for the formation of myelin in the peripheral nerve regeneration, being able to physically support nerve regeneration after injury. Implanted cells can be of autologous origin by scarifying a peripheral nerve. However, the studies reporting Schwann cell implantation in a SCI show limited success, being these cells of particular interest when combined with other SCI therapeutic strategies [114]. Olfactory ensheathing cells can be obtained from the olfactory bulb in a minimally invasive surgery and can also be of autologous origin. There are publications reporting the use of these cells alone [119], combined with other cell types [117] or in pieces of olfactory bulb [118]. Although these cells showed an inconsistent regenerative capacity in independently replicated experiments [120], the more recent results from the clinics seem to be encouraging [118, 119].

3.6. Other therapeutic strategies

In addition to the cellular- and molecular-based strategies for the treatment of SCI, other approaches are being clinically explored and applied, such as rehabilitation therapy. In fact, this is among the few approaches that have shown clear benefits [121]. Rehabilitation can promote sensorimotor recovery after SCI by promoting neuronal re-organization and functional plasticity [122]. Other procedures, such as early decompression after lesion and electrical stimulation are being investigated and are likely to be part of a SCI treatment regimen [123].

4. The biomaterials-based approach for spinal cord injury

As mentioned in the beginning of section 3, one of the strategies for SCI treatment concerns the *bridging* of the lesion. Here, biomaterials are major players. Nerve regeneration research based on the use of biomaterials was primarily focused on the development of scaffolds that can connect the lesion site, providing physical support and a path for axonal regrowth. These scaffolds have been evolving from the simple hollow conduit to more sophisticated devices with improved physical guidance architectures combined with molecules that can contribute for the nerve regeneration process (see Figure 4). The application of biomaterials in SCI is nowadays considered particularly interesting for the modification of the inhibitory environment at the lesion site, either by the release *in loco* of molecules incorporated in the matrix, or by the delivery of cells [123]. Scaffolds can be used as cell vectors, serving as reservoir of molecular or physical cues for cell survival and differentiation. Significant amount of research has been conducted on the design of the scaffolds and also on its combination with specific molecules or drugs and cells, as reviewed in the next sections.

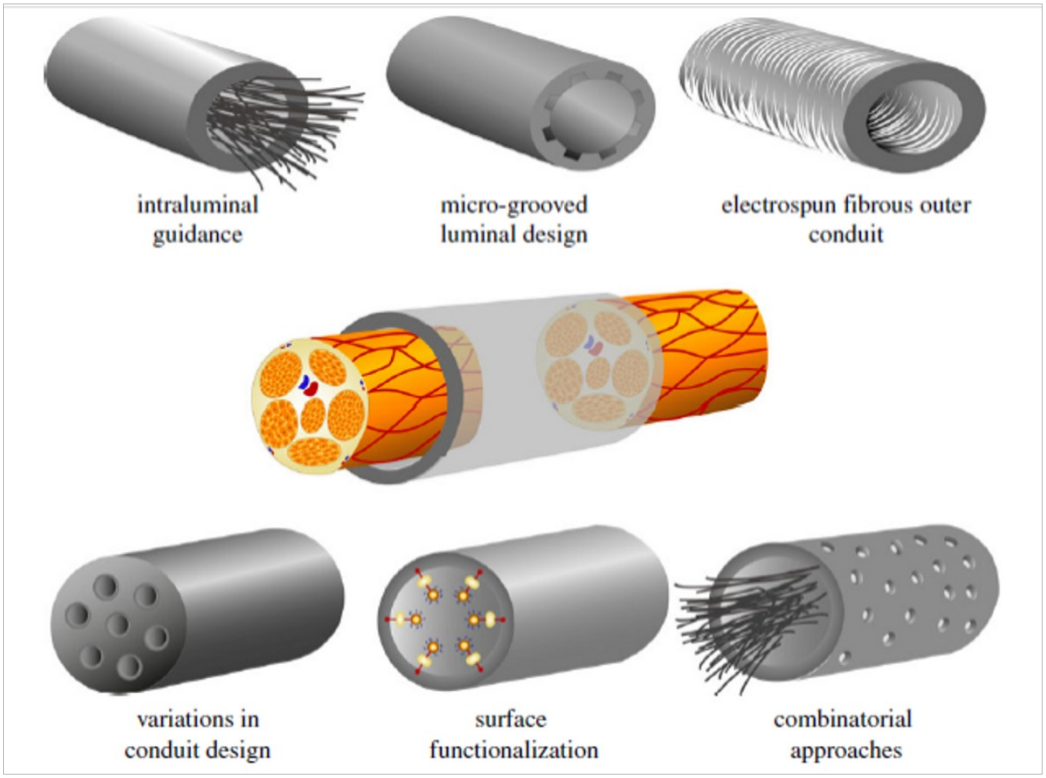

Figure 4. Different approaches on the design of nerve guidance channels. Reproduced from [124], Copyright (2012), with permission from Royal Society publishing.

4.1. Scaffold materials

The use of nerve conduits to bridge a nerve lesion was firstly explored for peripheral nervous system regeneration, as an alternative to autologous nerve grafting (see [125] for a review). Based on the evidence that neurons from the CNS can regenerate into peripheral nerve grafts [6], the development of nerve conduits for SCI was also proposed. Nerve conduits should ensure permeability to oxygen and nutrients, limited swelling, should be flexible but not kink [125], should allow sterilization and processing to the desired dimensions and to be easy to handle and suture [35].

Several materials have been used to prepare bridges for SCI. Those include biodegradable, and non-biodegradable polymers, either natural or synthetic. Although it is considered that the application *in vivo* of non-biodegradable materials has limited interest due to chronic nerve compression [126], materials like poly(acrylonitrile) /poly(vinylchloride) [127] or poly(2-hydroxyethyl methacrylate) [128] and copolymers with methyl methacrylate [129] have been implanted in the spinal cord. The mechanical properties of these materials closely resemble those of the spinal cord, characteristic considered important to avoid necrosis of the tissue in the interface tissue-implant [129]. Even so, non-degradable materials are not the focus of most current research efforts [130]. Silicone, another non-biodegradable material, has been used in the context of SCI research but mainly for testing the effect on axonal elongation of specific molecules [131], or extracellular components [126].

Biodegradable conduits hold the potential of an ultimate restoration of function without the need of removing the device [132] but, to achieve this goal, the polymer degradation rate should match the new tissue formation and maturation. The application of degradable materials encloses the concern of a potential inflammatory response triggered by the degradation process and products [132].

The use of synthetic materials to prepare nerve conduits has the advantage of manufacturing control and tuning the structure, mechanical properties and degradation rate. Among them, aliphatic polyesters, like poly(lactide) (PLA), poly(glycolide) (PGA) and their copolymers are the most explored [133-135], probably encouraged by the fact that these are FDA approved (see Table 1). Other popular synthetic polymer in the nerve conduits research field is poly(ε-caprolactone) (PCL) [136, 137], although the number of *in vivo* studies concerning its application in a SCI scenario is still limited. PCL has a very low degradation rate, and to tune its properties it has been co-polymerized with 1,3-trimethylene carbonate [138, 139] or ethyl ethylene phosphate [140]. Porous scaffolds of poly(trimethylene carbonate-co-ε-caprolactone) [P(TMC-CL)] showed to support peripheral nerve regeneration *in vivo* [141]. To enhance the bioactivity of conduits prepared from synthetic polymers, these have been modified with cell adhesion peptides [142, 143] or immobilized extracellular matrix proteins like fibronectin [134], or laminin [134, 135, 144]. The incorporation of extracellular components on nerve bridges holds the premise of improving cell adhesion and promoting axon pathfinding.

Alternatively, natural polymers are generally considered biocompatible, able to support cell migration and avoid the occurrence of toxic effects. These properties make natural polymers advantageous materials for the preparation of nerve tissue engineering constructs [126]. Chitosan [161, 162] and collagen [165] are popular natural materials used to prepare nerve conduits (for the peripheral or central nervous system). Other materials tested in the context of spinal cord injury include hyaluronic acid, agarose, fibrin, gelatin, gellan gum or alginate (see Table 1). To combine the advantages of both natural and synthetic polymers, blending have been actively investigated, as shown by the different combinations of PCL with gelatin [182], collagen [183] or chitosan [184].

Table 1. Materials studied for nerve regeneration and tested in SCI models.

	POLYMER	NATURE	TYPE OF BRIDGE	COMBINATIONS	REF.
SYNTHETIC POLYMERS	PLA *poly(lactide)*	Synthetic, degradable	Single walled conduit, electrospun fibres	Drug release	[145-147]
	PLGA *poly(lactide-co-glycolide)*	Synthetic, degradable	Multiple channel; electrospun fibres	Plasmid DNA; Schwann cells; self-assembling peptides for growth factor delivery; drug delivery	[148-152]
	PCL *poly(ε-caprolactone)*	Synthetic, degradable	Porous scaffold	Neural stem cells	[153, 154]
	Peptide amphiphiles	Synthetic; degradable	Hydrogel, fibres	Modified with IKVAV peptide	[143, 155]
	P(HEMA) *poly(2-hydroxyehtyl methacrylate) and copolymers*	Synthetic; non-degradable	Hydrogel; scaffold	Drug delivery; modified with SIKVAV	[128, 129, 156, 157]
	P(HPMA) *poly(N-2-hydroxypropyl methacrylate)*	Synthetic; non-degradable	Hydrogel	Modified with RGD; mesenchymal stem cells	[158-160]
NATURAL POLYMERS	Chitosan	Natural; degradable	Porous scaffold	Endothelial cells; Collagen hydrogel as filler; Bone marrow stem cells	[161-164]
	Collagen	Natural, degradable	Electrospun fibres; Oriented pore channels; hydrogel	Growth factors; chondroitinase ABC	[163, 165-167]
	Gelatin	Natural; degradable	Scaffold	Neuronal + endothelial cell lines	[168]
	Self assembling peptides	Natural; degradable	Hydrogel	Neural progenitors; Schwann cells	[169, 170]
	poly-β-hydroxybutyrate	Natural; degradable	Hydrogel	Schwann cells	[171]
	Agarose	Natural; degradable	Hydrogel/scaffold	Growth factors	[55, 172]
	Hyaluronic acid	Natural	Hydrogel	Growth factors	[173, 174]
	Fibrin	Natural, degradable	Hydrogel	Growth factors; chondroitinase ABC; Neural progenitor cells	[175-179]
	Alginate	Natural; slowly degradable	Hydrogel		[180]
	Gellan gum	Natural; degradable	Hydrogel	Modified with GRGDS; neural progenitor cells; olfactory ensheating cells.	[181]

Some of the above mentioned materials can be processed as solid conduits as well as injectable materials. The use of injectable materials is of particular interest in SCI lesions where dura matter is not compromised. In this case, injectable materials can fill the cavity formed without need for further lesion to implant a solid device [123]. Although polymers like chitosan or hyaluronic acid can form hydrogels, they need to be crosslinked. Traditionally, chemical agents like glutaraldheyde were used, but these were abandoned due to toxicity, being non-toxic crosslinking methods currently under investigation. In the SCI research, chitosan has been grafted with poly(ethylene glycol) as a mean to allow physical crosslinking driven by the presence of thermosensitive moieties [185]. Gupta and colleagues combined hyaluronic acid and methylcellulose to obtain a fast-gelling drug delivery system, compatible with the injection in the intrathecal space in SCI model [173]. However, this gel does not allow cell adhesion, being inappropriate to a direct application into the lesion cavity [173].

Fibrin is a natural polymer formed by enzymatic cleavage of fibrinogen by thrombin in the presence of calcium ions. It is widely used in clinical practice ("fibrin glue") as surgical haemostatic [186]. These gels can support axonal growth and are suitable for an implantation *in vivo* [175]. Fibrin has been actively investigated for the delivery of growth factors in the spinal cord [176, 177, 179]. The combination of fibrin with fibronectin gels improves axonal infiltration and integration with the host tissue after an incomplete lesion in the spinal cord [187]. Furthermore, fibrin hydrogels are very promising for cell transplantation, and have been applied in a number of recently published reports [178, 188], as will be described in more detail afterwards.

Self-assembling nanofibrous scaffolds gained in the last few years, considerable importance within the research field of injectable materials. Self-assembling peptides (SAP) are based on short amino acid sequences that self-assemble in response to mild stimulus, like the increase on temperature or ionic strength, allowing gelation in cell culture media or after injection *in vivo*. These synthetic hydrogels have been tested in a wide range of applications, namely for neuronal cell growth, being commercially available as PuraMatrix™ [189]. In SCI research, these hydrogels are commonly investigated for the delivery of cells, such as Schwann cells [170] and neural progenitor cells [169]. Some improvement on axonal growth through the scaffold is reported [169], but the most important benefit described for SAPs is on cell survival [169, 170]. To improve the ability of these hydrogels to contribute for regeneration after SCI, researchers focused on SAPs functionalization [190] or incorporation of molecules that can contribute for axonal regrowth [191]. Similarly to SAPs, peptide amphiphiles can self-assemble into nanofibrous hydrogels *in vivo* due to the environmental ionic strength. Peptide amphiphiles present the advantage of containing a region that can be modified with no significant interference in the gelation process [192]. It has been shown that the implantation of amphiphiles with IKVAV sequence (sequence from laminin adhesion protein) can promote a significant improvement on locomotor function in rats with a contusive [143, 155] or compressive SCI [155]. These peptides showed to reduce astrogliosis and enhance neuronal serotonergic innervation at the lesion site [143, 155]. Peptide amphiphiles are claimed to be biodegradable and, although detailed studies are still required, it is believed that the

degradation products will most probably not affect nerve regeneration [192]. Furthermore, they can also be used as drug delivery devices [193], putting forward these hydrogels as very promising materials to use as nerve conduits [192].

An important class of materials that has been proposed for the preparation of nerve conduits is the one of conductive polymers. It has been shown that electrical stimulation increases neurite outgrowth [194]; therefore, to provide scaffolds with conductive properties can positively contribute for the regeneration process. However, synthetic conductive polymers, like poly(pyrrole) and poly(aniline), have poor biocompatibility, biodegradability and are difficult to process in different scaffold designs. In view of the above, these polymers have been applied as coating or blends with other synthetic [195, 196] or natural [197] polymers as a mean to improve their biocompatibility while maintaining the electrical conductance and, ultimately allowing the stimulation of neurite outgrowth.

4.2. Scaffold design

It is well accepted that axons need guidance for regeneration and that growth is useless if axons wander randomly [198]. However, the use of hollow conduits in the spinal cord showed limited success [145, 162, 163]. Oudega and co-workers implanted a PLA single walled conduit in a complete transection SCI model and showed that the tube collapsed soon after implantation, compromising axonal regeneration [145]. Conduits made of chitosan [163] or chitosan modified with laminin by plasma treatment [162] were implanted in the spinal cord after excision of piece of tissue, but no improvement on axonal regrowth or function were detected comparing to injured rats without implanted device. Furthermore, there is mounting evidence that axons orient their processes according to the substrate and are sensible to patterns on the surface [199-202], suggesting that to include these features in nerve conduits can improve the guidance performance of the device. In view of the above, the development of an internal lumen for the conduits is being investigated, namely the incorporation of smaller channels, gels, or nanofibres as illustrated in Figure 5. These can favour cell attachment due to a higher surface area and can also serve for the incorporation of other molecular cues, like extracellular matrix components and growth factors [203].

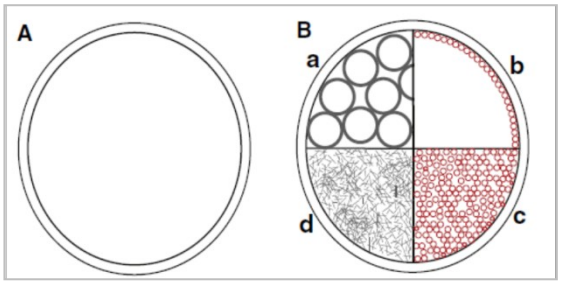

Figure 5. Cross-section illustration of nerve conduits. (A) basic hollow nerve conduit with a void lumen; (B) nerve conduit comprising different luminal structures: a) multichannel, b) inner wall surface furnished with nanofibres, c) array of nanofibres, d) gel or extracellular matrix or other materials. Adapted from [204], Copyright (2012), with permission from Elsevier.

Multiple channel bridges of poly(D,L-lactide-co-glycolide) (PLGA) have been prepared by gas foaming and particulate leaching [205]. The conduits containing channels between 150-250 μm maintained their integrity 13 days after subcutaneous implantation [205]. When implanted in the spinal cord, limited macrophage infiltration is found and the conduits are stable at least for 6 weeks after implantation [148]. Furthermore, the preparation of these conduits is compatible with the delivery of bioactive growth factors [205] or DNA [149]. To develop more complex internal lumen architectures, the design of moulds by computer aided design and solid freeform fabrication has been proposed [206]. Using this approach 7 channel conduits were prepared by injection moulding using a number of synthetic polymers. After implantation in a complete transection model for SCI combined with Schwann cells [150, 206], conduits of oligo(polyethylene glycol) fumarate positively charged hydrogel showed better results in terms of number of axons colonizing the scaffold comparing to PLGA scaffolds. Nonetheless, none of the materials tested achieved a functional improvement 4 weeks after lesion [150].

Although still not tested *in vivo*, collagen multichannel conduits based on electrospun fibres are being investigated and show great potential due to the very high surface area of the structure, mimicking the fascicles in nerve [207]. The preparation of scaffolds with oriented microchannels has also been explored using freeze-drying technique for polymers like collagen [167] or gelatin [168] and blends with chitosan [208].

The combination of hydrogels and hollow conduits have been mainly investigated for peripheral nerve repair [209, 210]. In the context of SCI, a large-scale study was performed using a chitosan conduit filled with a semi-fluid collagen. It was reported a significant improvement on the number of axons that can cross the bridge in rats where collagen was used to fill the chitosan tube, leading also to a significant increment in the Basso, Beattie and Bresnahan locomotor rating scale [163]. Other studies combine nerve conduits with hydrogels and cells, but these combinatorial approaches will be reviewed in section 4.3.

4.2.1. Electrospun scaffolds

In the last few years, the tissue engineering field has directed much attention to the preparation of nanofibrous scaffolds, since their structure emulates the extracellular matrix. The nanofibrous scaffolds provide large surface area to volume ratio and interconnected porous geometry [211].

Comparing to other techniques available for the preparation of nanofibrous scaffolds, like self-assembling, electrospinning is the most popular. It is simple and cost-effective; it can be applied to a wide range of materials (synthetic and natural polymers, proteins, polymer blends, polymer suspensions with nanoparticles, or active agents, metals and ceramics) [212, 213]. The method was first described more than a century ago and the first patent dates from 1934, by Formhals [214]. However, only more recently the popularity of electrospinning had increased, as can be perceived from the recent exponential increase in the number of publications [215]. Fibre thickness and morphology can be controlled by adjusting electrospinning parameters, like solution properties (viscosity, elasticity, conductivity and surface-tension), electric field strength, distance between the spinneret and the collecting plate (see Figure 6), temperature and humidity [216]. Electrospun fibres can be used to fill nerve conduits, but also for the preparation of the conduit itself. The electrospinning technique also allows some control on the scaffold size, shape, thickness and fibre orientation by adjustments on the grounded target [217]. The use of aligned nanofibres is particularly promising on the nerve regeneration field [133, 140, 218, 219].

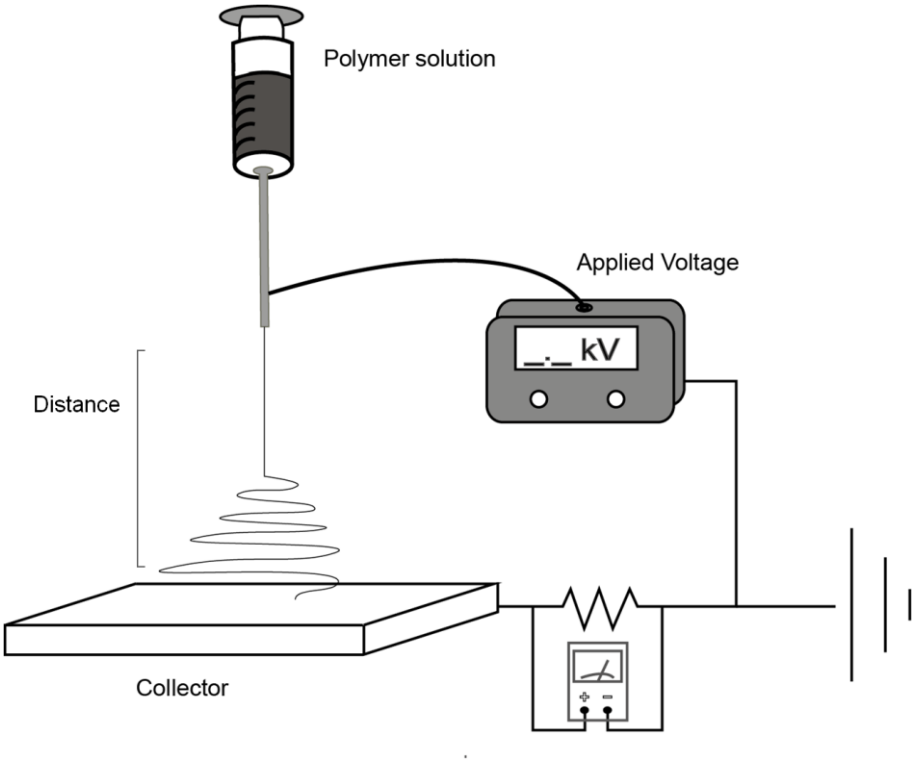

Figure 6. Illustration of an electrospinning setup.

Electrospun scaffolds have been broadly investigated for peripheral nerve regeneration [133, 135, 140, 182, 218, 220-222], and more recently, also explored in the context of SCI [146, 151, 152, 165, 223-226]. The first report testing electrospun fibres in a SCI scenario was published in 2007. Meiners and colleagues implanted a fabric based on randomly-oriented polyamide fibres in a

hemisection SCI model. The results were unsatisfactory, since the fabric tends to fold, impairing axonal outgrowth [223]. This study highlighted the importance of developing oriented nanofibrillar scaffolds for directing axonal growth. Indeed, it has been shown that neurite extension is increased when cells are cultured on aligned fibres of PCL or PLA, comparing to anisotropic substrates [218, 227]. Furthermore, the alignment of astrocytes [224] or olfactory ensheathing cells [228] on aligned electrospun fibres has also been demonstrated. The lack of alignment of glial cells after injury is associated to the regeneration failure; therefore, the use of these substrates where also glial cells can organize can further contribute for the regeneration process.

Fibre alignment showed also to play a role on adult stem cell differentiation, potentiating differentiation into the neuronal lineage when in differentiation cell culture media [229]. Previous reports describe that there is a higher number of cells expressing Tuj1 (marker for neurons) and O4 (oligodendrocyte marker) when cells are cultured on aligned PCL nanofibres as compared to random fibres. Conversely, the number of cells that differentiate into astrocytes is diminished [225].

The topography of the electrospun substrates was also found to influence the behaviour of immune cells. This issue has been investigated with particular focus on monocyte and macrophages. It has been shown that when cultured on electrospun fibres of PLA [230] or PCL [231] macrophages secrete less pro-inflammatory cytokines comparing to cells cultured on solvent-cast films, suggesting that the use of these biomimetic approach improves biocompatibility of the surfaces [230]. To modulate macrophage response via topographic cues provided by nerve conduits is a relevant approach towards spinal cord regeneration taking in consideration their role on secondary injury after SCI [77]. Although microglia is the responsible for the early pro-inflammatory environment after SCI [17], little is known about the response of these cells to surface topography. The effect of nanostructured silicone on BV-2 (a microglia cell line) cell adhesion was investigated, showing that cells can undergo marked morphogenic changes, according to feature size (30 nm - 2 μm) [232]. Additionally, it was demonstrated that microglia can interact mechanically with nanostructured 3D features, like 4.7 μm pillars, adapting actin cytoskeleton to these structures [233]. These studies clearly demonstrate morphologic plasticity of microglia [232-234], however, it is still necessary to understand if this can have an impact on cell function.

Despite the fact that the overall reports indicate that the use of electrospun fibres on nerve conduits can be beneficial for the regeneration process, the number of studies that tested electrospun scaffolds in SCI is still low. To the best of our knowledge the first report using electrospun conduits in a SCI *in vivo* model was published in 2011. Hurtado and co-workers tested a rolled conduit of PLA random and aligned micrometer fibres (Figure 7, A) after complete transection of the spinal cord. Although the functional recovery was not assessed in the study, the

authors showed a robust axonal regeneration in conduits with aligned fibres, 4 weeks after implantation. Interestingly, their results suggest that the regeneration is supported by astrocyte migration [146]. A preliminary *in vivo* study using collagen nanofibrous scaffold (Figure 7, C) showed limited success after 4 weeks of implantation [165]. The results are believed to be related to the degradation of the conduit and the size of the fibres. Fibres with a mean diameter around 200 µm [165] seem to be less effective guiding axonal growth than micrometer fibres used in other studies [146], although the role of fibre diameter on axonal growth after SCI needs to be investigated in more detail [165].

An alternative scaffold design using electrospun fibres was proposed by Gelain and colleagues [151]. The authors implanted layers of electrospun tubes with 210 µm diameter filled with self-assembling peptides and fixed by a PLGA / PCL electrospun sealing lamina (Figure 7, B) 4 weeks after contusive lesion. To implant the scaffold, the scar tissue and debris were removed and then the resulting cavity was filled. The results showed significant axonal growth inside and between the channels, spanning the lesion. Functional motor recovery was also observed, being statistical significance achieved only 22 weeks after scaffold implantation [151].

Nanofibrous scaffolds have also been applied in SCI research as patches for the delivery of rolipram (Figure 7, D) [152, 226], a small molecule that can enhance cAMP activity in neurons and suppress inflammatory response, favouring nerve regeneration [235]. It has been shown that locomotor function is improved comparing to unloaded patches from the third week on after implantation. To better control the release of the drug and increase drug loading, the electrospun fibres were combined with an alginate hydrogel. However, the use of high drug doses showed to lead to toxic effects and an increased mortality rate [226].

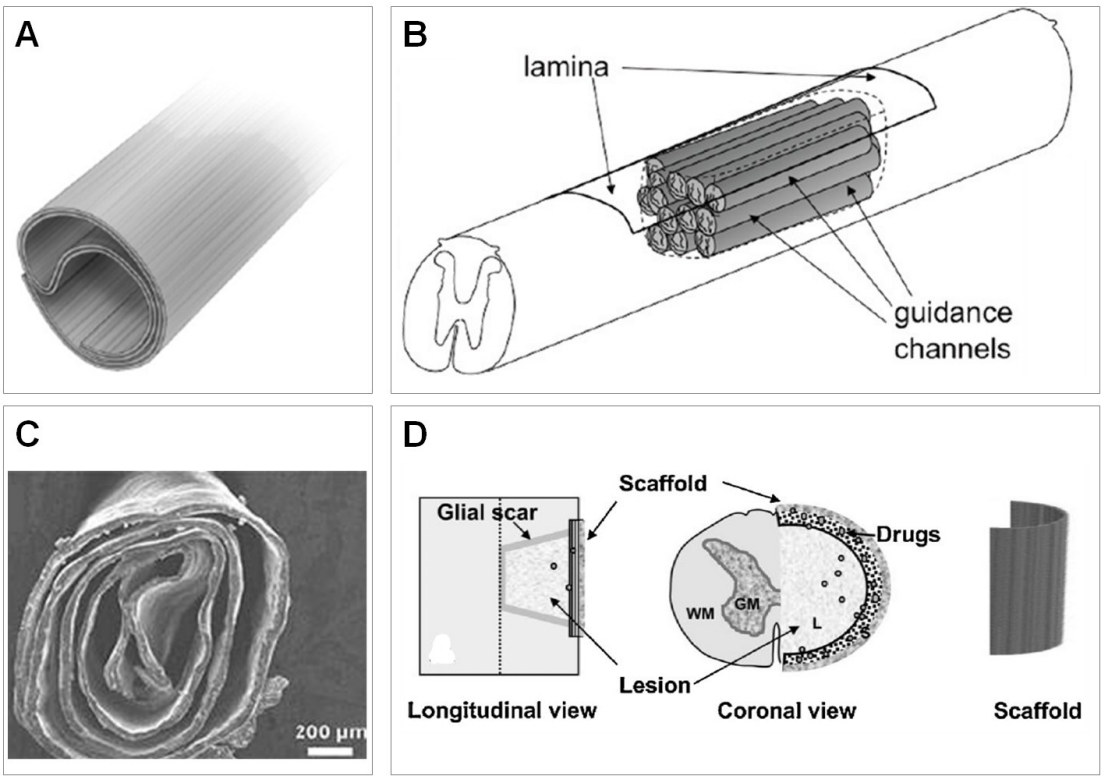

Figure 7. Example of electrospinning-based strategies tested in SCI *in vivo* models. A) Poly(lactide) conduit (adapted from [146], Copyright (2011), with permission from Elsevier). B) Multiple channel electrospun conduit (adapted from [151], Copyright (2011), with permission from American Chemical Society). C) Collagen conduit prepared by [165]. D) Electrospun poly(lactide)/ poly(lactide-co-glycolide) patch for the delivery of rolipram (Adapted from [152], Copyright (2010), with permission from WILEY-VCH Verlag GmbH & Co. KGaA, Weinheim).

4.3. Combinatorial strategies

So far in this review the strategies proposed to treat SCI were presented individually. However, it is currently believed that combinatorial strategies are needed to address such a complex condition [4], and there is an increasing number of reports combining conduits, gels, growth factors and cells, as reviewed in the next paragraphs.

4.3.1. Drug releasing bridges

In SCI research hydrogels based on hyaluronan and methyl cellulose has been extensively explored for the delivery of neurotrophic factors [156, 173] and other bigger proteins (IgG used as model) when encapsulated in PLGA microparticles [156]. The release of these proteins is dependent on their molecular weight and net charge; therefore, different kinetics are achieved for each of the molecules. The release of neurotrophic factors was also explored using a poly(ethylene glycol)-based photopolymerizable hydrogel [236] or fibrin [177], showing functional improvements after a SCI comparing to unloaded hydrogels.

Not only growth factors have been delivered at a spinal cord lesion via release from hydrogels. An agarose hydrogel containing PLGA nanoparticles loaded with methylprednisolone implanted in a contusion model of SCI showed to reduce lesion volume and macrophage infiltration [55]. The localized delivery has been proposed to reduce side effects associated to high amount of the drug administered systemically [55]. Chondroitinase ABC has also been delivered through fibrin hydrogels in a injured spinal cord [176], and alternatively, from electrospun fibres [166]. Indeed, hydrogels are particularly interesting as drug delivery vectors for intrathecal injection after SCI. However, when physical support is also required, other materials have to be applied. PLGA multiple lumen conduits were investigated for the delivery of NGF [205]; and PLA electrospun fibres loaded with 6-aminonicotinamide were studied as mean to limit astrocyte proliferation [147]. Collagen fibres were also prepared for the delivery of NT-3 and chondroitinase ABC [166]. Although these studies still require *in vivo* testing, the incorporation of growth factors cocktails in nerve conduits have already demonstrated to be a valuable strategy to improve functional recovery after SCI [151].

4.3.2. Drug releasing bridges with cells

The delivery of growth factors can also be used to improve the survival of cells implanted at the injury site or to modulate stem cell differentiation/proliferation after injection. Johnson and co-workers used a sub-acute dorsal hemisection SCI model to test the effect of embryonic neural progenitor cell implantation when in a fibrin gel loaded with growth factors (NT-3 and platelet derived growth factor). The authors reported an increased cell survival and differentiation into neural lineages; however, and particularly in growth factor loaded-hydrogels, overproliferation of a subset of the implanted cells occurred and was accompanied with loss of function [178]. More exciting results were recently published after implanting neural progenitor cells embedded in a fibrin matrix containing a cocktail of growth factors (including: brain-derived growth factor, NT-3, platelet-derived growth factor, insulin-like growth factor 1, epidermal growth factor, basic fibroblast growth factor, acidic fibroblast growth factor, glial-cell-line-derived neurotrophic factor, hepatocyte growth factor, and calpain inhibitor). The authors claimed long-distance axonal regeneration without the need of other drugs to ameliorate the inhibitory environment. Additionally, two stem cell lines were tested with similar results, being one already under clinical trials for amyotrophic lateral sclerosis, putting this study a step ahead for testing in clinical trials [188].

An alternative to growth factor entrapment in polymeric scaffolds is the genetic modification of the cells prior implantation, as a mean to convert the cell into a growth factor supplier. The premise is that the implantation of cells expressing growth factors can promote their survival and/or modulate the differentiation into neuronal lineages. Different engineered cells were already implanted *in vivo* including Schwann cells expressing NGF [237], bone marrow cells expressing BDNF [238], fibroblasts expressing GDNF [239], or olfactory ensheathing cells expressing NT-3 [240].

Recently, Gao and co-workers published promising results after implanting mesechymal stem cells expressing BDNF seeded on an agarose injectable gel. The number of axons that can cross the bridge is significantly higher when the cells seeded on the polymeric bridge are expressing the growth factor, as compared to cells expressing GFP, where the number of axons is similar to the implantation of the scaffold without cells [172]. The use of genetically-modified cells still have legal and ethical implications that should be solved [241].

Scaffolds containing genetic material can serve as depots for the *in situ* delivery of genes to cells at a lesion, potentially inducing the expression of a therapeutic protein for longer periods and higher concentrations, as compared to direct protein delivery [242]. In the context of nerve regeneration, PLGA disks loaded with poly(ethylenimine)-DNA nanoparticles containing a plasmid encoding for NGF showed to promote axonal elongation in dorsal root ganglia neurons co-cultured with human embryonic kidney (HEK) 293T cells [243]. Particularly in a SCI scenario, lipid-DNA particles were incorporated in a PLGA channel bridge and a high expression of the reporter gene was detected in the spinal cord during three weeks [134]. However, to achieve functional improvements the implantation of conduits containing more efficient gene delivery vectors (lentivirus encoding NT-3 or BDNF) was needed [244]. Alternatively, the use of nanoparticles for the delivery of small interference RNA (siRNA) incorporated in fibres was also proposed [245, 246], but these strategies still need to prove their efficiency *in vivo*.

5. References

1. Schwab JM, Brechtel K, Mueller CA, Failli V, Kaps HP, Tuli SK, and Schluesener HJ (2006). "Experimental strategies to promote spinal cord regeneration - An integrative perspective". *Progress in Neurobiology*, 78 (2): 91-116.

2. Ramer LM, Ramer MS, and Steeves JD (2005). "Setting the stage for functional repair of spinal cord injuries: A cast of thousands". *Spinal Cord*, 43 (3): 134-161.

3. Rowland JW, Hawryluk GW, Kwon B, and Fehlings MG (2008). "Current status of acute spinal cord injury pathophysiology and emerging therapies: promise on the horizon". *Neurosurgical focus*, 25 (5): E2.

4. McCreedy DA and Sakiyama-Elbert SE (2012). "Combination therapies in the CNS: Engineering the environment". *Neuroscience Letters*, 519 (2): 115-121.

5. Yiu G and He Z (2006). "Glial inhibition of CNS axon regeneration". *Nature Reviews Neuroscience*, 7 (8): 617-627.

6. David S and Aguayo AJ (1981). "Axonal elongation into peripheral nervous system 'bridges' after central nervous system injury in adult rats". *Science*, 214 (4523): 931-933.

7. Richardson PM, Issa VMK, and Aguayo AJ (1984). "Regeneration of long spinal axons in the rat". *Journal of Neurocytology*, 13 (1): 165-182.

8. Bareyre FM, Kerschensteiner M, Raineteau O, Mettenleiter TC, Weinmann O, and Schwab ME (2004). "The injured spinal cord spontaneously forms a new intraspinal circuit in adult rats". *Nature Neuroscience*, 7 (3): 269-277.

9. Fitch MT and Silver J (2008). "CNS injury, glial scars, and inflammation: Inhibitory extracellular matrices and regeneration failure". *Experimental Neurology*, 209 (2): 294-301.

10. Woerly S (2000). "Restorative surgery of the central nervous system by means of tissue engineering using Neurogen implants". *Neurosurgical Review*, 23 (2): 59-77.

11. He J, Wang XM, Spector M, and Cui FZ (2012). "Scaffolds for central nervous system tissue engineering". *Frontiers of Materials Science*, 6 (1): 1-25.

12. Donnelly DJ and Popovich PG (2008). "Inflammation and its role in neuroprotection, axonal regeneration and functional recovery after spinal cord injury". *Experimental Neurology*, 209 (2): 378-388.

13. Schnell L (1999). "Acute inflammatory responses to mechanical lesions in the CNS: Differences between brain and spinal cord". *European Journal of Neuroscience*, 11 (10): 3648-3658.

14. Sullivan PG, Krishnamurthy S, Patel SP, Pandya JD, and Rabchevsky AG (2007). "Temporal characterization of mitochondrial bioenergetics after spinal cord injury". *Journal of Neurotrauma*, 24 (6): 991-999.

15. Fawcett JW and Asher RA (1999). "The glial scar and central nervous system repair". *Brain Research Bulletin*, 49 (6): 377-391.

16. Kreutzberg GW (1996). "Microglia: A sensor for pathological events in the CNS". *Trends in Neurosciences*, 19 (8): 312-318.

17. Hausmann ON (2003). "Post-traumatic inflammation following spinal cord injury". *Spinal Cord*, 41 (7): 369-378.

18. Taoka Y, Okajima K, Murakami K, Johno M, and Naruo M (1998). "Role of neutrophil elastase in compression-induced spinal cord injury in rats". *Brain Research*, 799 (2): 264-269.

19. Schwartz M, Moalem G, Leibowitz-Amit R, and Cohen IR (1999). "Innate and adaptive immune responses can be beneficial for CNS repair". *Trends in Neurosciences*, 22 (7): 295-299.

20. Segal JL, Gonzalez E, Yousefi S, Jamshidipour L, and Brunnemann SR (1997). "Circulating levels of IL-2R, ICAM-1, and IL-6 in spinal cord injuries". *Archives of Physical Medicine and Rehabilitation*, 78 (1): 44-47.

21. Ridet JL, Malhotra SK, Privat A, and Gage FH (1997). "Reactive astrocytes: Cellular and molecular cues to biological function". *Trends in Neurosciences*, 20 (12): 570-577.

22. Tang X, Davies JE, and Davies SJA (2003). "Changes in distribution, cell associations, and protein expression levels of NG2, neurocan, phosphacan, brevican, versican v2, and tenascin-C during acute to chronic maturation of spinal cord scar tissue". *Journal of Neuroscience Research*, 71 (3): 427-444.

23. Jeroen Pasterkamp R, Anderson PN, and Verhaagen J (2001). "Peripheral nerve injury fails to induce growth of lesioned ascending dorsal column axons into spinal cord scar tissue expressing the axon repellent Semaphorin3A". *European Journal of Neuroscience*, 13 (3): 457-471.

24. Bundesen LQ, Scheel TA, Bregman BS, and Kromer LF (2003). "Ephrin-B2 and EphB2 regulation of astrocyte-meningeal fibroblast interactions in response to spinal cord lesions in adult rats". *Journal of Neuroscience*, 23 (21): 7789-7800.

25. McKeon RJ, Schreiber RC, Rudge JS, and Silver J (1991). "Reduction of neurite outgrowth in a model of glial scarring following CNS injury is correlated with the expression of inhibitory molecules on reactive astrocytes". *Journal of Neuroscience*, 11 (11): 3398-3411.

26. Silver J and Miller JH (2004). "Regeneration beyond the glial scar". *Nature Reviews Neuroscience*, 5 (2): 146-156.

27. Oohira A, Matsui F, Tokita Y, Yamauchi S, and Aono S (2000). "Molecular interactions of neural chondroitin sulfate proteoglycans in the brain development". *Archives of Biochemistry and Biophysics*, 374 (1): 24-34.

28. Bovolenta P and Fernaud-Espinosa I (2000). "Nervous system proteoglycans as modulators of neurite outgrowth". *Progress in Neurobiology*, 61 (2): 113-132.

29. Tan CL, Kwok JCF, Patani R, Ffrench-Constant C, Chandran S, and Fawcett JW (2011). "Integrin activation promotes axon growth on inhibitory chondroitin sulfate proteoglycans by enhancing integrin signaling". *Journal of Neuroscience*, 31 (17): 6289-6295.

30. Koprivica V, Cho KS, Park JB, Yiu G, Atwal J, Gore B, Kim JA, Lin E, Tessier-Lavigne M, Chen DF, and He Z (2005). "Neuroscience: EGFR activation mediates inhibition of axon regeneration by myelin and chondroitin sulfate proteoglycans". *Science*, 310 (5745): 106-110.

31. Monnier PP, Sierra A, Schwab JM, Henke-Fahle S, and Mueller BK (2003). "The Rho/ROCK pathway mediates neurite growth-inhibitory activity associated with the chondroitin sulfate proteoglycans of the CNS glial scar". *Molecular and Cellular Neuroscience*, 22 (3): 319-330.

32. Filbin MT (2003). "Myelin-associated inhibitors of axonal regeneration in the adult mammalian CNS". *Nature Reviews Neuroscience*, 4 (9): 703-713.

33. Dubreuil CI, Winton MJ, and McKerracher L (2003). "Rho activation patterns after spinal cord injury and the role of activated Rho in apoptosis in the central nervous system". *Journal of Cell Biology*, 162 (2): 233-243.

34. Schwab ME and Caroni P (1988). "Oligodendrocytes and CNS myelin are nonpermissive substrates for neurite growth and fibroblast spreading *in vitro*". *Journal of Neuroscience*, 8 (7): 2381-2393.

35. Schmidt CE and Leach JB (2003). "Neural tissue engineering: Strategies for repair and regeneration". *Annual Review of Biomedical Engineering*, 5: 293-347.

36. Caroni P and Schwab ME (1988). "Antibody against myelin associated inhibitor of neurite growth neutralizes nonpermissive substrate properties of CNS white matter". *Neuron*, 1 (1): 85-96.

37. Schwab ME (2004). "Nogo and axon regeneration". *Current Opinion in Neurobiology*, 14 (1): 118-124.

38. Murphy KJ, Miller AM, Thelma R, Cowley F, Fionnuala Cox F, and Lynch MA (2011). "The age- and amyloid-β-related increases in Nogo B contribute to microglial activation". *Neurochemistry International*, 58 (2): 161-168.

39. Liu BP, Fournier A, GrandPra T, and Strittmatter SM (2002). "Myelin-associated glycoprotein as a functional ligand for the Nogo-66 receptor". *Science*, 297 (5584): 1190-1193.

40. Niederast B, Oertle T, Fritsche J, McKinney RA, and Bandtlow CE (2002). "Nogo-A and myelin-associated glycoprotein mediate neurite growth inhibition by antagonistic regulation of RhoA and Rac1". *Journal of Neuroscience*, 22 (23): 10368-10376.

41. Borrie SC, Baeumer BE, and Bandtlow CE (2012). "The Nogo-66 receptor family in the intact and diseased CNS". *Cell and Tissue Research*, 349 (1): 105-117.

42. Huber AB, Kolodkin AL, Ginty DD, and Cloutier JF, *Signaling at the growth cone: Ligand-receptor complexes and the control of axon growth and guidance*, in *Annual Review of Neuroscience*. 2003, Palo Alto, Calif., Annual Reviews, inc. p. 509-563.

43. Wang KC, Kim JA, Sivasankaran R, Segal R, and He Z (2002). "p75 interacts with the Nogo receptor as a co-receptor for Nogo, MAG and OMgp". *Nature*, 420 (6911): 74-78.

44. Nobes CD and Hall A (1995). "Rho, Rac, and Cdc42 GTPases regulate the assembly of multimolecular focal complexes associated with actin stress fibers, lamellipodia, and filopodia". *Cell*, 81 (1): 53-62.

45. Dergham P, Ellezam B, Essagian C, Avedissian H, Lubell WD, and McKerracher L (2002). "Rho signaling pathway targeted to promote spinal cord repair". *Journal of Neuroscience*, 22 (15): 6570-6577.

46. Benson MD, Romero MI, Lush ME, Lu QR, Henkemeyer M, and Parada LF (2005). "Ephrin-B3 is a myelin-based inhibitor of neurite outgrowth". *Proceedings of the National Academy of Sciences of the United States of America*, 102 (30): 10694-10699.

47. Moreau-Fauvarque C, Kumanogoh A, Camand E, Jaillard C, Barbin G, Boquet I, Love C, Jones EY, Kikutani H, Lubetzki C, Dusart I, and Chédotal A (2003). "The transmembrane semaphorin Sema4D/CD100, an inhibitor of axonal growth, is expressed on oligodendrocytes and upregulated after CNS lesion". *Journal of Neuroscience*, 23 (27): 9229-9239.

48. Barnes PJ (1998). "Anti-inflammatory actions of glucocorticoids: Molecular mechanisms". *Clinical Science*, 94 (6): 557-572.

49. Bracken MB, Shepard MJ, Collins WF, Holford TR, Young W, Baskin DS, Eisenberg HM, Flamm E, Leo-Summers L, Maroon J, Marshall LF, Perot Jr PL, Piepmeier J, Sonntag VKH, Wagner FC, Wilberger JE, and Winn HR (1990). "A randomized, controlled trial of methylprednisolone or naloxone in the treatment of acute spinal-cord injury. Results of the Second National Acute Spinal Cord Injury Study". *New England Journal of Medicine*, 322 (20): 1405-1411.

50. Short DJ, El Masry WS, and Jones PW (2000). "High dose methylprednisolone in the management of acute spinal cord injury - A systematic review from a clinical perspective". *Spinal Cord*, 38 (5): 273-286.

51. Sipski ML and Pearse DD (2006). "Methylprednisolone and other confounders to spinal cord injury clinical trials". *Nature Clinical Practice Neurology*, 2 (8): 402-403.

52. Kwon BK, Tetzlaff W, Grauer JN, Beiner J, and Vaccaro AR (2004). "Pathophysiology and pharmacologic treatment of acute spinal cord injury". *The Spine Journal*, 4 (4): 451-464.

53. (2004). "Effect of intravenous corticosteroids on death within 14 days in 10 008 adults with clinically significant head injury (MRC CRASH trial): Randomised placebo-controlled trial". *Lancet*, 364 (9442): 1321-1328.

54. Kim Yt, Caldwell JM, and Bellamkonda RV (2009). "Nanoparticle-mediated local delivery of methylprednisolone after spinal cord injury". *Biomaterials*, 30 (13): 2582-2590.

55. Chvatal SA, Kim YT, Bratt-Leal AM, Lee H, and Bellamkonda RV (2008). "Spatial distribution and acute anti-inflammatory effects of Methylprednisolone after sustained local delivery to the contused spinal cord". *Biomaterials*, 29 (12): 1967-1975.

56. Lee JM, Yan P, Xiao Q, Chen S, Lee KY, Hsu CY, and Xu J (2008). "Methylprednisolone protects oligodendrocytes but not neurons after spinal cord injury". *Journal of Neuroscience*, 28 (12): 3141-3149.

57. Schrater A, Lustenberger RM, Obermair FJ, and Thallmair M (2009). "High-dose corticosteroids after spinal cord injury reduce neural progenitor cell proliferation". *Neuroscience*, 161 (3): 753-763.

58. Schiller MD and Mobbs RJ (2012). "The historical evolution of the management of spinal cord injury". *Journal of Clinical Neuroscience*, 19 (10): 1348-1353.

59. *Clinical Trials.gov*. cited 2014; Available from: http://www.clinicaltrials.gov/.

60. Ghezzi P and Brines M (2004). "Erythropoietin as an antiapoptotic, tissue-protective cytokine". *Cell Death and Differentiation*, 11 (SUPPL. 1).

61. Rabchevsky AG, Patel SP, and Springer JE (2011). "Pharmacological interventions for spinal cord injury: Where do we stand? How might we step forward?". *Pharmacology and Therapeutics*, 132 (1): 15-29.

62. Leist M, Gliezzi P, Grasso G, Bianchi R, Vilia P, Fratelli M, Savino C, Bianchi M, Nielsen J, Gerwien J, Kallunki P, Kirstine Larsen A, Helboe L, Christensen S, Pedersen LO, Nielsen M, Torup L, Sager T, Sfacteria A, Erbayraktar S, Erbayraktar Z, Gokmen N, Yilmaz O, Cerami-Hand C, Xie QW, Coleman T, Cerami A, and Brines M (2004). "Derivatives of erythropoitein that are tissue protective but not erythropoietic". *Science*, 305 (5681): 239-242.

63. Matis GK and Birbilis TA (2009). "Erythropoietin in spinal cord injury". *European Spine Journal*, 18 (3): 314-323.

64. Lee SM, Yune TY, Kim SJ, Park DW, Lee YK, Kim YC, Oh YJ, Markelonis GJ, and Oh TH (2003). "Minocycline Reduces Cell Death and Improves Functional Recovery after Traumatic Spinal Cord Injury in the Rat". *Journal of Neurotrauma*, 20 (10): 1017-1027.

65. Stirling DP, Khodarahmi K, Liu J, McPhail LT, McBride CB, Steeves JD, Ramer MS, and Tetzlaff W (2004). "Minocycline Treatment Reduces Delayed Oligodendrocyte Death, Attenuates Axonal Dieback, and Improves Functional Outcome after Spinal Cord Injury". *Journal of Neuroscience*, 24 (9): 2182-2190.

66. Casha S, Zygun D, McGowan MD, Bains I, Yong VW, and Hurlbert RJ (2012). "Results of a phase II placebo-controlled randomized trial of minocycline in acute spinal cord injury". *Brain*, 135 (4): 1224-1236.

67. Ates O, Cayli SR, Gurses I, Turkoz Y, Tarim O, Cakir CO, and Kocak A (2007). "Comparative neuroprotective effect of sodium channel blockers after experimental spinal cord injury". *Journal of Clinical Neuroscience*, 14 (7): 658-665.

68. Markus A, Patel TD, and Snider WD (2002). "Neurotrophic factors and axonal growth". *Current Opinion in Neurobiology*, 12 (5): 523-531.

69. Oudega M and Hagg T (1996). "Nerve growth factor promotes regeneration of sensory axons into adult rat spinal cord". *Experimental Neurology*, 140 (2): 218-229.

70. Bradbury EJ, Khemani S, King VR, Priestley JV, and McMahon SB (1999). "NT-3 promotes growth of lesioned adult rat sensory axons ascending in the dorsal columns of the spinal cord". *European Journal of Neuroscience*, 11 (11): 3873-3883.

71. Sharma HS, *Neuroprotective effects of neurotrophins and melanocortins in spinal cord injury: An experimental study in the rat using pharmacological and morphological approaches*, in *Annals of the New York Academy of Sciences*. 2005, New York, The Academy. p. 407-421.

72. Apfel SC, *Nerve growth factor for the treatment of diabetic neuropathy: What went wrong, what went right, and what does the future hold?*, in *International review of neurobiology*. 2002, New York Ny : Academic Press. p. 393-413.

73. Rossignol S, Schwab M, Schwartz M, and Fehlings MG (2007). "Spinal cord injury: Time to move?". *Journal of Neuroscience*, 27 (44): 11782-11792.

74. Popovich PG and Longbrake EE (2008). "Can the immune system be harnessed to repair the CNS?". *Nature Reviews Neuroscience*, 9 (6): 481-493.

75. Brewer KL, Bethea JR, and Yezierski RP (1999). "Neuroprotective effects of interleukin-10 following excitotoxic spinal cord injury". *Experimental Neurology*, 159 (2): 484-493.

76. Vidal PM, Lemmens E, Dooley D, and Hendrix S (2013). "The role of " anti-inflammatory" cytokines in axon regeneration". *Cytokine and Growth Factor Reviews*, 24 (1): 1-12.

77. Popovich PG, Guan Z, Wei P, Huitinga I, Van Rooijen N, and Stokes BT (1999). "Depletion of hematogenous macrophages promotes partial hindlimb recovery and neuroanatomical repair after experimental spinal cord injury". *Experimental Neurology*, 158 (2): 351-365.

78. Schwartz M, London A, and Shechter R (2009). "Boosting T-cell immunity as a therapeutic approach for neurodegenerative conditions: The role of innate immunity". *Neuroscience*, 158 (3): 1133-1142.

79. Rapalino O, Lazarov-Spiegler O, Agranov E, Velan GJ, Yoles E, Fraidakis M, Solomon A, Gepstein R, Katz A, Belkin M, Hadani M, and Schwartz M (1998). "Implantation of stimulated homologous macrophages results in partial recovery of paraplegic rats". *Nature Medicine*, 4 (7): 814-821.

80. Mantovani A, Sica A, Sozzani S, Allavena P, Vecchi A, and Locati M (2004). "The chemokine system in diverse forms of macrophage activation and polarization". *Trends in Immunology*, 25 (12): 677-686.

81. Mosser DM and Edwards JP (2008). "Exploring the full spectrum of macrophage activation". *Nature Reviews Immunology*, 8 (12): 958-969.

82. Lammertse DP, Jones LAT, Charlifue SB, Kirshblum SC, Apple DF, Ragnarsson KT, Falci SP, Heary RF, Choudhri TF, Jenkins AL, Betz RR, Poonian D, Cuthbert JP, Jha A, Snyder DA, and Knoller N (2012). "Autologous incubated macrophage therapy in acute, complete spinal cord injury: Results of the phase 2 randomized controlled multicenter trial". *Spinal Cord*, 50 (9): 661-671.

83. Hauben E, Butovsky O, Nevo U, Yoles E, Moalem G, Agranov E, Mor F, Leibowitz-Amit R, Pevsner E, Akselrod S, Neeman M, Cohen IR, and Schwartz M (2000). "Passive or active immunization with myelin basic protein promotes recovery from spinal cord contusion". *Journal of Neuroscience*, 20 (17): 6421-6430.

84. Ziv Y, Avidan H, Pluchino S, Martino G, and Schwartz M (2006). "Synergy between immune cells and adult neural stem/progenitor cells promotes functional recovery from spinal cord injury". *Proceedings of the National Academy of Sciences of the United States of America*, 103 (35): 13174-13179.

85. Bradbury EJ, Moon LDF, Popat RJ, King VR, Bennett GS, Patel PN, Fawcett JW, and McMahon SB (2002). "Chondroitinase ABC promotes functional recovery after spinal cord injury". *Nature*, 416 (6881): 636-640.

86. Garcia-Alias G, Lin R, Akrimi SF, Story D, Bradbury EJ, and Fawcett JW (2008). "Therapeutic time window for the application of chondroitinase ABC after spinal cord injury". *Experimental Neurology*, 210 (2): 331-338.

87. Crespo D, Asher RA, Lin R, Rhodes KE, and Fawcett JW (2007). "How does chondroitinase promote functional recovery in the damaged CNS?". *Experimental Neurology*, 206 (2): 159-171.

88. Lemons ML, Sandy JD, Anderson DK, and Howland DR (2003). "Intact aggrecan and chondroitin sulfate-depleted aggrecan core glycoprotein inhibit axon growth in the adult rat spinal cord". *Experimental Neurology*, 184 (2): 981-990.

89. Zhao RR, Muir EM, Alves JN, Rickman H, Allan AY, Kwok JC, Roet KCD, Verhaagen J, Schneider BL, Bensadoun JC, Ahmed SG, Yáñez-Muñoz RJ, Keynes RJ, Fawcett JW, and Rogers JH (2011). "Lentiviral vectors express chondroitinase ABC in cortical projections and promote sprouting of injured corticospinal axons". *Journal of Neuroscience Methods*, 201 (1): 228-238.

90. Massey JM, Hubscher CH, Wagoner MR, Decker JA, Amps J, Silver J, and Onifer SM (2006). "Chondroitinase ABC digestion of the perineuronal net promotes functional collateral sprouting in the cuneate nucleus after cervical spinal cord injury". *Journal of Neuroscience*, 26 (16): 4406-4414.

91. Schnell L and Schwab ME (1990). "Axonal regeneration in the rat spinal cord produced by an antibody against myelin-associated neurite growth inhibitors". *Nature*, 343 (6255): 269-272.

92. Gonzenbach RR and Schwab ME (2008). "Disinhibition of neurite growth to repair the injured adult CNS: Focusing on Nogo". *Cellular and Molecular Life Sciences*, 65 (1): 161-176.

93. Gonzenbach RR, Zoerner B, Schnell L, Weinmann O, Mir AK, and Schwab ME (2012). "Delayed anti-Nogo-A antibody application after spinal cord injury shows progressive loss of responsiveness". *Journal of Neurotrauma*, 29 (3): 567-578.

94. Li S and Strittmatter SM (2003). "Delayed systemic Nogo-66 receptor antagonist promotes recovery from spinal cord injury". *Journal of Neuroscience*, 23 (10): 4219-4227.

95. Steward O, Sharp K, Yee KM, and Hofstadter M (2008). "A re-assessment of the effects of a Nogo-66 receptor antagonist on regenerative growth of axons and locomotor recovery after spinal cord injury in mice". *Experimental Neurology*, 209 (2): 446-468.

96. Lehmann M, Fournier A, Selles-Navarro I, Dergham P, Sebok A, Leclerc N, Tigyi G, and McKerracher L (1999). "Inactivation of rho signaling pathway promotes CNS axon regeneration". *Journal of Neuroscience*, 19 (17): 7537-7547.

97. McKerracher L and Higuchi H (2006). "Targeting Rho to stimulate repair after spinal cord injury". *Journal of Neurotrauma*, 23 (3-4): 309-317.

98. Fehlings MG, Theodore N, Harrop J, Maurais G, Kuntz C, Shaffrey CI, Kwon BK, Chapman J, Yee A, Tighe A, and McKerracher L (2011). "A phase I/IIa clinical trial of a recombinant Rho protein antagonist in acute spinal cord injury". *Journal of Neurotrauma*, 28 (5): 787-796.

99. Mitchell JA, Akarasereenont P, Thiemermann C, Flower RJ, and Vane JR (1993). "Selectivity of nonsteroidal antiinflammatory drugs as inhibitors of constitutive and inducible cyclooxygenase". *Proceedings of the National Academy of Sciences of the United States of America*, 90 (24): 11693-11697.

100. Rainsford KD (2009). "Ibuprofen: pharmacology, efficacy and safety". *Inflammopharmacology*, 17 (6): 275-342.

101. Fu Q, Hue J, and Li S (2007). "Nonsteroidal anti-inflammatory drugs promote axon regeneration via RhoA inhibition". *Journal of Neuroscience*, 27 (15): 4154-4164.

102. Wang X, Budel S, Baughman K, Gould G, Song KH, and Strittmatter SM (2009). "Ibuprofen enhances recovery from spinal cord injury by limiting tissue loss and stimulating axonal growth". *Journal of Neurotrauma*, 26 (1): 81-95.

103. Madura T, Tomita K, and Terenghi G (2011). "Ibuprofen improves functional outcome after axotomy and immediate repair in the peripheral nervous system". *Journal of Plastic, Reconstructive and Aesthetic Surgery*, 64 (12): 1641-1646.

104. Xing B, Li H, Wang H, Mukhopadhyay D, Fisher D, Gilpin CJ, and Li S (2011). "RhoA-inhibiting NSAIDs promote axonal myelination after spinal cord injury". *Experimental Neurology*, 231 (2): 247-260.

105. Dill J, Patel AR, Yang XL, Bachoo R, Powell CM, and Li S (2010). "A molecular mechanism for ibuprofen-mediated RhoA inhibition in neurons". *Journal of Neuroscience*, 30 (3): 963-972.

106. Sharp KG, Yee KM, Stiles TL, Aguilar RM, and Steward O (2013). "A re-assessment of the effects of treatment with a non-steroidal anti-inflammatory (ibuprofen) on promoting axon regeneration via RhoA inhibition after spinal cord injury". *Experimental Neurology*, 248: 321-327.

107. Kopp MA, Liebscher T, Niedeggen A, Laufer S, Brommer B, Jungehulsing GJ, Strittmatter SM, Dirnagl U, and Schwab JM (2012). "Small-molecule-induced Rho-inhibition: NSAIDs after spinal cord injury". *Cell and Tissue Research*, 349 (1): 119-132.

108. Zhao P, Waxman SG, and Hains BC (2007). "Extracellular signal-regulated kinase-regulated microglia-neuron signaling by prostaglandin E_2 contributes to pain after spinal cord injury". *Journal of Neuroscience*, 27 (9): 2357-2368.

109. Ma W, St-Jacques B, and Cruz Duarte P (2012). "Targeting pain mediators induced by injured nerve-derived COX_2 and PGE_2 to treat neuropathic pain". *Expert Opinion on Therapeutic Targets*, 16 (6): 527-540.

110. Redondo-Castro E and Navarro X (2014). "Chronic ibuprofen administration reduces neuropathic pain but does not exert neuroprotection after spinal cord injury in adult rats". *Experimental Neurology*, 252: 95-103.

111. Pêgo AP, Kubinova S, Cizkova D, Vanicky I, Mar FM, Sousa MM, and Sykova E (2012). "Regenerative medicine for the treatment of spinal cord injury: More than just promises?". *Journal of Cellular and Molecular Medicine*, 16 (11): 2564-2582.

112. Ruff CA, Wilcox JT, and Fehlings MG (2012). "Cell-based transplantation strategies to promote plasticity following spinal cord injury". *Experimental Neurology*, 235 (1): 78-90.

113. Thuret S, Moon LDF, and Gage FH (2006). "Therapeutic interventions after spinal cord injury". *Nature Reviews Neuroscience*, 7 (8): 628-643.

114. Tetzlaff W, Okon EB, Karimi-Abdolrezaee S, Hill CE, Sparling JS, Plemel JR, Plunet WT, Tsai EC, Baptiste D, Smithson LJ, Kawaja MD, Fehlings MG, and Kwon BK (2011). "A systematic review of cellular transplantation therapies for spinal cord injury". *Journal of Neurotrauma*, 28 (8): 1611-1682.

115. McDonald JW, Liu XZ, Qu Y, Liu S, Mickey SK, Turetsky D, Gottlieb DI, and Choi DW (1999). "Transplanted embryonic stem cells survive, differentiate and promote recovery in injured rat spinal cord". *Nature Medicine*, 5 (12): 1410-1412.

116. Hill CE, Moon LDF, Wood PM, and Bunge MB (2006). "Labeled Schwann cell transplantation: Cell loss, host Schwann cell replacement, and strategies to enhance survival". *Glia*, 53 (3): 338-343.

117. Amemori T, Jendelová P, Růžičková K, Arboleda D, and Syková E (2010). "Co-transplantation of olfactory ensheathing glia and mesenchymal stromal cells does not have synergistic effects after spinal cord injury in the rat". *Cytotherapy*, 12 (2): 212-225.

118. Lima C, Escada P, Pratas-Vital J, Branco C, Arcangeli CA, Lazzeri G, Maia CA, Capucho C, Hasse-Ferreira A, and Peduzzi JD (2010). "Olfactory mucosal autografts and rehabilitation for chronic traumatic spinal cord injury". *Neurorehabilitation and neural repair*, 24 (1): 10-22.

119. Huang H, Xi H, Chen L, Zhang F, and Liu Y (2012). "Long-term outcome of olfactory ensheathing cell therapy for patients with complete chronic spinal cord injury". *Cell Transplantation*, 21 (SUPPL. 1): S23-S31.

120. Steward O, Sharp K, Selvan G, Hadden A, Hofstadter M, Au E, and Roskams J (2006). "A re-assessment of the consequences of delayed transplantation of olfactory lamina propria following complete spinal cord transection in rats". *Experimental Neurology*, 198 (2): 483-499.

121. Fouad K and Tetzlaff W (2012). "Rehabilitative training and plasticity following spinal cord injury". *Experimental Neurology*, 235 (1): 91-99.

122. Knikou M (2012). "Plasticity of corticospinal neural control after locomotor training in human spinal cord injury". *Neural Plasticity*, 2012.

123. Wilcox JT, Cadotte D, and Fehlings MG (2012). "Spinal cord clinical trials and the role for bioengineering". *Neuroscience Letters*, 519 (2): 93-102.

124. Daly W, Yao L, Zeugolis D, Windebank A, and Pandit A (2012). "A biomaterials approach to peripheral nerve regeneration: Bridging the peripheral nerve gap and enhancing functional recovery". *Journal of the Royal Society Interface*, 9 (67): 202-221.

125. de Ruiter GC, Malessy MJ, Yaszemski MJ, Windebank AJ, and Spinner RJ (2009). "Designing ideal conduits for peripheral nerve repair". *Neurosurgical focus*, 26 (2): E5.

126. Ciardelli G and Chiono V (2006). "Materials for peripheral nerve regeneration". *Macromolecular Bioscience*, 6 (1): 13-26.

127. Chau CH, Shum DK, Li H, Pei J, Lui YY, Wirthlin L, Chan YS, and Xu XM (2004). "Chondroitinase ABC enhances axonal regrowth through Schwann cell-seeded guidance channels after spinal cord injury". *The FASEB journal* 18 (1): 194-196.

128. Giannetti S, Lauretti L, Fernandez E, Salvinelli F, Tamburrini G, and Pallini R (2001). "Acrylic hydrogel implants after spinal cord lesion in the adult rat". *Neurological Research*, 23 (4): 405-409.

129. Tsai EC, Dalton PD, Shoichet MS, and Tator CH (2004). "Synthetic hydrogel guidance channels facilitate regeneration of adult rat brainstem motor axons after complete spinal cord transection". *Journal of Neurotrauma*, 21 (6): 789-804.

130. Straley KS, Foo CWP, and Heilshorn SC (2010). "Biomaterial design strategies for the treatment of spinal cord injuries". *Journal of Neurotrauma*, 27 (1): 1-19.

131. Hattori T, Matsuyama Y, Sakai Y, Ishiguro N, Hirata H, and Nakamura R (2008). "Chondrotinase ABC enhances axonal regeneration across nerve gaps". *Journal of Clinical Neuroscience*, 15 (2): 185-191.

132. Friedman JA, Windebank AJ, Moore MJ, Spinner RJ, Currier BL, Yaszemski MJ, Bartolomei J, Piepmeier JM, Chu G, Fehlings MG, Hodge Jr CJ, and Wagner Jr FC (2002). "Biodegradable polymer grafts for surgical repair of the injured spinal cord". *Neurosurgery*, 51 (3): 742-752.

133. Corey JM, Lin DY, Mycek KB, Chen Q, Samuel S, Feldman EL, and Martin DC (2007). "Aligned electrospun nanofibers specify the direction of dorsal root ganglia neurite growth". *Journal of Biomedical Materials Research - Part A*, 83 (3): 636-645.

134. De Laporte L, Lei Yan A, and Shea LD (2009). "Local gene delivery from ECM-coated poly(lactide-co-glycolide) multiple channel bridges after spinal cord injury". *Biomaterials*, 30 (12): 2361-2368.

135. Koh HS, Yong T, Chan CK, and Ramakrishna S (2008). "Enhancement of neurite outgrowth using nano-structured scaffolds coupled with laminin". *Biomaterials*, 29 (26): 3574-3582.

136. Yucel D, Kose GT, and Hasirci V (2010). "Polyester based nerve guidance conduit design". *Biomaterials*, 31 (7): 1596-1603.

137. Nisbet DR, Rodda AE, Horne MK, Forsythe JS, and Finkelstein DI (2009). "Neurite infiltration and cellular response to electrospun polycaprolactone scaffolds implanted into the brain". *Biomaterials*, 30 (27): 4573-4580.

138. Pêgo AP, Poot AA, Grijpma DW, and Feijen J (2001). "Copolymers of trimethylene carbonate and epsilon-caprolactone for porous nerve guides: Synthesis and properties". *Journal of Biomaterials Science, Polymer Edition*, 12 (1): 35-53.

139. Pêgo AP, Poot AA, Grijpma DW, and Feijen J (2003). "Biodegradable elastomeric scaffolds for soft tissue engineering". *Journal of Controlled Release*, 87 (1-3): 69-79.

140. Chew SY, Mi R, Hoke A, and Leong KW (2007). "Aligned protein-polymer composite fibers enhance nerve regeneration: A potential tissue-engineering platform". *Advanced Functional Materials*, 17 (8): 1288-1296.

141. Vleggeert-Lankamp CLAM, Wolfs J, Pêgo AP, Van Den Berg R, Feirabend H, and Lakke E (2008). "Effect of nerve graft porosity on the refractory period of regenerating nerve fibers: Laboratory investigation". *Journal of Neurosurgery*, 109 (2): 294-305.

142. de Luca AC, Stevens JS, Schroeder SLM, Guilbaud JB, Saiani A, Downes S, and Terenghi G (2013). "Immobilization of cell-binding peptides on poly-ε-caprolactone film surface to biomimic the peripheral nervous system". *Journal of Biomedical Materials Research - Part A*, 101 (2): 491-501.

143. Tysseling-Mattiace VM, Sahni V, Niece KL, Birch D, Czeisler C, Fehlings MG, Stupp SI, and Kessler JA (2008). "Self-assembling nanofibers inhibit glial scar formation and promote axon elongation after spinal cord injury". *Journal of Neuroscience*, 28 (14): 3814-3823.

144. Matsumoto K, Ohnishi K, Kiyotani T, Sekine T, Ueda H, Nakamura T, Endo K, and Shimizu Y (2000). "Peripheral nerve regeneration across an 80-mm gap bridged by a polyglycolic acid (PGA)-collagen tube filled with laminin-coated collagen fibers: A histological and electrophysiological evaluation of regenerated nerves". *Brain Research*, 868 (2): 315-328.

145. Oudega M, Gautier SE, Chapon P, Fragoso M, Bates ML, Parel JM, and Bartlett Bunge M (2001). "Axonal regeneration into Schwann cell grafts within resorbable poly(α-hydroxyacid) guidance channels in the adult rat spinal cord". *Biomaterials*, 22 (10): 1125-1136.

146. Hurtado A, Cregg JM, Wang HB, Wendell DF, Oudega M, Gilbert RJ, and McDonald JW (2011). "Robust CNS regeneration after complete spinal cord transection using aligned poly-l-lactic acid microfibers". *Biomaterials*, 32 (26): 6068-6079.

147. Schaub NJ and Gilbert RJ (2011). "Controlled release of 6-aminonicotinamide from aligned, electrospun fibers alters astrocyte metabolism and dorsal root ganglia neurite outgrowth". *Journal of Neural Engineering*, 8 (4): 046026.

148. Yang Y, De Laporte L, Zelivyanskaya ML, Whittlesey KJ, Anderson AJ, Cummings BJ, and Shea LD (2009). "Multiple Channel Bridges for Spinal Cord Injury: Cellular Characterization of Host Response". *Tissue Engineering Part A*, 15 (11): 3283-3295.

149. De Laporte L, Yang Y, Zelivyanskaya ML, Cummings BJ, Anderson AJ, and Shea LD (2009). "Plasmid releasing multiple channel bridges for transgene expression after spinal cord injury". *Molecular Therapy*, 17 (2): 318-326.

150. Chen BK, Knight AM, Madigan NN, Gross L, Dadsetan M, Nesbitt JJ, Rooney GE, Currier BL, Yaszemski MJ, Spinner RJ, and Windebank AJ (2011). "Comparison of polymer scaffolds in rat spinal cord: A step toward quantitative assessment of combinatorial approaches to spinal cord repair". *Biomaterials*, 32 (32): 8077-8086.

151. Gelain F, Panseri S, Antonini S, Cunha C, Donega M, Lowery J, Taraballi F, Cerri G, Montagna M, Baldissera F, and Vescovi A (2011). "Transplantation of nanostructured composite scaffolds results in the regeneration of chronically injured spinal cords". *ACS Nano*, 5 (1): 227-236.

152. Zhu Y, Wang A, Shen W, Patel S, Zhang R, Young WL, and Li S (2010). "Nanofibrous patches for spinal cord regeneration". *Advanced Functional Materials*, 20 (9): 1433-1440.

153. Hwang DH, Kim HM, Kang YM, Joo IS, Cho CS, Yoon BW, Kim SU, and Kim BG (2011). "Combination of multifaceted strategies to maximize the therapeutic benefits of neural stem cell transplantation for spinal cord repair". *Cell Transplantation*, 20 (9): 1361-1379.

154. Wong DY, Leveque JC, Brumblay H, Krebsbach PH, Hollister SJ, and LaMarca F (2008). "Macro-architectures in spinal cord scaffold implants influence regeneration". *Journal of Neurotrauma*, 25 (8): 1027-1037.

155. Tysseling VM, Sahni V, Pashuck ET, Birch D, Hebert A, Czeisler C, Stupp SI, and Kessler JA (2010). "Self-assembling peptide amphiphile promotes plasticity of serotonergic fibers following spinal cord injury". *Journal of Neuroscience Research*, 88 (14): 3161-3170.

156. Baumann MD, Kang CE, Stanwick JC, Wang Y, Kim H, Lapitsky Y, and Shoichet MS (2009). "An injectable drug delivery platform for sustained combination therapy". *Journal of Controlled Release*, 138 (3): 205-213.

157. Kubinová Š, Horák D, Kozubenko N, Vaněček V, Proks V, Price J, Cocks G, and Syková E (2010). "The use of superporous Ac-CGGASIKVAVS-OH-modified PHEMA scaffolds to promote cell adhesion and the differentiation of human fetal neural precursors". *Biomaterials*, 31 (23): 5966-5975.

158. Hejcl A, Lesný P, Prádný M, Michálek J, Jendelová P, Stulík J, and Syková E (2008). "Biocompatible hydrogels in spinal cord injury repair". *Physiological research / Academia Scientiarum Bohemoslovaca*, 57 Suppl 3: S121-132.

159. Hejčl A, Šedý J, Kapcalová M, Toro DA, Amemori T, Lesný P, Likavčanová-Mašínová K, Krumbholcová E, Přádný M, Michálek J, Burian M, Hájek M, Jendelová P, and Syková E (2010). "HPMA-RGD hydrogels seeded with mesenchymal stem cells improve functional outcome in chronic spinal cord injury". *Stem Cells and Development*, 19 (10): 1535-1546.

160. Loh NK, Woerly S, Bunt SM, Wilton SD, and Harvey AR (2001). "The regrowth of axons within tissue defects in the cns is promoted by implanted hydrogel matrices that contain BDNF and CNTF producing fibroblasts". *Experimental Neurology*, 170 (1): 72-84.

161. Amaral IF, Neiva I, Ferreira da Silva F, Sousa SR, Piloto AM, Lopes CDF, Barbosa MA, Kirkpatrick CJ, and Pêgo AP (2013). "Endothelialization of chitosan porous conduits via immobilization of a recombinant fibronectin fragment (rhFNIII 7-10)". *Acta Biomaterialia*, 9 (3): 5643-5652.

162. Cheng H, Huang YC, Chang PT, and Huang YY (2007). "Laminin-incorporated nerve conduits made by plasma treatment for repairing spinal cord injury". *Biochemical and Biophysical Research Communications*, 357 (4): 938-944.

163. Li X, Yang Z, Zhang A, Wang T, and Chen W (2009). "Repair of thoracic spinal cord injury by chitosan tube implantation in adult rats". *Biomaterials*, 30 (6): 1121-1132.

164. Chen X, Yang Y, Yao J, Lin W, Li Y, Chen Y, Gao Y, Gu X, and Wang X (2011). "Bone marrow stromal cells-loaded chitosan conduits promote repair of complete transection injury in rat spinal cord". *Journal of Materials Science: Materials in Medicine*, 22 (10): 2347-2356.

165. Liu T, Houle JD, Xu J, Chan BP, and Chew SY (2012). "Nanofibrous collagen nerve conduits for spinal cord repair". *Tissue Engineering - Part A*, 18 (9-10): 1057-1066.

166. Liu T, Xu J, Chan BP, and Chew SY (2012). "Sustained release of neurotrophin-3 and chondroitinase ABC from electrospun collagen nanofiber scaffold for spinal cord injury repair". *Journal of Biomedical Materials Research - Part A*, 100 A (1): 236-242.

167. Madaghiele M, Sannino A, Yannas IV, and Spector M (2008). "Collagen-based matrices with axially oriented pores". *Journal of Biomedical Materials Research - Part A*, 85 (3): 757-767.

168. Saglam A, Perets A, Canver AC, Li HL, Kollins K, Cohen G, Fischer I, Lazarovici P, and Lelkes PI (2012). "Angioneural Crosstalk in Scaffolds with Oriented Microchannels for Regenerative Spinal Cord Injury Repair". *Journal of Molecular Neuroscience*: 1-13.

169. Guo J, Su H, Zeng Y, Liang YX, Wong WM, Ellis-Behnke RG, So KF, and Wu W (2007). "Reknitting the injured spinal cord by self-assembling peptide nanofiber scaffold". *Nanomedicine: Nanotechnology, Biology, and Medicine*, 3 (4): 311-321.

170. Moradi F, Bahktiari M, Joghataei MT, Nobakht M, Soleimani M, Hasanzadeh G, Fallah A, Zarbakhsh S, Hejazian LB, Shirmohammadi M, and Maleki F (2012). "BD PuraMatrix peptide hydrogel as a culture system for human fetal Schwann cells in spinal cord regeneration". *Journal of Neuroscience Research*, 90 (12): 2335-2348.

171. Novikova LN, Pettersson J, Brohlin M, Wiberg M, and Novikov LN (2008). "Biodegradable poly-β-hydroxybutyrate scaffold seeded with Schwann cells to promote spinal cord repair". *Biomaterials*, 29 (9): 1198-1206.

172. Gao M, Lu P, Bednark B, Lynam D, Conner JM, Sakamoto J, and Tuszynski MH (2013). "Templated agarose scaffolds for the support of motor axon regeneration into sites of complete spinal cord transection". *Biomaterials*, 34 (5): 1529-1536.

173. Gupta D, Tator CH, and Shoichet MS (2006). "Fast-gelling injectable blend of hyaluronan and methylcellulose for intrathecal, localized delivery to the injured spinal cord". *Biomaterials*, 27 (11): 2370-2379.

174. Park J, Lim E, Back S, Na H, Park Y, and Sun K (2010). "Nerve regeneration following spinal cord injury using matrix metalloproteinase-sensitive, hyaluronic acid-based biomimetic hydrogel scaffold containing brain-derived neurotrophic factor". *Journal of Biomedical Materials Research - Part A*, 93 (3): 1091-1099.

175. Herbert CB, Nagaswami C, Bittner GD, Hubbell JA, and Weisel JW (1998). "Effects of fibrin micromorphology on neurite growth from dorsal root ganglia cultured in three-dimensional fibrin gels". *Journal of Biomedical Materials Research*, 40 (4): 551-559.

176. Hyatt AJT, Wang D, Kwok JC, Fawcett JW, and Martin KR (2010). "Controlled release of chondroitinase ABC from fibrin gel reduces the level of inhibitory glycosaminoglycan chains in lesioned spinal cord". *Journal of Controlled Release*, 147 (1): 24-29.

177. Johnson PJ, Parker SR, and Sakiyama-Elbert SE (2009). "Controlled release of neurotrophin-3 from fibrin-based tissue engineering scaffolds enhances neural fiber sprouting following subacute spinal cord injury". *Biotechnology and Bioengineering*, 104 (6): 1207-1214.

178. Johnson PJ, Tatara A, McCreedy DA, Shiu A, and Sakiyama-Elbert SE (2010). "Tissue-engineered fibrin scaffolds containing neural progenitors enhance functional recovery in a subacute model of SCI". *Soft Matter*, 6 (20): 5127-5137.

179. Taylor SJ, Rosenzweig ES, McDonald Iii JW, and Sakiyama-Elbert SE (2006). "Delivery of neurotrophin-3 from fibrin enhances neuronal fiber sprouting after spinal cord injury". *Journal of Controlled Release*, 113 (3): 226-235.

180. Prang P, Müller R, Eljaouhari A, Heckmann K, Kunz W, Weber T, Faber C, Vroemen M, Bogdahn U, and Weidner N (2006). "The promotion of oriented axonal regrowth in the injured spinal cord by alginate-based anisotropic capillary hydrogels". *Biomaterials*, 27 (19): 3560-3569.

181. Silva NA, Cooke MJ, Tam RY, Sousa N, Salgado AJ, Reis RL, and Shoichet MS (2012). "The effects of peptide modified gellan gum and olfactory ensheathing glia cells on neural stem/progenitor cell fate". *Biomaterials*, 33 (27): 6345-6354.

182. Alvarez-Perez MA, Guarino V, Cirillo V, and Ambrosio L (2010). "Influence of gelatin cues in PCL electrospun membranes on nerve outgrowth". *Biomacromolecules*, 11 (9): 2238-2246.

183. Prabhakaran MP, Venugopal J, Chan CK, and Ramakrishna S (2008). "Surface modified electrospun nanofibrous scaffolds for nerve tissue engineering". *Nanotechnology*, 19 (45).

184. Bhattarai N, Li Z, Gunn J, Leung M, Cooper A, Edmondson D, Veiseh O, Chen MH, Zhang Y, Ellenbogen RG, and Zhang M (2009). "Natural-synthetic polyblend nanofibers for biomedical applications". *Advanced Materials*, 21 (27): 2792-2797.

185. Bhattarai N, Ramay HR, Gunn J, Matsen FA, and Zhang M (2005). "PEG-grafted chitosan as an injectable thermosensitive hydrogel for sustained protein release". *Journal of Controlled Release*, 103 (3): 609-624.

186. Eyrich D, Göpferich A, and Blunk T, *Fibrin in tissue engineering*, in *Advances in experimental medicine and biology*. 2006, New York, Plenum Press. p. 379-392.

187. King VR, Alovskaya A, Wei DYT, Brown RA, and Priestley JV (2010). "The use of injectable forms of fibrin and fibronectin to support axonal ingrowth after spinal cord injury". *Biomaterials*, 31 (15): 4447-4456.

188. Lu P, Wang Y, Graham L, McHale K, Gao M, Wu D, Brock J, Blesch A, Rosenzweig ES, Havton LA, Zheng B, Conner JM, Marsala M, and Tuszynski MH (2012). "Long-distance growth and connectivity of neural stem cells after severe spinal cord injury". *Cell*, 150 (6): 1264-1273.

189. Zhang S (2003). "Fabrication of novel biomaterials through molecular self-assembly". *Nature Biotechnology*, 21 (10): 1171-1178.

190. Gelain F, Cigognini D, Caprini A, Silva D, Colleoni B, Donegá M, Antonini S, Cohen BE, and Vescovi A (2012). "New bioactive motifs and their use in functionalized self-assembling peptides for NSC differentiation and neural tissue engineering". *Nanoscale*, 4 (9): 2946-2957.

191. Zhang W, Zhan X, Gao M, Hamilton AD, Liu Z, Jiang Y, Su H, Dai X, He B, Kang X, Zeng Y, Wu W, and Guo J (2012). "Self-assembling peptide nanofiber scaffold enhanced with RhoA inhibitor CT04 improves axonal regrowth in the transected spinal cord". *Journal of Nanomaterials*, 2012; nr 54.

192. Tan A, Rajadas J, and Seifalian AM (2012). "Biochemical engineering nerve conduits using peptide amphiphiles". *Journal of Controlled Release*, 163 (3): 342-352.

193. Webber MJ, Matson JB, Tamboli VK, and Stupp SI (2012). "Controlled release of dexamethasone from peptide nanofiber gels to modulate inflammatory response". *Biomaterials*, 33 (28): 6823-6832.

194. Schmidt CE, Shastri VR, Vacanti JP, and Langer R (1997). "Stimulation of neurite outgrowth using an electrically conducting polymer". *Proceedings of the National Academy of Sciences of the United States of America*, 94 (17): 8948-8953.

195. Lee JY, Bashur CA, Goldstein AS, and Schmidt CE (2009). "Polypyrrole-coated electrospun PLGA nanofibers for neural tissue applications". *Biomaterials*, 30 (26): 4325-4335.

196. Prabhakaran MP, Ghasemi-Mobarakeh L, Jin G, and Ramakrishna S (2011). "Electrospun conducting polymer nanofibers and electrical stimulation of nerve stem cells". *Journal of Bioscience and Bioengineering*, 112 (5): 501-507.

197. Huang J, Hu X, Lu L, Ye Z, Zhang Q, and Luo Z (2010). "Electrical regulation of Schwann cells using conductive polypyrrole/chitosan polymers". *Journal of Biomedical Materials Research - Part A*, 93 (1): 164-174.

198. Geller HM and Fawcett JW (2002). "Building a bridge: Engineering spinal cord repair". *Experimental Neurology*, 174 (2): 125-136.

199. Mahoney MJ, Chen RR, Tan J, and Mark Saltzman W (2005). "The influence of microchannels on neurite growth and architecture". *Biomaterials*, 26 (7): 771-778.

200. Yao L, Wang S, Cui W, Sherlock R, O'Connell C, Damodaran G, Gorman A, Windebank A, and Pandit A (2009). "Effect of functionalized micropatterned PLGA on guided neurite growth". *Acta Biomaterialia*, 5 (2): 580-588.

201. Fan YW, Cui FZ, Hou SP, Xu QY, Chen LN, and Lee IS (2002). "Culture of neural cells on silicon wafers with nano-scale surface topograph". *Journal of Neuroscience Methods*, 120 (1): 17-23.

202. Schnell E, Klinkhammer K, Balzer S, Brook G, Klee D, Dalton P, and Mey J (2007). "Guidance of glial cell migration and axonal growth on electrospun nanofibers of poly-ε-caprolactone and a collagen/poly-ε-caprolactone blend". *Biomaterials*, 28 (19): 3012-3025.

203. Wang M, Zhai P, Chen X, Schreyer DJ, Sun X, and Cui F (2011). "Bioengineered scaffolds for spinal cord repair". *Tissue Engineering - Part B: Reviews*, 17 (3): 177-194.

204. Madduri S and Gander B (2012). "Growth factor delivery systems and repair strategies for damaged peripheral nerves". *Journal of Controlled Release*, 161 (2): 274-282.

205. Yang Y, De Laporte L, Rives CB, Jang JH, Lin WC, Shull KR, and Shea LD (2005). "Neurotrophin releasing single and multiple lumen nerve conduits". *Journal of Controlled Release*, 104 (3): 433-446.

206. Moore MJ, Friedman JA, Lewellyn EB, Mantila SM, Krych AJ, Ameenuddin S, Knight AM, Lu L, Currier BL, Spinner RJ, Marsh RW, Windebank AJ, and Yaszemski MJ (2006). "Multiple-channel scaffolds to promote spinal cord axon regeneration". *Biomaterials*, 27 (3): 419-429.

207. Jeffries EM and Wang Y (2012). "Biomimetic micropatterned multi-channel nerve guides by templated electrospinning". *Biotechnology and Bioengineering*, 109 (6): 1571-1582.

208. Hu XY, Huang JH, Ye ZX, Xia L, Li M, Lv BC, Shen XF, and Luo ZJ (2009). "A Novel Scaffold with Longitudinally Oriented Microchannels Promotes Peripheral Nerve Regeneration". *Tissue Engineering Part A*, 15 (11): 3297-3308.

209. Lee AC, Yu VM, Lowe Iii JB, Brenner MJ, Hunter DA, Mackinnon SE, and Sakiyama-Elbert SE (2003). "Controlled release of nerve growth factor enhances sciatic nerve regeneration". *Experimental Neurology*, 184 (1): 295-303.

210. Midha R, Munro CA, Dalton PD, Tator CH, and Shoichet MS (2003). "Growth factor enhancement of peripheral nerve regeneration through a novel synthetic hydrogel tube". *Journal of Neurosurgery*, 99 (3): 555-565.

211. Murugan R and Ramakrishna S (2006). "Nano-featured scaffolds for tissue engineering: A review of spinning methodologies". *Tissue Engineering*, 12 (3): 435-447.

212. Greiner A and Wendorff JH (2007). "Electrospinning: A fascinating method for the preparation of ultrathin fibers". *Angewandte Chemie - International Edition*, 46 (30): 5670-5703.

213. Zhang Y, Chwee TL, Ramakrishna S, and Huang ZM (2005). "Recent development of polymer nanofibers for biomedical and biotechnological applications". *Journal of Materials Science: Materials in Medicine*, 16 (10): 933-946.

214. Formhals A. 1934. US Patent version number: 1,975,504.

215. *Scopus*. cited 2014; Available from: http://www.scopus.com/search/form.url.

216. Liang D, Hsiao BS, and Chu B (2007). "Functional electrospun nanofibrous scaffolds for biomedical applications". *Advanced Drug Delivery Reviews*, 59 (14): 1392-1412.

217. Barnes CP, Sell SA, Boland ED, Simpson DG, and Bowlin GL (2007). "Nanofiber technology: Designing the next generation of tissue engineering scaffolds". *Advanced Drug Delivery Reviews*, 59 (14): 1413-1433.

218. Patel S, Kurpinski K, Quigley R, Gao H, Hsiao BS, Poo MM, and Li S (2007). "Bioactive nanofibers: Synergistic effects of nanotopography and chemical signaling on cell guidance". *Nano Letters*, 7 (7): 2122-2128.

219. Gupta D, Venugopal J, Prabhakaran MP, Dev VRG, Low S, Choon AT, and Ramakrishna S (2009). "Aligned and random nanofibrous substrate for the *in vitro* culture of Schwann cells for neural tissue engineering". *Acta Biomaterialia*, 5 (7): 2560-2569.

220. Chew SY, Wen J, Yim EKF, and Leong KW (2005). "Sustained release of proteins from electrospun biodegradable fibers". *Biomacromolecules*, 6 (4): 2017-2024.

221. Christopherson GT, Song H, and Mao HQ (2009). "The influence of fiber diameter of electrospun substrates on neural stem cell differentiation and proliferation". *Biomaterials*, 30 (4): 556-564.

222. Ghasemi-Mobarakeh L, Prabhakaran MP, Morshed M, Nasr-Esfahani MH, and Ramakrishna S (2008). "Electrospun poly(epsilon-caprolactone)/gelatin nanofibrous scaffolds for nerve tissue engineering". *Biomaterials*, 29 (34): 4532-4539.

223. Meiners S, Ahmed I, Ponery AS, Amor N, Harris SL, Ayres V, Fan Y, Chen Q, Delgado-Rivera R, and Babu AN (2007). "Engineering electrospun nanofibrillar surfaces for spinal cord repair: A discussion". *Polymer International*, 56 (11): 1340-1348.

224. Chow WN, Simpson DG, Bigbee JW, and Colello RJ (2007). "Evaluating neuronal and glial growth on electrospun polarized matrices: Bridging the gap in percussive spinal cord injuries". *Neuron Glia Biology*, 3 (2): 119-126.

225. Xie J, Willerth SM, Li X, Macewan MR, Rader A, Sakiyama-Elbert SE, and Xia Y (2009). "The differentiation of embryonic stem cells seeded on electrospun nanofibers into neural lineages". *Biomaterials*, 30 (3): 354-362.

226. Downing TL, Wang A, Yan ZQ, Nout Y, Lee AL, Beattie MS, Bresnahan JC, Farmer DL, and Li S (2012). "Drug-eluting microfibrous patches for the local delivery of rolipram in spinal cord repair". *Journal of Controlled Release*, 161 (3): 910-917.

227. Yao L, O'Brien N, Windebank A, and Pandit A (2009). "Orienting neurite growth in electrospun fibrous neural conduits". *Journal of Biomedical Materials Research - Part B Applied Biomaterials*, 90 (2): 483-491.

228. Shen Y, Qian Y, Zhang H, Zuo B, Lu Z, Fan Z, Zhang P, Zhang F, and Zhou C (2010). "Guidance of olfactory ensheathing cell growth and migration on electrospun silk fibroin scaffolds". *Cell Transplantation*, 19 (2): 147-157.

229. Lim SH, Liu XY, Song H, Yarema KJ, and Mao HQ (2010). "The effect of nanofiber-guided cell alignment on the preferential differentiation of neural stem cells". *Biomaterials*, 31 (34): 9031-9039.

230. Saino E, Focarete ML, Gualandi C, Emanuele E, Cornaglia AI, Imbriani M, and Visai L (2011). "Effect of electrospun fiber diameter and alignment on macrophage activation and secretion of proinflammatory cytokines and chemokines". *Biomacromolecules*, 12 (5): 1900-1911.

231. Cao H, McHugh K, Chew SY, and Anderson JM (2010). "The topographical effect of electrospun nanofibrous scaffolds on the *in vivo* and *in vitro* foreign body reaction". *Journal of Biomedical Materials Research - Part A*, 93 (3): 1151-1159.

232. Persheyev S, Fan Y, Irving A, and Rose MJ (2011). "BV-2 microglial cells sense micro-nanotextured silicon surface topology". *Journal of Biomedical Materials Research - Part A*, 99 A (1): 135-140.

233. Minev IR, Moshayedi P, Fawcett JW, and Lacour SP (2013). "Interaction of glia with a compliant, microstructured silicone surface". *Acta Biomaterialia*, 9 (6): 6936-6942.

234. Amadio S, De Ninno A, Montilli C, Businaro L, Gerardino A, and Volonté C (2013). "Plasticity of primary microglia on micropatterned geometries and spontaneous long-distance migration in microfluidic channels". *BMC Neuroscience*, 14.

235. Pearse DD, Pereira FC, Marcillo AE, Bates ML, Berrocal YA, Filbin MT, and Bunge MB (2004). "cAMP and Schwann cells promote axonal growth and functional recovery after spinal cord injury". *Nature Medicine*, 10 (6): 610-616.

236. Piantino J, Burdick JA, Goldberg D, Langer R, and Benowitz LI (2006). "An injectable, biodegradable hydrogel for trophic factor delivery enhances axonal rewiring and improves performance after spinal cord injury". *Experimental Neurology*, 201 (2): 359-367.

237. Tuszynski MH, Weidner N, McCormack M, Miller I, Powell H, and Conner J (1998). "Grafts of genetically modified Schwann cells to the spinal cord: Survival, axon growth, and myelination". *Cell Transplantation*, 7 (2): 187-196.

238. Lu P, Jones LL, and Tuszynski MH (2005). "BDNF-expressing marrow stromal cells support extensive axonal growth at sites of spinal cord injury". *Experimental Neurology*, 191 (2): 344-360.

239. Lo WC, Hsu CH, Wu ATH, Yang LY, Chen WH, Chiu WT, Lai WF, Wu CH, Gelovani JG, and Deng WP (2008). "A novel cell-based therapy for contusion spinal cord injury using GDNF-delivering NIH3T3 cells with dual reporter genes monitored by molecular imaging". *Journal of Nuclear Medicine*, 49 (9): 1512-1519.

240. Yu-Hai M, Zhang Y, Cao L, Su JC, Wang ZW, Xu AB, and Zhang SC (2010). "Effect of neurotrophin-3 genetically modified olfactory ensheathing cells transplantation on spinal cord injury". *Cell Transplantation*, 19 (2): 167-177.

241. Hutmacher DW and Garcia AJ (2005). "Scaffold-based bone engineering by using genetically modified cells". *Gene*, 347 (1): 1-10.

242. Salvay DM and Shea LD (2006). "Inductive tissue engineering with protein and DNA-releasing scaffolds". *Molecular BioSystems*, 2 (1): 36-48.

243. Houchin-Ray T, Swift LA, Jang JH, and Shea LD (2007). "Patterned PLG substrates for localized DNA delivery and directed neurite extension". *Biomaterials*, 28 (16): 2603-2611.

244. Tuinstra HM, Aviles MO, Shin S, Holland SJ, Zelivyanskaya ML, Fast AG, Ko SY, Margul DJ, Bartels AK, Boehler RM, Cummings BJ, Anderson AJ, and Shea LD (2012). "Multifunctional, multichannel bridges that deliver neurotrophin encoding lentivirus for regeneration following spinal cord injury". *Biomaterials*, 33 (5): 1618-1626.

245. Mittnacht U, Hartmann H, Hein S, Oliveira H, Dong M, Pêgo AP, Kjems J, Howard KA, and Schlosshauer B (2010). "Chitosan/siRNA nanoparticles biofunctionalize nerve implants and enable neurite outgrowth". *Nano Letters*, 10 (10): 3933-3939.

246. Chen M, Gao S, Dong M, Song J, Yang C, Howard KA, Kjems J, and Besenbacher F (2012). "Chitosan/siRNA nanoparticles encapsulated in PLGA nanofibers for siRNA delivery". *ACS Nano*, 6 (6): 4835-4844.

CHAPTER III

Effect of surface topography on microglia - implications for central nervous tissue engineering*

Liliana R Pires[1, 2], Daniela N Rocha[1,2], Luigi Ambrosio[3], Ana Paula Pêgo[1, 2,4]

1 – INEB – Instituto de Engenharia Biomédica, Universidade do Porto, Rua do Campo Alegre 823, 4150-180 Porto, Portugal.

2 – Universidade do Porto – Faculdade de Engenharia, Rua Roberto Frias, s/n, 4200-465 Porto, Portugal.

3 – Institute of Composite and Biomedical Materials, National Research Council, P. le Tecchio 80, 80125 Naples, Italy.

4 – Universidade do Porto – Instituto de Ciências Biomédicas Abel Salazar, Rua de Jorge Viterbo Ferreira 228, 4050-313 Porto, Portugal.

Submitted for publication

Abstract

Microglia play an important role in the central nervous system (CNS) homeostasis and response to injury that has been overlooked so far in the field of tissue engineering. Here the response of primary microglia cells to topographic cues provided by electrospun fibres and flat films of poly(trimethylene carbonate-co-ε-caprolactone) [P(TMC-CL)] was investigated, envisaging the design of instructive surfaces that can contribute to the challenging process of CNS regeneration. It was observed that cell morphology is remarkably affected by the substrate topography, mirroring the surface main features. Cells cultured on flat substrates presenting a round shape, while cells with elongated processes being observed on the electrospun fibres. Unexpectedly, a higher concentration of the pro-inflammatory cytokine TNFα was detected in cell culture media from microglia cultured on fibres. Still, it was observed that astrogliosis is not exacerbated when astrocytes are cultured in the presence of microglia conditioned media obtained from cultures in contact with either substrates. Furthermore, a significant percentage of microglia was found to participate in the process of myelin phagocytosis, with the formation of multinucleated giant cells being only observed on P(TMC-CL) films. Altogether, the results presented suggest that microglia in contact with the tested substrates is triggered towards a pro-regenerative phenotype. Furthermore, the present findings highlight the role of microglia in the context of CNS tissue engineering and the need to consider these cells as active contributors to the regeneration process.

Keywords:

Microglia; surface topography; electrospinning; myelin; multinucleated giant cell; nerve tissue engineering.

1. Introduction

Microglia, the resident immune cells of the central nervous system (CNS), play a key role on the maintenance of CNS homeostasis and in the management of tissue response to injury, although representing only about 10% of the total number of glial cells [1]. Microglia can secrete both pro-inflammatory cytokines that may lead to cell death, or anti-inflammatory molecules and neurotrophic factors that contribute to neuroprotection and regeneration [2]. Furthermore, in the context of an insult to the CNS, microglia is involved in the clearance of myelin debris that accumulate due to Wallerian degeneration. This process is of paramount importance as the accumulation of debris has been associated with the inhibition of axonal regeneration [3]. Consequently, the diversity of microglia activities turn these cells into an interesting target for new therapies in the context of CNS regeneration [4].

It is now well established that topographic cues can have a considerable influence on cellular processes such as cell adhesion and differentiation (see [5, 6] for a review). The role of surface topography on cells from the CNS has been investigated under the scope of the development of tissue engineering scaffolds. Neurons have been under the spotlight of the research in the field, so far. It has been shown that fibrous topographies support axonal guidance and growth [7-9], as well as stem cell differentiation into the neuronal lineage [10, 11]. Similarly, micropatterned surfaces have been successfully applied to promote directional axonal growth and neural stem cell differentiation [12]. The number of studies concerning the influence of topographic cues on glial cells is, on the other hand, still limited and these have been focused on astrocytes, mainly due to their key role on the formation of the glial scar in response to an insult to the CNS [13]. Astrocytes have been found to orient their filamentous structure according to the topography of the surface [14-17]. Moreover, although some authors did not found significant alterations on astrocyte activation when cells were seeded on a fibrous surface in comparison to cells cultured on flat solvent cast films (assessed in terms of glial fibrillary acidic protein (GFAP) and vimentin protein expression) [15], others claimed that the contact of astrocytes with fibres is able to promote a decrease on GFAP expression [16] and an increase on glutamate uptake, what can contribute for neuroprotection in vivo [17]. Furthermore, by using micropatterned grooved scaffolds, mature astrocytes were found to be reverted into radial glia-like cells, and consequently to a more pro-regenerative phenotype [18]. These studies highlight that by providing appropriate physical stimuli it is possible to bias the response of glial cells to injury.

Despite the important role ascribed to microglia, studies on microglia-material interaction are still in the infancy and have been focused on materials/structures for the design of implantable electrodes. The chemistry of the surface was found to influence the cytokine release profile of microglia depending on its hydrophobicity [19]. In what concerns topography, the effect of nanostructured silicone or poly(dimethylsiloxane) surfaces on microglia morphology, adhesion [20, 21] or motility [20] were also investigated. More recently, it was demonstrated that microglia interacts mechanically with silicone micropillars on a surface, being affected by surface stiffness [22].

Foreseeing the design of a tissue engineering scaffold that can contribute to regeneration in the CNS, we explored the use of poly(trimethylene carbonate-co-ε-caprolactone) [P(TMC-CL)] to obtain matrices with different topographic cues. The preparation of fibres of this biodegradable polymer by electrospinning was previously reported [23], as well as its remarkable properties in the context of tissue engineering for the peripheral [24, 25] and the central nervous system regeneration [26]. Noteworthy, P(TMC-CL) showed to stimulate cortical neuron polarization and promote axonal elongation. Moreover, even in the presence of myelin, cortical neurons cultured on P(TMC-CL) films were found to extend more neurites, showing P(TMC-CL)'s ability to tame myelin inhibition in a CNS lesion scenario [26]. Here we investigate microglia response to different topographic cues provided by electrospun fibres and solvent-cast films of P(TMC-CL) in order to obtain important clues towards the design of instructive surfaces that can contribute to the challenging process of CNS regeneration.

2. Materials and Methods

2.1. Polymer synthesis and characterization

The statistical P(TMC-CL) copolymer was prepared by ring-opening polymerization and subsequently purified as previously described [24]. Chemical composition of the purified copolymer was assessed by 1H nuclear magnetic resonance (NMR) and found to contain 11% mol of TMC, being in accordance to the monomer ratio charged (10% mol TMC). The average number molecular weight and polydispersity index of the purified polymer were determined by size exclusion chromatography [23] and were found to be 8.2×10^4 and 1.61, respectively.

2.2. Substrate preparation

P(TMC-CL) fibres were prepared by electrospinning as previously described [23]. In brief, 10% (w/v) P(TMC-CL) solutions in dichloromethane (DCM, Merck, Germany) were dispensed at a controlled flow rate of 1 $ml.h^{-1}$ using a syringe pump (Ugo Basille, Italy). An electric field of 1 $kV.cm^{-1}$ was applied (Gamma High Voltage source, FL, USA) between the spinneret (inner diameter 0.8 mm) and the flat collector (15x15 cm). Fibres were collected during 1-1.5 hrs onto 13 mm glass coverslips (Menzel-Glaser, Germany) distributed on top of aluminium foil.

P(TMC-CL) films were prepared by solvent casting as follows. A P(TMC-CL) solution in DCM (6% (w/v)) was casted onto a glass petri dish. The solvent was left to evaporate overnight under a DCM saturated atmosphere at room temperature (20-25°C).

After preparation, electrospun fibres and solvent cast films were vacuum dried during 24 hrs (vacuum oven, Raypa, Spain). Subsequently, 14 mm discs were punched out, packed under vacuum after an Argon purge and sterilized by gamma irradiation (25 kGy, ^{60}Co source).

2.3. Surface characterization

P(TMC-CL) samples were sputter-coated with gold-palladium for 90 seconds (SPI Supplies, PA, USA). Afterwards, the P(TMC-CL) surfaces were observed by scanning electron microscopy (SEM) using a FEI Quanta 400FEG microscope (FEI, the Netherlands). Fibre diameter was quantified from SEM micrographs using image analysis software (Image J, version 1.39, NIH, MD, USA). Fibre mean diameter and fibre diameter distribution were calculated from at least 100 measurements from 3 independent samples.

2.4. Primary cell isolation and culture

Primary cultures of microglia and astrocytes were obtained from postnatal (1-2 days) Wistar rat pups based on previously described procedures [27, 28]. All experiments involving animals and their care were conducted in compliance with institutional ethical guidelines and with the approval of Portuguese Veterinary Authorities – Direcção-Geral de Alimentação e Veterinária (DGAV). Briefly, pups were decapitated, the meninges were carefully stripped off and cortices dissected. Subsequently, the tissue was enzimatically digested using a papain solution (0.2 units.ml^{-1}, Sigma-Aldrich Química, Portugal) for 30 min at 37ºC. The tissue was further dissociated using a pipette and, subsequently, plated into tissue culture treated flasks (Thermo Scientific, Thermo Fisher Scientific, Portugal). The mixed glial cultures were maintained for 8 to 10 days at 37°C in high-glucose Dulbecco's modified Eagle medium (DMEM) supplemented with 10% (v/v) of heat inactivated (56°C, 30 min) foetal bovine serum (FBS) and 1% (v/v) penicillin/streptomycin (P/S, 10,000 U.ml^{-1} penicillin, 10,000 µg.ml^{-1} streptomycin), all supplied by Gibco (Life technologies S.A., Spain).

To obtain microglia, after culture confluence, the mixed glial cultures were shaken for 1 hr using an orbital shaker (IKA, Germany) at 160 rpm and 37ºC. The supernatant enriched with microglia was collected and centrifuged (200 g, 5 minutes). Microglial cell culture purity was quantified after immunolabelling using CD11b antibody (1:200, Abcam, Belgium) and found to be above 90% (see details in supporting information) in accordance to previous reports that used a similar isolation technique [19, 29]. 6x10^{4} viable cells.ml^{-1} were seeded on P(TMC-CL) substrates secured at the bottom of a 24-well plate with a silicone o-ring (Epidor, Spain) and cultured in DMEM/F12 medium (Gibco) supplemented with 10% FBS and 1% P/S for 1 or 5 days.

After collecting microglia, mixed glial cultures were shaken for additional 22 hrs to remove oligodendrocytes. The remaining cell layer, mainly composed by astrocytes, was maintained in culture in supplemented DMEM.

2.5. Cytoskeleton immunolabelling

To analyze cell morphology, cells were fixed with paraformaldehyde (4% (w/v), in phosphate buffered saline – PBS) and immunostained for F-actin as follows. Cell external fluorescence was

quenched using 50 mM NH_4Cl (Merck) for 10 minutes. After washing with PBS (three times, 5 minutes) cells were permeabilized with 0.1% (v/v) Triton X-100 (in PBS) for 5 minutes. Afterwards, cells were washed with PBS, incubated with 5% (w/v) bovine serum albumin (BSA, Merck) in PBS for 30 minutes and, thereafter, incubated with Alexa Fluor® 488 Phalloidin (1:40 Invitrogen, Life Technologies). Subsequently, cells were washed with PBS and stained with 4',6-diamidino-2-phenylindole (DAPI, 0.1 $\mu g.ml^{-1}$ in PBS, Sigma-Aldrich). Samples were observed under an inverted fluorescence microscope (Axiovert 200, Zeiss, Germany) or confocal microscope (Leica Microsystems, Germany).

2.6. Microglia morphology analysis

Microglia morphology was analysed using the Fraclac plug-in for ImageJ. The box counting fractal dimension (DB) [30] as well as morphometrics based on the convex hull were calculated. Images of the cytoskeleton (F-actin) of individual cells (n = 50) were applied, after conversion to binary images and manually outlining the cell contour. Morphometric parameters calculated include area and circularity, and results are presented in pixels.

2.7. Cytokine quantification

At the defined time point, cell culture supernatants from microglia seeded on different P(TMC-CL) substrates were collected and, after centrifugation (16,000g, 4ºC, 10 minutes) to remove cell debris, stored at -20ºC for posterior analysis. Cell culture media from cells activated with lipopolysaccharide (LPS, 100 $ng.ml^{-1}$, 3 hrs, Sigma-Aldrich) was also analyzed to serve as positive control for microglia activation [31].

Tumour necrosis factor-α (TNFα, RayBiotech, GA, USA) and interleukin-10 (IL-10, Biolegend, CA, USA) were quantified from microglia culture supernatants by enzyme-linked immunosorbent assay (ELISA) following manufacturer instructions.

2.8. Myelin phagocytosis assay

Myelin phagocytosis by microglia when seeded on different substrates was evaluated as follows. Rat brain myelin was obtained as previously described [32]. Five days after microglia seeding, a myelin suspension was added to the cell culture media to a final concentration of 2.5 $\mu g.ml^{-1}$ [33]. After 24 hrs in contact with myelin, cells were washed, stained for CD11b and subsequently fixed and permeabilized as described above. Cells were counterstained using myelin binding protein (MBP) antibody (1:200, Chemicon, Millipore, MA, USA) at 4ºC, overnight followed by 1 hr of incubation with Alexa Fluor® 488 donkey anti-rat IgG (1:1,000, Invitrogen, Life Technologies). DAPI was applied to label cell nuclei. Cultures were observed using an inverted fluorescence microscope (Axiovert, Zeiss) and the percentage of cells with detectable MBP was used as a measure for myelin ingestion.

2.9. Effect of microglia conditioned media on astrocyte metabolic activity and gene expression

Astrocytes ($4x10^4$ viable cells.ml^{-1}) (passage 4-7) were seeded on 24-well plates using supplemented DMEM. After adhesion overnight, the cell culture medium was changed by microglia conditioned media collected after 5 days in contact with P(TMC-CL) substrates. As a control condition (non-treated cells), astrocyte cultures were conducted in supplemented DMEM/F12 (microglia culture medium, see section 2.4).

Cell metabolic activity was assessed after 24 and 72 hrs by two different methods. Cellular ATP content was measured using Celltiter-Glo® (Promega, WI, USA), following the manufacturer instructions. To assess resazurin metabolization, cells were incubated (4 hrs, 37°C) with a resazurin (Sigma-Aldrich) solution (0.1 mg.ml^{-1}, in PBS) and the fluorescence (λex=530nm, λem=590nm) in the cell culture medium was measured (SynergyMx, Biotek, Portugal).

Gene expression of genes related to astrogliosis, namely glial fibrillary acidic protein (GFAP), collagen IV and vimentin was assessed. Cell lysis and RNA purification were performed using Quick-RNA MiniPrep from Zymo Research (CA, USA), according to the manufacturer's instructions. Reverse transcription was done with SuperScript III (Invitrogen). Primer sequences are provided in supporting information. Hypoxanthine-guanine phosphoribosyltransferase (Hprt) was applied as reference gene. PCR was performed using HotStarTaq DNA polymerase (Qiagen, USA) for 34 cycles. Quantification of band intensity was done using ImageLab software, version 3.0 (Bio-Rad, Portugal).

2.10. Statistical analysis

Statistical analysis was performed using PRISM 5.0 software (GraphPad, CA, USA). A parametric t-test was applied to assess differences on cell morphology parameters. Statistical differences between groups on cytokine concentration, astrogliosis markers and myelin phagocytosis were calculated applying the nonparametric Mann-Whitney test. A p-value lower than 0.05 was considered statistically significant.

3. Results

3.1. Substrate characterization

By using different processing techniques (electrospinning and solvent casting), distinctive P(TMC-CL) surface topographies were obtained, as observed in the representative SEM micrographs presented in Figure 1. Solvent cast films show a spherulitic morphology (Figure 1, A, B) characteristic of a semicrystalline material [34]. The preparation of P(TMC-CL) fibres by electrospinning was previously optimized [23]. Under the conditions selected for the present study, the prepared electrospun membranes show a typical fibrous and randomly oriented structure

(Figure 1, C, D). Bead defects are not observed. Mean fibre diameter was determined to be 1.09 ± 0.1 µm, being fibre diameter distribution as depicted in Figure 1, E.

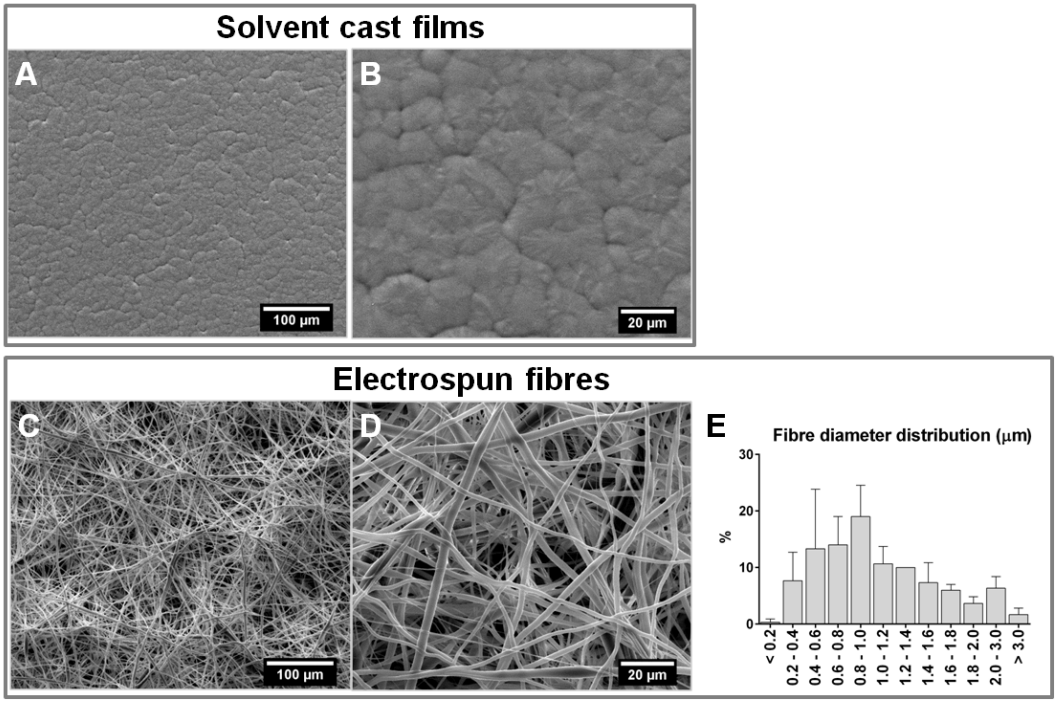

Figure 1. Scanning electron microscopy (SEM) photomicrographs of the prepared P(TMC-CL) surfaces. (A and B) Films obtained by solvent casting; and (C and D) fibres obtained by electrospinning. (E) Fibre diameter distribution as calculated from 100 measurements from 3 independent samples; bars represent mean values and error bars show standard deviation.

3.2. Effect of surface topography on microglia

3.2.1 Microglia morphology

The morphology of microglia cells when seeded on different P(TMC-CL) surface topographies was analyzed after immunolabelling of F-actin. Cell cytoskeleton organization was found to be significantly affected by the surface topography, as can be observed in Figure 2. On P(TMC-CL) films, microglia presents a round shape and long protrusions (Figure 2, A). Conversely, microglia seeded on P(TMC-CL) electrospun fibres show a smaller and more elongated cytoplasm (Figure 2, B), being actin concentrated at the points of cell adhesion along the fibre (Figure 2, B). Image analysis shows that microglia seeded on P(TMC-CL) films has an increased complexity comparing to cells cultured on fibres, as indicated by the higher box counting fractal dimension DB [30]. Moreover, cell area was also found to be significantly increased on microglia seeded on P(TMC-CL) films (Figure 2, C). Although no statistical differences were found comparing mean values of circularity, it can be observed from the graphs representing the percentage of cells distributed in equally weighted grades (Figure 2, D), that on P(TMC-CL) films a higher percentage of cells show a circularity close to 1 – the theoretical circularity of a circle.

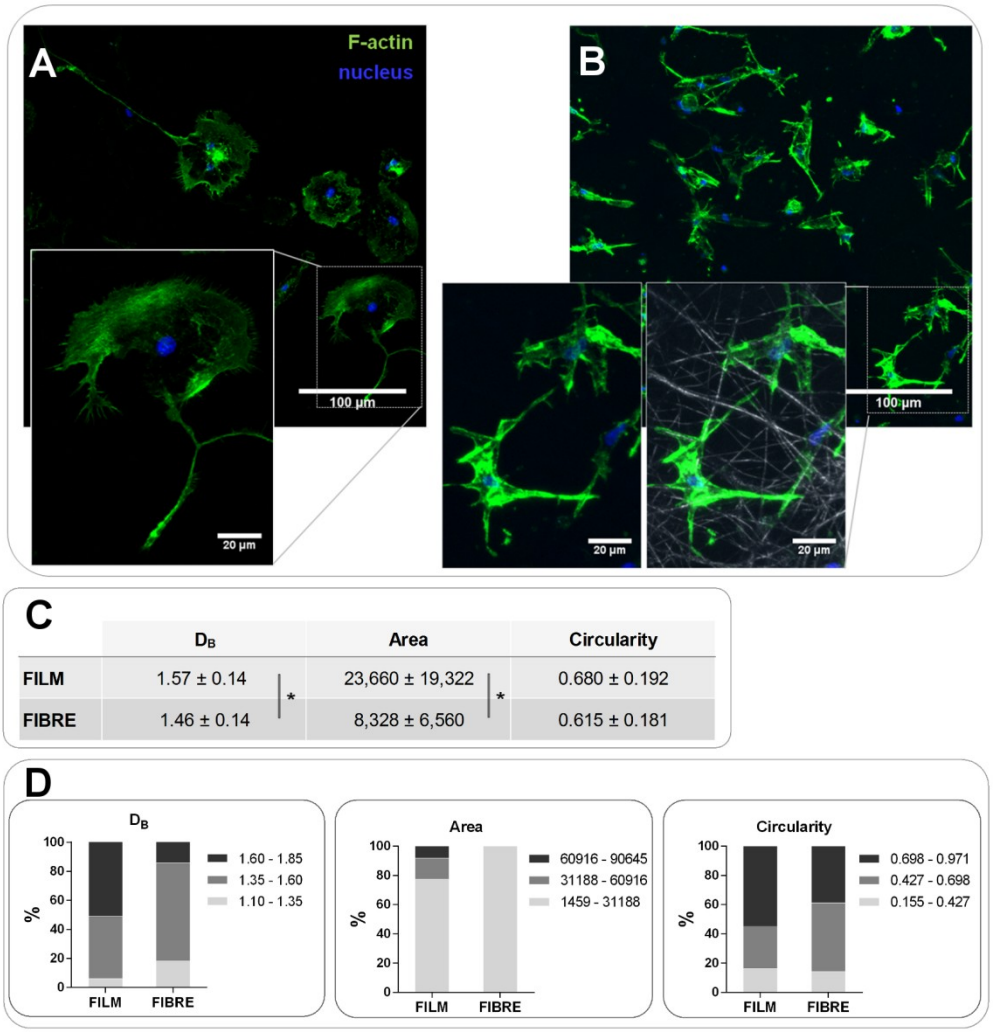

C	D_B	Area	Circularity
FILM	1.57 ± 0.14 *	23,660 ± 19,322 *	0.680 ± 0.192
FIBRE	1.46 ± 0.14	8,328 ± 6,560	0.615 ± 0.181

Figure 2. Microglia morphology when cultured (5 days) on P(TMC-CL) substrates. (A and B) Confocal Z-projection images of F-actin and cell nuclei of microglia seeded on P(TMC-CL) (A) films or (B) fibres. In the presented detail of (B) it is also shown the fibrous structure of the electrospun mat (gray). (C and D) Characterization of microglia morphology by image analysis using box counting fractal dimension (DB) and morphometrics based on convex hull (n=50). (C) Average ± standard deviation values for the morphological parameters investigated: DB, cell area and circularity. (D) Graphic representation of the percentage of cells with different grade for each parameter. Three equalized grades were defined. * denotes statistical significance, $p < 0.05$.

3.2.2 Cytokine release profile

Variations on microglia morphology have been traditionally associated with distinct functional states [35, 36]. Therefore, to evaluate if the differences found on microglia morphology, as a consequence of the different P(TMC-CL) surface topography, can lead to alterations on cytokine release profile, IL-10 and TNFα were quantified in the cell culture medium at day 1 and 5 of culture (Figure 3). Although the differences did not achieve statistical significance, higher concentration of the anti-inflammatory cytokine IL-10 was detected on the cell culture medium from microglia cultured on P(TMC-CL) fibres, comparing to medium obtained from cells seeded on solvent cast films (Figure 3, A). Additionally, TNFα was found to be increased in cell culture

medium of cells adhered to P(TMC-CL) fibrous topography as compared to cells adhered on solvent cast films (Figure 3, B), being this difference statistically significant at day 1 of culture. It is worthwhile mentioning that a sharp increase on TNFα concentration was observed when microglia was stimulated with LPS (Figure 3, C).

Analyzing the concentration of these cytokines in the cell culture media over time, it can be observed that when cells were cultured in contact with P(TMC-CL) fibres IL-10 concentration tended to increase, whereas TNFα was maintained. In the case of cells cultured on P(TMC-CL) films, no alteration on cytokine concentration was detected between the two time points of analysis (Figure 3).

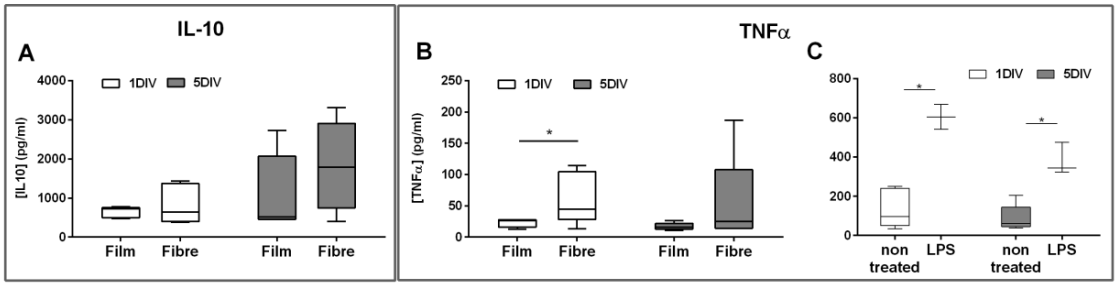

Figure 3. Box-whiskers plot representing the concentration of (A) IL-10 and (B and C) TNFα released to the cell culture medium by primary microglia over time. Cells were cultured in P(TMC-CL) films or electrospun fibres during 1 and 5 days (n=5). Non-treated cells (n=5) and cells treated with lipopolysacharide (LPS) (n=3) were cultured on regular glass coverslips. DIV - days *in vitro*. * denotes statistical significance, $p < 0.05$.

3.2.3. Myelin phagocytosis

One of the key functions of microglia in the aftermath of a lesion to the CNS is the clearance of myelin debris. since myelin accumulation exposes inhibitory molecules converting the lesion region in a non-permissive substrate for axonal regrowth [3]. To investigate if the surface topography can influence microglia ability to phagocytise myelin, myelin was added in suspension to cells cultured on the different substrates and the percentage of cells engulfing myelin was quantified after immunolabelling.

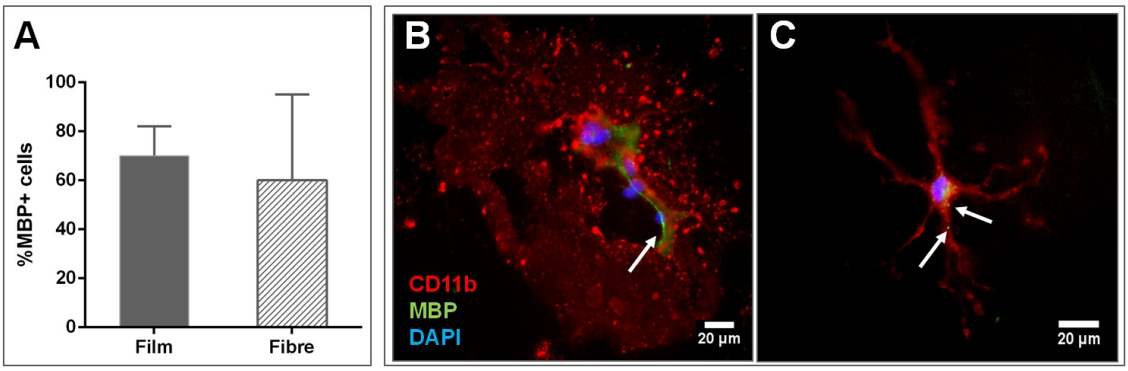

Figure 4. Myelin phagocytosis assay. (A) Quantification of the percentage of microglia cells that co-localize with myelin. Bars represent mean values and error bars show standard deviation (n=3). (B and C) representative fluorescence microscopy images of microglia cultured on P(TMC-CL) (B) films or (C) fibres when in contact with myelin. Arrows indicate myelin inside the cells.

The overall percentage of microglia found to engulf myelin was above 60% for both cells cultured on P(TMC-CL) films and fibres, tending this parameter to be higher for cells seeded on films (Figure 4, A).

As previously mentioned, cell morphology is markedly influenced by the P(TMC-CL) surface topography. Figure 4 shows that it is further affected by the presence of myelin. The round cells with long protrusions found on P(TMC-CL) films (see Figure 2) were able to form multinucleated giant cells (MGC) when in contact with myelin (Figure 4, B). On the other hand, in the microglia cultures performed in contact with fibrous substrates, MGC were not observed. Conversely, cells tend to increase the number of ramifications (Figure 4, C).

3.3. Effect of microglia conditioned media on primary astrocyte cultures

3.3.1 Astrocyte metabolic activity

The increase on astrocyte proliferation is one of the events associated with reactive astrogliosis, which is widely used as a pathological hallmark of the injured CNS [37]. Microglia cells are the immune regulators of astrogliosis [38], namely by releasing a variety of cytokines [37]. To understand if microglia cultured on different (TMC-CL) topographies can release factors with an impact on astrocytes, astrocyte metabolic activity was assessed after being cultured with microglia conditioned media. Measures of metabolic activity were applied as indicative of cell proliferation.

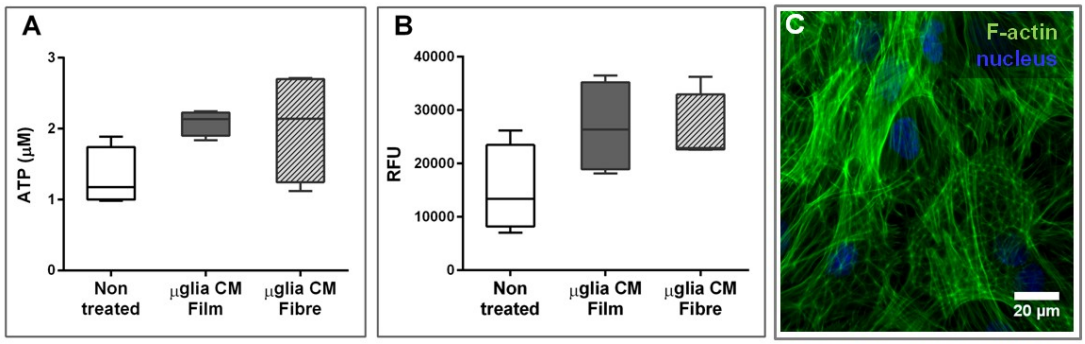

Figure 5. Box-whisker plots (n=4) showing (A) ATP production and (B) resazurin metabolism by astrocytes when in contact with microglia conditioned media (µglia CM) during 24 hrs. The medium was recovered from microglial cultures after 5 days in contact with P(TMC-CL) films or fibres. Non-treated cells were maintained in supplemented DMEM/F12 media. (C) F-actin labelling of astrocytes incubated with microglia conditioned media obtained from cultures on fibrous topography.

Cell metabolic activity of astrocytes when in contact with microglia conditioned media showed a tendency to increase as compared to non-treated cells (Figure 5, A, B). Conditioned media obtained from microglia cultures on P(TMC-CL) fibres or solvent cast films were found to have similar effect on astrocyte metabolic activity (Figure 5, A, B). Comparable results were obtained when astrocyte metabolic activity was assessed after 72 hrs in contact with microglia conditioned media (data not shown). Figure 5, C shows the typical morphology [39] of the astrocytic cell

culture. No alterations were identified after incubating astrocytes with the different microglia conditioned media under investigation.

3.3.2. Astrocyte gene expression

Astrogliosis has been associated to the up-regulation of some genes, namely GFAP and vimentin [13]. Collagen type IV is the main constituent of the glial scar and its expression is increased in astrocytes in response to injury [40].

Astrocyte expression of astrogliosis gene markers was found not to be significantly affected by microglia conditioned media in comparison to non-treated cells (Figure 6). Additionally, the topography of the surface on which microglia was cultured do not shown an effect on GFAP, vimentin, or collagen type IV gene expression.

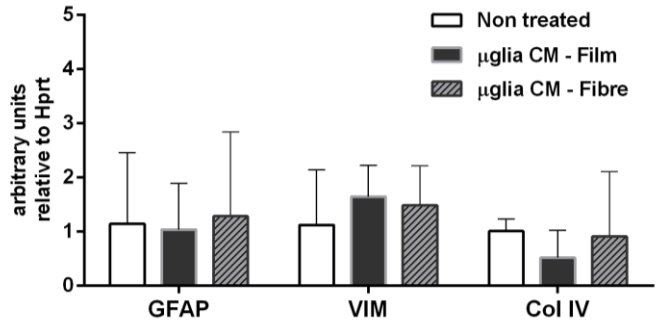

Figure 6. mRNA expression of glial fibrillary acidic protein (GFAP), vimentin (VIM) and collagen type IV (Col IV) on astrocytes when in contact with microglia conditioned media. Conditioned media was obtained from microglia seeded on P(TMC-CL) solvent cast films, or electrospun fibres, after 5 days in culture. Non treated cells were maintained in supplemented DMEM/F12. Bars represent mean values and error bars show standard deviation (n=4).

4. Discussion

In the past few years, the understanding of the role of topographic cues has gained substantial relevance in the context of the design of tissue engineering scaffolds for nerve regeneration. Focus was primarily directed to neuronal cells [7, 9, 11] but more recent studies are contributing to shed some light on the effect of this parameter on other CNS cellular key players, as astrocytes [15-18]. It is known that microglia, the immune cells of the CNS, play a critical role on CNS homeostasis as well as being in the frontline of the tissue response to injury [1]. Particularly, microglia cells can release cytokines and other molecules, activating cells at the lesion site, recruiting others, and modulating its own function in an autocrine effect [38]. However, taking the role of microglia in a lesion scenario into consideration, the impact of the surface properties, in particular of surface topography, on the microglia response has been overlooked at large. This was the main goal of the present study.

As previously reported for other cell types [6], in this work it was shown that microglia organize their cytoskeleton according to the topography of the surface to which they adhere. On P(TMC-CL) solvent cast films, microglia presents a rounder shape and long protrusions, whereas on fibres, cell cytoskeleton elongates along the fibre direction and cell area is smaller. Variations on microglia cell shape have been commonly taken as indication of distinct functional states. Amoeboid features have been traditionally associated with increased phagocytic activity and a pro-inflammatory profile, whereas a ramified morphology has been associated with a quiescent state [35, 36]. The morphological aspects of the microglia seeded on both tested substrates do not show neither the marked amoeboid nor the ramified features. It was demonstrated that cells cultured on P(TMC-CL) films are larger (increased area) and tend to present an increased circularity what can be considered an indication of a more pro-inflammatory phenotype. However, the concentration of TNFα found in the cell culture medium from microglia in contact with these films is low, as compared to the one detected on cultures in contact with electrospun fibres, particularly at day one of culture. These results indicate that when different topographic cues are involved, microglia shape is not a parameter based on which one can directly predict its functional state. A similar issue has been previously raised by Bartneck and colleagues when comparing macrophages cultured on 2D or 3D substrates [41]. The authors claimed that the effect on cell morphology and the expression of surface-markers is strongly affected by the biomaterial where cells adhere to and suggest that, for macrophages in contact with biomaterials, cytokine release should be taken as main criterion instead of surface-markers for macrophage phenotype classification [41]. The analysis of microglia morphology using box counting analysis can, however, bring new insights into this topic. The presented results show that cells seeded on P(TMC-CL) films have a higher complexity comparing to cells on fibres, as measured by DB parameter. It has been suggested that microglia in resting state has an increased complexity [30]. Thus, in the present context, DB is a morphological parameter that better correlates with the cytokine release profile of microglia cultured on the different surface topographies.

Interestingly, the effect of the surface topography on the cytokine release by primary microglia herein reported shows a different trend comparing to that described for macrophages. Previous studies using poly(L-lactide) [42], or poly(ε-caprolactone) [43] demonstrated that the concentration of pro-inflammatory molecules is lower in cultures in contact with electrospun fibrous surfaces, as compared to cells on solvent cast films. Surface topographies that induce macrophage elongation were found to favour macrophage polarization into an anti-inflammatory phenotype, and, although the mechanisms are still not fully described, it was suggested that polarization via topographic signalling is mediated by actin cytoskeleton contractility [44]. The differences found in the present study on microglia behaviour highlight the need for studying microglia in detail. Even though sharing relevant lineage features with macrophages, these cells can react differently to stimuli, as previously reported when testing different chemical factors [33, 45].

In the context of an insult to the CNS, the contribution of microglia to the clearance of debris is of primary importance, as an inefficient removal of myelin debris is associated with the inhibition of

nerve regeneration [3]. It has been demonstrated that myelin phagocytosis is affected by the stimulation of microglia with different cytokines [33]. Thus, in the present work it was investigated whether culturing cells on substrates with a different topography can have an impact on microglia-mediated phagocytosis. A previous report showed that microglia in basal conditions or stimulated with anti-inflammatory cytokines (IL-4 and IL-13) were more efficient on myelin phagocytosis, being found that 70-75% of these cells were able to incorporate myelin in a phagocytosis assay. Conversely, less than 50% of the cells engulfed myelin if stimulated with LPS and interferon-γ [33]. In the context of Alzheimer's disease, it has been demonstrated that the accumulation of pro-inflammatory molecules such as LPS, IL-1β or β-amyloid fibrils induces microglia dysfunction, limiting their phagocytosis activity [46]. In the present study, the percentage of cells that engulfed myelin was found to be above 60% for cultures conducted either on P(TMC-CL) solvent cast films or on fibrous topography. This result suggests that the P(TMC-CL) surfaces provide physical and/or chemical cues that promote phagocytosis without the need of additional chemical stimuli, and may actively contribute for the establishment of a pro-regenerative environment.

Despite the fact that the percentage of cells that engulfed myelin was found not to be influenced by the topographic cues provided by the surface, a remarkable difference was observed on the morphology of microglia when in the presence of myelin. Microglia seeded on P(TMC-CL) films were found to form multinucleated giant cells (MGCs), a phenomenon that was not observed when cells were adhered to fibres. Though the morphology of microglia cells was affected by the surface topography as described above, the formation of MGC was clearly a consequence of the presence of myelin, as this event was not detected in its absence. The role of MGCs derived from microglia has been poorly discussed in the open literature. These cells have been found to accumulate with age [47], being also associated with some neuropathologies, namely HIV-related dementia [48]. Microglia activation to form MGCs can be triggered by inflammatory cytokines [49-51] as well as in response to phagocytosis of cell debris [50, 52]. MGCs have an increased phagocytic activity [52] what could represent an advantage when large amounts of debris accumulate due to Wallerian degeneration. The results obtained in this work do not directly point to an increased percentage of cells engaged in phagocytosis when microglia was cultured in the presence of the P(TMC-CL) films in which MGCs were detected. However, it is important to note that in the calculation of the percentage of cells with engulfed myelin, multinuclear cells were considered as one cellular entity. To the best of our knowledge this is the first study that analyzes the effect of biomaterials on microglia in light of MGC formation. A recent publication using monocyte-derived macrophages demonstrates that orthogonal features on chitosan scaffolds favoured macrophage fusion and MGC formation, comparing to a diagonal architecture [53]. Nonetheless, the authors were able to correlate this effect with the increase of TNFα in the cell culture media. In the present study, the concentration of TNFα when cells were seeded on P(TMC-CL) films was found to be low, suggesting that this cytokine was not involved on the stimulation of MGC formation. It cannot be excluded that concentration of TNFα was altered in the presence of myelin, but if it was the case, it remains to be clarified why only in cells seeded on P(TMC-CL) films. In this context, the topography of the substrate may be influencing directly the

formation of MGCs. In our interpretation of the obtained results, the surface provided by electrospun fibres may be hampering cytoskeleton re-arrangement, cytoplasm enlargement and cell fusion compromising, therefore, the formation of MGC in comparison to what occurs on solvent cast films.

There is increasing evidence that a reciprocal modulation between microglia and astrocytes takes place after CNS injury [54]. Microglia are the first cells arriving to the lesion site and the cytokines released by these cells, namely TNFα and IL-1β, can induce astrocyte proliferation, influencing the glial scar formation [55]. On the other hand, molecules produced by astrocytes are believed to modulate microglia activation in the chronic phase of injury [54]. Taking these aspects into consideration, in this study it was investigated how the response of microglia to different surface topographies can influence astrocyte activation markers. Microglia conditioned media was applied to astrocyte primary cultures and it was found that none of the markers investigated was significantly up-regulated. It is worthwhile mentioning that in these experiments microglia activation with LPS led to a dramatic increase on TNFα concentration in the cell culture medium in comparison to that detected for microglia seeded on P(TMC-CL) fibres or films. This result points to the fact that the amount of TNFα produced by cells when seeded on P(TMC-CL) substrates may not be sufficient to trigger a significant activation of microglia that could, consequently, have an impact on astrocytes. The obtained results are in accordance with a previous study reporting no alteration on astrogliosis markers when astrocytes were treated with conditioned media from resting microglia [56].

5. Conclusion

This work describes for the first time the effect of scaffold surface topography – fibres and flat films – on primary microglia cells. Overall the results presented show that both structures provide topographic cues that can modulate microglia towards a pro-regenerative phenotype, while remarkable differences were found on cell morphology, in line with the topography of the surface. Accordingly, it was pointed out that, when different surface topographies are under investigation, cell behaviour cannot be anticipated from cellular shape. Although TNFα concentration was found to be increased in response to fibrous substrates, overall, the factors released by the cells were not able to trigger astrogliosis, independently of the surface's topography. Noteworthy, a significant percentage of microglia seeded on P(TMC-CL) substrates was found to participate on the phagocytosis of myelin, putting forward these materials as supportive of tissue regeneration in the context of an insult to the CNS.

Acknowledgements

This work was financed by FEDER funds through the Programa Operacional Factores de Competitividade – COMPETE and by Portuguese funds through FCT – Fundação para a Ciência

e a Tecnologia in the framework of the project PEst-C/SAU/LA0002/2011 and PTDC/CTM-NAN/115124/2009. LR Pires and DN Rocha thank FCT for their PhD grants (SFRH / BD / 46015 / 2008 and SFRH / BD / 64079 / 2009). Authors acknowledge the Centro de Materiais da Universidade do Porto (CEMUP; REEQ/1062/CTM/2005 from FCT) for SEM and 1H NMR analysis. The authors wish to thank Renato Socodato for the fruitful discussions.

References

[1] Aguzzi A, Barres BA, Bennett ML. Microglia: Scapegoat, saboteur, or something else? Science. 2013;339:156-61.

[2] David S, Kroner A. Repertoire of microglial and macrophage responses after spinal cord injury. Nat Rev Neurosci. 2011;12:388-99.

[3] Schwab JM, Brechtel K, Mueller CA, Failli V, Kaps HP, Tuli SK, et al. Experimental strategies to promote spinal cord regeneration - An integrative perspective. Prog Neurobiol. 2006;78:91-116.

[4] Hernandez-Ontiveros DG, Tajiri N, Acosta S, Giunta B, Tan J, Borlongan CV. Microglia activation as a biomarker for traumatic brain injury. Front Neurol. 2013;26:30.

[5] Curtis A, Wilkinson C. Topographical control of cells. Biomaterials. 1997;18:1573-83.

[6] Martínez E, Engel E, Planell JA, Samitier J. Effects of artificial micro- and nano-structured surfaces on cell behaviour. Ann Anat. 2009;191:126-35.

[7] Liu T, Houle JD, Xu J, Chan BP, Chew SY. Nanofibrous collagen nerve conduits for spinal cord repair. Tissue Eng Part A. 2012;18:1057-66.

[8] Nisbet DR, Rodda AE, Horne MK, Forsythe JS, Finkelstein DI. Neurite infiltration and cellular response to electrospun polycaprolactone scaffolds implanted into the brain. Biomaterials. 2009;30:4573-80.

[9] Yucel D, Kose GT, Hasirci V. Polyester based nerve guidance conduit design. Biomaterials. 2010;31:1596-603.

[10] Xie J, Willerth SM, Li X, Macewan MR, Rader A, Sakiyama-Elbert SE, et al. The differentiation of embryonic stem cells seeded on electrospun nanofibers into neural lineages. Biomaterials. 2009;30:354-62.

[11] Lim SH, Liu XY, Song H, Yarema KJ, Mao HQ. The effect of nanofiber-guided cell alignment on the preferential differentiation of neural stem cells. Biomaterials. 2010;31:9031-9.

[12] Recknor JB, Sakaguchi DS, Mallapragada SK. Directed growth and selective differentiation of neural progenitor cells on micropatterned polymer substrates. Biomaterials. 2006;27:4098-108.

[13] Pekny M, Nilsson M. Astrocyte activation and reactive gliosis. Glia. 2005;50:427-34.

[14] Chow WN, Simpson DG, Bigbee JW, Colello RJ. Evaluating neuronal and glial growth on electrospun polarized matrices: Bridging the gap in percussive spinal cord injuries. Neuron Glia Biol. 2007;3:119-26.

[15] Cao H, Marcy G, Goh ELK, Wang F, Wang J, Chew SY. The Effects of Nanofiber Topography on Astrocyte Behavior and Gene Silencing Efficiency. Macromol Biosci. 2012;12:666-74.

[16] Min SK, Kim SH, Kim CR, Paik SM, Jung SM, Shin HS. Effect of topography of an electrospun nanofiber on modulation of activity of primary rat astrocytes. Neurosci Lett 2013;534:80-4.

[17] Zuidema JM, Hyzinski-García MC, Van Vlasselaer K, Zaccor NW, Plopper GE, Mongin AA, et al. Enhanced GLT-1 mediated glutamate uptake and migration of primary astrocytes directed by fibronectin-coated electrospun poly-l-lactic acid fibers. Biomaterials. 2014;35:1439-49.

[18] Mattotti M, Alvarez Z, Ortega JA, Planell JA, Engel E, Alcántara S. Inducing functional radial glia-like progenitors from cortical astrocyte cultures using micropatterned PMMA. Biomaterials. 2012;33:1759-70.

[19] Leung BK, Biran R, Underwood CJ, Tresco PA. Characterization of microglial attachment and cytokine release on biomaterials of differing surface chemistry. Biomaterials. 2008;29:3289-97.

[20] Amadio S, De Ninno A, Montilli C, Businaro L, Gerardino A, Volonté C. Plasticity of primary microglia on micropatterned geometries and spontaneous long-distance migration in microfluidic channels. BMC Neurosci. 2013;14.

[21] Persheyev S, Fan Y, Irving A, Rose MJ. BV-2 microglial cells sense micro-nanotextured silicon surface topology. J Biomed Mater Res A. 2011;99 A:135-40.

[22] Minev IR, Moshayedi P, Fawcett JW, Lacour SP. Interaction of glia with a compliant, microstructured silicone surface. Acta Biomater. 2013;9:6936-42.

[23] Pires LR, Guarino V, Oliveira MJ, Ribeiro CC, Barbosa MA, Ambrosio L, et al. Ibuprofen-loaded poly(trimethylene carbonate-co-ε-caprolactone) electrospun fibers for nerve regeneration. J Tissue Eng Regen Med. 2013:Accepted for publication.

[24] Pêgo AP, Poot AA, Grijpma DW, Feijen J. Copolymers of trimethylene carbonate and epsilon-caprolactone for porous nerve guides: Synthesis and properties. J Biomater Sci Polym Ed. 2001;12:35-53.

[25] Pêgo AP, Poot AA, Grijpma DW, Feijen J. Biodegradable elastomeric scaffolds for soft tissue engineering. J Control Release. 2003;87:69-79.

[26] Rocha DN, Brites P, Fonseca C, Pêgo AP. Poly(Trimethylene Carbonate-co-ε-Caprolactone) Promotes Axonal Growth. PLoS One. 2014; 9(2):e88593.

[27] McCarthy K, de Vellis J. Preparation of separate astroglial and oligodendroglial cell cultures from rat cerebral tissue. J Cell Biol. 1980;85:890-902.

[28] Barateiro A, Miron VE, Santos SD, Relvas JB, Fernandes A, ffrench-Constant C, et al. Unconjugated Bilirubin Restricts Oligodendrocyte Differentiation and Axonal Myelination. Mol Neurobiol. 2012:1-13.

[29] Cristóvão AC, Saavedra A, Fonseca CP, Campos F, Duarte EP, Baltazar G. Microglia of rat ventral midbrain recovers its resting state over time in vitro: Let microglia rest before work. J Neurosci Res. 2010;88:552-62.

[30] Karperien A, Ahammer H, Jelinek HF. Quantitating the subtleties of microglial morphology with fractal analysis. Front Cell Neurosci. 2013:1-34.

[31] Chang Y, Lee J, Hsieh C, Hsiao G, Chou D, Sheu J. Inhibitory effects of ketamine on lipopolysaccharide-induced microglial activation. Mediators Inflamm. 2009;2009:705379.

[32] Norton WT, Poduslo SE. Myelination in rat brain: Method of myelin isolation. J Neurochem. 1973;21:749-57.

[33] Durafourt BA, Moore CS, Zammit DA, Johnson TA, Zaguia F, Guiot MC, et al. Comparison of polarization properties of human adult microglia and blood-derived macrophages. Glia. 2012;60:717-27.

[34] Pêgo AP, Vleggeert-Lankamp CLAM, Deenen M, Lakke EAJF, Grijpma DW, Poot AA, et al. Adhesion and growth of human schwann cells on trimethylene carbonate (co)polymers. J Biomed Mater Res A. 2003;67:876-85.

[35] Streit WJ, Walter SA, Pennell NA. Reactive microgliosis. Prog Neurobiol. 1999;57:563-81.

[36] Shechter R, Schwartz M. Harnessing monocyte-derived macrophages to control central nervous system pathologies: No longer if' but how'. J Pathol. 2013;229:332-46.

[37] Sofroniew MV, Vinters HV. Astrocytes: Biology and pathology. Acta Neuropathol. 2010;119:7-35.

[38] Zhang D, Hu X, Qian L, O'Callaghan JP, Hong JS. Astrogliosis in CNS pathologies: Is there a role for microglia? Mol Neurobiol. 2010;41:232-41.

[39] Duarri A, Lopez de Heredia M, Capdevila-Nortes X, Ridder MC, Montolio M, López-Hernández T, et al. Knockdown of MLC1 in primary astrocytes causes cell vacuolation: A MLC disease cell model. Neurobiol Dis. 2011;43:228-38.

[40] Liesi P, Kauppila T. Induction of type IV collagen and other basement-membrane-associated proteins after spinal cord injury of the adult rat may participate in formation of the glial scar. Exp Neurol. 2002;173:31-45.

[41] Bartneck M, Heffels KH, Pan Y, Bovi M, Zwadlo-Klarwasser G, Groll J. Inducing healing-like human primary macrophage phenotypes by 3D hydrogel coated nanofibres. Biomaterials. 2012;33:4136-46.

[42] Saino E, Focarete ML, Gualandi C, Emanuele E, Cornaglia AI, Imbriani M, et al. Effect of electrospun fiber diameter and alignment on macrophage activation and secretion of proinflammatory cytokines and chemokines. Biomacromolecules. 2011;12:1900-11.

[43] Chen S, Jones JA, Xu Y, Low HY, Anderson JM, Leong KW. Characterization of topographical effects on macrophage behavior in a foreign body response model. Biomaterials. 2010;31:3479-91.

[44] McWhorter FY, Wang T, Nguyen P, Chung T, Liu WF. Modulation of macrophage phenotype by cell shape. Proc Natl Acad Sci USA. 2013;110:17253-8.

[45] Lambert C, Ase AR, Séguéla P, Antel JP. Distinct migratory and cytokine responses of human microglia and macrophages to ATP. Brain Behav Immun. 2010;24:1241-8.

[46] Pan XD, Zhu YG, Lin N, Zhang J, Ye QY, Huang HP, et al. Microglial phagocytosis induced by fibrillar β-amyloid is attenuated by oligomeric β-amyloid: Implications for Alzheimer's disease. Mol Neurodegener. 2011;6.

[47] Hart AD, Wyttenbach A, Hugh Perry V, Teeling JL. Age related changes in microglial phenotype vary between CNS regions: Grey versus white matter differences. Brain Behav Immun. 2012;26:754-65.

[48] Tambuyzer BR, Ponsaerts P, Nouwen EJ. Microglia: Gatekeepers of central nervous system immunology. J Leukoc Biol. 2009;85:352-70.

[49] Lively S, Schlichter LC. The microglial activation state regulates migration and roles of matrix-dissolving enzymes for invasion. J Neuroinflam. 2013;10: 75.

[50] Hornik TC, Neniskyte U, Brown GC. Inflammation induces multinucleation of Microglia via PKC inhibition of cytokinesis, generating highly phagocytic multinucleated giant cells. J Neurochem. 2014; 128(5):650-61.

[51] Mosley K, Cuzner ML. Receptor-mediated phagocytosis of myelin by macrophages and microglia: Effect of opsonization and receptor blocking agents. Neurochem Res. 1996;21:481-7.

[52] Beyer M, Gimsa U, Eyüpoglu IY, Hailer NP, Nitsch R. Phagocytosis of neuronal or glial debris by microglial cells: Upregulation of MHC class II expression and multinuclear giant cell formation in vitro. Glia. 2000;31:262-6.

[53] Almeida CR, Serra T, Oliveira MI, Planell JA, Barbosa MA, Navarro M. Impact of 3-D printed PLA- and chitosan-based scaffolds on human monocyte/macrophage responses: Unraveling the effect of 3-D structures on inflammation. Acta Biomater. 2014; 10(2): 613-22.

[54] Gao Z, Zhu Q, Zhang Y, Zhao Y, Cai L, Shields CB, et al. Reciprocal modulation between microglia and astrocyte in reactive gliosis following the CNS injury. Mol Neurobiol. 2013;48:690-701.

[55] Buffo A, Rolando C, Ceruti S. Astrocytes in the damaged brain: Molecular and cellular insights into their reactive response and healing potential. Biochem Pharmacol. 2010;79:77-89.

[56] Röhl C, Lucius R, Sievers J. The effect of activated microglia on astrogliosis parameters in astrocyte cultures. Brain Res. 2007;1129:43-52.

Supporting information

1. Microglial culture purity

The purity of microglial cultures was assessed by immunocytochemistry after labelling the conducted cultures with an antibody against CD11b (Abcam), following the manufacturer instructions. In brief, 24 hrs after seeding, cell culture medium was removed and the cells washed with phosphate buffered saline (PBS). The cells were incubated 20 minutes with CD11b antibody (diluted in DMEM, 1:200) at 37ºC and, subsequently, with the secondary antibody (20 minutes, 1:500, anti-mouse AlexaFluor® 488, Invitrogen). Cells were then fixed using 4% (w/v) paraformaldehyde, permeabilized with Triton X-100 (0.2% (v/v) in PBS) and counterstained with 4',6-diamidino-2-phenylindole (DAPI, 0.1 µg.ml^{-1} in PBS, Sigma). Cells were observed using an inverted fluorescence microscope (Axiovert, Zeiss) and the percentage of CD11b+ cells was calculated relative to the total number of cells (number of nuclei labelled with DAPI) and found to be above 90% (Figure 1, A).

Microglia cultures were also labelled for glial fibrilary acidic protein (GFAP) antibody in order to assess possible culture contamination with astrocytes. In brief, after fixation, cells were permeabilized 0.2% (v/v) Triton X-100 solution containing 5% (v/v) of normal goat serum (NGS, Sigma-Aldrich) during 30 minutes. Afterwards an anti-GFAP (Dako, 1:500) solution containing 1% (v/v) NGS and 0.15% (v/v) Triton X-100 was added and incubated overnight at 4°C. After washing with PBS (three times, 5 minutes), the cells were incubated with anti-rabbit AlexaFluor® 568 (Invitrogen) for 1 hr at room temperature. Cells were thereafter counterstained with DAPI as described above. The occurrence of GFAP positive cells was rare, consisting in less than 5% of the total number of cells (Figure 1, B).

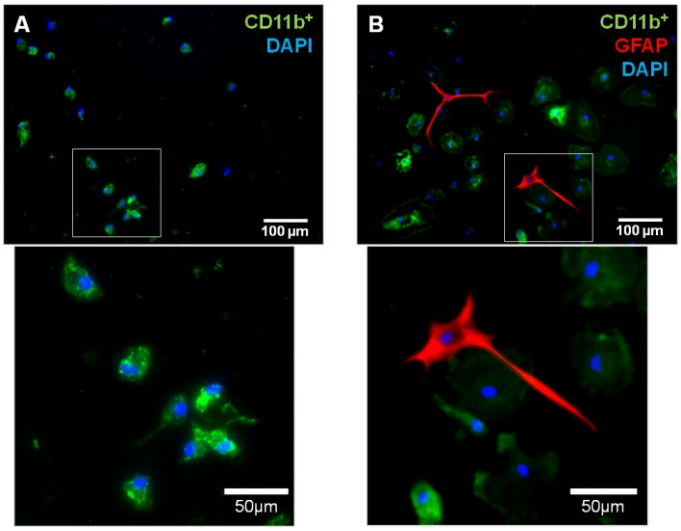

Figure 1. Microglia cultures immunolabelling. (A) CD11b^{+} cell detection or (B) combined with GFAP, an astrocytic marker.

2. Primer sequences applied in RT-PCR

Primer sequences used for RT-PCR were as follows:

GFAP sense	5'AGGCTGGAGGCGGAGAAC3'
GFAP anti-sense	5'GCTGTGAGGTCTGGCTTGG3'
Vimentin sense	5'CGTGATGTCCGCCAGCAGTATG3'
Vimentin anti-sense	5'GGCATCCACTTCGCAGGTGAG3'
Collagen IV sense	5'AAGGCGAGGAAGGCATCATG3'
Collagen IV anti-sense	5'GGGTGAGTAGGCTGGAGGTC3'
Hprt sense	5'ATGGACTGATTATGGACAGGACTG3'
Hprt anti-sense	5'GCAGGTCAGCAAAGAACTTATAGC3'

CHAPTER IV

Ibuprofen-loaded poly(trimethylene carbonate-co-ε-caprolactone) electrospun fibres for nerve regeneration*

Liliana R Pires[1, 2], Vincenzo Guarino[3], Maria J Oliveira[1, 4], Cristina C Ribeiro[1,5], Mário A Barbosa[1, 2, 6], Luigi Ambrosio[3], Ana Paula Pêgo[1, 2, 6]

1 – INEB – Instituto de Engenharia Biomédica, Universidade do Porto, Rua do Campo Alegre 823, 4150-180 Porto, Portugal.

2 – Universidade do Porto – Faculdade de Engenharia, Rua Roberto Frias, s/n, 4200-465 Porto, Portugal.

3 – Institute of Composite and Biomedical Materials, National Research Council, P. le Tecchio 80, 80125 Naples, Italy.

4 – Departamento de Patologia e Oncologia- Faculdade de Medicina- Universidade do Porto – Alameda Prof. Hernâni Monteiro, 4200-319 Porto, Portugal.

5 – ISEP – Instituto Superior de Engenharia do Porto, Departamento de Física, Porto, Portugal.

6 – Universidade do Porto – Instituto de Ciências Biomédicas Abel Salazar, Rua de Jorge Viterbo Ferreira 228, 4050-313 Porto, Portugal.

** Journal of Tissue Engineering and Regenerative Medicine in press (DOI: 10.1002/term.1792)*

Abstract

The development of scaffolds that combine the delivery of drugs with the physical support provided by electrospun fibres holds great potential in the field of nerve regeneration. Here it is proposed the incorporation of ibuprofen, a well-known non-steroidal anti-inflammatory drug, in electrospun fibres of the statistical copolymer poly(trimethylene carbonate-co-ε-caprolactone) [P(TMC-CL)] to serve as a drug delivery system to enhance axonal regeneration in the context of a spinal cord lesion, by limiting the inflammatory response. P(TMC-CL) fibres were electrospun from mixtures of dichloromethane (DCM) and dimethylformamide (DMF). The solvent mixture applied influenced fibre morphology, as well as mean fibre diameter, which decreased as the DMF content in solution increased. Ibuprofen-loaded fibres were prepared from P(TMC-CL) solutions containing 5% ibuprofen (w/w of polymer). Increasing drug content to 10% led to jet instability, resulting in the formation of a less homogeneous fibrous mesh. Under the optimized conditions, drug-loading efficiency was above 80%. Confocal Raman mapping showed no preferential distribution of ibuprofen in P(TMC-CL) fibres. Under physiological conditions ibuprofen was released in 24 h. The release process being diffusion-dependent for fibres prepared from DCM solutions, in contrast to fibres prepared from DCM–DMF mixtures where burst release occurred. The biological activity of the drug released was demonstrated using human-derived macrophages. The release of prostaglandin E2 to the cell culture medium was reduced when cells were incubated with ibuprofen-loaded P(TMC-CL) fibres, confirming the biological significance of the drug delivery strategy presented. Overall, this study constitutes an important contribution to the design of a P(TMC-CL)-based nerve conduit with anti-inflammatory properties.

Keywords

Confocal Raman microscopy; drug delivery; electrospinning; ibuprofen; inflammation; nerve guide

1. Introduction

The first patent on electrospinning dates from 1934 by Formhals (1934). More recently, the technique was 'reinvented', becoming very popular for the preparation of tissue engineering scaffolds (Martins et al., 2007; Agarwal et al., 2009). Electrospinning allows the fabrication of nanofibrous scaffolds that can emulate the extracellular matrix, providing a biomimetic environment for cell growth, polarization and differentiation. In addition, a number of parameters in the electrospinning setup can be adjusted in order to modulate fibre diameter and orientation, as well as scaffold size and shape. The possibility of preparing aligned fibres has been especially explored in the context of nerve repair (Xie et al., 2010; Lee and Arinzeh, 2011). Previous reports show that neurons align their cellular processes in the direction of electrospun fibres *in vitro* (Corey et al., 2007; Yao et al., 2009). A similar outcome was observed *in vivo*, both in the peripheral (Yu et al., 2011; Jiang et al., 2012) and in the central nervous system (Hurtado et al., 2011). Electrospun scaffolds can also serve as drug delivery devices. Owing to the versatility of the electrospinning technique, different types of molecules can be incorporated in fibres. For nerve regeneration applications, fibres have been loaded with neurotrophins (Chew et al., 2005; Liu et al., 2012) or drugs, like 6-aminonicotinamide, known to limit astrocyte proliferation (Schaub and Gilbert, 2011). To promote central nervous system regeneration, the combination of nanofibrous scaffolds with molecules that can locally hinder the inhibitory environment after a lesion is of particular interest (Liu et al., 2012).

Inflammation is one of the secondary events activated after a central nervous system lesion and one of the most relevant targets in nerve regeneration strategies (Thuret et al., 2006; Fitch and Silver, 2008). Although the role of inflammation in central nervous system regeneration is currently an issue of active debate (Chan, 2008; Schwartz et al., 2009), the results of clinical trials that involved assessment of drugs with described anti-inflammatory properties, namely the antibiotic minocycline (Casha et al., 2012), support strategies targeting the modulation of the inflammatory response.

This report proposes the incorporation of ibuprofen in electrospun fibres as a drug delivery system to enhance axonal regeneration in the context of a spinal cord lesion by limiting the inflammatory response. Ibuprofen is a non-steroidal anti-inflammatory drug and its action is attributed to the inhibitory effect on cyclooxygenase (COX). This enzyme is responsible for the conversion of arachidonic acid in prostaglandins, the latter being associated with pain, fever and acute inflammatory reaction (Mitchell et al., 1993; Rainsford, 2009). In addition to the classical view of the action of ibuprofen, the release of prostaglandin E2 (PGE_2) has been more recently associated with neuropathic pain after spinal cord injury (Zhao et al., 2007). Consequently, targeting the COX pathway is currently indicated as a new avenue to treat this condition (Ma et al., 2012), providing added value to the strategy proposed in this manuscript.

Poly(trimethylene carbonate-co-ε-caprolactone) [P(TMC-CL)] is a biodegradable elastomer previously studied in the field of nerve regeneration research. The polymer possesses mechanical properties and a degradation profile appropriate to serve as nerve conduit (Pêgo et al., 2001,

2003) and it has shown to be able to support peripheral nerve regeneration *in vivo* (Vleggeert-Lankamp et al., 2008). In the present work, it is proposed that P(TMC-CL) serve as polymeric matrix for the delivery of ibuprofen. The optimization of electrospun P(TMC-CL) fibre preparation, the incorporation of the drug and its release profile and bioactivity are investigated.

2. Materials and methods

2.1. Polymer synthesis

Poly(trimethylene carbonate-co-ε-caprolactone) was prepared by ring-opening polymerization as previously described (Pêgo et al., 2001). In brief, ε-caprolactone (CL) (Merck, Darmstadt, Germany) was dried overnight (calcium hydride; Sigma-Aldrich Química, Sintra, Portugal) and distilled before the polymerization with trimethylene carbonate (TMC, used as received from Boehringer Ingelheim, Ingelheim am Rhein, Germany). Polymerization was carried out in evacuated and sealed glass ampoules using stannous octoate (Sigma-Aldrich) as catalyst (2×10^{-4} mol per mol of monomer). After 3 days of reaction at 130 °C the polymer obtained was purified by dissolution in chloroform (BDH-Prolabo, Carnaxide, Portugal) and subsequent precipitation into a tenfold volume of ethanol (96%, v/v; AGA, Prior Velho, Portugal). The chemical composition of the copolymer was assessed by ^{1}H nuclear magnetic resonance (NMR) and found to contain 11% mol of TMC, which is in accord with the monomer ratio charged (10% mol TMC). The molecular weight of the obtained polymer was determined by size exclusion chromatography using chloroform as the mobile phase. The average weight molecular weight was found to be 8.2×10^{4} g/mol and the polydispersity index was 1.61.

2.2. P(TMC-CL) and ibuprofen-loaded P(TMC-CL) fibre preparation by electrospinning

Initially, a range of electrospinning parameters was assessed. The parameters tested included polymer concentration in the electrospun solution (6–10%, w/v), polymer solvent [dichloromethane (DCM; Merck), chloroform (Sigma-Aldrich) and N,N-dimethylformamide (DMF), Merck)], flow rate (0.1–1.5ml/h), and electric field applied (0.5–1 kV /cm). Based on the morphology of the fibres obtained (data not shown) the selected conditions for the subsequent experiments were: P(TMC-CL) solutions (10%, w/v) dispensed at a flow rate of 1ml/h using a syringe pump (Ugo Basile, Italy); an electric field (Gamma High Voltage source; Ormond Beach, FL, USA) of 1 kV/cm applied between the spinneret (inner diameter 0.8mm) and a flat copper plate (15×15 cm) separated by 14 cm; DCM and DMF mixtures used as solvent at the volume ratios of 1:0, 6:1, 3:1 and 1:1. Fibres were collected into an aluminium foil for 1–1.5 h. After vacuum drying (vacuum oven, Raypa, Barcelona, Spain) for 24 h, 14mm discs were punched out from the electrospun membranes and stored at room temperature (20-25 °C) until further use.

Ibuprofen-loaded fibres were obtained by adding 5% and 10% of ibuprofen powder (w/w of polymer) to the polymer solution 5 h before electrospinning. Pharmaceutical grade ibuprofen (purity>99%) was kindly supplied by Sérgio Simões (Bluepharma, Coimbra, Portugal).

2.3. Fibre characterization

2.3.1. Fibre morphology

Fibre morphology was analysed by scanning electron microscopy (SEM). A low vacuum (5 kV) Phenom™ G2 (Phenom-World, Eindhoven, the Netherlands) and a Quanta 400FEG ESEM (FEI, Eindhoven, the Netherlands) microscopes were used. Fibre diameter was quantified from SEM micrographs using image analysis software (Image J, version 1.39; NIH, Bethesda, MD, USA). Fibre mean diameter and fibre diameter distribution were calculated from at least 100 measurements from three independent samples.

2.3.2. Drug loading efficiency

^{1}H NMR spectroscopy was used in order to quantify ibuprofen in the P(TMC-CL) electrospun meshes. The analyses were performed in an AVANCE III 400 spectrometer (Bruker Corporation, Barcelona, Spain), operating at 400MHz. The ^{1}H chemical shifts were internally referenced to the tetramethylsilane (TMS; Eurisotop, Saint-Aubin, France) signal (0.00 ppm) for spectra recorded in $CDCl_3$ (Sigma-Aldrich). Ibuprofen-loaded P(TMC-CL) fibres were dissolved in $CDCl_3$ before analysis. Characteristic peaks from ibuprofen and P(TMC-CL) were used to identify both species. The drug loading efficiency was calculated from the ratio between the area of the signal at δ=2.45 ppm corresponding to the CH_2 group of ibuprofen (2H), and the area of the peak corresponding to the resonance of the α-methylene (δ=2.30, 2H, CH_2) of polymeric caprolactone.

2.3.3. Ibuprofen distribution in P(TMC-CL) fibres

Ibuprofen powder and P(TMC-CL) fibres prepared from 1:0 and 3:1 DCM–DMF mixtures with and without ibuprofen incorporated (5%, w/w, of polymer) were analysed using Fourier transform infrared spectroscopy (FTIR) and confocal Raman microscopy.

The FTIR characterization was performed using a Perkin Elmer 2000 spectrometer (Perkin Elmer, Waltham, MA, USA) and an attenuated total reflectance (ATR) accessory (SplitPea™; Harrick Scientific, Pleasantville, NY USA), provided with a silicon internal reflection element and configured for external reflectance mode, where the spectra were acquired from a 200 μm diameter sampling area. A nitrogen purge was performed before each experiment. All samples were run at a spectral resolution of 4/cm and 200 scans were accumulated in order to obtain a high signal-to-noise level. The band at 1675–1775/cm was deconvoluted by applying the derivative and curve fitting algorithms using PEAKFIT from AISN Software (Florence, Oregon,

USA). Initial peak positions were obtained from second derivative spectra of the raw data. A Lorentzian band-shape was used to fit the contours.

Confocal Raman microscopy analyses were performed using a LabRAM HR 800 confocal Raman microscope system (Horiba Jobin Yvon, Lille, France) comprising a spectrometer and a fully integrated Olympus BX41 confocal microscope (Olympus Iberia, S.A.U., Lisboa, Portugal). Raman spectra were generated using a 514 nm laser diode as excitation source, focused on the sample with a x100 objective, a confocal hole of 100 μm and an exposure time of 100 s. For the experimental setup used, the spatial resolution is between 0.5 μm and 1 μm. The scattered light was dispersed by a grating with 1800 lines/mm (Jobin-Yvon) at 4/cm spectral resolution. Spectral analysis was carried out using LABSPEC5 software (Horiba Jobin Yvon). Imaging experiments on fibres were performed by scanning the laser beam over the region of interest and accumulating a full Raman spectrum at each pixel. Raman images were constructed by plotting the integrated intensity of the vibrational bands of interest as a function of position. For these experiments, fibres with a diameter > 2 μm were selected and step size for data acquisition was approximately 0.6 μm. The spectral range measured was 1400–1800/cm and the mapping area varied according to the fibre dimension.

2.4. Drug-release studies

The amount of ibuprofen released from the electrospun P(TMC-CL) fibres was evaluated as follows. Samples loaded with 5% of ibuprofen (w/w of polymer) were incubated at 37 °C and 120 rpm (Orbital Shaker Oven; IKA, Staufen, Germany) in phosphate buffered saline (PBS) at the final concentration of 5 mg/ml (mass of fibres/volume of PBS). At defined time-points (0.5, 1, 2, 4, 6, 8, and 24 h) the releasing medium was refreshed. Ultraviolet/ visible spectroscopy (UV/Vis) at 230nm (SynergyMx; Biotek, Carnaxide, Portugal) was used to monitor the amount of ibuprofen released. Values were interpolated from an ibuprofen calibration curve (see the Supporting Information, Figure S4). Cumulative release was calculated relative to the maximum loading of 5% (w/w of polymer). The drug release kinetics was analysed using the Higuchi simplified model:

$$M_t = M_\infty = k\sqrt{t} \quad (1)$$

where M_t/M_∞ represents cumulative ibuprofen release, t is time of incubation and k is a constant reflecting the design variables of the system (Siepmann and Peppas, 2001).

2.5. Biological effect of ibuprofen on human macrophages

2.5.1. Peripheral blood-derived monocyte isolation

Human peripheral blood-derived monocytes were isolated from Buffy coats (kindly donated by Instituto Português do Sangue, Porto, Portugal) by negative selection using Rosettesep™ (StemCell Technologies, Grenoble, France) as previously described (Oliveira et al., 2012). A day after isolation, adherent cells were collected applying a 5mM solution of ethylenediamine

tetraacetic acid (EDTA; BDH-Prolabo) and reseeded on glass coverslips at a cell density of 1.25×10^5 cells/cm^2. The cell population contained >70% of CD14 positive cells and no contamination by CD3-positive T lymphocytes, as determined by flow cytometry (Oliveira et al., 2012). Cells were allowed to differentiate in RPMI medium (Gibco, Life technologies S.A., Madrid, Spain) supplemented with 10% of heat-inactivated (56 °C, 30 min) fetal bovine serum (Lonza, Barcelona, Spain) for additional 8 days. Ten days after isolation, monocyte-derived macrophages were stimulated with 10 ng/ml lipopolysaccharide (LPS; Sigma) for 72 h. Specific cell treatments were performed after LPS activation.

2.5.2. Cell culture

The effect of ibuprofen on macrophage metabolic activity was assessed by means of a resazurin-based assay. In brief, different ibuprofen solutions in ethanol–water mixtures (7:3) were prepared and added (5 µl) to the cell culture media (500 µl) in order to obtain a final drug concentration ranging from 0.001 mg/ml to 1 mg/ml. Cell metabolic activity was evaluated at 24 h and 72 h after treatment. At the defined time-point cells were incubated (4 h, 37 °C) with a resazurin (Sigma-Aldrich) solution (0.1mg/ml, in PBS) and the fluorescence (λex=530nm, λem=590nm) in the cell culture medium was measured (SynergyMx; Biotek). Results are represented as percentage of cell viability relative to cells treated with equal volume of the ibuprofen solvent (5 µl).

In order to evaluate the bioactivity of ibuprofen released from P(TMC-CL) electrospun fibres, fibre discs (14mm) were incubated with macrophages for 72 h. The fibres tested were prepared from 1:0 DCM–DMF solutions loaded with 5% ibuprofen (w/w of polymer). The punched discs weighed between 0.9 mg and 3 mg. Fibre sterilization was performed by irradiating (gamma rays, 25 kGy, ^{60}Co source) samples previously packed under vacuum. Fibre discs were suspended in the well without direct contact with the cells. Macrophages treated with ibuprofen in the medium (final concentration 0.1mg/ml), as well as cells cultured in presence of unloaded P(TMC-CL) fibres, were used as control.

2.5.3. Immunofluorescence

To analyse cell morphology, macrophages were fixed with 4% (w/v) paraformaldehyde (Merck) and immunostained for α-tubulin and F-actin as follows. Cell external fluorescence was quenched by treating the cells with 50mM NH_4Cl for 10 min. Subsequently, cells were permeabilized with 0.1% (v/v) Triton X-100 (in PBS) for 5 min. After washing with PBS, cells were incubated with 5% (w/v) bovine serum albumin (BSA; Sigma-Aldrich) in PBS for 30 min and, thereafter, incubated with the primary antibody mouse anti-α-tubulin (1:4000; Sigma-Aldrich) for 1 h. Subsequently, cells were thoroughly washed and incubated with Alexa Fluor 594 goat anti-mouse IgG (1:1000; Invitrogen, Life technologies Madrid, Spain) for 45 min. F-actin was stained for 15 min using 5 µM Phalloidin-FITC (Sigma-Aldrich). Cells were washed with PBS and mounted on Vectashield with 4′,6- diamidino-2-phenylindole (DAPI; Vector Laboratories, Peterborough, UK). Samples were

observed under an inverted fluorescence microscope (Axiovert 200; Zeiss, Oberkochen, Germany).

2.5.4. PGE_2 and quantification of cytokines

At the defined time-point (72 h after treatment), cell culture supernatants were collected and, after centrifugation (16000 g, 4 °C, 10min) to remove cell debris, stored at –20 °C for posterior analysis. The concentration in the cell culture supernatant of PGE_2 (Cayman Chemical, Ann Arbor, MI, USA), interleukin 6 (IL-6), IL-10 and tumour necrosis factor-α (TNFα) were quantified by enzyme-linked immunosorbent assay (ELISA; Biolegend, San Diego, CA, USA) following the manufacturer's instructions. Results are presented normalized for the total protein content in the cell culture medium, as determined by the DC protein assay (Bio-Rad, Amadora, Portugal).

2.6. Statistical analysis

Statistical analysis was performed using PRISM 5.0 software (GraphPad, La Jolla, CA, USA). Statistical differences between two groups were calculated applying a t-test when analysing results from PGE_2 and release of cytokines. Mean fibre diameters obtained when using different solvent combinations loaded or unloaded with ibuprofen were analysed using non-parametric Kruskal–Wallis test and Bonferroni correction for multiple comparisons. A p-value lower than 0.05 was considered statistically significant.

3. Results

3.1. Characterization of P(TMC-CL) and ibuprofen-loaded P(TMC-CL) fibres

3.1.1. Fibre morphology

The influence of solvent composition on P(TMC-CL) fibre morphology was evaluated by testing different DCM–DMF mixtures (Figure 1, Table 1). Fibres prepared from 1:0 DCM–DMF solutions showed a broad diameter distribution. Improved homogeneity of the fibres was observed when increasing the DMF fraction in solution, as shown by the narrowing of the fibre diameter distribution (Figure 1). The fibre mean diameter was found to be 1.09±0.10 μm for fibres prepared from 1:0 DCM–DMF solutions, decreasing to 0.48±0.03 μm for fibres prepared from 1:1 DCM–DMF solutions (Table 1).

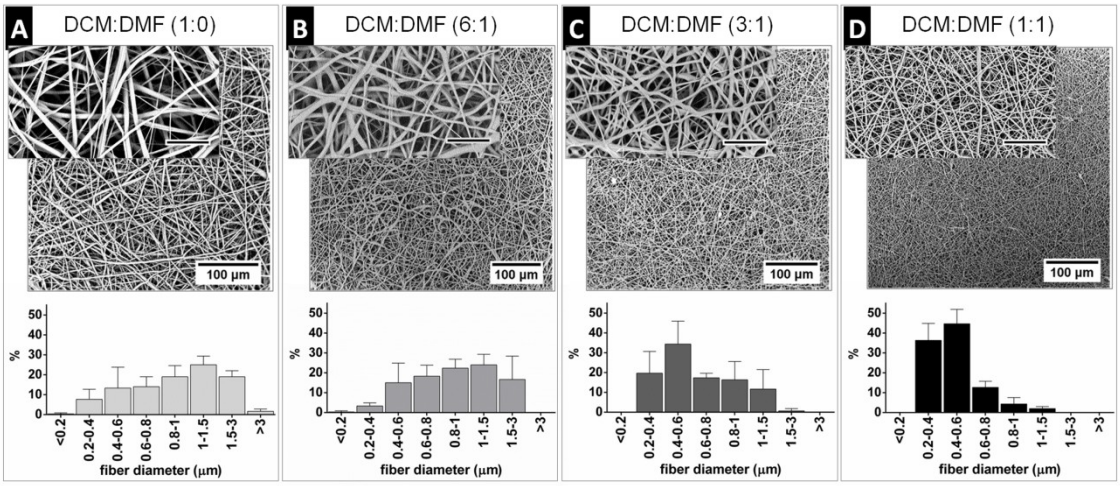

Figure 1. Representative scanning electron microscopy photomicrographs of poly(trimethylene carbonate-co-ε-caprolactone) [P(TMC-CL)] fibres and fibre diameter distribution (n=3). Samples were prepared using P(TMC-CL) solutions in a dichloromethane (DCM)–N,N-dimethylformamide (DMF) mixture with increasing amounts of DMF: **(A)** 1:0 DCM–DMF; **(B)** 6:1 DCM–DMF; **(C)** 3:1 DCM–DMF; **(D)** 1:1 DCM–DMF. Higher magnification images scale bar=20 µm.

Table 1: Poly(trimethylene carbonate-co-ε-caprolactone) [P(TMC-CL)] electrospun fibres diameter.

	Fibre diameter (µm)			
	1:0 DCM-DMF	6:1 DCM-DMF	3:1 DCM-DMF	1:1 DCM-DMF
Non-loaded	1.09 ± 0.10	1.02 ± 0.19	0.67 ± 0.12	0.48 ± 0.03
Ibuprofen 5%	0.84 ± 0.08	0.91 ± 0.09	0.76 ± 0.06	–
Ibuprofen 10%	1.2 ± 0.05	0.91 ± 0.2	0.84 ± 0.12	–

Mean diameter ± standard deviation (n=3) of P(TMC-CL) fibres prepared from dichloromethane (DCM)–N,N-dimethylformamide (DMF) solutions at ratios of 1:0, 6:1, 3:1 and 1:1 in the absence or presence of 5% and 10% of ibuprofen (w/w of polymer), respectively. Standard deviation represents variability between different samples.

Ibuprofen-loaded P(TMC-CL) fibres were prepared by adding 5 % and 10 % of the drug (w/w of polymer) to the polymer solution before electrospinning. Electrospinning parameters applied were the same as those optimized for the preparation of the non-loaded fibres. When 5% of ibuprofen (w/w of polymer) was added to the P(TMC-CL) solution, smaller fibres were formed, as indicated by the decrease in mean fibre diameter in comparison with unloaded fibres (Table 1). When analysing the effect of the solvent composition on the morphology of 5% ibuprofen-loaded fibres, under the conditions tested, fibres prepared from 1:1 DCM–DMF solutions fused (Figure 2). For this reason, a 1:1 DCM–DMF solutions was not tested for 10% ibuprofen loaded fibres. No significant differences in terms of mean fibre diameter were detected when comparing loaded fibres prepared from 1:0, 6:1 and 3:1 DCM–DMF solutions. However, in terms of fibre diameter distribution a higher percentage of bigger fibres (> 3 µm) were formed from 1:0 DCM–DMF

solutions (Figure 2). When fibres were prepared from solutions with 10% ibuprofen (w/w of polymer), the high drug content led to jet instability, resulting in a less homogeneous fibre mesh.

Under these conditions a tendency towards the formation of defects and large-diameter fibres was observed, as indicated by the fibre diameter distribution graphs (Figure 2), albeit the mean fibre diameter was not remarkably affected (Table 1). For fibres prepared from 3:1 DCM–DMF solutions, in particular, fusion of the deposited fibres was also observed.

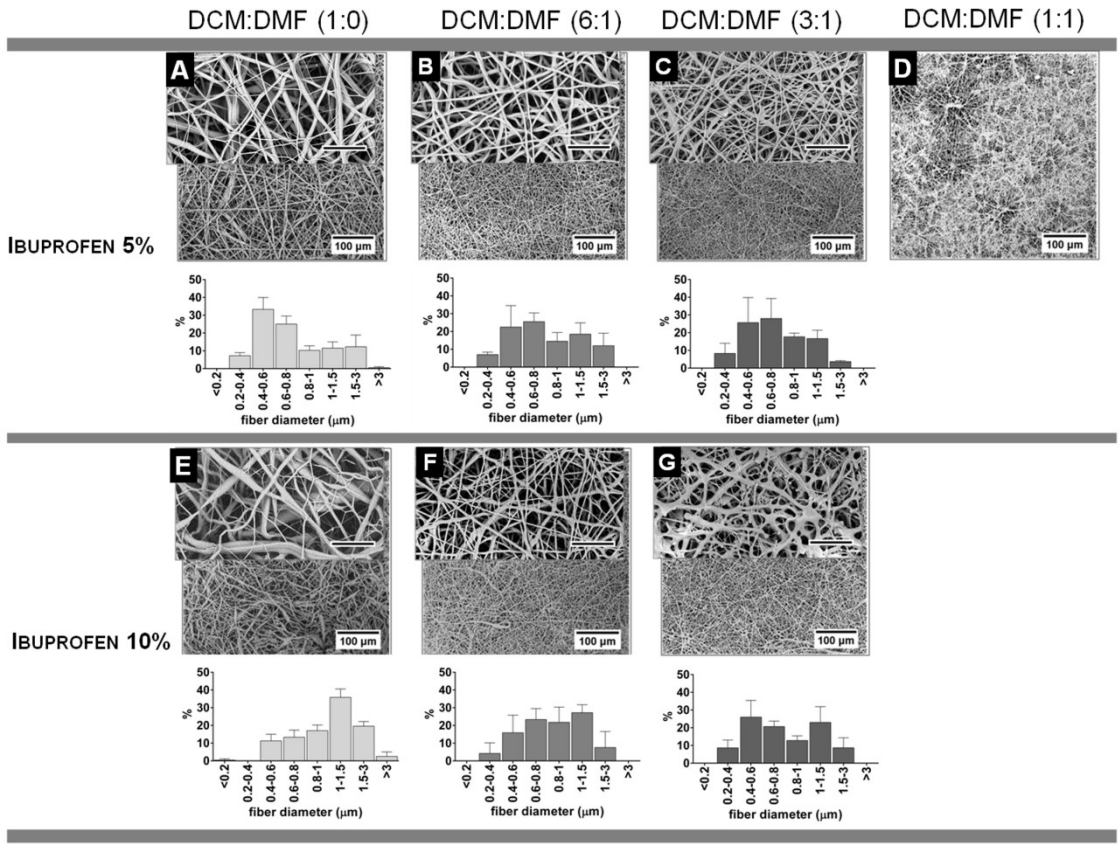

Figure 2. Scanning electron microscopy photomicrographs of ibuprofen-loaded poly(trimethylene carbonate-co-ε-caprolactone) [P(TMC-CL)] fibres and respective fibre diameter distribution (n=3). Fibres were obtained from solutions containing 5% **(A–D)** and 10% **(E–G)** of ibuprofen (w/w of polymer) and applying different dichloromethane (DCM)–N,N-dimethylformamide (DMF) mixtures as solvent: **(A,E)** 1:0 DCM–DMF; **(B,F)** 6:1 DCM–DMF; **(C,G)** 3:1 DCM–DMF; **(D)** 1:1 DCM–DMF. Higher magnification images scale bar=20 µm.

3.1.2. Drug loading and distribution

The chemical composition of ibuprofen-loaded P(TMC-CL) fibres was analysed by means of three spectroscopic techniques: ^{1}H NMR, ATR-FTIR and Raman.

By ^{1}H NMR spectroscopy, ibuprofen was clearly distinguished from P(TMC-CL) signals (see the Supporting information, Figure S1). The amount of drug relative to the polymer was quantified using this technique. It was found that in the 5% ibuprofen (w/w of polymer) loaded P(TMC-CL) fibres the actual loading was 4.21±0.02 % (w/w of polymer; n=3), corresponding to a loading efficiency of over 80%.

As NMR provides information about the bulk chemical composition of the prepared samples, to obtain complementary chemical characterization of the fibres, these were also analysed by ATR-FTIR. Figure 3A shows the spectra of ibuprofen-loaded P(TMC-CL) fibres prepared from 1:0 DMC-DMF solution, unloaded fibres and ibuprofen powder. The most intense bands of ibuprofen are located at 2955, 1721 and 1231/cm, being assigned to CH_3 asymmetric stretching, C=O stretching and C–C stretching, respectively (see full FTIR spectra in Figure S2). These bands cannot be distinguished in the ibuprofen-loaded fibres because of overlapping with the polymer signals. Although weak, the band corresponding to the aromatic C=C stretching vibration of ibuprofen (1509/cm) can be identified in the ibuprofen-loaded P(TMC-CL) fibre spectrum, confirming the presence of the drug in the fibres (Figure 3A). In order to identify the presence of subtle spectral changes in the region of the most intense bands of ibuprofen and P(TMC-CL) (1670–1800/cm) a second derivatization and curve fitting of the raw data was performed. Figure 3AI, AII shows that the number of bands in that particular zone of the spectrum increases in the loaded polymer samples further supporting the presence of ibuprofen in the fibres. Analysis of the ibuprofen-loaded P(TMC-CL) spectrum compared with those of P(TMC-CL) and ibuprofen showed no differences other than the characteristic bands of the starting materials, suggesting that no chemical interaction between ibuprofen and the polymer occurred. ATR-FTIR analysis of P(TMC-CL) fibres prepared from 3:1 DCM–DMF solutions was also performed and similar spectra were obtained.

As a complementary technique to FTIR P(TMC-CL), individual fibres were analysed by confocal Raman spectroscopy. By using this technique it was possible to identify the C–C stretching (1610/cm) on the fingerprint region of ibuprofen (Figure 3B). The presence of this clear marker band allowed the use of Raman mapping to determine and compare the spatial distribution of ibuprofen in P(TMC-CL) fibres prepared with 1:0 and 3:1 DCM–DMF solutions. Data was acquired on an area of the fibre as shown in Figure 3CI, DI. Mapping was performed by rationing the ibuprofen fingerprint region to the background signal in two different spectral regions: 1510–1525/cm and 1645–1665/cm. Regions with high concentration of ibuprofen are depicted in bright green, while regions with low ibuprofen concentration are shown in black (see Figure 3E). Although drug distribution is not completely homogeneous, results show no preferential distribution of the drug at fibre edges or in the centre for both ibuprofen containing fibres prepared from 1:0 and 3:1 DCM–DMF P(TMC-CL) solutions (Figure 3 (CII, DII)).

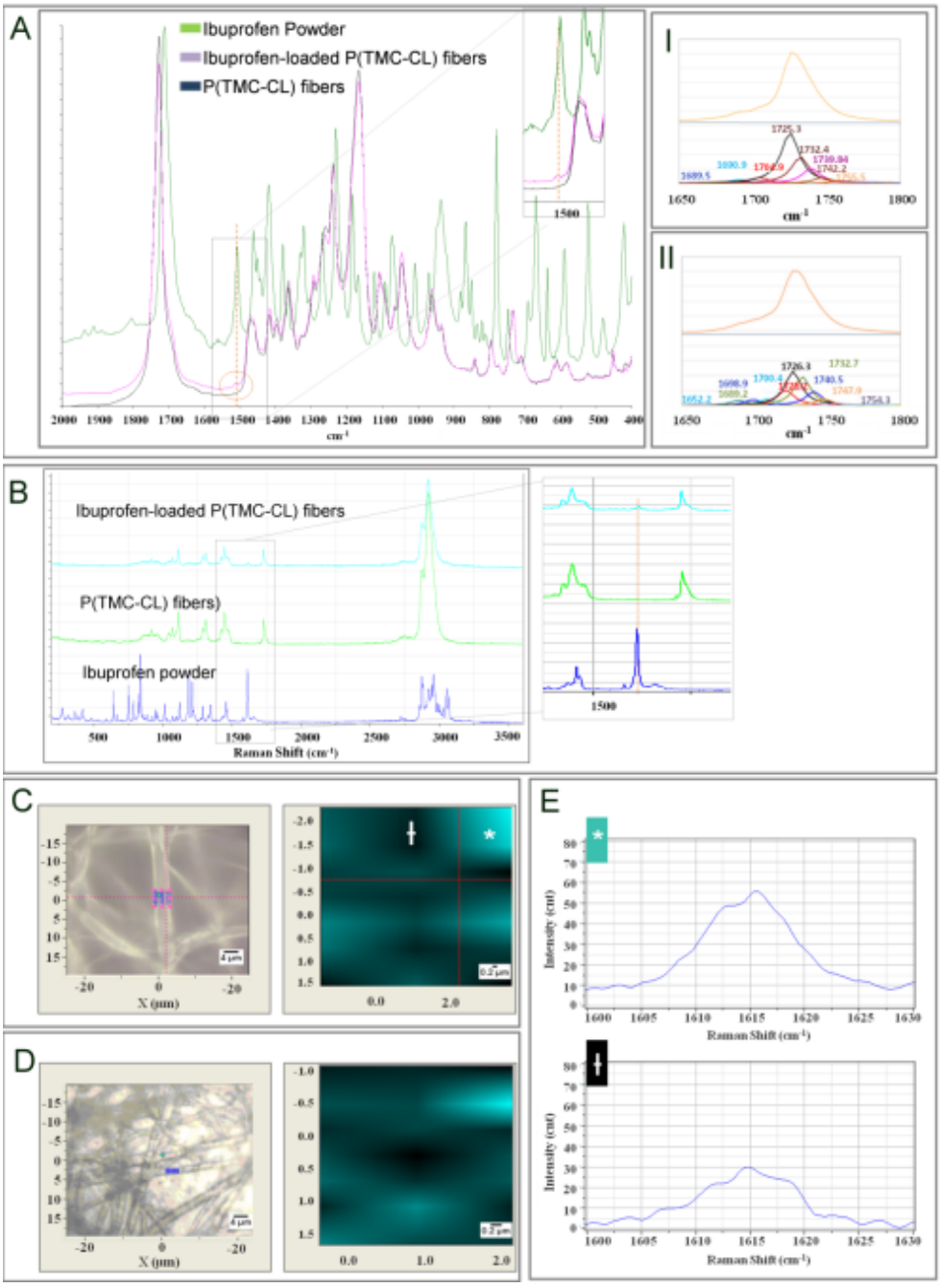

Figure 3. (A) Attenuated total reflectance–Fourier transform infrared spectroscopy spectrum of ibuprofen-loaded poly(trimethylene carbonate-co-ϵ-caprolactone) [P(TMC-CL)] fibres prepared from 1:0 dichloromethane (DCM)–N,N-dimethylformamide (DMF) solutions (pink). The spectra of ibuprofen (in green) and non-loaded fibres (blue) is shown for comparison. Curve fitting in the spectral region between 1670/cm and 1800/cm of **(I)** P(TMC-CL) fibres and **(II)** ibuprofen-loaded P(TMC-CL) fibres. **(B)** Raman spectra of ibuprofen (dark blue), P(TMC-CL) fibres (green), and ibuprofen-loaded P(TMC-CL) fibres (light blue) obtained from 1:0 DCM–DMF solutions. **(C, D)** Confocal Raman microscopy analysis of ibuprofen-loaded P(TMC-CL) fibres. **(I)** In images blue indicates the region analysed from ibuprofen-loaded P(TMC-CL) fibres prepared from **(C)** 1:0 DCM–DMF and **(D)** 3:1 DCM–DMF solutions, respectively (axis indicates distance in µm). **(II)** For each sample the mapping of the 1610/cm ibuprofen Raman band relative to background bands (1510–1525/cm and 1645–1665/cm; axis indicates distance in µm) is presented. These are representative images from three different areas analysed. The overlay of the spectra obtained for each point is presented in Figure S3 (see Supporting Information). Regions with high concentration of ibuprofen are depicted in bright green (*) and regions with lower concentration are depicted in dark green (+). **(E)** Representative spectra of these regions are shown.

3.2. Drug-release studies

The release of ibuprofen from P(TMC-CL) fibres was evaluated in PBS at 37°C, to mimic physiological conditions. The amount of ibuprofen released was interpolated from a calibration curve and the percentage of cumulative release was calculated relative to the maximum loading of 5% (w/w of polymer).

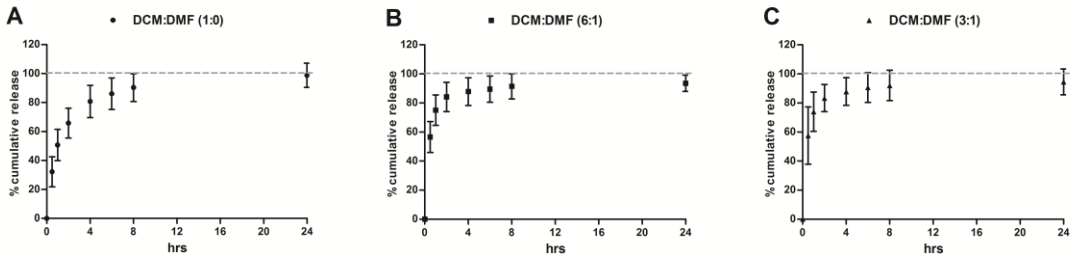

Figure 4. Cumulative release of ibuprofen from poly(trimethylene carbonate-co-ϵ-caprolactone) [P(TMC-CL)] fibres in phosphate buffered saline (PBS) (37 °C). Samples were prepared from **(A)** 1:0 dichloromethane (DCM)–N,N-dimethylformamide (DMF), **(B)** 6:1 DCM–DMF and **(C)** 3:1 DCM–DMF solutions containing 5% ibuprofen (w/w of polymer). Fibre concentration in PBS was 5 mg/ml (n=9).

Under the experimental conditions tested, ibuprofen was released from the P(TMC-CL) fibres within the first 24 h of incubation in PBS (37°C), independently of the solvent mixture used for fibre preparation. None, or residual amounts of ibuprofen were detected in the releasing medium when loaded fibres were incubated for longer periods (data not shown). In the case of fibres prepared from 6:1 and 3:1 DCM–DMF solutions, a burst release appeared to occur (Figure 4B, C). In contrast, the release kinetics of ibuprofen from fibres prepared in 1:0 DCM– DMF was slower, suggesting time-dependency (Figure 4A).

Analysing ibuprofen release using the Higuchi model it was found that the release profile of ibuprofen from P(TMC-CL) fibres prepared from 1:0 DCM–DMF solutions fitted better in the model, indicating that the release is diffusion dependent for the first 8 h of incubation in PBS (see fitting curve in Figure S5). Observation of the fibres after the drug release experiments showed that fibre morphology was maintained upon drug release (Figure S6).

3.3. Biological evaluation

Ibuprofen anti-inflammatory properties have been associated to its inhibitory action on COX (Mitchell et al., 1993). This enzyme is responsible for the formation of prostaglandins (such as PGE_2) from arachidonic acid, and is related with the inflammatory response (for a review see Rainsford, 2009). To ensure that the ibuprofen incorporated into the P(TMC-CL) fibres exerted its biological activity, the release of cytokines and PGE_2 by monocyte-derived human macrophages was quantified after incubating the cells with the fibres or soluble ibuprofen (positive control).

Taking advantage of the fact that P(TMC-CL) density is similar to water density and consequently the discs hang in cell culture medium, the fibres were incubated without direct contact with the adhered cells. This set up made it possible to distinguish the effect of the drug from any effect triggered by the polymer surface, as macrophage response and differentiation is affected by surface chemistry (Brodbeck et al., 2002), and by its topography (Cao et al., 2010). In this study the aim was to discern the effect of the released drug regardless of cell–material interaction.

3.3.1. Effect of ibuprofen on macrophage cell viability and morphology

To assess ibuprofen cytotoxic profile on monocyte-derived human macrophages, the drug was added in its soluble form to the cell culture medium to a final concentration ranging from 0.001–1mg/ml. Ibuprofen solvent (ethanol 70% v/v) was also applied as a negative control. The graph presented in Figure 5A indicates that, at the highest concentration tested (1mg/ml), ibuprofen was toxic for macrophages, significantly reducing cell viability (< 10%). Similar results were obtained when cell metabolic activity was assessed 24 h post-treatment (data not shown). Taking into consideration these results, 0.1mg/ml soluble of ibuprofen was applied in the following experiments as control.

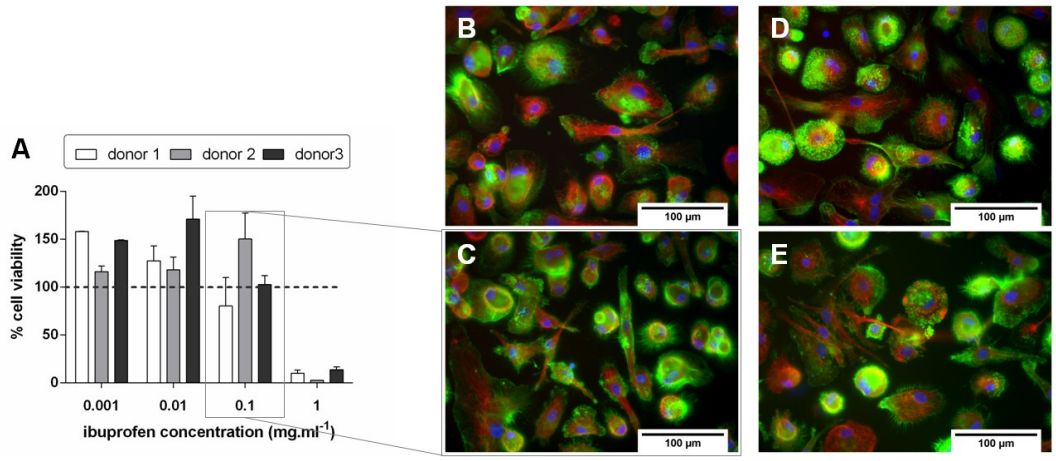

Figure 5. (A) Macrophage viability when incubated for 72 h with ibuprofen at different concentrations. The percentage of viable cells was calculated relative to cells treated with ibuprofen solvent (ethanol 70% v/v). Bars represent mean values and error bars show standard deviation. Results are representative of three independent experiments. **(B–E)** Actin–tubulin cytoskeleton immunolabelling of macrophages. Macrophages were incubated for 72 h in the presence of **(B)** ethanol 70% (v/v), **(C)** ibuprofen 0.1mg/ml, **(D)** poly(trimethylene carbonate-co-ε-caprolactone) [P(TMC-CL)] fibres, and **(E)** ibuprofen-loaded P(TMC-CL) fibres. Scale bar=100 µm. α-Tubulin is shown in red, F-actin in green and the cell nucleus in blue. Magnified images of each condition are also presented (scale bar=20 µm).

The effect of ibuprofen-loaded P(TMC-CL) fibres on macrophage morphology was investigated by observing the distribution pattern of cytoskeleton proteins (α-tubulin and F-actin). Therefore, human primary macrophages were incubated for 72 h with soluble ibuprofen at a final concentration of 0.1 mg/ml, with ethanol (70% v/v, ibuprofen solvent), with P(TMC-CL) fibres or

with ibuprofen-loaded P(TMC-CL) fibres. In all the experimental conditions tested macrophages showed evidence of heterogeneous cell morphology, with round-shaped cells and F-actin staining concentrated at the cell periphery in podosome-like structures, and elongated cells with less intense and peripheral F-actin staining. In contrast, α- tubulin staining was always homogeneously distributed along the cell body and according the cell axis (Figure 5). No significant differences in terms of macrophage morphology were observed between the different experimental conditions.

3.3.2. Anti-inflammatory properties of ibuprofen loaded P(TMC-CL) fibres

To assess if the ibuprofen released from ibuprofen-loaded P(TMC-CL) electrospun fibres is bioactive, the concentration of soluble PGE_2 produced by exposed macrophages was quantified in the cell culture supernatants after 72 h of incubation.

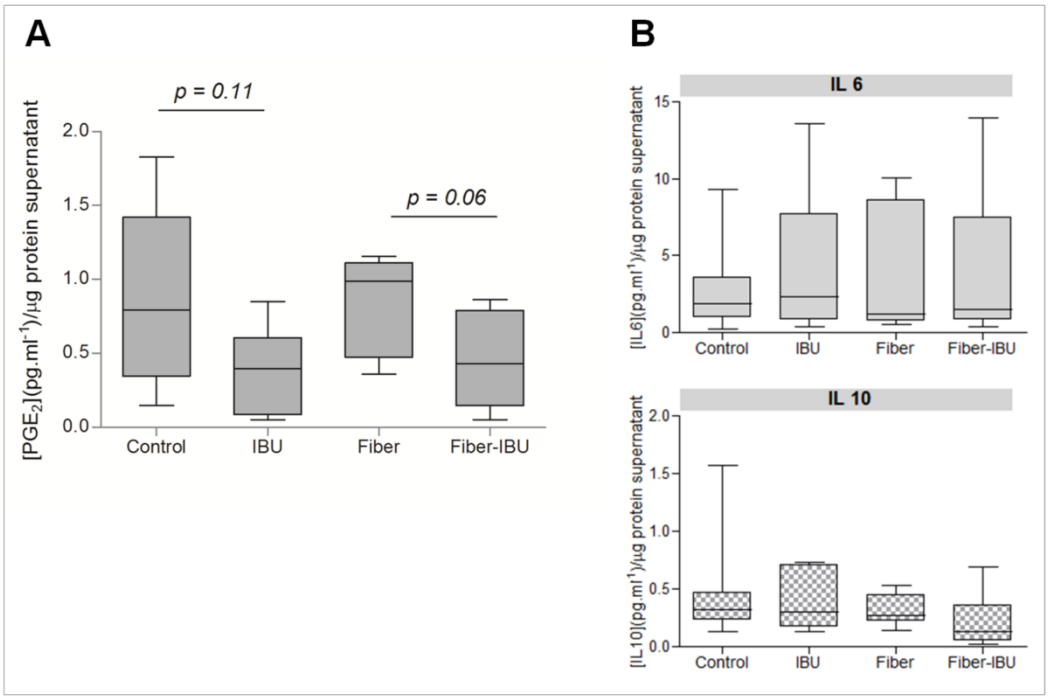

Figure 6. Effect of ibuprofen on **(A)** prostaglandin E2 (PGE_2) and **(B)** cytokine [interleukin (IL)-6 and IL-10] release by human macrophages. Results are expressed as box-whisker plots showing the quantification of **(A)** PGE_2 or **(B)** IL-6 and IL-10 released into the cell culture medium after 72 h in contact with soluble ibuprofen added in solution to the cell culture medium or released from P(TMC-CL) electrospun fibres. The P(TMC-CL) fibres were prepared from 1:0 dichloromethane (DCM)–N,N-dimethylformamide (DMF) solutions. Cells incubated with non-loaded fibres (Fibre) or with ibuprofen (IBU) solvent (ethanol 70% v/v, Control) were used as controls. Results were obtained from cells from five independent donors and seven samples and are normalized by the total amount of protein in the supernatant. The p-value calculated by t-test.

The results (Figure 6) indicate that when ibuprofen is added to the medium the release of PGE_2 decreases, suggesting that COX is being inhibited. The same tendency is observed when comparing the effect of ibuprofen-loaded fibres and non-loaded fibres (Figure 6), although none of

the differences achieved statistical significance. In terms of inhibition, considering the mean values, when ibuprofen is added in solution there is a 56% decrease in PGE_2 release, while ibuprofen released from P(TMC-CL) electrospun fibres can reduce the release of PGE_2 by 47%. However, when comparing the effect of ibuprofen released from P(TMC-CL) fibres directly with control conditions one should take into account that the amount of drug that can be released from P(TMC-CL) fibres is in a concentration range and can slightly differ from the control concentration used in this assay.

The effect of ibuprofen on the release of IL-6, IL-10 and TNFα was also evaluated. Under the experimental conditions of this study, ibuprofen was found to induce no significant effect on the release of IL-6 or IL-10 when added in solution or when released from electrospun P(TMC-CL) fibres (Figure 6). The concentration of TNFα secreted into the cell culture medium was found to be below the detection limit (3.5 pg/ml) of the ELISA assay (data not shown).

4. Discussion

The preparation of nerve conduits by electrospinning holds the promise of allowing easy preparation of fibres, at the nanometre scale, that can guide axonal growth and be loaded with biologically active molecules able to enhance nerve regeneration processes (Lee and Arinzeh, 2011). In the present work, the aim was to prepare fibres of a statistical copolymer of TMC and CL with low TMC content (11 mol%) by electrospinning and to load these with an anti-inflammatory drug. The idea beyond this strategy is to design scaffolds that can provide physical support for nerve cell growth, and that simultaneously minimize, at the lesion site, the inflammatory reaction that could counteract nerve regeneration. The preparation of electrospun structures based on a block copolymer of TMC and CL (Jia et al., 2006) or blends of P(TMC) and P(CL) (Han et al., 2010) have been reported in the literature. Nevertheless, a statistical copolymer holds the advantage of reducing the formation of crystalline domains and reducing phase separation within the polymer structure, which is desirable when envisaging the use of these materials in implantable devices (Pêgo et al., 2001). The authors have previously reported on the use of selected statistical P(TMC-CL) for the preparation of microporous and macroporous conduits for nerve reconstruction in the peripheral nervous system. P(TMC-CL) with a high CL content has been shown to possess adequate mechanical properties and degradation rate to be used in a nerve regeneration strategy (Pêgo et al., 2001, 2003), as it is able to support nerve regeneration *in vivo* (Vleggeert-Lankamp et al., 2008). This paper describes for the first time the preparation of electrospun fibres from this copolymer.

By using different DCM–DMF mixtures in the electrospinning solution it was possible to prepare fibrous meshes with variable mean fibre diameter. Increasing the DMF content in solution, mean fibre diameter was decreased from 1.09 μm to 0.48μm. DMF is a high conductivity solvent, and its use in the preparation of solutions for electrospinning leads to an increase in jet splaying and a reduction of fibre diameter (Hsu and Shivkumar, 2004). Typically, DMF is used below 30% in

solution, as described for the preparation of fibres of P(CL) (Bölgen et al., 2005) and P(CL)/P(TMC) blends (Han et al., 2010). Herein, the preparation of fibres from solutions containing up to 50% of DMF was explored. Results show that by increasing the DMF content one can obtain very homogeneous fibre meshes, with narrower fibre diameter distribution and smaller mean fibre diameter. However, the use of 1:1 DCM–DMF solutions was revealed to be unsuitable for the preparation of ibuprofen-loaded P(TMC-CL) fibres at the drug concentrations tested. It was previously described that the incorporation of drugs in electrospinning solutions can lead to an increase in solution conductivity (Kim et al., 2004). This increase, combined with the high DMF content, may cause fibres to bind together because of the high conductivity (Heikkilä and Harlin, 2008) and high boiling point of DMF, which prevent solvent evaporation during fibre deposition (Hsu and Shivkumar, 2004).

Ibuprofen-loaded fibres were obtained from 1:0, 6:1 and 3:1 DCM–DMF mixtures. In terms of morphology, when applying a 5% of ibuprofen (w/w of polymer) load, a tendency towards a decrease in mean fibre diameter is observed compared with unloaded fibres. This effect is particularly noticeable for 1:0 DCM–DMF solutions, probably because the presence of the drug led to a more marked increase in solution conductivity compared with solutions containing DMF (Kim et al., 2004). Although the differences in terms of mean fibre diameter are not significant, when loading 10% ibuprofen in solution, jet stability and solvent evaporation are reduced, the latter being particularly evident in the case of the 3:1 DCM–DMF solution. The increase in jet instability with higher drug loading has also been reported previously (Natu et al., 2010).

The presence of ibuprofen in P(TMC-CL) fibres was clearly demonstrated by ATR-FTIR and Raman spectroscopy. Both techniques showed that the chemical stability of ibuprofen is maintained after electrospinning. In addition, no alterations in the characteristic peaks of P(TMC-CL) and ibuprofen are seen in ibuprofen-loaded P(TMC-CL) spectrum, indicating that there is no significant chemical interaction between the polymer and the drug, as previously observed in ibuprofen-loaded cellulose acetate fibres (Tungprapa et al., 2007).

The ibuprofen release kinetics from P(TMC-CL) fibres were assessed in physiological medium (PBS, 37 °C). Results demonstrate that ibuprofen is released within the first 24 h after incubation in PBS, independently of the solvent mixture used for the preparation of the fibres. It was previously reported that the expression of cycloxygenase-2 peaks 3 h after spinal cord injury (SCI), and is maintained for 3 days (Adachi et al., 2005). In this context, the release of ibuprofen in the early hours after the lesion can provide the expected therapeutic benefit. A complete ibuprofen release in the first 24 h of incubation under physiological conditions has also been reported using cellulose acetate fibres (Tungprapa et al., 2007). In terms of kinetics, we found an initial burst release for fibres prepared from 6:1 and 3:1 DCM–DMF mixtures. However, in the case of fibres prepared from 1:0 DCM–DMF the release was found to be diffusion dependent, as it fits the Higuchi model for drug release (Siepmann and Peppas, 2001). Indeed, the cumulative amount of ibuprofen correlates with the square root of the time (R^2>0.94) for the first 8 h of incubation for fibres prepared from 1:0 DCM–DMF solutions. Conversely, no linearity was observed for ibuprofen

release from P(TMC-CL) fibres prepared from the 3:1 and 6:1 DCM–DMF solutions. It was hypothesized that the presence of DMF in solution could affect the drug distribution within the fibre, leading to a burst release compared with fibres prepared from solutions without DMF. To address this point samples were analysed using confocal Raman microscopy. To the best of the authors' knowledge this is the first report using confocal Raman microscopy to assess drug distribution in an electrospun fibre. Mapping experiments by confocal Raman allowed screening of specific areas within an electrospun fibre. By using a step slightly smaller than the theoretical size of the spot of the laser beam (0.7 μm), mapping experiments provided the profiling of all the sample area and discrimination of subtle differences in composition (Adar, 2008). The mapping of the drug in P(TMC-CL) fibres showed that ibuprofen distribution was not completely homogenous. Nevertheless, at the spatial resolution offered by the experimental setup used, no preferential localization of the drug was identified that could be correlated with the burst release (for example, at the fibre edge). In addition, no significant differences were detected when comparing fibres prepared from 1:0 and 3:1 DCM–DMF solutions, suggesting that, at the submicrometer scale, the drug distribution is independent of the solvent mixture applied during electrospinning. The results indicate that other parameters are probably playing a role in ibuprofen release, for example the fibre diameter (Cui et al., 2006). Although no significant differences were detected in terms of mean fibre diameter, the fibre diameter distribution was different between these two types of samples. In fibres prepared from 1:0 DCM–DMF mixtures the presence of a small percentage of fibres with a large diameter (> 3 μm) was observed and could have contributed to delaying the release of the drug by increasing the drug diffusion pathway within the polymeric fibre structure.

Owing to the important role of macrophages as effectors of an inflammatory response and as these cells are targets of ibuprofen, primary human monocyte-derived macrophages were selected to evaluate ibuprofen bioactivity after the release from electrospun fibres. Macrophages are highly dynamic and versatile cells, and their response to exogenous stimuli is generally accompanied by alterations in actin assembly/disassembly and cell morphology. These alterations may occur as a consequence of a number of effects such as surface topography (Cao et al., 2010), drugs (Chiou et al., 2003) or soluble factors (Shinji et al., 1991; Porcheray et al., 2005). Thus, the effect of ibuprofen-loaded P(TMC-CL) fibres on macrophage morphology was investigated by observing the distribution patterns of cytoskeleton proteins (α-tubulin and F-actin). The results show no major alterations of actin/tubulin cytoskeleton organization in macrophages incubated with ibuprofen or ibuprofen-loaded P(TMC-CL) fibres. However, it cannot be excluded that, to be perceived, considerable alterations would need to have occurred in the heterogeneous macrophage cell population under study. Cells incubated with ibuprofen-loaded P(TMC-CL) fibres secreted less PGE_2 into the cell culture medium than did non-loaded fibres. Although the result did not accomplish the statistical significance ($p=0.06$) because of the high variability between cell donors, this result strongly suggests that the drug incorporated in the electrospun fibres retains its bioactivity. This result is reinforced by the fact that the percentage of inhibition obtained (47%) is similar to that found with treatment with ibuprofen in solution (56%).

In addition to the classical view of ibuprofen activity, acting on the prostaglandin pathway, there is mounting evidence that lowering levels of eicosanoids is not the only mechanism by which ibuprofen exerts its effects (Stuhlmeier et al., 1999; Zhou et al., 2003). Stuhlmeier and co-workers (1999) showed that ibuprofen can inhibit the nuclear translocation of the nuclear factor kappa B (NF-kB), a transcription factor critical for the up-regulation of expression of pro-inflammatory genes. These reports prompted evaluation of the concentration of pro-inflammatory cytokines (TNFα and IL-6) and an anti-inflammatory cytokine (IL–10) in the cell culture medium in this study. Under the experimental conditions applied in this study, no significant levels of TNFα were found in the cell culture medium. For IL-6 and IL-10, no major differences were found when comparing cytokine levels secreted by cells incubated with ibuprofen-loaded P(TMC-CL) fibres or non-loaded fibres. Similar results were obtained when cells were treated with ibuprofen in the medium (0.1mg/ml), suggesting that under the set conditions the drug exerts no effect on the cytokine release profile. In the literature divergent effects on cytokine release are ascribed to ibuprofen. Some authors have shown that ibuprofen induces a decrease in the secretion of TNFα and IL-1β by mononuclear cells (Stuhlmeier et al., 1999; Lamanna et al., 2012), whereas a concentration-dependent increase of TNFα and IL-6 has been observed by others (Sirota et al., 2001; Lee and Chuang, 2010). Recently, Lamanna and colleagues (2012) reported the inhibition of TNFα secretion by a macrophage cell line when cells were incubated with a high concentration of ibuprofen (1mg/ml). However, when applying this concentration, the authors (Lamanna et al., 2012) also found ibuprofen-mediated cytotoxicity and, in agreement with the results of the present study, incubating cells with 0.1mg/ml of ibuprofen was found to have no effect on IL-6 and TNFα release into the culture medium.

5. Conclusions

Fibres from P(TMC-CL) were successfully prepared by electrospinning. It is shown here that by adjusting the solvent composition, one can change the mean fibre diameter in a controlled manner. An anti-inflammatory drug can be loaded in P(TMC-CL) fibres, the release kinetics being dependent on fibre morphology, which is tuned by the solvent mixture applied for preparation of the electrospinning solution. Ibuprofen was found to maintain its chemical stability and bioactivity after electrospinning, as demonstrated by the fact that the drug was able to reduce the amount of PGE_2 secreted into the cell culture medium by human macrophages. The use of confocal Raman microscopy as a mean to assess the drug distribution within electrospun fibres is also proposed for the first time, being a promising technique to provide new cues on the drug-release process.

The results provide an important insight into the design of a P(TMC-CL)-based nerve conduit combining physical cues provided by the fibres with an anti-inflammatory signalling molecule, which, together, can assist nerve regeneration.

Acknowledgements

This work was financed by FEDER funds through the Programa Operacional Factores de Competitividade – COMPETE and by Portuguese funds through FCT – Fundação para a Ciência e a Tecnologia in the framework of the project PEst-C/SAU/ LA0002/2011 and PTDC/CTM-NAN/115124/2009, PTDC/SAUONC/112511/2009. L.R.P. thanks FCT for her PhD grant (SFRH /BD / 46015 / 2008) and M.J.O. is a FCT Ciência 2007 fellow. The authors acknowledge Centro de Materiais da Universidade do Porto (CEMUP; REEQ/1062/CTM/2005 from FCT) for the ^{1}H NMR analysis.

Conflict of interest

The authors have declared that there is no conflict of interest.

References

Adachi K, Yimin Y, Satake K et al. 2005; Localization of cyclooxygenase-2 induced following traumatic spinal cord injury. *Neurosci Res* **51**: 73–80.

Adar F. 2008; Raman images from raman maps – spatial resolution, mapping speed, and multivariate techniques for constructing the image. *Spectroscopy* **23**: 14–21.

Agarwal S, Wendorff JH, Greiner A. 2009; Progress in the field of electrospinning for tissue engineering applications. *Adv Mater* **21**: 3343–3351.

Bölgen N, Menceloglu YZ, Acatay K, Vargel I, Piskin E. 2005; *In vitro* and *in vivo* degradation of non-woven materials made of poly(ϵ-caprolactone) nanofibres prepared by electrospinning under different conditions. *J Biomater Sci Polym Ed* **16**: 1537–1555.

Brodbeck WG, Nakayama Y, Matsuda T et al. 2002; Biomaterial surface chemistry dictates adherent monocyte/macrophage cytokine expression *in vitro*. *Cytokine* **18**: 311–319.

Cao H, McHugh K, Chew SY et al. 2010; The topographical effect of electrospun nanofibrous scaffolds on the *in vivo* and *in vitro* foreign body reaction. *J Biomed Mater Res A* **93**: 1151–1159.

Casha S, Zygun D, McGowan MD et al. 2012; Results of a phase II placebo-controlled randomized trial of minocycline in acute spinal cord injury. *Brain* **135**: 1224–1236.

Chan CC. 2008; Inflammation: beneficial or detrimental after spinal cord injury? *Recent Pat CNS Drug Discov* **3**: 189–199.

Chew SY, Wen J, Yim EKF et al. 2005; Sustained release of proteins from electrospun biodegradable fibres. *Biomacromolecules* **6**: 2017–2024.

Chiou WF, Shum AYC, Peng CH et al. 2003; Piperlactam S suppresses macrophage migration by impeding F-actin polymerization and filopodia extension. *Eur J Pharmacol* **458**: 217–225.

Corey JM, Lin DY, Mycek KB et al. 2007; Aligned electrospun nanofibres specify the direction of dorsal root ganglia neurite growth. *J Biomed Mater Res A* **83**: 636–645.

Cui W, Li X, Zhu X et al. 2006; Investigation of drug release and matrix degradation of electrospun poly(DL-lactide) fibres with paracetanol inoculation. *Biomacromolecules* **7**: 1623–1629.

Fitch MT, Silver J. 2008; CNS injury, glial scars, and inflammation: Inhibitory extracellular matrices and regeneration failure. *Exp Neurol* **209**: 294–301.

Formhals A. 1934; US patent (1,975,504).

Han J, Branford-White CJ, Zhu LM. 2010; Preparation of poly(ϵ-caprolactone)/ poly(trimethylene carbonate) blend nanofibres by electrospinning. *Carbohydr Polym* **79**: 214–218.

Heikkilä P, Harlin A. 2008; Parameter study of electrospinning of polyamide-6. *Eur Polym J* **44**: 3067–3079.

Hsu CM, Shivkumar S. 2004; N,Ndimethylformamide additions to the solution for the electrospinning of poly(ϵ- caprolactone) nanofibres. *Macromol Mater Eng* **289**: 334–340.

Hurtado A, Cregg JM, Wang HB et al. 2011; Robust CNS regeneration after complete spinal cord transection using aligned poly-l-lactic acid microfibres. *Biomaterials* **32**: 6068–6079.

Jia YT, KimHY, Gong J et al. 2006; Electrospun nanofibres of block copolymer of trimethylene carbonate and ecaprolactone. *J Appl Polym Sci Symp* **99**: 1462–1470.

Jiang X,Mi R, Hoke A et al. 2012; Nanofibrous nerve conduit-enhanced peripheral nerve regeneration. *J Tissue Eng Regen Med*. DOI: 10.1002/term.1531. [Epub ahead of print]

KimK, Luu YK, Chang C et al. 2004; Incorporation and controlled release of a hydrophilic antibiotic using poly(lactide-co-glycolide)-based electrospun nanofibrous scaffolds. *J Control Release* **98**: 47–56.

Lamanna G, Russier J, Dumortier H et al. 2012; Enhancement of anti-inflammatory drug activity by multivalent adamantine-based dendrons. *Biomaterials* **33**: 5610–5617.

Lee YJ, Chuang YC. 2010; Ibuprofen augments pro-inflammatory cytokine release in a mouse model of Vibrio vulnificus infection. *Microbiol Immunol* **54**: 542–550.

Lee YS, Arinzeh TL. 2011; Electrospun nanofibrous materials for neural tissue engineering. Polymers 3: 413–426.

Liu T, Xu J, Chan BP et al. 2012; Sustained release of neurotrophin-3 and chondroitinase ABC from electrospun collagen nanofibre scaffold for spinal cord injury repair. *J Biomed Mater Res A* **100A**: 236–242.

Ma W, St-Jacques B, Cruz Duarte P. 2012; Targeting pain mediators induced by injured nerve-derived COX_2 and PGE_2 to treat neuropathic pain. *Expert Opin Ther Targets* **16**: 527–540.

Martins A, Araújo JV, Reis RL et al. 2007; Electrospun nanostructured scaffolds for tissue engineering applications. *Nanomedicine* **2**: 929–942.

Mitchell JA, Akarasereenont P, Thiemermann C et al. 1993; Selectivity of nonsteroidal antiinflammatory drugs as inhibitors of constitutive and inducible cyclooxygenase. *Proc Natl Acad Sci USA* **90**:11693–11697.

Natu MV, de Sousa HC, Gil MH. 2010; Effects of drug solubility, state and loading on controlled release in bicomponent electrospun fibres. *Int J Pharm* **397**:50–58.

Oliveira MI, Santos SG, Oliveira MJ et al. 2012; Chitosan drives anti-inflammatory macrophage polarisation and proinflammatory dendritic cell stimulation. *Eur Cell Mater* **24**: 136–153.

Pêgo AP, Poot AA, Grijpma DW et al. 2001; Copolymers of trimethylene carbonate and epsilon-caprolactone for porous nerve guides: Synthesis and properties. *J Biomater Sci Polym Ed* **12**: 35–53.

Pêgo AP, Poot AA, Grijpma DW et al. 2003; Biodegradable elastomeric scaffolds for soft tissue engineering. *J Control Release* **87**: 69–79.

Porcheray F, Viaud S, Rimaniol AC et al. 2005; Macrophage activation switching: an asset for the resolution of inflammation. *Clin Exp Immunol* **142**: 481–489.

Rainsford KD. 2009; Ibuprofen: pharmacology, efficacy and safety. *Inflammopharmacology* **17**: 275–342.

Schaub NJ, Gilbert RJ. 2011; Controlled release of 6-aminonicotinamide from aligned, electrospun fibres alters astrocyte metabolism and dorsal root ganglia neurite outgrowth. *J Neural Eng* **8**: 046026.

Schwartz M, London A, Shechter R. 2009; Boosting T-cell immunity as a therapeutic approach for neurodegenerative conditions: The role of innate immunity. *Neuroscience* **158:** 1133–1142.

Shinji H, Kaiho S, Nakano T et al. 1991; Reorganization of microfilaments in macrophages after LPS stimulation. *Exp Cell Res* **193**: 127–133.

Siepmann J, Peppas NA. 2001; Modeling of drug release from delivery systems based on hydroxypropyl methylcellulose (HPMC). *Adv Drug Deliv Rev* **48**: 139–157.

Sirota L, Shacham D, Punsky I et al. 2001; Ibuprofen affects pro- and anti-inflammatory cytokine production by mononuclear cells of preterm newborns. *Biol Neonate* **79**: 103–108.

Stuhlmeier KM, Li H, Kao JJ. 1999; Ibuprofen: New explanation for an old phenomenon. *Biochem Pharmacol* **57**: 313–320.

Thuret S, Moon LDF, Gage FH. 2006; Therapeutic interventions after spinal cord injury. *Nat Rev Neurosci* **7**: 628–643.

Tungprapa S, Jangchud I, Supaphol P. 2007; Release characteristics of four model drugs from drug-loaded electrospun cellulose acetate fibre mats. *Polymer* **48**: 5030–5041.

Vleggeert-Lankamp CLAM, Wolfs J, Pêgo AP et al. 2008; Effect of nerve graft porosity on the refractory period of regenerating nerve fibres: laboratory investigation. *J Neurosurg* 109: 294–305.

Xie J, MacEwan MR, Schwartz AG et al. 2010; Electrospun nanofibres for neural tissue engineering. Nanoscale 2: 35–44.

Yao L, O'Brien N, Windebank A et al. 2009; Orienting neurite growth in electrospun fibrous neural conduits. *J Biomed Mater Res B Appl Biomater* **90**: 483–491.

Yu W, Zhao W, Zhu C et al. 2011; Sciatic nerve regeneration in rats by a promising electrospun collagen/poly(ϵ-caprolactone) nerve conduit with tailored degradation rate. *BMC Neurosci* **12**: 68.

Zhao P, Waxman SG, Hains BC. 2007; Extracellular signal-regulated kinase-regulated microglia-neuron signaling by prostaglandin E2 contributes to pain after spinal cord injury. *J Neurosci* **27**: 2357–2368.

Zhou Y, Su Y, Li BL et al. 2003; Nonsteroidal anti-inflammatory drugs can lower amyloidogenic A beta(42) by inhibiting Rho. *Science* **302**: 1215–1217.

Supporting information

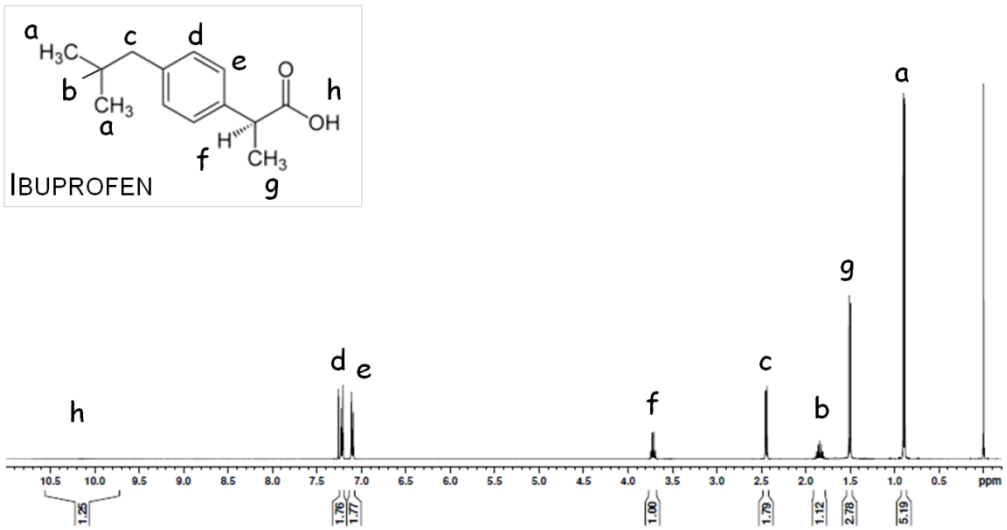

Figure S1. ^{1}H Nuclear magnetic resonance spectrum of ibuprofen-loaded poly(trimethylene carbonate-co-ε-caprolactone) [P(TMC-CL)] fibres, showing the identification of ibuprofen characteristic peaks.

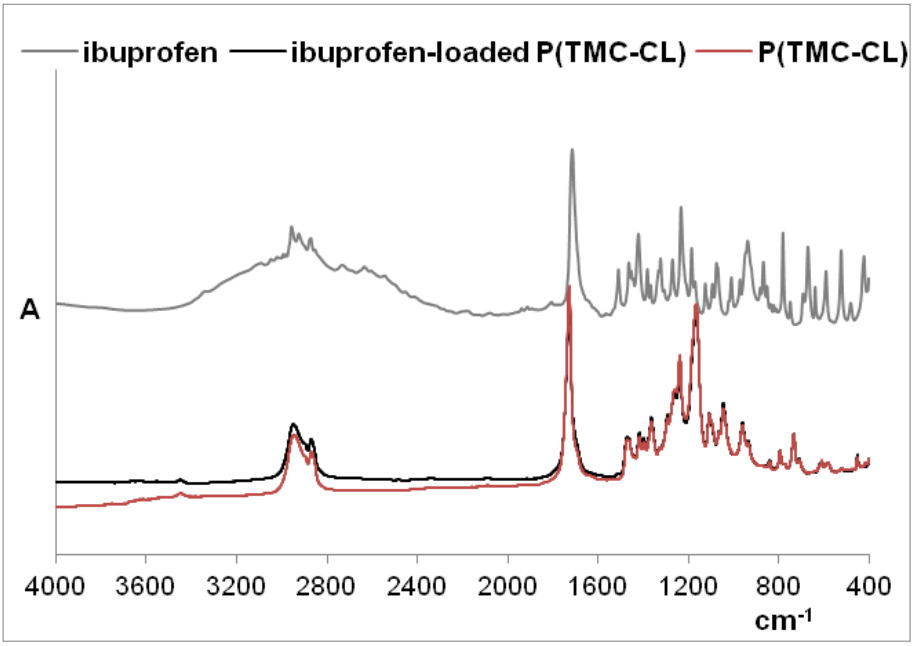

Figure S2. Full attenuated total reflectance Fourier transform infrared spectrum of ibuprofen (grey), ibuprofen-loaded poly(trimethylene carbonate-co-ε-caprolactone) [P(TMC-CL)] fibres (black) and P(TMC-CL) (red).

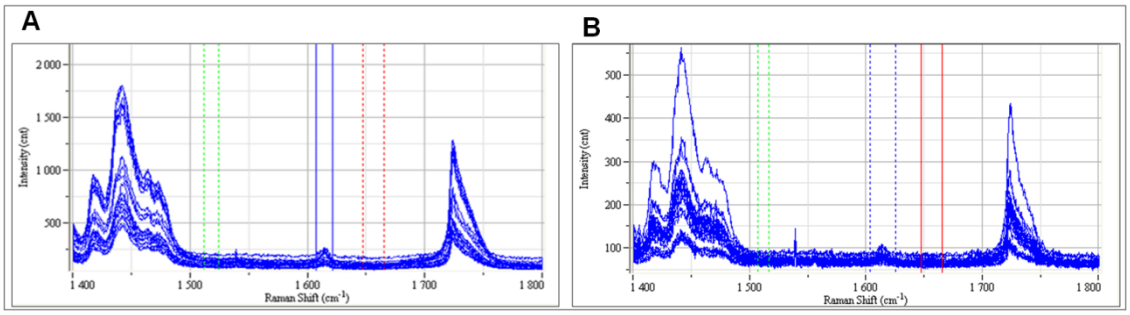

Figure S3. Overlay Overlay of spectra obtained from mapping experiments of ibuprofen-loaded poly(trimethylene carbonate-co-ε-caprolactone) [P(TMC-CL)] fibres prepared from (A) 1:0 dichloromethane (DCM)–N,N-dimethylformamide (DMF) and (B) 3:1 DCM–DMF solutions.

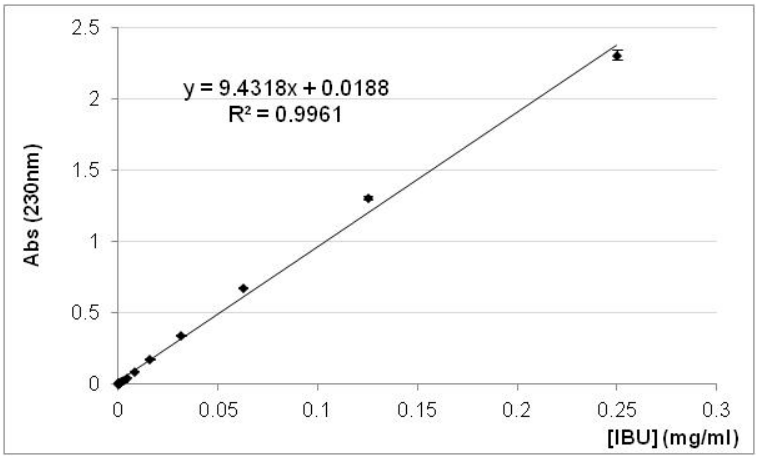

Figure S4. Standard calibration curve obtained for ibuprofen.

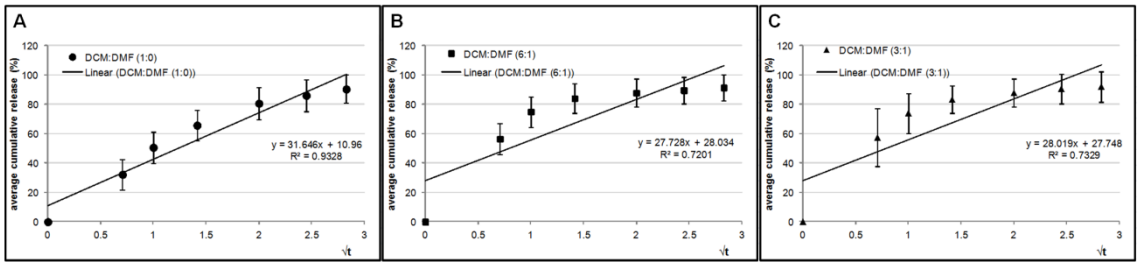

Figure S5. Fittings according to Higuchi model for drug release for fibres prepared from **(A)** 1:0 dichloromethane (DCM)–N,N-dimethylformamide (DMF), **(B)** 6:1 DCM:DMF and **(C)** 3:1 DCM–DMF.

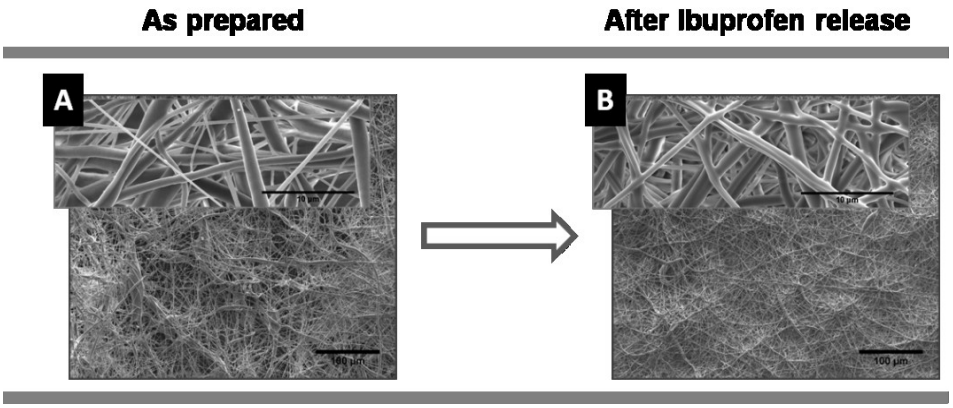

Figure S6. Scanning electron microscopy photomicrographs of ibuprofen-loaded poly(trimethylene carbonate-co-ε-caprolactone) [P(TMC-CL)] fibres prepared from 1:0 dichloromethane (DCM)–N,N-dimethylformamide (DMF) solution (A) before and (B) after ibuprofen release.

CHAPTER V

Ibuprofen-loaded scaffolds for spinal cord injury regeneration – targeting RhoA at the lesion site

Liliana R Pires[1,2], Cátia DF Lopes[1,3], Daniela N Rocha[1,2], Luigi Ambrosio[4], Mónica M Sousa[5], Ana Paula Pêgo[1,2,6]

1 – INEB – Instituto de Engenharia Biomédica, Universidade do Porto, Rua do Campo Alegre, 823, 4150-180 Porto, Portugal.

2 – Universidade do Porto – Faculdade de Engenharia, Rua Roberto Frias, s/n, 4200-465 Porto, Portugal.

3 – Universidade do Porto – Faculdade de Medicina, Alameda Prof. Hernâni Monteiro, 4200-319 Porto, Portugal

4 – Institute of Composite and Biomedical Materials, National Research Council, P. le Tecchio 80, 80125 Naples, Italy

5 – Nerve Regeneration Group, IBMC - Instituto de Biologia Molecular e Celular, Universidade do Porto, Rua do Campo Alegre, 823, 4150-180 Porto, Portugal.

6 – Universidade do Porto – Instituto de Ciências Biomédicas Abel Salazar, Largo Prof. Abel Salazar, 4099-003 Porto, Portugal.

Abstract

It is now well accepted that a therapeutic strategy for spinal cord injury demands a multi-target approach. Here we propose the use of a poly(trimethylene carbonate-co-ε-caprolactone) [P(TMC-CL)]-based scaffold that gathers physical guidance cues provided by electrospun aligned fibres and the delivery of ibuprofen as a mean to reduce the inhibitory environment at the lesion site by targeting RhoA activation. Bilayer scaffolds were prepared being composed by a solvent cast film onto which electrospun aligned fibres have been deposited. Both layers were loaded with the ibupofen. The release of the drug was found to occur in the first 24 hrs of incubation when this was assessed *in vitro* under physiological conditions. The bioactivity of the released drug was demonstrated by the inhibition of RhoA activation when the neuronal ND7/23 cells were challenged with lysophosphatidic acid. The ibuprofen-loaded bilayer scaffolds were successfully implanted *in vivo* in a dorsal hemisection SCI model. The implantation of the scaffold did not compromise animal survival. The effect of scaffold implantation and ibuprofen release on RhoA activity, and the histological characterization of the tissues are under investigation.

Keywords

Spinal cord injury; Ibuprofen; electrospinning, RhoA.

1. Introduction

Injury to the spinal cord is marked by the disruption of ascending and descending axonal pathways, interrupting the communication between the brain and other parts of the body. In the adult central nervous system (CNS) axonal regrowth after injury, necessary to restore connectivity, is prevented by the lack of physical support and by the presence of inhibitory molecules in the extracellular milieu (see [1, 2] for a review). The Ras homolog gene family, member A (RhoA) is considered a key convergence effector for several of these molecules involved in inhibitory processes. It has been demonstrated that the use of RhoA antagonists can promote axonal regeneration and functional recovery [3-5]. Consequently, limiting RhoA activation has been pointed out as a promising therapeutic approach for spinal cord injury (SCI).

In 2003, it was reported for the first time that some non-steroidal anti-inflammatory drugs, namely ibuprofen, can inhibit RhoA signalling [6]. Some years later, it was demonstrated that ibuprofen can prevent myelin mediated inhibition of neurite outgrowth *in vitro* [7] and, in different *in vivo* models of SCI, the administration of ibuprofen showed to promote corticospinal axonal regeneration [7] and functional recovery [7, 8]. A re-assessment study [9] aiming at replicating the first results obtained with ibuprofen on SCI [7] has recently confirmed that ibuprofen inhibits RhoA activation, although the significant improvement on corticospinal axonal regeneration was not achieved [9]. The administration of ibuprofen has also been associated with the reduction of neuropathic pain [10] and the increase of oligodendrocyte survival and axonal myelination [11], further supporting the use of the drug in the context of SCI.

Ibuprofen has been used worldwide for pain relief, lowering fever and acute inflammatory reaction based on its action as an inhibitor of cyclooxygenases [12, 13]. Due to its widespread use, ibuprofen long-term administration presents an acceptable risk profile and reduced economical costs [14], holding a great potential to become a new therapeutic tool for SCI [14].

Considering the increasing evidence that the multi-faced inhibitory nature of SCI will imply a combinatorial therapeutic approach [15], the present work aimed at designing a scaffold that can be implanted at the lesion site after SCI, providing guidance for axonal growth and also the delivery of ibuprofen as a mean to convert the lesion site in a more permissive substrate for regeneration. Here we explore the application of poly(trimethylene carbonate-co-ε-caprolatone) [P(TMC-CL)], a synthetic copolymer previously applied for the preparation of nerve conduits [16], as starting material for the development of a scaffold based on longitudinally aligned nanofibres. In a SCI scenario, the use of aligned fibrous scaffolds is of particular interest as these structures can provide physical guidance cues for neurons, allowing cellular processes to orient in the direction of the fibres *in vitro* [17, 18] and ultimately leading to improved regeneration *in vivo* [19]. It has been demonstrated that P(TMC-CL) can support peripheral nerve regeneration *in vivo* [20] and, in the context of the CNS, P(TMC-CL) showed to stimulate neuronal polarization and axonal elongation, favouring neurite outgrowth when in an inhibitory environment [21]. Our group has previously described the preparation of P(TMC-CL) fibres by electrospinning and demonstrated that these structures can combine the delivery of ibuprofen, yielding fibres with anti-inflammatory

properties [22]. Here the inhibition of RhoA pathway by ibuprofen-loaded P(TMC-CL) scaffolds was investigated both *in vitro* and *in vivo*.

2. Materials and Methods

2.1. Scaffolds preparation and design

Bilayer scaffolds were prepared using a statistical P(TMC-CL) copolymer. The copolymer was prepared by ring-opening polymerization and subsequently purified as previously described [23]. In brief, ε-caprolactone (CL) (Merck, Germany) was dried overnight (calcium hydride; Sigma-Aldrich Química, Portugal) and distilled before the polymerization with trimethylene carbonate (TMC, used as received from Boehringer Ingelheim, Germany). Polymerization was carried out in evacuated and sealed glass ampoules using stannous octoate (Sigma-Aldrich Química, Portugal) as catalyst (2×10^{-4} mol per mol of monomer). After 3 days of reaction at 130°C the polymer obtained was purified by dissolution in chloroform (BDH-Prolabo, Portugal) and subsequent precipitation into a tenfold volume of ethanol (96%, v/v; AGA, Portugal). The chemical composition of the purified copolymer was assessed by ^{1}H nuclear magnetic resonance (NMR) and found to contain 11% mol of TMC, being in accordance to the monomer ratio charged (10% mol TMC). The average number molecular weight and polydispersity index of the purified polymer were determined by size exclusion chromatography [22] and were found to be $8.2\text{x}10^{4}$ and 1.61, respectively.

Bilayer scaffolds were composed by an outer layer comprising a P(TMC-CL) film prepared by solvent casting, and an inner layer, made of preferentially aligned electrospun P(TMC-CL) fibres (Figure 5, A). To prepare solvent cast films, a 6% (w/v) P(TMC-CL) solution in dichloromethane (DCM; Merck, Germany) was casted onto a glass mould. The solvent was left to evaporate overnight under a DCM saturated atmosphere at room temperature (20-25 ºC) and subsequently, the films were vacuum dried for 24 hrs (vacuum oven, Raypa, Spain). For the preparation of ibuprofen-loaded scaffolds, 5% of ibuprofen (w/w of polymer) was added to the polymer solution and slowly stirred for 5 hrs, before casting. Pharmaceutical grade ibuprofen (purity>99%) was kindly supplied by Sérgio Simões (Bluepharma, Portugal).

Based on previous findings from our group [22], P(TMC-CL) electrospun fibres were prepared as follows. P(TMC-CL) was dissolved overnight in a mixture of DCM and N,N-dimethylformamide (DMF, Merck) at a volume ratio of 3:1. When preparing ibuprofen-loaded fibres, the drug (5% (w/w of polymer)) was added to the polymer solution and stirred for 5 hrs before electrospinning. The prepared solutions were dispensed at a controlled flow rate of 1 $ml.h^{-1}$ using a syringe pump (Ugo Basille, Italy). The blunt needle serving as spinneret (inner diameter 0.8 mm) was placed at 13 cm from the collector and an 18 kV electric field was applied (Gamma High Voltage source; FL, USA). The fibres were collected onto P(TMC-CL) solvent cast films covering a cylindrical drum (10 cm diameter, 15 cm of length, Yflow, Spain) rotating at 3000 rpm. The fibres were collected during 2.5 hrs and subsequently the scaffolds were vacuum dried for 24 hrs. 6x5 mm bilayer scaffolds were

punched out and packed under vacuum after an argon purge. Samples were sterilized by gamma irradiation (25 kGy, ^{60}Co source) prior further use.

2.2. Scaffolds characterization

The scaffolds were observed by scanning electron microscopy (SEM) using a FEI Quanta 400FEG microscope (FEI, the Netherlands) after being sputter-coated with gold-palladium for 90 seconds (SPI Supplies, PA, USA). Fibre diameter and alignment were quantified from SEM micrographs using Image analysis software (Image J, version 1.39, NIH, MD, USA). The fibre mean diameter was calculated from, at least, 100 measurements from 3 independent samples. To calculate fibre alignment, the preferential direction of the alignment was defined for each image and subsequently the angle formed between the fibres and this axis was measured. Results are presented as percentage relative to the total number of fibres measured from 3 independent samples.

2.3. Drug release quantification

The amount of ibuprofen released from P(TMC-CL) scaffolds was evaluated as follows. Samples were incubated at 37ºC and 120 rpm (Orbital Shaker Oven, IKA, Germany) in phosphate buffered saline (PBS) at the final concentration of 5 mg.ml^{-1} (mass of fibres/volume of PBS). At defined time points (0.5, 1, 2, 4, 6, 8, 24 and 48 hrs), the releasing medium was refreshed. The amount of ibuprofen released was quantified by high-pressure liquid chromatography (HPLC). In brief, the equipment used was an HPLC system (LaChrom Elite®, Hitachi Portugal) equipped with a variable wavelength diode array detector (L-2455). Separation was performed using a Lichrosorb RP-18 column (5 µm, 12.5 x 0.4 cm, Merck) and a mobile phase consisting on a mixture of acetonitrile and ortho-phosphoric acid 0.015 M (45:55, (v/v), all supplied by Merck). Flow rate was set to 2.5 ml.h^{-1} and separation occurred at 40ºC, whereas detection was performed at 25ºC. Ibuprofen was detected at 230 nm after 10 µl sample injection. Cumulative release was calculated relative to the theoretical maximum loading of 5% (w/w of polymer).

2.4. Cell Culture

ND7/23 cell line (mouse neuroblastoma (N18 tg 2) x rat dorsal root ganglion neuron hybrid) was obtained from ECACC (United Kingdom) and routinely cultured in Dulbecco's Modified Eagle Medium (DMEM) with Glutamax, supplemented with 10% (v/v) of heat inactivated (56ºC, 30 minutes) foetal bovine serum (FBS) and 1% penicillin/streptomycin (PS, 10,000 units.ml^{-1} penicillin and 10,000 µg.ml^{-1} streptomycin), all supplied by Gibco (Life technologies S.A., Spain).

To test the effect of ibuprofen on these cells, ND7/23 cells were sub-cultured using supplemented DMEM at a cellular density of 2x10^4 viable cells.cm^{-2}. To promote cell differentiation, 24 hrs after seeding the cell culture medium was replaced by differentiation medium containing 0.5% FBS, 1%

PS, 200 nM nerve growth factor (NGF, Calbiochem, Merck), and 1 mM cyclic adenosine monophosphate (cAMP, Sigma-Aldrich). Cells were allowed to differentiate for 2 days before further treatment.

2.5. Effect of ibuprofen on ND7/23 cell metabolic activity

The effect of ibuprofen on ND7/23 cell metabolic activity was assessed by means of a resazurin-based assay. In brief, different ibuprofen solutions in ethanol:water (7:3) were prepared and added (5 µl) to the cell culture medium (500 µl) in order to obtain a final drug concentration ranging from 50 to 2000 µM. After a 24 hrs treatment, cells were incubated (4 hrs, 37 °C) with a resazurin (Sigma-Aldrich) solution (0.1 $mg.ml^{-1}$, in PBS). Fluorescence (λ_{ex}= 530 nm, λ_{em}= 590 nm) in the cell culture medium was measured (SynergyMx, Biotek, Portugal). Results are represented as percentage of cell metabolic activity relative to cells treated with equal volume of the ibuprofen solvent (5 µl).

2.6. *In vitro* inhibition of RhoA activation by ibuprofen

To investigate whether ibuprofen released from P(TMC-CL) scaffolds could influence RhoA activation in ND7/23 cells, extracts from the ibuprofen-loaded scaffolds (Ibuprofen scaffold) were firstly prepared as follows. Scaffolds were incubated in DMEM at 37ºC (80 rpm) during 72 hrs. The volume of DMEM used was adjusted according to the weight of scaffolds in order to achieve, after the total release of ibuprofen, a theoretical drug concentration of 500 µM. The concentration was selected based on a previous report showing ibuprofen-mediated inhibition of RhoA pathway in the PC12 cell line [7]. The obtained extracts were then tested on differentiated ND7/23 cells. In brief, after a starving period of 2 hrs in DMEM without serum, cell culture medium was replaced by the ibuprofen-containing extracts obtained from the P(TMC-CL) scaffolds. Ibuprofen solution (100x in ethanol:water (7:3)) was added to the cell culture media to a final concentration of 500 µM to serve as control (Ibuprofen soluble). After 30 minutes, the cells were activated with 45 µM of lysophosphatidic acid (LPA, Sigma-Aldrich) for 10 minutes. Non-treated cells were applied as negative control, and cells activated with LPA served as positive control for RhoA activation.

RhoA activation was assessed using Rhotekin RBD-coupled beads (Millipore, MA, USA) according to manufacturer instructions. Cell lysates were prepared using Mg^{2+} lysis buffer (MLB) containing 25 mM HEPES, 1% Tergitol (v/v) and 10 mM $MgCl_2$ (Sigma-Aldrich), and 150 mM NaCl, 1% (w/v) EDTA and 10% (v/v) glycerol from BDH-Prolabo (Portugal) and a protease inhibitors cocktail (Sigma-Aldrich). Lysates were clarified by centrifugation (20,000xg, 4ºC, 5 minutes) and snap frozen prior further use. Total protein content was quantified using DC protein assay (Bio-Rad, Portugal). Lysates containing 1 mg of total protein were incubated with RBD-coupled beads during 1 hr at 4ºC under slow rotation. After two washing steps, the beads were resuspended in 2x laemmli buffer (Bio-Rad) containing β-mercaptoethanol, boiled at 95ºC (10 minutes) and filtered using Mobicol filters (35 µm, Mobitec, Germany). Bound GTP-RhoA along

with 25 µg of total lysate were separated in a 12% (w/v) SDS-polyacrilamide gel and detected by western blot. Briefly, gels were transferred to Hybond nitrocellulose ECL membrane (Amersham, GE Healthcare Europe GmbH, Portugal) and blocked in a 5% skim milk in PBS containing 0.1% (v/v) Tween-20 (PBS-T). The membranes were incubated overnight with a mouse anti-RhoA antibody (1:500, sc-418; Santa Cruz Biotechnology, CA, USA) followed by a 1 hr incubation with horseradish peroxidase-labelled sheep anti-mouse IgG (1:3,000, Amersham). After extensive washing the immunoreactive bands were detected using WesternBright Quantum Chemiluminescent Substrate (Advansta, CA, USA) and visualized by autoradiography on an Amersham Hyperfilm ECL (GE Healthcare Europe). The relative intensity of protein bands was analyzed using Quantity One (version 4.6) program (Bio-Rad). Results are expressed as the ratio between the activated protein form of RhoA (RhoA-GTP) and the total protein (RhoA).

2.7. Preliminary *in vivo* testing – dorsal hemisection model

All experiments involving animals and their care were conducted in compliance with institutional ethical guidelines and with the approval of Portuguese Veterinary Authorities – Direcção Geral de Veterinária (DGAV). Female adult Wistar rats (10 - 13 weeks) were anesthetized with ketamine/medetomidine (100 $mg.kg^{-1}$ ketamine; 1 $mg.kg^{-1}$ medetomidine). Laminectomies were performed at the 8 and 9 vertebrae and the spinal dura mater was incised to expose the spinal cord. Dorsal hemisection at the T9 level was performed using a micro-scissor. The scaffolds (6x5 mm) were implanted underneath the dura, immediately after the lesion was carried out. The fibrous side of the scaffolds was placed in contact with the spinal cord, ensuring that fibres were longitudinally aligned with the axonal pathways. The surgery site was closed in layers using absorbable suture (Surgicryl, Smi, Belgium). Atipamezole (1 $mg.kg^{-1}$) was administrated to counteract anaesthesia. The rats were kept in heating pads 24 hrs after surgery and abdominal massage was performed twice a day to help bladder evacuation. Butorphanol (1 $mg.kg^{-1}$) was administrated twice a day during the first two days after surgery to manage pain.

A total of twenty animals undergone surgery and were distributed in three experimental groups as follows: (A) non-treated (n=6); (B) P(TMC-CL) scaffold (n=7); (C) ibuprofen-loaded P(TMC-CL) scaffold (n=7). All the animals were subjected to dorsal hemisection as described above being that animals from group A were subjected to no further treatment, and animals from group B and C were implanted with P(TMC-CL) scaffolds, plain or loaded with ibuprofen, respectively. Five days after implantation, the animals were euthanized. The scaffold was removed and 1 cm of the spinal cord tissue centred at the lesion site was collected and divided sagitally. Part of the tissue was snap frozen in dry ice and stored at -80 ºC for posterior RhoA quantification. The second portion of the spinal cord, was fixed using 4% (w/v) paraformaldehyde at 4ºC (overnight). The samples were then transferred to a 30% (w/v) sucrose solution containing 0.1% (w/v) sodium azide for cryoprotection and stored at -20ºC before cryostat sectioning.

2.7.1. Histology and Immunohistochemistry

Spinal cord tissue was embedded on optimum cutting medium (OCT, Thermo Scientific, Thermo Fisher Scientific, Portugal) and cut onto 16 µm thick sections using a cryostat (Thermo Scientific). Sections were mounted onto glass coverslips (Superfrost, VWR) and stored at -20ºC till further use.

Sections were stained using haematoxilin and eosin according to standard procedures.

For immunohistochemistry, cryostat sections were firstly incubated with 0.1% (w/v) sodium borohydride (5 minutes) and ammonium chloride (50 mM, 15 minutes). Afterwards, sections were incubated 1 hr at 37ºC with blocking buffer containing 5% (v/v) normal donkey serum (Sigma-Aldrich) and 0.3% (v/v) Triton X-100 in PBS. The primary antibody for glial fibrillary acidic protein (GFAP, rabbit anti GFAP, Dako) was diluted in the blocking buffer (1:500) and incubated with the cryosections overnight at 4ºC. Subsequently, sections were incubated 1 hr at room temperature with Alexa 488-conjugated anti-rabbit secondary antibody (Invitrogen, 1:1,000). Afterwards, Hoechst solution (Invitrogen, 1:30,000) was applied (15 minutes at room temperature) in order to label cell nuclei. Stained sections were coverslipped using Fluoromount (Sigma-Aldrich) and kept at -20ºC until analysis. The immunolabelled tissue sections were analyzed using an inverted fluorescence microscope (Axiovert 200, Zeiss, Germany) .

2.8. Statistical analysis

Statistical analysis was performed using the Graphpad Prism 5.0 software (GraphPad, CA, USA). Statistical differences were calculated using one-way ANOVA followed by the Dunnett's test for multiple comparisons. A p value lower than 0.05 was considered statistically significant.

3. Results

3.1. Scaffold morphology

By combining solvent casting and electrospinning a bilayer scaffold was prepared. The obtained scaffolds were analysed by SEM and representative images are presented in Figure 1. The surface of the solvent cast flat outer layer reveals a spherulitic morphology, typical of a semicrystalline material [24] (Figure 1, A, C; E, G). The inner layer composed by electrospun fibres shows a preferentially longitudinally aligned fibrous structure (Figure 1, B, D, F, H). The presence of ibuprofen alters jet stability as denoted by the formation of bended fibres (Figure 1, F and H). Nonetheless, on the whole, the fibre mean diameter and alignment were not significantly altered as one can observe by comparing non-loaded and ibuprofen-loaded fibres. Fibre mean diameter was found to be 0.661 and 0.646 µm for non-loaded and ibuprofen-loaded fibres, respectively (Figure 1, K).

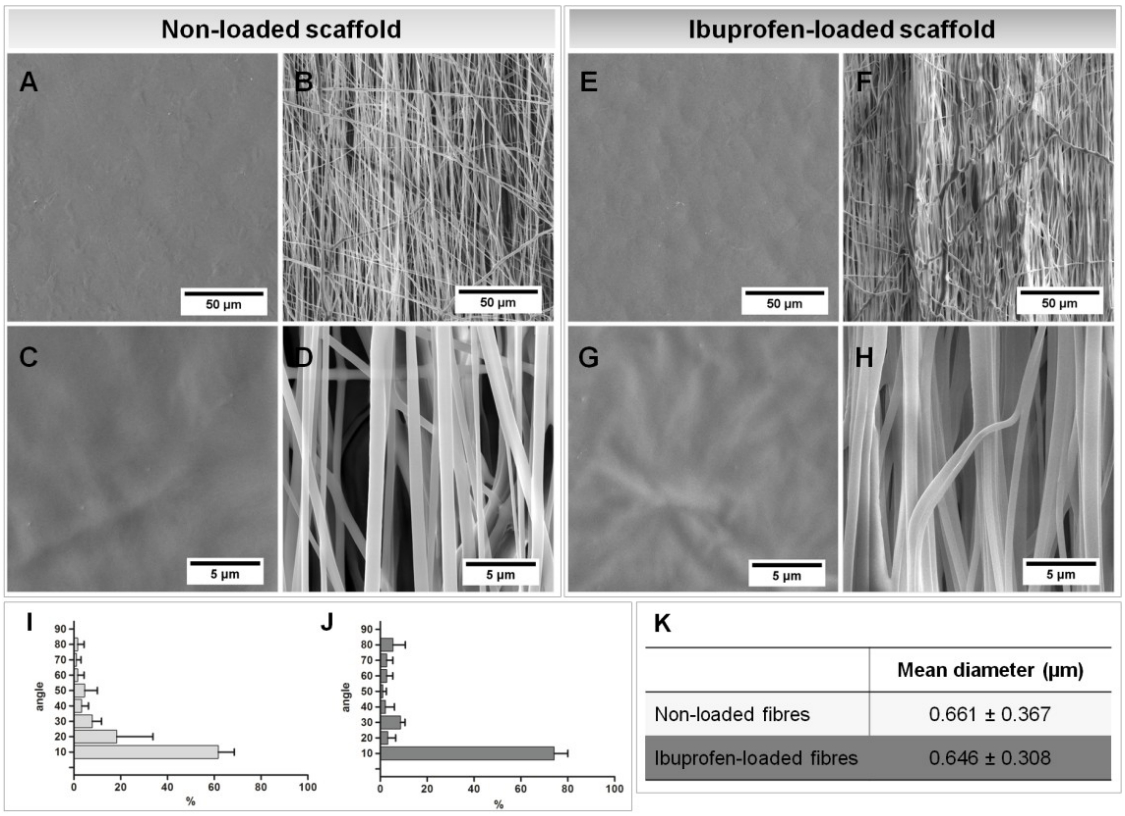

Figure 1. Characterization of the P(TMC-CL) scaffolds under investigation. Scanning electron microscopy photomicrographs of **(A-D)** non-loaded and **(E-H)** ibuprofen-loaded scaffolds. Images A, C, E and G show the outer layer of the scaffold composed by solvent cast films; images B, D, F and H shows the inner layer made of preferentially aligned fibres prepared by electrospinning. **(I and J)** Graphic representation of the quantification of fibre alignment for (I) non-loaded and (J) ibuprofen-loaded fibres. Bars represent average and error bars show standard deviation (n=3). **(K)** Fibre mean diameter as calculated from at least 100 measurements (n=3).

3.2. Drug release from P(TMC-CL) scaffolds

The release of ibuprofen from P(TMC-CL) bilayer scaffolds was evaluated when in PBS at 37ºC. The percentage of cumulative release was calculated relative to a theoretical maximum loading of 5% (w/w of polymer).

Under the experimental conditions tested, ibuprofen was released from the P(TMC-CL) scaffolds within the first 24 hrs of incubation in PBS (37°C) (Figure 2). When fibres were incubated in PBS for longer period, none or residual amounts of ibuprofen were detected, being that the limit of quantitation of the applied experimental setup was determined to be 0.001 $mg.ml^{-1}$. The scaffolds were analysed by SEM after drug release and the fibrous morphology was maintained (data not shown).

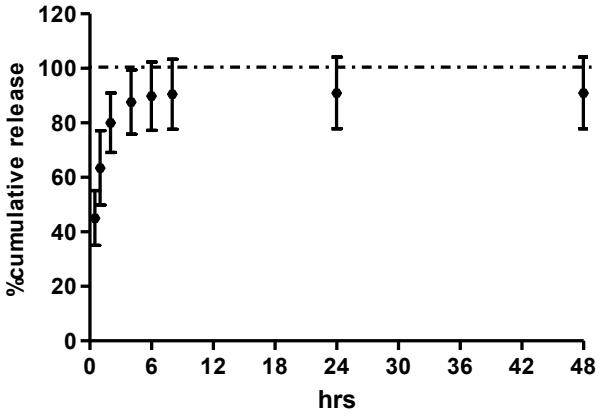

Figure 2. Cumulative release of ibuprofen from P(TMC-CL) scaffolds when incubated in PBS (37°C), as determined by HPLC. Average ± standard deviation are represented (n=7).

3.3. Effect of ibuprofen on ND7/23 cell line

3.3.1. Cell viability

To determine whether ibuprofen can affect ND7/23 cells, cell metabolic activity was assessed as measure for cellular viability. The drug was added in its soluble form to the cell culture medium to a final concentration ranging from 50 to 2000 µM. Ibuprofen solvent (ethanol:water (7:3)) was used as reference and is represented as ibuprofen concentration 0 µM.

The graph presented in Figure 3 shows that when cells are incubated during 24 hrs in the presence of ibuprofen at a final concentration higher than 500 µM, the cell metabolic activity is reduced in a concentration-dependent manner. No significant difference on cell metabolic activity was observed when cells were treated with ibuprofen up to 500 µM.

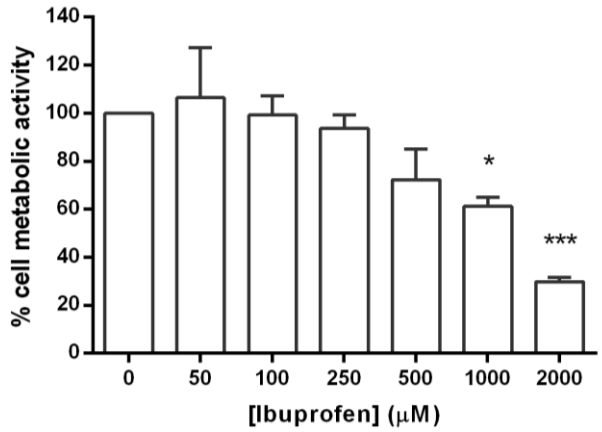

Figure 3. Cell viability of ND7/23 differentiated cells after incubation with different concentrations of ibuprofen. Bars represent mean values and error bars show standard deviation (n=4). Percentage calculated relative to the cells treated with ibuprofen solvent (ethanol:water (7:3)). *p< 0.05; ***p<0.001 relative to control.

3.3.2. RhoA activation

Pre-treatment of cells with ibuprofen has previously shown to limit RhoA-induced activation, namely by LPA [7]. To investigate if ibuprofen released from P(TMC-CL) bilayer scaffolds retains its bioactivity and can have an effect on the RhoA pathway, RhoA activation was assessed in treated ND7/23 cells after stimulation with LPA. The cells were pre-treated with extracts from P(TMC-CL) ibuprofen-loaded scaffolds, or with medium supplemented with ibuprofen solution. Non-activated cells (no LPA stimulation) and cells activated with LPA, but non-treated with ibuprofen were used as negative and positive control, respectively.

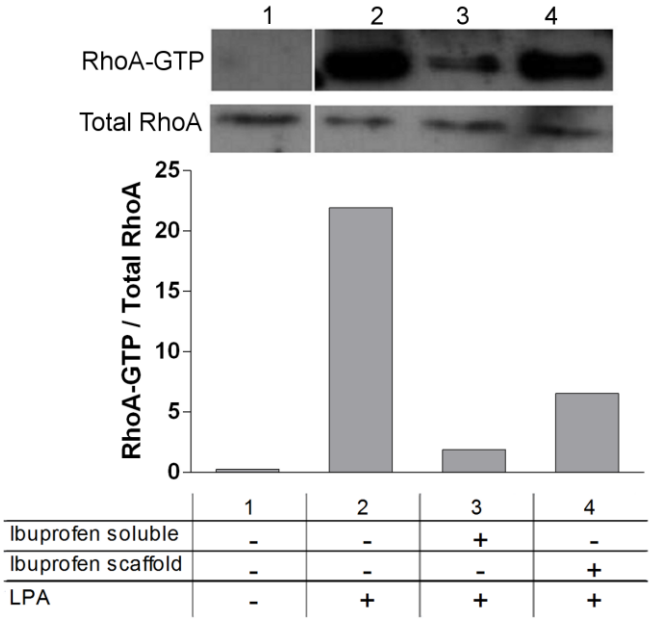

Figure 4. RhoA activation on ND7/23 cells as determined by western blot after precipitation of the active form of RhoA (RhoA-GTP). Stimulation with LPA (45 µM, 10 minutes, 2-LPA) and pre-treatment with ibuprofen (3-Ibuprofen soluble) or ibuprofen released from P(TMC-CL) scaffolds (4-Ibuprofen scaffold) were tested. The RhoA basal activation was also assessed (lane 1).

The activated form of RhoA was not detected in non-stimulated ND7/23 cells. Treatment with LPA leads to an increase on RhoA activation as demonstrated by the detected high levels of RhoA-GTP (Figure 4, lane 2). Similarly to the effect observed when cells were incubated with soluble ibuprofen, cells treated with extracts of the ibuprofen-loaded P(TMC-CL) scaffolds showed a significant reduction (approximately 5 times) of the LPA-mediated RhoA activation (Figure 4).

3.4. Preliminary *in vivo* testing of ibuprofen-loaded P(TMC-CL) scaffolds

The developed P(TMC-CL) bilayer scaffolds were tested in an *in vivo* situation by implantation in contact with a spinal cord immediately after dorsal hemisection (Figure 5).

As shown in Figure 5, the P(TMC-CL) scaffolds were placed at the lesion site wrapping the spinal cord tissue. We found that the scaffolds bend properly to allow fixation in the bone and close contact with the spinal cord tissue. Five days after implantation, the retrieved scaffolds were found to be covered by fibrous tissue, and no signs of scaffold degradation were observed (Figure 5, C).

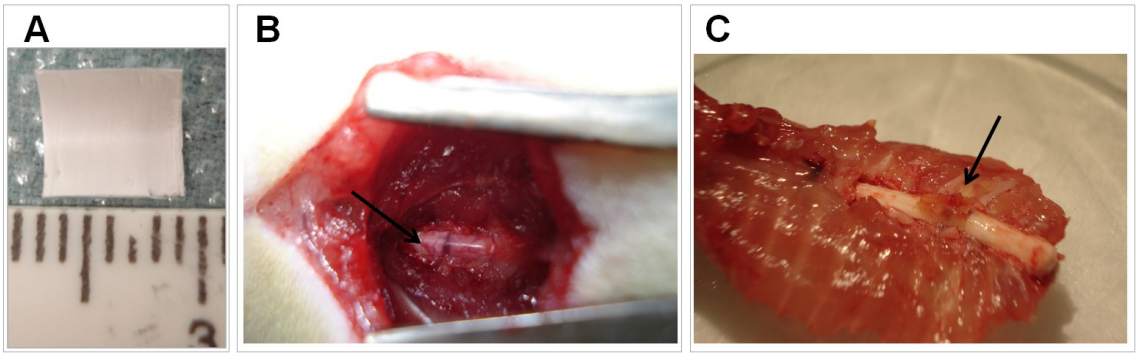

Figure 5. Photographs of the aspect of the bilayer P(TMC-CL) scaffold **(A)** prior implantation (gamma sterilized); **(B)** after implantation in an injured (dorsal hemisection) spinal cord; and **(C)** as collected after animal euthanasia (5 days post implantation). Arrows indicate the P(TMC-CL) scaffold.

From the twenty animals used in this experiment, one, from group B, was excluded due to poor health at the day 5 of the experiment. This unique event was considered to be independent from the treatment, as animals with SCI are generally more susceptible to infections [25]. The implantation of ibuprofen-loaded P(TMC-CL) scaffolds did not compromise animal survival after SCI.

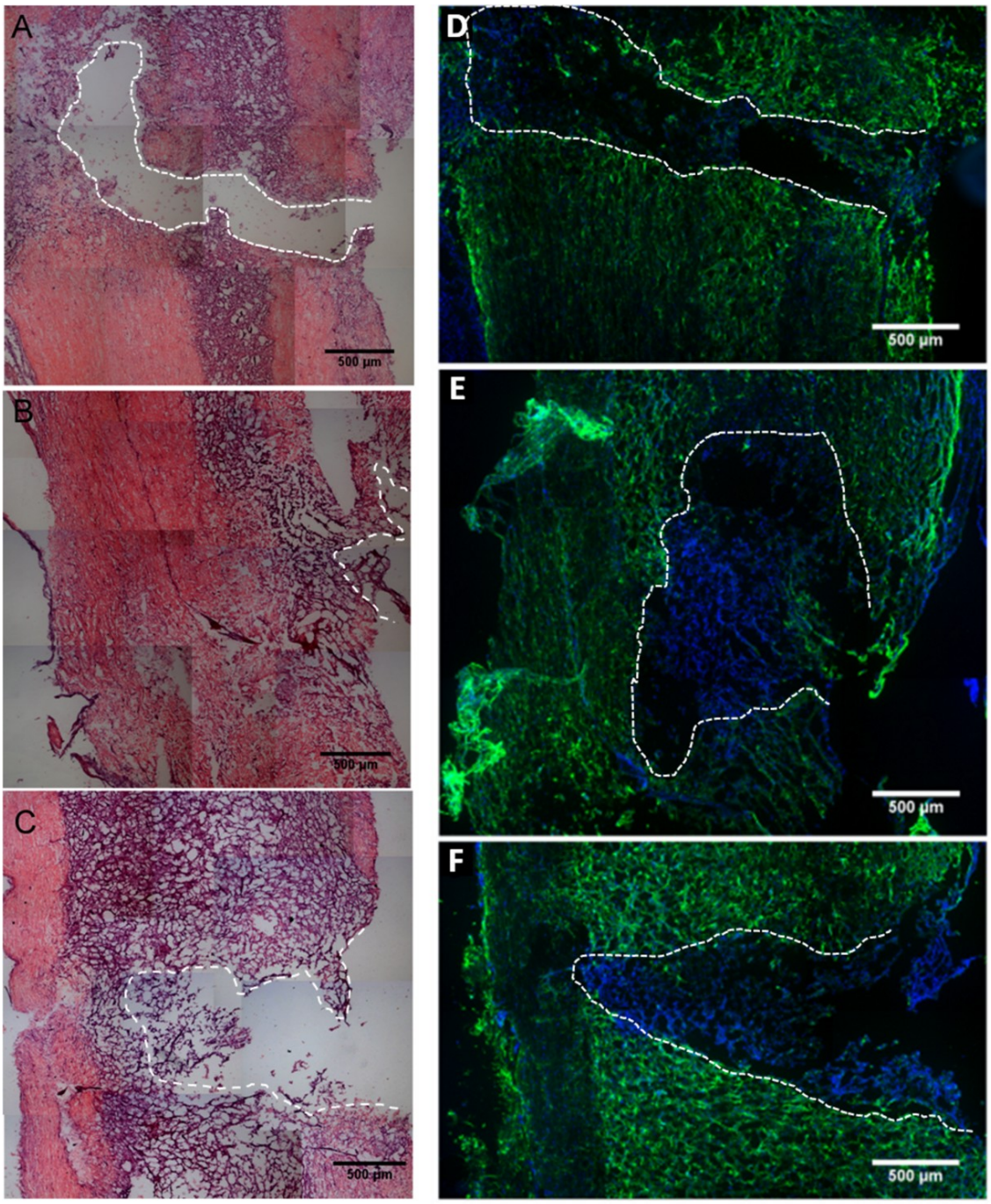

Figure 6. Light microscopy images of the haematoxylin-eosin staining **(A-C)** and fluorescence microscopy images of GFAP (green) and DAPI (blue) immunolabelling **(D-F)** of cryosections from the spinal cord of **(A and D)** control animal dorsal hemisection and animals with implanted **(B and E)** P(TMC-CL) scaffold or **(C and F)** ibuprofen-loaded scaffold. Tissue was collected 5 days after implantation. The images show the region of the lesion (delimited in white).

The histological evaluation of the tissues collected is ongoing. Figure 6 shows the preliminary analysis of one tissue from each experimental group. Figure 6 (A, B, C) shows the haemotoxilin-eosin staining of the area of the lesion in tissues from group A (non-treated), group B (P(TMC-CL) scaffold) and group C (ibuprofen-loaded P(TMC-CL) scaffold), respectively. In the case of group

B, the region of the lesion is more difficult to demarcate, as it seems more spread than in the other tissues, where it is clearly identified. It is worthwhile mentioning that in the animals where P(TMC-CL) scaffolds were implanted, the scaffold was separated from the spinal cord prior cryopreservation of the tissue. This process seems to have affected tissue cohesion and cause the appearance of additional debris in the stained sections (see Figure 6, B). Comparing the tissue from group A and C, the images from haemotoxilin-eosin staining suggest that the extension of the tissue damage is different among groups. When analysing the cryosections immunolabelleded for GFAP, it can be observed that on group B and C (Figure 6, E and F) a higher number of cells is found in the lesion site, suggesting significant cellular infiltration. Nevertheless, the number of GFAP positive cells in that region was found to be residual. This observation is not replicated in group A (Figure 6, D), where signs of astrogliosis (GFAP positive cells) are detected at the time of the evaluation.

4. Discussion

It is commonly accepted that a multi-target strategy will be required to tackle the challenge of promoting nerve regeneration after SCI [15]. Following the primary injury that interrupts axonal pathways, the rewiring of the system is limited due to the lack of physical support, the activation of inhibitory pathways, and, ultimately, due to the formation of a glial scar that physically halts axonal re-connection. In the present work, we describe the preparation of a bilayer scaffold that can provide physical support, guidance cues and can serve as vehicle for the *in situ* delivery of ibuprofen, a drug expected to be able to reduce the inhibitory environment at the lesion site.

The use of aligned electrospun fibres to guide axonal growth has been previously explored in the literature both for the peripheral and the central nervous system regeneration (see [26] for a review). In the first report using aligned electrospun fibres in a SCI scenario, the authors claimed a robust rostral regeneration, four weeks after implantation of poly(L-lactide) longitudinally aligned fibres. The success of the strategy was ascribed to the anisotropy of the substrates as modest regeneration was observed when randomly oriented fibres or solvent cast films were implanted [19]. Here, we report the successful preparation of P(TMC-CL) preferentially aligned fibres. Fibre mean diameter was found to be around 650 nm, in accordance with that previously described for randomly oriented structures using the same solvent mixture [22]. The aligned fibres were collected onto solvent cast films in order to improve the final mechanical properties of the scaffold. Nanofibrous scaffolds have, in general, weaker mechanical properties than bulky structures [27], particularly when constituted by aligned fibres [28]. This can compromise the success of an implantable device, as demonstrated in a previous study showing that the folding of an electrospun fibrous fabric impaired nerve regeneration [29].

The vectorization through scaffolds of molecules that have a positive effect on regeneration holds a great potential to become a therapeutic strategy for SCI. It was previously shown that the implantation after lesion of a nanofibrous patch with rolipram physically adsorbed to poly(L-

lactide)-based electrospun fibres lead to an improved functional recovery from the third week on, comparing to non-loaded scaffolds that showed a similar result as non-treated animals [28]. In the present study, it is proposed the use of ibuprofen incorporated in a P(TMC-CL) scaffold, based on the reported inhibitory action of the drug on the RhoA pathway [7, 8]. Bilayer ibuprofen-loaded scaffolds were prepared by mixing the drug with the polymer solution prior to electrospinning and solvent casting, for the preparation of the inner and outer scaffold layer, respectively. It was observed that the drug released from the scaffolds is bioactive as confirmed by the hindrance of RhoA activation in a neuronal-like cell population challenged with LPA – a known RhoA activator. This result encouraged the testing of P(TMC-CL) bilayer scaffolds in an *in vivo* SCI model.

The ibuprofen release profile from the P(TMC-CL) bilayer scaffolds conducted in sink conditions indicated that the majority of the drug is released within the first 24 hrs of incubation. When translating this data to an *in vivo* scenario, one can expect that this release will be delayed as in the conducted studies the media was completely refreshed at each evaluation time point, what favours the washing out of the drug from the scaffold. Moreover, we hypothesized that a significant release of ibuprofen in the initial stages of the tissue response after a lesion can also play a role on the early inflammatory response triggered, namely reducing microglia activation [10] and that this can positively contribute to regeneration in the aftermath of a SCI [30].

The results reported in this manuscript concerning the *in vivo* performance of the developed P(TMC-CL) scaffolds are still preliminary. This experiment aimed at constituting a proof-of-concept from the feasibility of using ibuprofen-loaded bilayer scaffolds for inhibiting RhoA activation. In that view, the study was designed to address the early response on the RhoA pathway and not attempt to assess axonal regeneration or achieve functional improvements. So far, we demonstrated that the implantation of P(TMC-CL) scaffolds can be successfully achieved and does not compromised animal survival rate. Although we were not expecting any deleterious effect caused by the implantation of P(TMC-CL) scaffolds, some concern existed about the drug loading applied. The published studies using ibuprofen for treatment of SCI report the subcutaneous administration of the drug at the dose of 60 $mg.kg^{-1}.day^{-1}$ [7, 8]. In the present study the drug loading in the P(TMC-CL) scaffolds was in average 500 $\mu g.cm^{-2}$, corresponding to approximately 0.75 $mg.kg^{-1}$. However, it must be noted that in the present study, the release of the drug occurs *in situ*, as the scaffold is in direct contact with the spinal cord tissue. A previous work using rolipram loaded patches implanted in contact with the spinal cord, showed that implantation of high drug doses (65 $\mu g.cm^{-2}$) lead to an increase on animal mortality rate [31]. It should be mentioned however, that the effective dose of ibuprofen and rolipram are significantly different, and improvements on regeneration after SCI by the administration of rolipram are achieved by the subcutaneous administration of 1 $mg.kg^{-1}$ of drug [32], 60 times less than that reported for ibuprofen [7, 8].

The preliminary histological characterization of the tissues collected from animals treated with ibuprofen-loaded P(TMC-CL) bilayer scaffolds showed that at the time of evaluation (5 days after the lesion) considerable cellular infiltration occurred at the lesion site, but no signs of astrogliosis

were identified so far. In comparison, the untreated animals showed already signs of the presence of a glial scar at the lesion site, as indicated by the presence of GFAP positive cells. The ongoing characterization of the infiltrated cells will shed light on the effect of the released ibuprofen on the modulation of the lesion microenvironment. Ultimately, the quantification of RhoA activation in tissues in contact with ibuprofen-loaded scaffolds will contribute for disclosing the potential of the proposed strategy in providing a more permissive milieu for axonal regeneration.

5. Conclusion and Future Perspectives

This study describes the successful preparation of bilayer P(TMC-CL) scaffolds containing longitudinally aligned P(TMC-CL) fibres, and loaded with ibuprofen. It is demonstrated that ibuprofen released from P(TMC-CL) scaffolds can effectively reduce RhoA activation in ND7/23 cells putting forward these scaffolds to be applied in a SCI scenario.

A preliminary *in vivo* experiment was performed and showed, so far, that the scaffolds can be implanted in the spinal cord after injury. No effect on animal survival was observed. The detailed histological characterization of the retrieved tissues is ongoing and will provide critical information on the success of the proposed strategy, bringing also new insights to future improvements on scaffold design. Drug loading, or the drug release profile are parameters that can be modulated in order to develop a scaffold that better supports cells in the hostile environment of SCI.

To assess the effect of the strategy proposed in this study on axonal growth or functional recovery after SCI, it is necessary to perform an extended experiment in which the scaffolds are implanted for a longer period. This study is key to evaluate the effect of the early inhibition of RhoA pathway on regeneration and also the contribution of P(TMC-CL) and fibre alignment in the process.

Acknowledgements

This work was financed by FEDER funds through the *Programa Operacional Factores de Competitividade* – COMPETE and by Portuguese funds through FCT – *Fundação para a Ciência e a Tecnologia* in the framework of the project PEst-C/SAU/LA0002/2011 and PTDC/CTM-NAN/115124/2009. LR Pires and DN Rocha thank FCT for their PhD grants (SFRH / BD / 46015 / 2008 and SFRH / BD / 64079 / 2009). The authors wish to thank Ana Marques and Marlene Morgado for the technical assistance. Authors acknowledge the *Centro de Materiais da Universidade do Porto* (CEMUP; REEQ/1062/CTM/2005 from FCT) for SEM and ^{1}H NMR analysis and to Sérgio Simões for the kind help making available the use of HPLC equipment at Bluepharma (Coimbra).

References

1. Schwab JM, Brechtel K, Mueller CA, Failli V, Kaps HP, Tuli SK, and Schluesener HJ (2006). "Experimental strategies to promote spinal cord regeneration - An integrative perspective". *Progress in Neurobiology*, 78 (2): 91-116.

2. Silver J and Miller JH (2004). "Regeneration beyond the glial scar". *Nature Reviews Neuroscience*, 5 (2): 146-156.

3. Dergham P, Ellezam B, Essagian C, Avedissian H, Lubell WD, and McKerracher L (2002). "Rho signaling pathway targeted to promote spinal cord repair". *Journal of Neuroscience*, 22 (15): 6570-6577.

4. McKerracher L and Higuchi H (2006). "Targeting Rho to stimulate repair after spinal cord injury". *Journal of Neurotrauma*, 23 (3-4): 309-317.

5. Monnier PP, Sierra A, Schwab JM, Henke-Fahle S, and Mueller BK (2003). "The Rho/ROCK pathway mediates neurite growth-inhibitory activity associated with the chondroitin sulfate proteoglycans of the CNS glial scar". *Molecular and Cellular Neuroscience*, 22 (3): 319-330.

6. Zhou Y, Su Y, Li BL, Liu F, Ryder JW, Wu X, Gonzalez-DeWhitt PA, Gelfanova V, Hale JE, May PC, Paul SM, and Ni BH (2003). "Nonsteroidal anti-inflammatory drugs can lower amyloidogenic A beta(42) by inhibiting Rho". *Science*, 302 (5648): 1215-1217.

7. Fu Q, Hue J, and Li S (2007). "Nonsteroidal anti-inflammatory drugs promote axon regeneration via RhoA inhibition". *Journal of Neuroscience*, 27 (15): 4154-4164.

8. Wang X, Budel S, Baughman K, Gould G, Song KH, and Strittmatter SM (2009). "Ibuprofen enhances recovery from spinal cord injury by limiting tissue loss and stimulating axonal growth". *Journal of Neurotrauma*, 26 (1): 81-95.

9. Sharp KG, Yee KM, Stiles TL, Aguilar RM, and Steward O (2013). "A re-assessment of the effects of treatment with a non-steroidal anti-inflammatory (ibuprofen) on promoting axon regeneration via RhoA inhibition after spinal cord injury". *Experimental Neurology*, 248: 321-327.

10. Redondo-Castro E and Navarro X (2014). "Chronic ibuprofen administration reduces neuropathic pain but does not exert neuroprotection after spinal cord injury in adult rats". *Experimental Neurology*, 252: 95-103.

11. Xing B, Li H, Wang H, Mukhopadhyay D, Fisher D, Gilpin CJ, and Li S (2011). "RhoA-inhibiting NSAIDs promote axonal myelination after spinal cord injury". *Experimental Neurology*, 231 (2): 247-260.

12. Mitchell JA, Akarasereenont P, Thiemermann C, Flower RJ, and Vane JR (1993). "Selectivity of nonsteroidal antiinflammatory drugs as inhibitors of constitutive and inducible cyclooxygenase". *Proceedings of the National Academy of Sciences of the United States of America*, 90 (24): 11693-11697.

13. Rainsford KD (2009). "Ibuprofen: pharmacology, efficacy and safety". *Inflammopharmacology*, 17 (6): 275-342.

14. Kopp MA, Liebscher T, Niedeggen A, Laufer S, Brommer B, Jungehulsing GJ, Strittmatter SM, Dirnagl U, and Schwab JM (2012). "Small-molecule-induced Rho-inhibition: NSAIDs after spinal cord injury". *Cell and Tissue Research*, 349 (1): 119-132.

15. McCreedy DA and Sakiyama-Elbert SE (2012). "Combination therapies in the CNS: Engineering the environment". *Neuroscience Letters*, 519 (2): 115-121.

16. Pêgo AP, Poot AA, Grijpma DW, and Feijen J (2003). "Biodegradable elastomeric scaffolds for soft tissue engineering". *Journal of Controlled Release*, 87 (1-3): 69-79.

17. Corey JM, Lin DY, Mycek KB, Chen Q, Samuel S, Feldman EL, and Martin DC (2007). "Aligned electrospun nanofibers specify the direction of dorsal root ganglia neurite growth". *Journal of Biomedical Materials Research - Part A*, 83 (3): 636-645.

18. Yao L, O'Brien N, Windebank A, and Pandit A (2009). "Orienting neurite growth in electrospun fibrous neural conduits". *Journal of Biomedical Materials Research - Part B Applied Biomaterials*, 90 (2): 483-491.

19. Hurtado A, Cregg JM, Wang HB, Wendell DF, Oudega M, Gilbert RJ, and McDonald JW (2011). "Robust CNS regeneration after complete spinal cord transection using aligned poly-l-lactic acid microfibers". *Biomaterials*, 32 (26): 6068-6079.

20. Vleggeert-Lankamp CLAM, Wolfs J, Pêgo AP, Van Den Berg R, Feirabend H, and Lakke E (2008). "Effect of nerve graft porosity on the refractory period of regenerating nerve fibers: Laboratory investigation". *Journal of Neurosurgery*, 109 (2): 294-305.

21. Rocha DN, Brites P, Fonseca C, and Pêgo AP (2014). "Poly(Trimethylene Carbonate-co-ε-Caprolactone) Promotes Axonal Growth". *Plos One*, 9(2): e88593.

22. Pires LR, Guarino V, Oliveira MJ, Ribeiro CC, Barbosa MA, Ambrosio L, and Pêgo AP (2013). "Ibuprofen-loaded poly(trimethylene carbonate-co-ε-caprolactone) electrospun fibers for nerve regeneration". *Journal of Tissue Engineering and Regenerative Medicine*: *Accepted for publication*.

23. Pêgo AP, Poot AA, Grijpma DW, and Feijen J (2001). "Copolymers of trimethylene carbonate and epsilon-caprolactone for porous nerve guides: Synthesis and properties". *Journal of Biomaterials Science, Polymer Edition*, 12 (1): 35-53.

24. Pêgo AP, Vleggeert-Lankamp CLAM, Deenen M, Lakke EAJF, Grijpma DW, Poot AA, Marani E, and Feijen J (2003). "Adhesion and growth of human schwann cells on trimethylene carbonate (co)polymers". *Journal of Biomedical Materials Research - Part A*, 67 (3): 876-885.

25. Balsara ZR, Ross SS, Dolber PC, Wiener JS, Tang Y, and Seed PC (2013). "Enhanced susceptibility to urinary tract infection in the spinal cord-injured host with neurogenic bladder". *Infection and Immunity*, 81 (8): 3018-3026.

26. Xie J, MacEwan MR, Schwartz AG, and Xia Y (2010). "Electrospun nanofibers for neural tissue engineering". *Nanoscale*, 2 (1): 35-44.

27. Teo WE and Ramakrishna S (2006). "A review on electrospinning design and nanofibre assemblies". *Nanotechnology*, 17 (14): R89-R106.

28. Zhu Y, Wang A, Shen W, Patel S, Zhang R, Young WL, and Li S (2010). "Nanofibrous patches for spinal cord regeneration". *Advanced Functional Materials*, 20 (9): 1433-1440.

29. Meiners S, Ahmed I, Ponery AS, Amor N, Harris SL, Ayres V, Fan Y, Chen Q, Delgado-Rivera R, and Babu AN (2007). "Engineering electrospun nanofibrillar surfaces for spinal cord repair: A discussion". *Polymer International*, 56 (11): 1340-1348.

30. Casha S, Zygun D, McGowan MD, Bains I, Yong VW, and Hurlbert RJ (2012). "Results of a phase II placebo-controlled randomized trial of minocycline in acute spinal cord injury". *Brain*, 135 (4): 1224-1236.

31. Downing TL, Wang A, Yan ZQ, Nout Y, Lee AL, Beattie MS, Bresnahan JC, Farmer DL, and Li S (2012). "Drug-eluting microfibrous patches for the local delivery of rolipram in spinal cord repair". *Journal of Controlled Release*, 161 (3): 910-917.

32. Schaal SM, Garg MS, Ghosh M, Lovera L, Lopez M, Patel M, Louro J, Patel S, Tuesta L, Chan WM, and da Pearse D (2012). "The Therapeutic Profile of Rolipram, PDE Target and Mechanism of Action as a Neuroprotectant following Spinal Cord Injury". *Plos One*, 7 (9): e43634.

CHAPTER VI

Imidazole-grafted chitosan mediated gene delivery: *in vitro* study on transfection, intracellular trafficking, and degradation*

Liliana R Pires[1, 2], Hugo Oliveira[1], Cristina C Barrias[1], Paula Sampaio[3], António J Pereira[3], Hélder Maiato[3], Sérgio Simões[4,5], Ana Paula Pêgo[1]

1 – INEB – Instituto de Engenharia Biomédica, NEWTherapies Group, Universidade do Porto, Rua do Campo Alegre 823, 4150-180 Porto, Portugal.

2 – Universidade do Porto – Faculdade de Engenharia, Rua Roberto Frias, s/n, 4200-465 Porto, Portugal.

3 – Instituto de Biologia Molecular e Celular (IBMC), Rua do Campo Alegre, 823, 4150-180 Porto, Portugal.

4 – Centro de Neurociências e Biologia Celular, Universidade de Coimbra, 3004-517 Coimbra, Portugal

5 – Departamento de Tecnologia Farmacêutica, Faculdade de Farmácia, Universidade de Coimbra, 3000-295 Coimbra, Portugal.

** Nanomedicine, 6(9): 1499-1512 (2011).*

Abstract

Aim: Study the mechanism of transfection mediated by imidazole-grafted chitosan (CHimi) nanoparticles, to propose new strategies to control and improve the expression of a delivered gene in the context of Regenerative Medicine. Methods: Biochemical and microscopy methods were used to establish transfection efficiency and nanoparticle intracellular trafficking. The role of CHimi degree of N-acetylation (DA) on transfection was explored. Results: CHimi was found to promote the expression of a delivered gene during a minimum seven-day period. Additionally, the production of a protein of interest could be upheld by consecutive transfections, without compromising cell viability. Transfection was found to be a time dependent process, requiring CHimi-DNA complex disassembling. The DA was found to have an impact on transfection kinetics in line with the observation that the rate of lysozyme-mediated nanoparticle degradation increases with the polymer DA. Conclusions: The adjustment of the CH degradation rate can be used as a tool for tuning the expression of a gene delivered by CH-based nanoparticle systems.

1. Introduction

The combination of gene delivery and tissue engineering strategies holds great promise in a regenerative medicine scenario, as a mean to promote the expression *in loco* of genes encoding for specific proteins that can play a role in regeneration [1]. This approach can overcome drawbacks associated with recombinant protein delivery, like short half-life and high cost of production [2]. Growth factors have been considered key elements due to their important role in regeneration. However, overexpression of these proteins could lead to abnormal cell behavior, since their action is commonly dose-dependent [3]. Therefore, control of gene delivery and its expression is of crucial importance. Accordingly, clinical application of strategies based on gene therapy and tissue engineering is strongly dependent on the development of vectors that can mediate the safe and effective delivery of genes, promoting a sustained and controlled expression of the encoded proteins.

A number of synthetic molecules has been explored to serve as vehicles for genetic material, as the most extensively studied being based on the use of cationic lipids like 2,3-bis[oleyl]oxipropyltrimethylammonium chloride (DOTMA) [4] or cationic polymers, such as poly(ethylene imine) (PEI) [5]. These systems can mediate promising transfection efficiencies and lead to transient expression of the transgene. However, the cytotoxicity and the lack of biodegradability of some of these vectors has been limiting their application in a regenerative medicine scenario [6-8].

Chitosan (CH) is a natural polysaccharide widely explored for biomedical applications, particularly due to its well-known biocompatibility. CH is a copolymer composed by N-acetyl glucosamine and glucosamine moieties that can be cleaved by hydrolytic enzymes, such as lysozyme [9]. The *in vivo* biodegradability makes CH use very attractive in regenerative medicine applications [10]. Several reviews were recently published concerning CH application in gene delivery, highlighting its potential and versatility [11-13]. Our group has previously showed that the incorporation of imidazole moieties into the CH backbone results in an increase of transfection efficiency comparing to the parental polymer [14]. The achieved improvement was found to be related to the higher buffering capacity of the modified CH, and consequent better escape of modified CH-DNA complexes from endosomal vesicles [14].

Foreseeing a regenerative medicine application, in this work we have performed a detailed and systematic study on the ability of imidazole-grafted CH-based vectors (CHimi) to mediate *in vitro* transfection under different experimental conditions. We focused on the evaluation of the reporter gene expression mediated by CHimi-based polymers as well as on the correlation of these observations with the intracellular trafficking of CHimi-DNA complexes in human embryonic kidney 293T cells. The obtained results led us to hypothesize that CH degradation could be influencing the expression of the delivered gene. Taking into consideration the role of the degree of N-acetylation (DA) on CH biodegradation [9], this hypothesis was explored by testing CHimi-based polymers with different DA.

2. Materials and Methods

2.1. Materials

Unless mentioned otherwise, all reagents were obtained from Sigma-Aldrich and were of analytical grade.

Technical grade chitosan (Chimarin™, DA 13%, apparent viscosity 8 mPa.s, supplied by Medicarb, Sweden) was purified and characterized prior further use. The average weight molecular weight ($\overline{M}w$), polydispersity, polydispersity index and DA of the purified polymer were found to be $1.2x10^5$, 2.1 and 16.4%, respectively (see below for experimental details) [14]. Endotoxin levels of CH extracts were found to be lower than 0.1 $EU.ml^{-1}$ [14], respecting the US Department of Health and Human Services guidelines for implantable devices [15].

Plasmids carrying β-galactosidase (pCMV-Sport β Gal, Invitrogen, 7.8 Kbp), green fluorescence protein (pCMV-GFP, 7.4 Kbp) or transthyretin (TTR) (pET-3a based plasmid, 4.9 Kbp) genes were used in this study. Plasmids were amplified in DH5α Escherichia coli (*E. coli*) and isolated using GENELUTE™ high performance endotoxin-free plasmid maxiprep kit according to the manufacturer instructions. Plasmid concentration and purity were determined spectrophotometrically (Beckman DU®650, USA). The ratio between optical density at 260 nm and 280 nm was found to be higher than 1.7.

2.2. Chemical modification of chitosan

Chitosan deacetylation. CH with a low DA was prepared by heterogeneous deacetylation [16] of the purified polymer (CH16), under argon atmosphere. The deacetylated polymer (CH05) was precipitated by addition of a mixture of water/ammonia 7:3 (v:v) and recovered by centrifugation, neutralized by washing with deionized water, freeze dried (Labconco) and, subsequently, vacuum dried at 60°C for 24 hrs.

Chitosan acetylation. CHs with different DA were obtained from re-acetylation of CH05 according to a previously described procedure [17]. The obtained polymers were purified as described above.

Imidazole grafting of chitosan. CH05, CH10, CH16 and CH18 were modified with imidazole-4-acetic acid sodium salt by amidation of the glucosamine residues using an EDC/NHS condensation system (1-Ethyl-3-[3-dimethylaminopropyl]carbodiimide hydrochloride – EDC; N-hydroxysuccinimide – NHS) [14]. Polymer stock solutions (0.1% (w/v)) were prepared according to a previously described procedure [14], and stored at 4°C till further use.

2.3. Polymer characterization

Fourier Transform – Infrared Spectroscopy (FT-IR) was performed in Perkin-Elmer 2000 system. Samples were prepared as potassium bromide (KBr) discs by mixing 2 mg of the polymer

(vacuum dried 24 hrs at 60°C) with 200 mg of KBr (dried 24 hrs at 105°C). The IR spectra were recorded, after a 5-min purge of the sample chamber with N_2, by accumulation of 200 interferograms, at a 4 cm^{-1} spectral resolution.

Size exclusion chromatography (SEC) was used to determine the molecular weight of CH05, CH10, CH16 and CH18. The modular system employed was composed by an isocratic pump (K-1001 Knaeur), a vacuum degasser (K-5002 Knaeur), a viscometer/right angle laser light scattering (RALLS) dual detector (T60 Viscotek), and a refractive index detector (K-5002 Knaeur) operating at the same wavelength as the RALLS detector (670 nm). Separations were performed in a set of PL aquagel-OH mixed columns. 0.2 M $NaCH_3COO$/0.5 M CH_3COOH was used as eluent at a flow rate of 1ml.min^{-1} and the *dn/dc* used for molecular weight calculations was 0.205 ml.g^{-1} [18]. Sample concentration in a 0.1 to 0.2% (w/v) range and an injection volume of 100 µl were applied. All measurements were performed in triplicate, at room temperature (RT).

2.4. CHimi-DNA particle preparation

CHimi-DNA particles were prepared by mixing, while vortexing, equal volumes of a CHimi solution in 5 mM CH_3COONa buffer pH 5.5 (0.1% (w/v)) and a plasmid DNA solution (in 25 mM Na_2SO_4), both previously heated at 55°C for 10 min. Complexes were allowed to form and stabilize for 15 min at RT before further use. Unless mentioned otherwise, complexes were prepared at a molar ratio of CH primary amines to DNA phosphate group (N/P) of 18.

2.5. CHimi-based particle characterization

Complexes were prepared as described above, using 10 µg of pCMV-GFP and 150 µg of CHimi, independently of the polymer DA. After stabilization, complexes were diluted to a final volume of 1 ml, using 5 mM CH_3COONa buffer (pH 5.5). Complex size and zeta potential were assessed using a Zetasizer Nano Zs (Malvern, UK). The Smoluchowski model was applied for zeta potential determination and cumulant analysis was used for mean particle size determination. All measurements were performed in triplicate, at 25°C.

2.6. Cell culture

293T human embryonic kidney endothelial cells were cultured under standard conditions in Dulbecco's Modified Eagle's Medium (DMEM) high glucose (4500 mg.l^{-1}) supplemented with 10% (v/v) heat-inactivated (56°C, 30 min) fetal bovine serum (FBS) and 1% (v/v) penicillin/streptomycin (10.000 U.ml^{-1} penicillin, 10.000 µg.ml^{-1} streptomycin) (all supplied by Gibco). Cells were routinely tested for mycoplasma contamination by PCR [19, 20].

2.7. Transfection

293T cells were seeded ($2.7x10^4$ viable cells.cm^{-2}) on poly-D-Lysine hydrobromide (PDL) coated 24-well tissue culture plates (Greiner Bio-one, CellStar), 24 hrs prior transfection. Cell culture medium was replaced for 500 µl of complete fresh medium 2 hrs before transfection. In all transfection experiments, complexes were added to the cells at a final DNA concentration of 1.3 µg.cm^{-2}. Cell culture medium was refreshed everyday.

2.8. *In vitro* gene expression studies

In this set of studies the plasmid carrying the β-galactosidase (β-gal) reporter gene was used.

The gene expression mediated by CHimi with a DA of 16% and two degrees of substitution with imidazole (13% - CH16imi1 and 22% - CH16imi2) was evaluated up to 168 hrs post-transfection. Cultures dilution was performed 72 hrs post-transfection. In brief, the cell monolayer was rinsed with pre-warmed phosphate buffered saline (PBS) and harvested by trypsinization (5 min, 37°C). Cells were re-suspended in supplemented DMEM (1 ml/well), diluted (7x) and re-seeded on PDL-coated 24-well plates.

The effect of multiple transfections on transfection activity (expressed as specific activity of β-gal) and cell viability was assessed as follows: 72 hrs post-transfection cells were harvested by trypsinization, as described above, and re-seeded on PDL-coated 24-well plates at the initial cell density ($2.7x10^4$ viable cells.cm^{-2}). 24 hrs after plating, cells were subjected to a second transfection. This procedure was repeated once more. In total three transfection treatments were performed. Transfection activity was evaluated at 48 and 72 hrs after each transfection. At each time point, cells were processed for β-gal activity evaluation according to manufacturer instructions (β-gal assay kit, Invitrogen). Non-transfected cells were used as blank. The total protein was determined by the BCA assay (Pierce), following the manufacturer instructions.

Cell viability was determined using a resazurin-based assay [21], as previously described [22]. Results are represented as percentage of metabolic activity of transfected cells relative to non-transfected cells.

2.9. Intracellular trafficking studies

Fluorescence microscopy studies

To allow the tracking of the CHimi-based particles inside cells, both polymer and plasmid DNA were fluorescently labeled. A rhodamine (λex=575 nm, λem=600 nm) activated derivative [5(6)-Carboxy-X-rhodamine N-succinimidyl ester, ROX (Fluka)] was used to label CH16imi1. In brief, 10 mg of CH16imi1 was dissolved overnight in 10 ml of a 1% (v/v) acetic acid solution and added to an equal volume ROX solution (0.13 mg.ml^{-1} in dehydrated methanol, Molecular Sieves, Merck). The reaction was let to occur for 3 hrs, under constant stirring, protected from light. The

fluorescently-labeled CH16imi1 ($CHimi_{ROX}$) was recovered by precipitation with 5 ml of 0.5 M NaOH. The precipitated polymer was washed with deionized water till no fluorescence was detected in the supernatant and, subsequently, freeze-dried. pCMV-GFP plasmid was fluorescently labeled using the commercial kit Label IT Cy5 (Mirus™) according to the manufacturer instructions. The fluorescently labeled DNA (DNA_{Cy5}) was recovered by precipitation in ethanol and concentration was assessed by spectrophotometry (λ=260 nm) (Beckman DU®650, USA).

Complexes prepared with the fluorescently labeled $CHimi_{ROX}$ and DNA_{Cy5} were used to transfect cells 24 hrs after seeding on PDL-coated glass coverslips. The intracellular localization of the complexes was analyzed in both live and fixed cells as follows. Twenty four hrs after cell seeding, the cultures on PDL glass coverslips (2.5 cm^2) were transferred into a closed chamber and incubated with L-15 medium (Gibco) supplemented with 10% (v/v) FBS and 1% (v/v) penicillin/streptomycin containing the complexes prepared with fluorescently labeled DNA and polymer. Cells were maintained at 37°C and images were acquired using an inverted epifluorescence microscope (Nikon eclipse TE2000-U) equipped with a Cool Snap HQ2 camera. Images were collected each hr during the first 6 hrs after transfection and at 24 hrs post-transfection. A series of z-sections were collected in order to capture images in all cell depth. At least five different areas of the sample were followed in time, in three independent experiments. At 48 hrs post-transfection images of GFP positive cells were collected. To prepare fixed cell samples, at defined time points (2, 4, 6, 24 and 48 hrs post-transfection), cultures on PDL glass coverslips (1.3 cm^2) transfected with fluorescently labeled polymer and DNA were rinsed with pre-warmed PBS and fixed for 15 min at 37°C with paraformaldehyde (4% (w/v), in PBS), supplemented with 2% (w/v) sucrose. After fixation, cell cytoskeleton and nuclei were stained. In brief, fixed cells were permeabilized according to a previously described procedure [23] and incubated with 1% (w/v) bovine serum albumin (BSA) for 1 hr. Cell nuclei were stained for 4 min with 4'-6-diamidino-2-phenylindole (DAPI, 0.1 $\mu g.ml^{-1}$ in PBS) and cell cytoskeleton filamentous actin (F-actin) was counterstained with Alexafluor 488-conjugated phalloidin (5 $U.ml^{-1}$, in PBS with 1% (w/v) BSA, 20 min, Molecular Probes). Samples were mounted in Vectashield (Vector) and observed by confocal laser scanning microscopy (CLSM, Leica Microsystems). Cytoskeleton staining was not performed in samples collected 48 hrs post-transfection in order to allow the detection of GFP positive cells. Cells were analyzed in depth by z-stacking. A minimum of 20 fields per time point were collected, from three independent experiments.

Cell-free gene expression assay

The occurrence of reporter gene transcription and/or translation, when in a complex form with CHimi-based polymer, was evaluated using a TNT® Quick Coupled Transcription/Translation System (Promega). This system allows protein production from genes under a T7 promoter. A pET-3a based plasmid encoding for the TTR protein [22] was used in this experiment to complex with CH16imi1. Following the manufacturer instructions, 1 μg of plasmid DNA was used in each

reaction. CHimi-based complexes were prepared by mixing 2 μl of DNA solution (in 25 mM Na_2SO_4 solution) with 13.4 μl of CH16imi1. The complex suspension was added to the TNT mix. The modification in complex formation procedure, as well as the experimental conditions of the assay (complex formation procedure, medium pH, temperature and ionic strength) showed not to alter the polymer ability to retain DNA in an agarose gel electrophoresis (data not shown). Since the final volume of the reaction mixture containing the complex solution exceeds the 50 μl recommended by the manufacturer, two controls were added to the experiment where the increase on the final reaction volume and the presence of CH_3COONa buffer pH 5.5 (CH16imi solvent) were equated. The reaction was let to occur for 90 min at 30°C. The reaction products were resolved by an SDS-polyacrylamide gel electrophoresis (SDS-PAGE) on a 15% (w/v) gel. The gel was dried and, since ^{35}S[methionine] was included in the reaction mixture, the presence of TTR protein was analyzed by phosphorimaging (Typhoon 8600 variable mode imager; Molecular Dynamics), after an overnight exposure. The position within the gel of the TTR band was confirmed by running in the same gel a molecular weight marker and the recombinant human TTR protein (produced in *E. Coli*) (data not shown).

2.10. DNase I protection assay CHimi-DNA particle stability and DNA protection

To evaluate the stability in physiological media of CHimi-DNA particles prepared with CHimi with different degree of acetylation, DNA electrophoretic mobility and DNase I protection were assessed. The electrophoretic mobility of DNA and CHimi-DNA complexes was analyzed in an agarose gel, as previously described [14]. Prior to running the gel, the complexes were prepared as described above and incubated for 20 minutes with equal volume of supplemented DMEM (10% FCS and 1% P/S). The gel was scanned using a Bio Rad Gel Doc™ XR system.

The ability of the polymer to protect DNA from DNase I degradation was assessed as follows. Complexes were suspended in buffer solution (10 mM Tris HCl, 150 mM NaCl, 1 mM $MgCl_2$; pH 7.4) and incubated with DNase I (1 U/μl, Fermentas) at 37ºC. Absorbance (260 nm) was recorded for 30 min, using a PowerWave™ Microplate Spectrophotometer (BioTek, USA).

2.11. Extent of internalization and transfection efficiency

The extent of internalization and transfection efficiency of complexes prepared with constant mass of pCMV-GFP and CHimi (independently of the polymer DA) were assessed by flow cytometry (FACSCalibur, BD Biosciences). For the internalization studies, pCMV-GFP was labeled with YoYo-1 (Invitrogen, 1:200 bp) prior to complex formation, according to the manufacturer instructions. After 2 hrs of contact with complexes, cells were processed for fluorescence activated cell sorting (FACS) analysis. Briefly, trypan blue (0.2% (w/v)) was added to the medium and incubated for 5 min in order to quench fluorescence external to cells [24]. Subsequently, the cells were washed with cold PBS, and harvested by trypsinization. After two washes with PBS,

cells were recovered in 100 µl of PBS containing 0.01% (w/v) of sodium azide. For transfection efficiency determination, cells were processed as described above, skipping the trypan blue incubation step. The number of cells expressing GFP was determined at 24, 48 and 72 hrs post-transfection. The individual fluorescence of 10,000 cells was quantified and results were analyzed using the FlowJo software (version 8.3.7). Results are expressed as the percentage of labeled DNA (for extent of internalization) or GFP positive cells (for transfection efficiency).

2.12. Enzymatic degradation of CHimi-based complexes

To assess CH-based particle degradation, complexes were prepared using a constant CHimi-pCMV-GFP mass ratio, independently of the polymer DA, and incubated with lysozyme in the presence of a fluorogenic substrate for the enzyme. In brief, 4-methylumbelliferyl β-D-N,N′,N″-triacetylchitotrioside (MU-$[GlcNAc]_3$) was dissolved in CH_3COONa (1M, pH=5.5):H_2O:DMF (1:1:1) [25] and added to freshly prepared CHimi-DNA complexes. Equimolar solutions of MU-$[GlcNAc]_3$ and CHimi (4.45 µM) were applied. Subsequently, the mixture was incubated with lysozyme (from chicken egg white) at a final concentration of 0.5 $mg.ml^{-1}$, at 37°C under constant stirring. After 1, 2, 3 and 4 hrs of reaction, NaOH was added to a final concentration of 0.05 M to stop the reaction. The fluorescence resulting from the enzymatic degradation of the substrate was measured (λexc=360nm; λem=455nm – Spectra Max Gemini XS; Molecular Devices). For each DA, CHimi-DNA complexes were incubated in the same conditions but without fluorogenic substrate, and used as blank.

2.13. Statistical data analysis

Data are presented as average ± standard deviation (SD). The statistical analysis of the results was performed using the non-parametric Mann-Whitney *U*-test. For multiple comparisons, homogeneity of variances was assessed by the Bartlett's test. If homogeneity of variances could be assumed the post-hoc Bonferroni test was performed, otherwise, the Dunnett T3 test was applied. Results were considered statistically significant when $p<0.05$. Calculations were performed using SPSS® software for Windows (version 16.0).

3. Results

3.1. *In vitro* gene expression study

In a previous work we have optimized CHimi mediated transfection [14] . It was found that the best transfection results are attained when CHimi-DNA complexes are prepared with CHimi containing 13% (CH16imi1) or 22% (CH16imi2) of the primary amines substituted with imidazole moieties, at an N/P molar ratio of 18. These two formulations were selected to be further studied in the present work. To follow CHimi-mediated gene expression over time, β-gal activity was evaluated during 7 days after transfection (Figure 1).

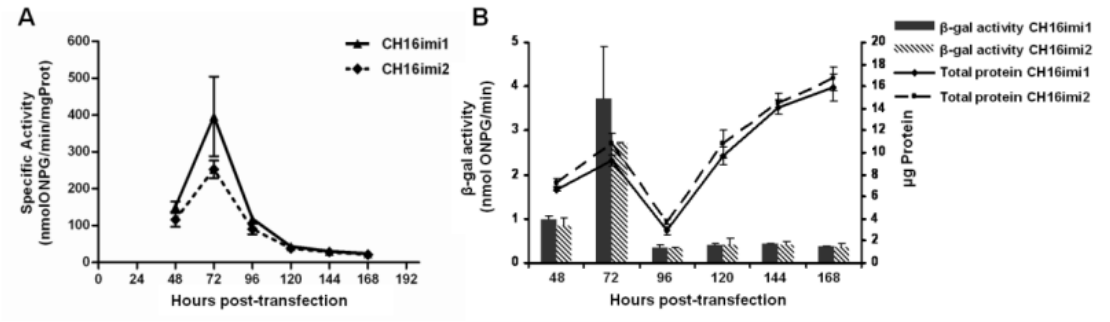

Figure 1. (A) Transfection activity as function of time for 293T cultures treated with CH16imi1- and CH16imi2-based vectors (N/P=18). Cells were trypsinized and diluted (7x) at 72 hrs post-transfection. **(B)** Independent plotting of β-gal activity and respective total cell protein content. Representative experiment out of the three performed (average ± SD; n=3).

Under the experimental conditions used, a transfection activity maximum is reached 72 hrs post-transfection for both polymers tested. After trypsinization, a significant decrease on β-gal specific activity was observed (Figure 1 (A)), in accordance to a previously published report [26]. Nevertheless, when the enzymatic activity (nmolONPG.min^{-1}) and the total cell protein content are plotted separately (Figure 1 (B)), one can observe that the decrease in enzymatic activity is of the same magnitude of the dilution performed (7x dilution) rather than resulting from an effective decrease in the production of the reporter protein. Furthermore, β-gal production remained stable in the period between 96 and 168 hrs post-transfection. Cell viability was monitored at the same time points. No significant alteration was found in terms of metabolic activity of cells transfected with CHimi-based polymers relative to non-transfected cells (Figure S1, supplementary material).

The possibility of performing successive transfection treatments using CHimi-based polymers, without compromising cell viability, was addressed *in vitro*. In terms of transfection activity the results show that cells can be re-transfected, maintaining high levels of the reporter gene expression (Figure 1 (A)). One should refer that a burst increase in transfection efficiency was observed at times, as illustrated in Figure 2 (A). This could be resulting from the series of trypsinization steps introduced every 3 days of culture that could not be circumvented in the implementation of this study. Even so, independently of the polymer system tested, cell viability relative to untreated cells remained above 80% after every treatment (see Figure 2 (B) for an example).

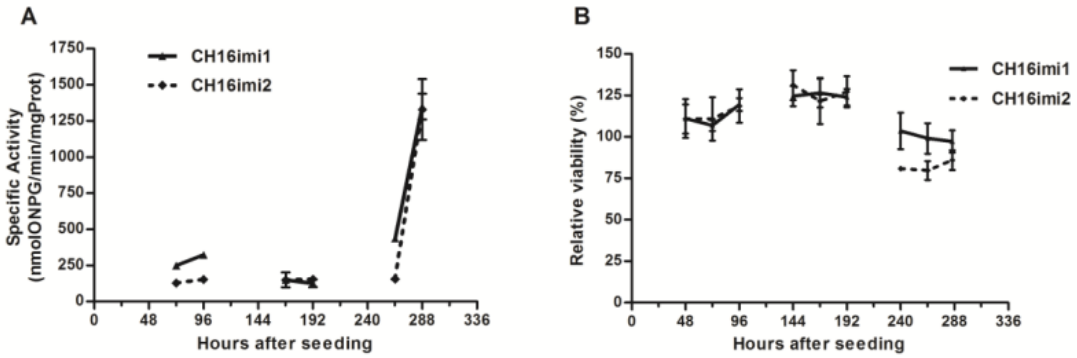

Figure 2. (A) Transfection activity and **(B)** relative cell viability of 293T cells after consecutive transfections with CH16imi-based vectors. Representative experiment out of the three performed (average ± SD; n=3).

3.2. Intracellular trafficking studies

In order to monitor the intracellular route of CHimi-DNA complexes after transfection, both CH16imi1 and DNA were covalently labeled with fluorescent tracers (rhodamine and Cy5, respectively). The ability of the labeled polymer to form complexes with DNA was confirmed by assessing the physical properties of the resulting particles. No significant differences were found in terms of complex size and zeta potential, comparing to those prepared with the non-labeled polymer (Table S1, supplementary material).

Live cell imaging

To follow fluorescently-labeled complexes ($CHimi_{ROX}$-DNA_{Cy5}) in live cells, a number of regions of the cell monolayer were monitored over time. Differential-interference contrast (DIC) combined with fluorescence images were acquired at different z-planes aiming at defining the localization of complexes inside the cell. A representative region of a sample at the first hrs after transfection is presented in Figure 3.

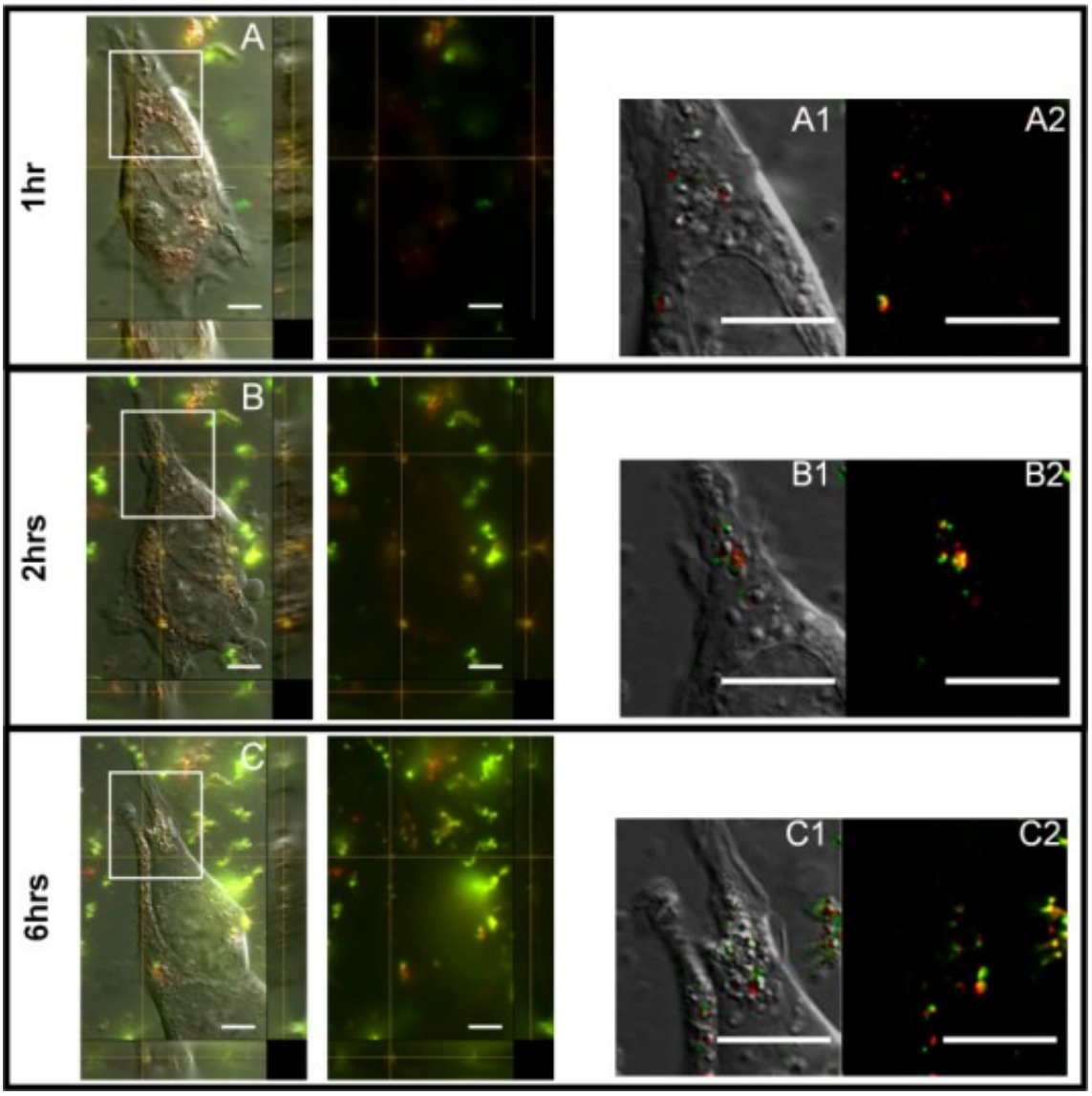

Figure 3. Fluorescence images combined with DIC images of 293T live cells at **(A)** 1, **(B)** 2, and **(C)** 6 hrs after transfection with complexes prepared with fluorescently labeled polymer and DNA. Images correspond to one central section from the z-stack acquired and the x-z and y-z section is presented. An amplification of the cells for each condition (A1, B1, and C1) and the correspondent fluorescence images (A2, B2, C2) is presented for each time point. The signal corresponding to $CHimi_{ROX}$ is shown in red and DNA_{Cy5} in green. Arrows indicate the location of $CHimi_{ROX}$-DNA_{Cy5} complexes. Scale bar = 10 μm.

Complexes could be detected bound to the cell membrane and also in the cell cytoplasm from the first hr post-transfection, up to 6 hrs post-transfection (Figure 3). The same scenario was found after 24 hrs post-transfection.

At 48 hrs post-transfection, fluorescently labeled complexes were still detected inside the cell cytoplasm, as well as bound to the cell membrane, both in GFP positive (Figure 4) and negative cells. The fluorescence signals from $CHimi_{ROX}$ and DNA_{Cy5} were found not to co-localize in some cases, although being detected in close proximity (see Figure 4 (3)).

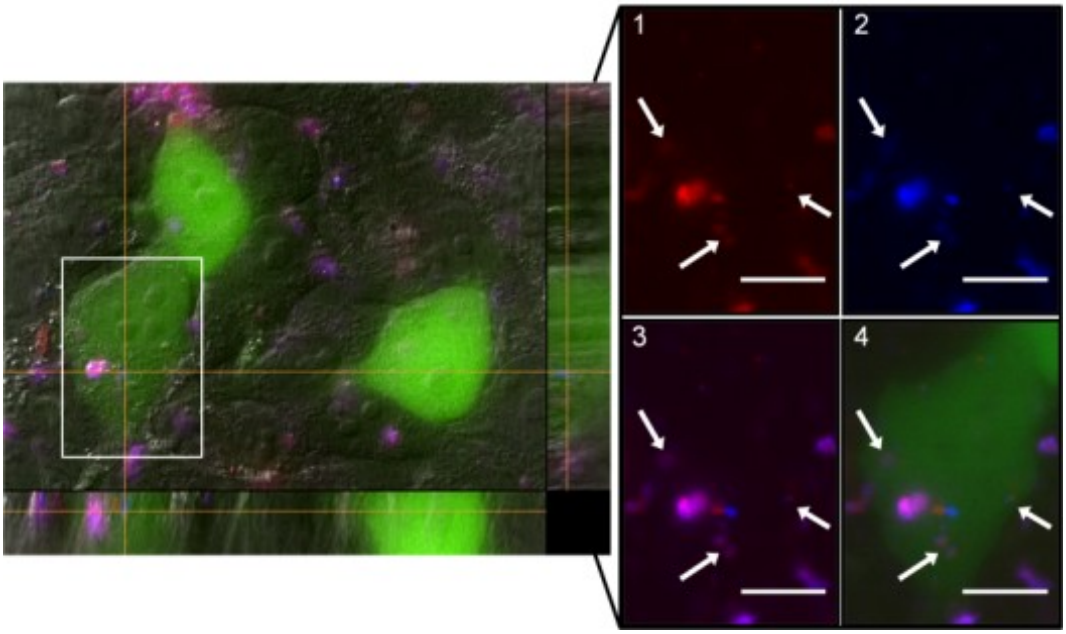

Figure 4. Z-section and the correspondent x-z and x-y section of 293T cells expressing GFP captured at 48 hrs post-transfection. The amplification of the fluorescence images corresponding to the area within the rectangle is shown in 1-4. The individual signals of (1) $CHimi_{ROX}$ and (2) DNA_{Cy5} are presented. (3) shows the merged image of $CHimi_{ROX}$ (in red) and DNA_{Cy5} (in blue). (4) combines also the GFP signal. Arrows indicate the location of $CHimi_{ROX}$-DNA_{Cy5} complexes within the GFP expressing cell. Scale bar = 10 µm.

Fixed cells analysis

The $CHimi_{ROX}$-DNA_{Cy5} complexes distribution was analyzed in fixed cells by CLSM at the same time points: 2, 6, and 48hrs after transfection. Representative images of each time point are presented in Figure 6.

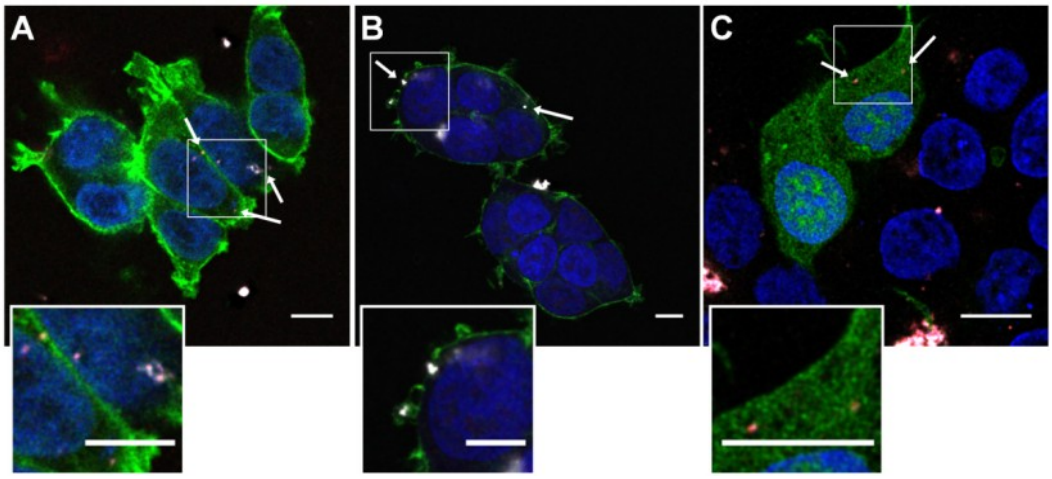

Figure 5. CLSM images captured at **(A)** 2, **(B)** 6, and **(C)** 48 hrs after transfection of 293T cells with $CHimi_{ROX}$-DNA_{Cy5} complexes. Images correspond to one central section from the z-stack acquired. The insert corresponds to an amplification of the specific area indicated in the original image. The fluorescence signal corresponding to $CHimi_{ROX}$ is shown in red and DNA_{Cy5} in gray. Cells were stained with DAPI (genomic DNA, blue) and phalloidin (filamentous actin, green; A-B). (C) Cells are shown in green due to GFP expression. Arrows indicate the location of $CHimi_{ROX}$-DNA_{Cy5} complexes. Scale bar = 10 µm. The images of each of the fluorescence channels are presented in supplementary material (Figure S2).

The analysis of the images obtained by CLSM showed that complexes can be found bound to the cell membrane as well as in the cytoplasm for all of the tested time points (see Figure 5 (A) for an illustration) and also in GFP positive cells (see Figure 5 (C)). $CHimi_{ROX}$ and DNA_{Cy5} signals were always co-localized.

In both studies, with live and fixed cells, it was not possible to localize a significant number of complexes inside the cell nucleus.

3.3. Cell-free gene expression assay

The importance of CHimi-DNA complex disassembling to the expression of the delivered gene was investigated through an *in vitro* transcription/translation assay. A pET-3a based plasmid encoding for the TTR protein was used to form complexes with CH16imi1.

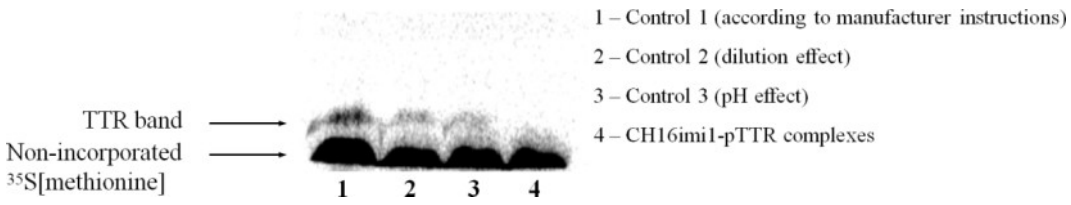

Figure 6. Phosphor imaging of the *in vitro* transcription/translation assay reaction products.

Four different reactions were performed and the resulting radioactive products can be visualized in the gel presented in Figure 6. TTR protein was not detected when pTTR was complexed with CHimi-based polymer (lane 4), whereas in all the controls performed (lane 1-3) the radioactive signal corresponding to TTR is identified.

3.4. Degree of acetylation role on CH-based nanoparticle transfection efficiency and degradation

Polymer Characterization

Through deacetylation of CH16 and posterior acetylation, three polymers with a range of DA were prepared, as determined by FT-IR spectra (Figure S4 supplementary material) according to Brugnerotto et. al. [27] (see Table 1). The molecular weight and the polydispersity index ($\overline{M}w/\overline{M}n$) of the resulting polymers were determined by SEC. No statistically significant variation was found when comparing the respective average number molecular weight ($\overline{M}n$) of the obtained polymers and the starting CH (CH16, see Table 1). Subsequently, both deacetylated and acetylated polymers were grafted with imidazole moieties following a previously described

procedure [14]. Briefly, grafting of the starting materials was explored with a molar ratio of imidazole-4-acetic acid sodium salt to glucosamine residues of 0.30. The obtained degree of substitution of each grafted polymer was assessed by FT-IR [14] (spectra in Figure S5 supplementary material) and it is presented in the Table 1. For the polymers with lower DA (CH16 and CH18) the obtained degree of substitution was lower than the expected value of 30% of imidazole moieties per mol of primary amino groups (22.1 and 23.4%, respectively). A possible explanation is that the lower polymer solubility could be limiting the reaction efficiency, as previously discussed [14].

Table 1. Degree of N-acetylation, percentage of the average number molecular weight ($\overline{M}w$) relative to the initial polymer (CH16), polydispersity index ($\overline{M}w/\overline{M}n$) and degree of substitution of primary amines of CH with imidazole moieties (imi) of the resulting polymers (average ± SD; n=3).

Polymer code	Degree of N-acetylation (%)	% $\overline{M}n$ relative to CH16	$\overline{M}w/\overline{M}n$	Polymer code	Degree of Substitution (imi)
CH05	5.2 ± 1.0	112 ± 9	1.9 ± 0.1	**CH05imi**	30.2 ± 1.4
CH10	9.8 ± 1.3	98 ± 9	1.9 ± 0.2	**CH10imi**	31.7 ± 1.4
CH16	16.4 ± 0.4	100 ± 9	2.2 ± 0.1	**CH16imi**	22.1 ± 4.0
CH18	17.7 ± 2.7	113 ± 8	1.9 ± 0.1	**CH18imi**	23.4 ± 0.9

CHimi-based particle characterization

The physical properties of the CHimi-DNA complexes prepared with a constant polymer to DNA mass ratio, using CHimi with different DA were determined. No significant variations in terms of particle size and zeta potential were detected between complexes prepared with the different polymers. Particle zeta potential was found to be around +20 mV, whereas the mean particle size ranged between 244 and 331 nm (Table 2).

Table 2. Zeta potential, average size (Z-Average), and polydispersity index (PdI) of CHimi-DNA complexes prepared with the pCMV-GFP plasmid and CHimi with different DA (average ± SD; n=3).

Polymer code	Zeta Potential (mV)	Z-Average (nm)	PdI
CH05imi	22.2 ± 0.8	244 ± 14	0.325 ± 0.085
CH10imi	20.9 ± 0.3	254 ± 58	0.359 ± 0.068
CH16imi	19.3 ± 2.0	331 ± 32	0.434 ± 0.050
CH18imi	21.9 ± 0.1	287 ±15	0.296 ± 0.012

CHimi-DNA particle stability and DNA protection

The ability of CHimi with variable DA to form stable particles with DNA and to protect the plasmid from nuclease degradation in physiological conditions was assessed. Results show that only naked DNA is able to migrate under an electrophoretic field, demonstrating that, independently of the CHimi DA, the complexes are stable in the presence of supplemented cell culture medium (Figure S3, supplementary material (A)). Furthermore, CHimi-based polymers are able to protect DNA from DNase I degradation. The performed assay is based on the fact that intact DNA molecules possess hypochromicity and that the absorbance at 260 nm increases upon enzymatic digestion [26]. The results show that naked DNA is fully degraded by DNase I following a 30 min incubation period, whereas for DNA complexed with CHimi-based polymers, the absorbance at 260 nm does not significantly increases upon incubation with the enzyme (Figure S3, supplementary material (B)).

Extent of internalization and transfection efficiency

The percentage of YoYo-1 positive cells was determined after 2 hrs of incubation of the cells with complexes based on CHimi with different DA. As shown in Figure 7 (A), internalization of complexes based in CH05imi, CH10imi or CH16imi was observed in approximately 30% of 293T cells. However, a significant lower extent of internalization was observed for CH18imi-based complexes.

Transfection efficiency mediated by CHimi-based complexes with variable DA was assessed for up to 72 hrs post-transfection (Figure 7 (B)). As can be observed, CH16imi is the most efficient polymer among the various CHs tested, being able to transfect over 40% of the cell population (at 72 hrs post-transfection). Although CH18imi-based complexes are able to be internalized by the cells, a significantly lower transfection efficiency is attained, in comparison to the other three polymers. The rate of internalization of CH18imi-DNA complexes is similar to the one obtained when naked DNA is added to cells (see representative histogram plots in Figure S6 supplementary material), being the later also ineffective transfecting cells [14]. For CH05imi-, CH10imi- and CH16imi-based complexes, transfection efficiency increased over time, in accordance to what was previously described in section 3.1. For CH10imi and CH16imi, the most significant increase of transfection occurred from 24 to 48 hrs post-transfection. However, in the case of CH05imi this effect was observed from 48 to 72 hrs post-transfection. A commercial formulation of PEI (Escort V® – Sigma) was used as a control for transfection experiments, and transfection efficiency was found to be above 80% at all the time points tested. A more detailed comparison between CHimi and PEI can be found in a previous publication [14].

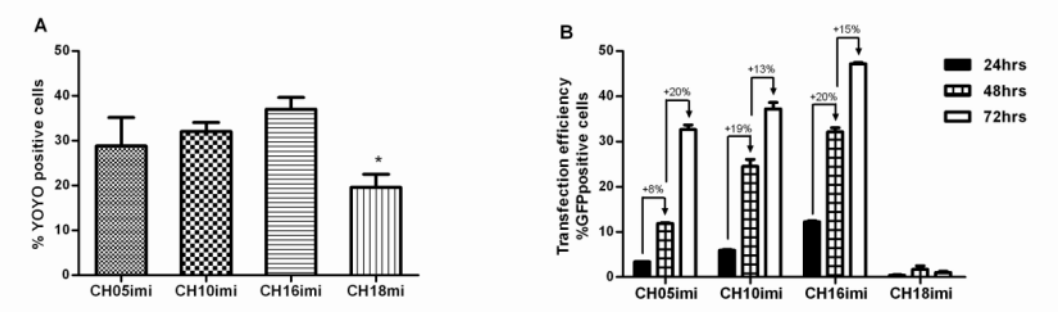

Figure 7. (A) Percentage of 293T cells positive for YoYo-1 after 2 hrs of incubation with CHimi-based complexes with variable DA. **(B)** Percentage of 293T cells expressing GFP at 24, 48 and 72 hrs post-transfection with CHimi-based complexes with variable DA. The increase in the percentage of GFP positive cells over time for each polymer is presented. Representative experiment out of the three performed (average ± SD; n=3). * denotes statistical significant differences relative to CH05imi, CH10imi and CH16imi (p<0.05). Representative histogram plots and mean fluorescence intensity data are presented in Figure S6, Figure S7 and Figure S8 of supplementary material.

Enzymatic degradation of CHimi-based nanoparticles

To evaluate the effect of the DA of CHimi on the degradation of CHimi-based complexes, a competition assay was setup using lysozyme as a model enzyme for CH intracellular degradation [9, 28-31]. The assay is based on the competition for lysozyme between a fluorogenic substrate (MU-[GlcNAc]$_3$) [25] and CHimi-based complexes. It is expected that a reduction on the fluorescence produced is observed when CHimi is competing with the fluorogenic substrate, since less substrate will be degraded.

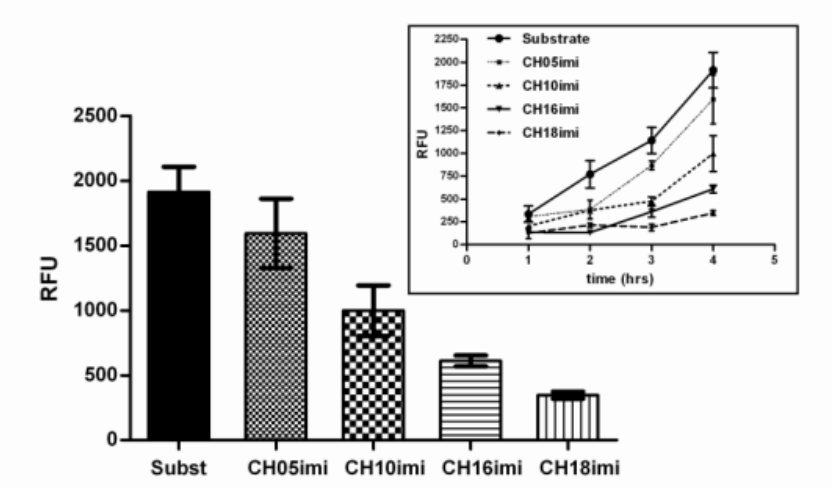

Figure 8. Extent of MU-[GlcNAc]$_3$ hydrolysis after 4 hrs of incubation with lysozyme in the absence or presence of CHimi-DNA complexes. Complexes were prepared with pCMV-GFP and CHimi with different DA. The insert shows the fluorescence produced as a function of time. Representative experiment out of the three performed (average ± SD; n=3).

As seen in Figure 8, a reduction in fluorescence can be observed as CHimi DA increases. The decrease on fluorescence results from less substrate being degraded, indicating that more

polymer degradation has occurred. This difference is identified also at earlier time points (insert of Figure 8), although being more evident as incubation time increases.

4. Discussion

The application of gene delivery strategies in regenerative medicine has been proposed as a promising approach to induce the production *in loco* of proteins that can play a role in tissue regeneration. In a previous study we showed that by grafting CH with imidazole moieties, transfection efficiency mediated by this polymer can be improved, without impairing cell viability [14]. In the present work, we aim at investigating the mechanism of transfection mediated by CHimi-based vectors, with the final objective of finding new avenues to further improve the system and tune the expression of a delivered gene.

It has been proposed that gene delivery mediated by CH is a time dependent process [32]; however, most of the related publications in this field report transfection efficiency in the 3 to 4 days after transfection [33-36]. Transfection experiments are usually conducted at high initial cell densities (>50% cell confluence), which may be considered a limiting factor regarding the maximum time period to render such evaluation feasible. Li and co-workers studied CH-mediated transfection up to 15 days post-transfection [37], but the cell culture conditions applied in that study were not described in detail. In the present work we introduced a trypsinization step 72 hrs post-transfection, as an experimental strategy to extend the time period for evaluation of transfection activity and cell viability, while maintaining cells in exponential growth conditions. Two CHs with a degree of substitution of primary amine with imidazole moieties of 13% (CH16imi1) and 22% (CH16imi2) were tested, as in previous studies in our laboratory these were found to be the most effective in mediating cell transfection [14]. The obtained results showed that both polymers could mediate a sustained expression of a reporter gene for the time period of the study - up to 7 days post-transfection. Additionally, successive transfections with CHimi-based carriers could be performed to uphold the levels of gene expression, without a significant reduction on cell viability.

The understanding of the intracellular mechanisms occurring during transfection is considered a valuable tool in the design of efficient and functional gene delivery systems [38, 39]. A number of intracellular trafficking studies has been conducted so far [40-45], nevertheless the importance of complex disassembling on transfection is yet to be established for the cationic polymer-based gene delivery systems, as recently discussed [46]. Some authors suggested that DNA can be transcribed while complexed with PEI [42], whereas in other studies it was hypothesized that the release of DNA from CH is the limiting step for an efficient *in vitro* transfection [47]. In an attempt to clarify whether disassembling of CHimi-DNA complex occurs and to better define the intracellular localization of such process, fluorescence microscopy studies were performed in live and fixed cells, using complexes prepared with fluorescently labeled CHimi and DNA. In both conditions $CHimi_{ROX}$-DNA_{Cy5} complexes could be detected inside 293T cells from the first hrs post-

transfection up to 48 hrs post-transfection, including in GFP expressing cells. In the process of assessing the occurrence of complex disassembling by fluorescent signal co-localization, an important difference was noted between conditions. In live cells the signal from $CHimi_{ROX}$ and DNA_{Cy5} did not always overlap, whereas in CLSM images of fixed cells $CHimi_{ROX}$ and DNA_{Cy5} were found to co-localize at all time periods. The disparity in the observations suggested that cell/complex movement could be responsible for the separation of signals observed during acquisition in live cells. By fast time-lapse consecutive acquisition of individual fluorescence channels, we were able to confirm that particles change position in the time frame of the image collection (data not shown). This artifact is not observed when using CLSM for live cell imaging, because different wavelengths are acquired simultaneously (see Figure S9 of supplementary material). Therefore, fluorescent microscopy studies were not able to clearly demonstrate complex disassembling; nonetheless these studies highlighted the importance of a cautious analysis of fluorescence images on intracellular trafficking studies. In our attempt to establish complex disassembling, we proposed an innovative assay in gene delivery studies. By an *in vitro* transcription/translation assay we were able to show that the production of the reporter protein is impaired when DNA is complexed with CHimi, clearly suggesting that disassembling is required for gene expression to occur.

The observed sustained gene expression profile combined with the fact that CHimi-DNA complexes could be found in cell cytoplasm up to 48 hrs post-transfection, indicate that gene expression mediated by CHimi is a time dependent process, as previously hypothesized for CH based gene delivery systems [32]. Furthermore, DNA transcription and/or translation were found to be impaired in the presence of the polymer, pointing out the importance of DNA release for the expression of the delivered gene. Being CH established as a biodegradable polymer [9, 48], we hypothesized that the complex disassembling process could be dependent on CH degradation, and, consequently, closely dependent on the polymer DA [9]. To address this question, transfection mediated by CHimi with different DA was explored. By the deacetylation of CH16 and posterior homogeneous acetylation [17], three polymers with a DA of 5, 10 and 18% were produced, while maintaining unchanged the initial molecular weight of the polymer. Imidazole moieties were subsequently grafted to each of the prepared CHs. The variation of CH DA neither did affect the CHimi-DNA complex physical properties, in accordance to a previous report [49], nor the CHimi ability to form stable complexes with DNA in the serum supplemented culture medium and to protect it from DNase I-mediated degradation under physiologic conditions. Nonetheless, significant differences were found in terms of complex internalization in 293T cells, as well as on transfection efficiency. Internalization of CH18imi-based complexes was found to be significantly lower than the other nanoparticle formulations. Furthermore, the internalized CH18imi-based nanoparticles showed a limited ability to transfect cells, comparing to the other tested systems. These results suggest that other factors rather than the extent of internalization are contributing to the observed transfection outcome. There is evidence in the open literature that a small difference on chitosan degree of acetylation can lead to significant changes on polymer properties [29], being the distribution of the acetylated monomers in the polymer chain one of the contributors to

this effect [9]. The effect of the DA on CH enzymatic degradation has been previously described namely for CH films [29] and scaffolds [31]. The data concerning CH degradation, when the polymer is incorporated in nanoparticles is limited and inconclusive, though. Campos et al. [30] had shown a slight decrease of CH-tri-polyphosphate nanoparticle size (DA 16%) after 4 hrs of incubation with lysozyme. Similar results were reported by Bernkop-Schnurch and colleagues using thiolated CH [50]. By applying an assay in which CHimi-based complexes compete with a fluorogenic substrate for lysozyme, we showed that as CHimi DA increases, less fluorescence is produced, indicating that the polymer present in the particles is being more extensively degraded. According to this result, CH18imi was found to be the polymer under investigation that degrades at the fastest rate, what can justify its low efficiency as a gene delivery vector. Upon internalization, the polymer may be readily degraded leading to a premature release of DNA, therefore compromising the plasmid DNA protection intracellularly and, consequently, impairing transfection. On the other hand, only a small decrease on fluorescence was observed when CH05imi-based particles competed for lysozyme, suggesting that the degradation of this polymer was limited. The slower degradation could justify the delayed expression of the reporter gene mediated by CH05imi, when in comparison to CH10imi and CH16imi. In the former case the boost on transfection efficiency occurs only after 48 hrs post-transfection. Additional indication of CHimi degradation was obtained by CLSM in an experiment where a $CHimi_{ROX}$-DNA_{Cy5} complex entrapped in a vesicle within the cell cytoplasm was followed by live imaging (time lapse video supplied in supporting info. For experimental details see caption of Figure S9, supplementary material). The fluorescence emitted by $CHimi_{ROX}$ was clearly reduced during the experiment, whereas the one emitted by DNA_{Cy5} is not altered (Figure S10, Supplementary material). The results provide experimental evidence for CH-based complexes degradation both *in vitro* and intracellularly, putting forward CH degradation rate as a parameter influencing transfection efficiency mediated by CHimi.

5. Conclusion

The opportunity to tune gene expression as a function of CHimi biodegradability, and the fact that this polymer promotes a sustained gene expression that can be upheld by successive transfections, emphasizes the potential of CHimi-based polymers as gene vectors *in vivo* in a regenerative medicine scenario. Therefore, our group is currently exploring different possibilities to incorporate CHimi-based polymers in the design of targeted nanoparticles aiming at cell-specific gene delivery to the peripheral nervous system [51].

Executive summary

In vitro gene expression study

CHimi-based vectors show appropriate properties to be used in a regenerative medicine scenario, being able to mediate a transient, and sustained expression of a delivered gene without cytotoxic

effects. Successive transfections with CHimi-based vectors can be carried out to uphold the levels of expression of a therapeutic protein without compromising cell viability.

Intracellular trafficking studies

The sustained gene expression is consistent with the fact that complexes are detected inside the cells up to 48hrs after transfection.

Cell-free gene expression assay

Complex disassembling is a critical step for the transcription and/or translation of the delivered gene. The *in vitro* transcription/translation assay proved to be a valuable tool in gene delivery studies to disclose the role of complex disassembling on gene expression.

Degree of acetylation role on CH-based nanoparticle transfection efficiency and degradation

CHimi, when complexed with DNA, can be enzymatically degraded. The degradation rate is directly dependent on the chitosan degree of acetylation. Gene expression kinetics can be related to the CHimi degradation.

Conclusion

CHimi-based polymers have high potential as gene vectors for an *in vivo* application in a regenerative medicine scenario. Tuning their degradation rate could be used as a strategy to adapt the overall expression process of a transgene to fulfill the therapeutic end.

Acknowledgements

This project was carried out under the Portuguese Foundation for Science and Technology (FCT) contract POCI/SAU-BMA/58170/2004. Work in the laboratory of Hélder Maiato was supported by the grants PTDC/BIA-BCM/66106/2006 and PTDC/SAU-OBD/66113/2006 from FCT and the Gulbenkian Programme on the Frontiers in Life Sciences. Liliana Pires (SFRH/BD/46015/2008) and Hugo Oliveira (SFRH/BD/22090/2005) acknowledge FCT for their PhD scholarships. The authors would like to thank Elsa Leitão and Maria Rosário Almeida (IBMC) for their help on the *in vitro* transcription/translation assay.

References

1. Hosseinkhani H, Hosseinkhani M, Gabrielson NP, Pack DW, Khademhosseini A, and Kobayashi H (2008). "DNA nanoparticles encapsulated in 3D tissue-engineered scaffolds enhance osteogenic differentiation of mesenchymal stem cells". *Journal of Biomedical Materials Research - Part A*, 85 (1): 47-60.

2. Salvay DM and Shea LD (2006). "Inductive tissue engineering with protein and DNA-releasing scaffolds". *Molecular BioSystems*, 2 (1): 36-48.

3. Carmeliet P (2000). "VEGF gene therapy: Stimulating angiogenesis or angioma-genesis?". *Nature Medicine*, 6 (10): 1102-1103.

4. Simões S, Filipe A, Faneca H, Mano M, Penacho N, Duzgunes N, and de Lima MP (2005). "Cationic liposomes for gene delivery". *Expert Opinion on Drug Delivery*, 2 (2): 237-254.

5. Lungwitz U, Breunig M, Blunk T, and Gopferich A (2005). "Polyethylenimine-based non-viral gene delivery systems". *European Journal of Pharmaceutics and Biopharmaceutics*, 60 (2): 247-266.

6. Lv H, Zhang S, Wang B, Cui S, and Yan J (2006). "Toxicity of cationic lipids and cationic polymers in gene delivery". *Journal of Controlled Release*, 114 (1): 100-109.

7. Itaka K, Ohba S, Miyata K, Kawaguchi H, Nakamura K, Takato T, Chung UI, and Kataoka K (2007). "Bone regeneration by regulated *in vivo* gene transfer using biocompatible polyplex nanomicelles". *Molecular Therapy*, 15 (9): 1655-1662.

8. Arote RB, Jere D, Jiang HL, Kim YK, Choi YJ, Cho MH, and Cho CS (2010). "Structure activity relationship for poly(ester amine)s as gene carriers". *Materials Technology*, 25 (3-4): 196-204.

9. Nordtveit RJ, Varum KM, and Smidsrød O (1994). "Degradation of fully water-soluble, partially N-acetylated chitosans with lysozyme". *Carbohydrate Polymers*, 23 (4): 253-260.

10. Dang JM and Leong KW (2006). "Natural polymers for gene delivery and tissue engineering". *Advanced Drug Delivery Reviews*, 58 (4): 487-499.

11. Kim TH, Jiang HL, Jere D, Park IK, Cho MH, Nah JW, Choi YJ, Akaike T, and Cho CS (2007). "Chemical modification of chitosan as a gene carrier *in vitro* and *in vivo*". *Progress in Polymer Science (Oxford)*, 32 (7): 726-753.

12. Lai WF and Lin MCM (2009). "Nucleic acid delivery with chitosan and its derivatives". *Journal of Controlled Release*, 134 (3): 158 - 168.

13. Mao SR, Sun W, and Kissel T (2010). "Chitosan-based formulations for delivery of DNA and siRNA". *Advanced Drug Delivery Reviews*, 62 (1): 12-27.

14. Moreira C, Oliveira H, Pires LR, Simões S, Barbosa MA, and Pêgo AP (2009). "Improving chitosan-mediated gene transfer by the introduction of intracellular buffering moieties into the chitosan backbone". *Acta Biomaterialia*, 5 (8): 2995-3006.

15. *US Department of Health and Human Services, Public Health Service, Food and Drug Administration, Guideline on Validation of the Limulus Amebocyte Lysate Test as an End-product Endotoxin Test for Human and Animal Parental Drugs, Biological Products, and Medical Devices*, W. US Department of Health and Human Services, DC Editor. 1987.

16. Mima S, Miya M, Iwamoto R, and Yoshikawa S (1983). "Highly deacetylated chitosan and its properties". *Journal of Applied Polymer Science*, 28 (6): 1909-1917.

17. Vachoud L, Zydowicz N, and Domard A (1997). "Formation and characterisation of a physical chitin gel". *Carbohydrate Research*, 302 (3-4): 169-177.

18. Terbojevich M, Cosani A, and Muzzarelli RAA (1996). "Molecular parameters of chitosans depolymerized with the aid of papain". *Carbohydrate Polymers*, 29 (1): 63-68.

19. Van Kuppeveld FJM, Van der Logt JTM, Angulo AF, Van Zoest MJ, Quint WGV, Niesters HGM, Galama JMD, and Melchers WJG (1992). "Genus- and species-specific identification of mycoplasmas by 16S rRNA amplification". *Applied and Environmental Microbiology*, 58 (8): 2606-2615.

20. van Kuppeveld FJM, van der Logt JTM, Angulo AF, van Zoest MJ, Quint WGV, Niesters HGM, Galama JMD, and Melchers WJG (1993). "Genus- and species-specific identification of mycoplasmas by 16S rRNA amplification". *Applied and Environmental Microbiology*, 59 (2): 655.

21. O'Brien J, Wilson I, Orton T, and Pognan F (2000). "Investigation of the Alamar Blue (resazurin) fluorescent dye for the assessment of mammalian cell cytotoxicity". *European Journal of Biochemistry*, 267 (17): 5421-5426.

22. Oliveira H, Fernandez R, Pires LR, Martins MCL, Simões S, Barbosa MA, and Pêgo AP (2010). "Targeted gene delivery into peripheral sensorial neurons mediated by self-assembled vectors composed of poly(ethylene imine) and tetanus toxin fragment c". *Journal of Controlled Release*, 143 (3): 350-358.

23. Dalby MJ, McCloy D, Robertson M, Wilkinson CDW, and Oreffo ROC (2006). "Osteoprogenitor response to defined topographies with nanoscale depths". *Biomaterials*, 27 (8): 1306-1315.

24. Innes NPT and Ogden GR (1999). "A technique for the study of endocytosis in human oral epithelial cells". *Archives of Oral Biology*, 44 (6): 519-523.

25. Van Steijn GJ, Nieuw Amerongen AV, Veerman ECI, Kasanmoentalib S, and Overdijk B (1999). "Chitinase in whole and glandular human salivas and in whole saliva of patients with periodontal inflammation". *European Journal of Oral Sciences*, 107 (5): 328-337.

26. Mao HQ, Roy K, Troung-Le VL, Janes KA, Lin KY, Wang Y, August JT, and Leong KW (2001). "Chitosan-DNA nanoparticles as gene carriers: synthesis, characterization and transfection efficiency". *Journal of Controlled Release*, 70 (3): 399-421.

27. Brugnerotto J, Lizardi J, Goycoolea FM, Arguelles-Monal W, Desbrieres J, and Rinaudo M (2001). "An infrared investigation in relation with chitin and chitosan characterization". *Polymer*, 42 (8): 3569-3580.

28. Nordtveit RJ, Varum KM, and Smidsrød O (1996). "Degradation of partially N-acetylated chitosans with hen egg white and human lysozyme". *Carbohydrate Polymers*, 29 (2): 163-167.

29. Tomihata K and Ikada Y (1997). "*In vitro* and *in vivo* degradation of films of chitin and its deacetylated derivatives". *Biomaterials*, 18 (7): 567-575.

30. De Campos AM, Diebold Y, Carvalho ELS, Sanchez A, and Alonso MJ (2004). "Chitosan nanoparticles as new ocular drug delivery systems: *In vitro* stability, *in vivo* fate, and cellular toxicity". *Pharmaceutical Research*, 21 (5): 803-810.

31. Ren D, Yi H, Wang W, and Ma X (2005). "The enzymatic degradation and swelling properties of chitosan matrices with different degrees of N-acetylation". *Carbohydrate Research*, 340 (15): 2403-2410.

32. Koping-Hoggard M, Tubulekas I, Guan H, Edwards K, Nilsson M, Varum KM, and Artursson P (2001). "Chitosan as a nonviral gene delivery system. Structure-property relationships and characteristics compared with polyethylenimine *in vitro* and after lung administration *In vivo*". *Gene Therapy*, 8 (14): 1108-1121.

33. Corsi K, Chellat F, Yahia L, and Fernandes JC (2003). "Mesenchymal stem cells, MG63 and HEK293 transfection using chitosan-DNA nanoparticles". *Biomaterials*, 24 (7): 1255-1264.

34. Zhao X, Yu SB, Wu FL, Mao ZB, and Yu CL (2006). "Transfection of primary chondrocytes using chitosan-pEGFP nanoparticles". *Journal of Controlled Release*, 112 (2): 223-8.

35. Jiang HL, Kim YK, Arote R, Nah JW, Cho MH, Choi YJ, Akaike T, and Cho CS (2007). "Chitosan-graft-polyethylenimine as a gene carrier". *Journal of Controlled Release*, 117 (2): 273-280.

36. Lee D, Zhang W, Shirley SA, Kong X, Hellermann GR, Lockey RF, and Mohapatra SS (2007). "Thiolated chitosan/DNA nanocomplexes exhibit enhanced and sustained gene delivery". *Pharmaceutical Research*, 24 (1): 157-167.

37. Li XW, Lee DKL, Chan ASC, and Alpar HO (2003). "Sustained expression in mammalian cells with DNA complexed with chitosan nanoparticles". *Biochimica et Biophysica Acta - Gene Structure and Expression*, 1630 (1): 7-18.

38. Roth CM and Sundaram S (2004). "Engineering synthetic vectors for improved DNA delivery: Insights from intracellular pathways". *Annual Review of Biomedical Engineering*, 6: 397-426.

39. Khalil IA, Kogure K, Akita H, and Harashima H (2006). "Uptake pathways and subsequent intracellular trafficking in nonviral gene delivery". *Pharmacological Reviews*, 58 (1): 32-45.

40. Godbey WT, Barry MA, Saggau P, Wu KK, and Mikos AG (2000). "Poly(ethylenimine)-mediated transfection: A new paradigm for gene delivery". *Journal of Biomedical Materials Research*, 51 (3): 321-328.

41. Ishii T, Okahata Y, and Sato T (2001). "Mechanism of cell transfection with plasmid/chitosan complexes". *Biochimica Et Biophysica Acta-Biomembranes*, 1514 (1): 51-64.

42. Bieber T, Meissner W, Kostin S, Niemann A, and Elsasser HP (2002). "Intracellular route and transcriptional competence of polyethylenimine-DNA complexes". *Journal of Controlled Release*, 82 (2-3): 441-454.

43. Huang M, Fong CW, Khor E, and Lim LY (2005). "Transfection efficiency of chitosan vectors: Effect of polymer molecular weight and degree of deacetylation". *Journal of Controlled Release*, 106 (3): 391-406.

44. Hashimoto M, Morimoto M, Saimoto H, Shigemasa Y, and Sato T (2006). "Lactosylated chitosan for DNA delivery into hepatocytes: The effect of lactosylation on the physicochemical properties and intracellular trafficking of pDNA/chitosan complexes". *Bioconjugate Chemistry*, 17 (2): 309-316.

45. Nam HY, Kwon SM, Chung H, Lee SY, Kwon SH, Jeon H, Kim Y, Park JH, Kim J, Her S, Oh YK, Kwon IC, Kim K, and Jeong SY (2009). "Cellular uptake mechanism and intracellular fate of hydrophobically modified glycol chitosan nanoparticles". *Journal of Controlled Release*, 135 (3): 259-267.

46. Won YY, Sharma R, and Konieczny SF (2009). "Missing pieces in understanding the intracellular trafficking of polycation/DNA complexes". *Journal of Controlled Release*, 139 (2): 88-93.

47. Koping-Hoggard M, Varum KM, Issa M, Danielsen S, Christensen BE, Stokke BT, and Artursson P (2004). "Improved chitosan-mediated gene delivery based on easily dissociated chitosan polyplexes of highly defined chitosan oligomers". *Gene Therapy*, 11 (19): 1441-1452.

48. Onishi H and Machida Y (1999). "Biodegradation and distribution of water-soluble chitosan in mice". *Biomaterials*, 20 (2): 175-182.

49. Lavertu M, Mel̀thot S, Tran-Khanh N, and Buschmann MD (2006). "High efficiency gene transfer using chitosan/DNA nanoparticles with specific combinations of molecular weight and degree of deacetylation". *Biomaterials*, 27 (27): 4815-4824.

50. Bernkop-Schnurch A, Heinrich A, and Greimel A (2006). "Development of a novel method for the preparation of submicron particles based on thiolated chitosan". *European Journal of Pharmaceutics and Biopharmaceutics*, 63 (2): 166-172.

51. Oliveira H, Pires LR, Fernandez R, Martins MCL, Simões S, and Pêgo AP (2010). "Chitosan-based gene delivery vectors targeted to the peripheral nervous system". *Journal of Biomedical Materials Research - Part A*, 95 (3 A): 801-810.

Supporting information

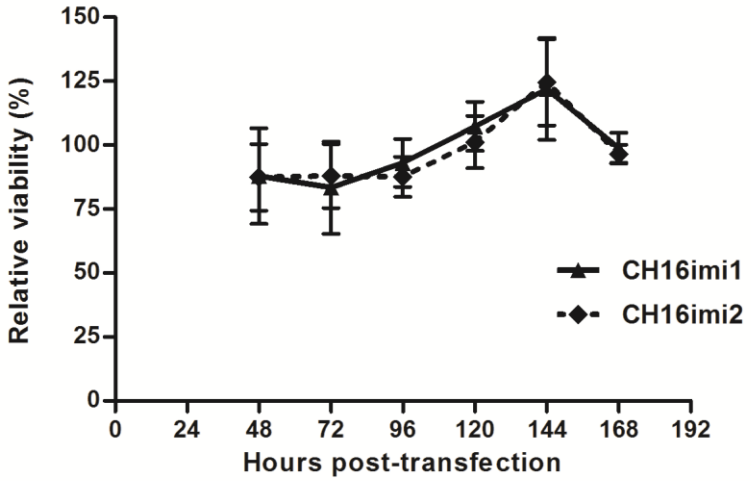

Figure S1. Cell viability as a function of post-transfection time. Relative viability was defined as the percentage of metabolic activity of transfected cells relative to non-transfected cells. Representative experiment out of the three performed (average ± SD; n=6).

Table S1. Zeta potential, average size (Z-Average) and polydispersity index (PdI) of CHimi1-DNA based complexes. Measurements were performed in acetate buffer 5 mM (pH 5.5) at 25°C. Zeta potential was calculated according to the Smoluchowski model. $CHimi_{ROX}$ indicates the fluorescent labeled polymer (average ± SD; n=3).

Polymer code	Zeta Potential (mV)	Z-Average (nm)	PdI
CH16imi1	18.6 ± 1.9	223 ± 26	0.358 ± 0.031
$CHimi_{ROX}$	20.5 ± 4.7	216 ± 45	0.333 ± 0.060

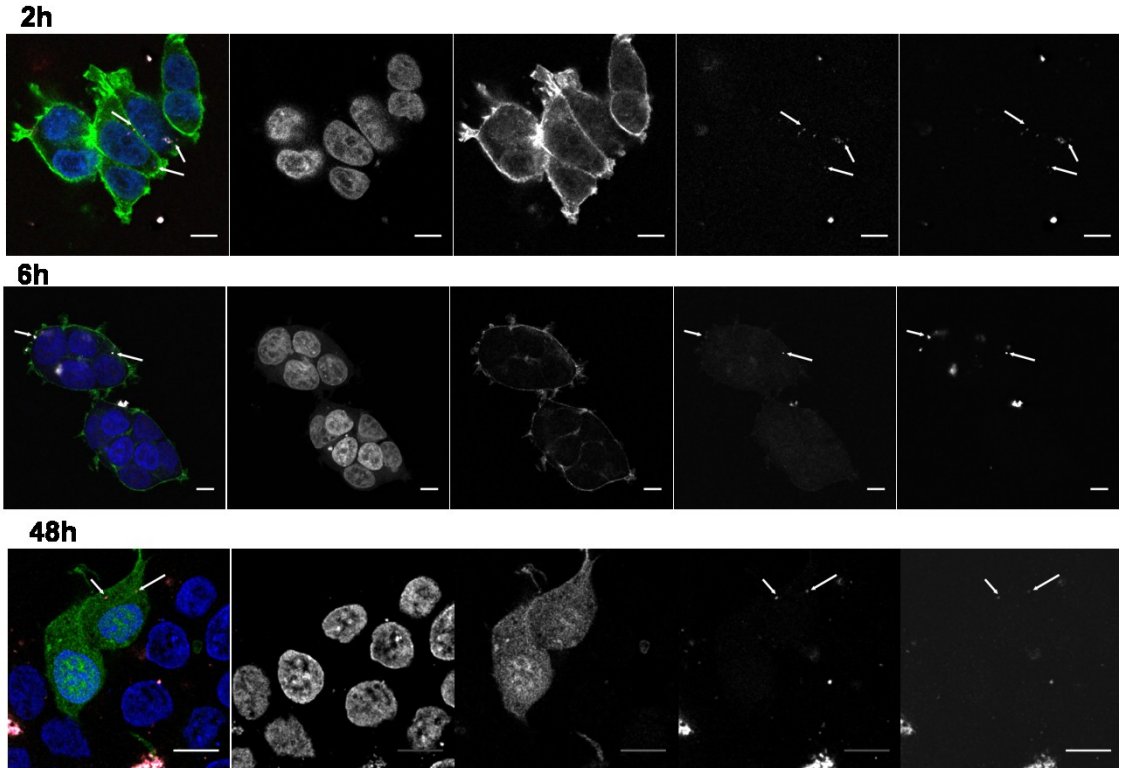

Figure S2. CLSM images obtained at 2, 6, and 48 hrs after transfecting 293T cells with $CHimi_{ROX}$-DNA_{Cy5} complexes. Merged and individual signals are presented. In merged images $CHimi_{ROX}$ is shown in red, DNA_{Cy5} in gray, genomic DNA is stained in blue and phalloidin (filamentous F-actin) is in green. At 48 hrs post-transfection GFP positive cells are depicted in green. White arrows indicate $CHimi_{ROX}$-DNA_{Cy5} complexes. Scale bar: 10 µm.

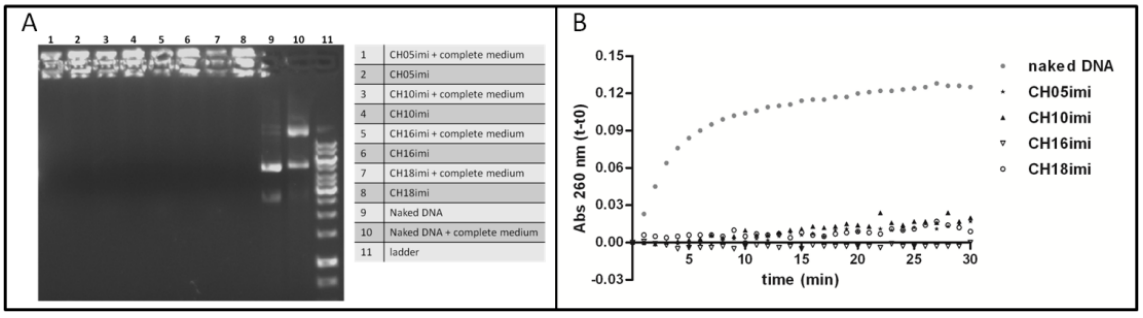

Figure S3. CHimi-DNA particle stability and protection. Complexes were prepared with the same polymer mass, independently of the DA. Naked DNA was used as control. (A) Agarose gel electrophoresis of naked DNA and CHimi–DNA complexes in the presence/absence of supplemented DMEM (10% FCS and 1% PS). (B) Variation of absorbance values at 260 nm (t-t_0) as a function of time after addition of DNase I (pH 7.4, 37°C).

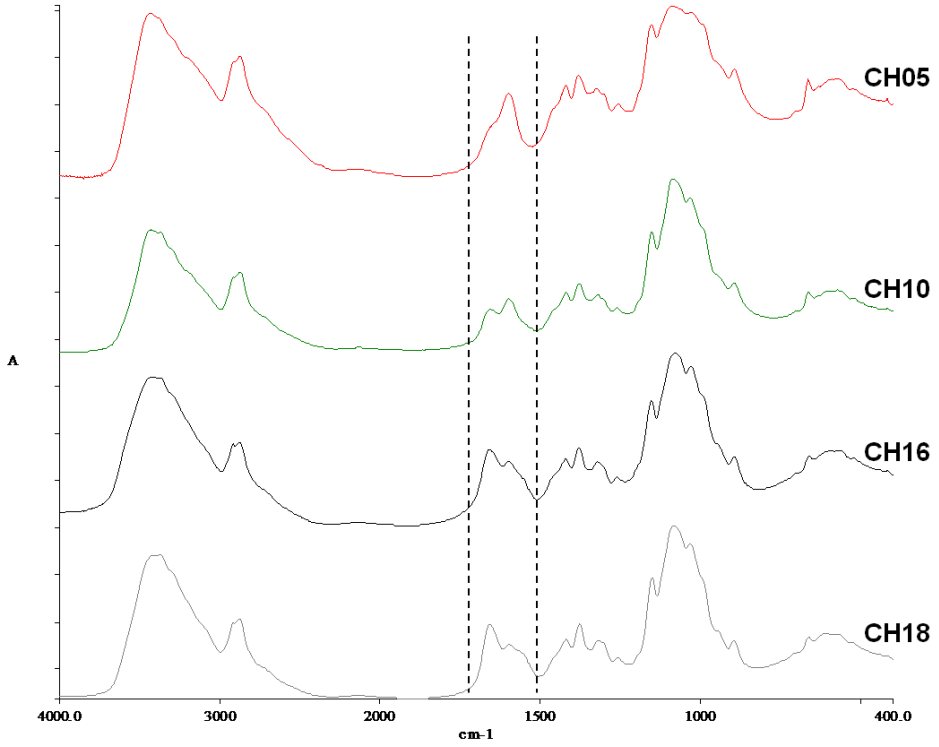

Figure S4. FT-IR spectra of chitosan with different degree of acetylation prepared in this study.

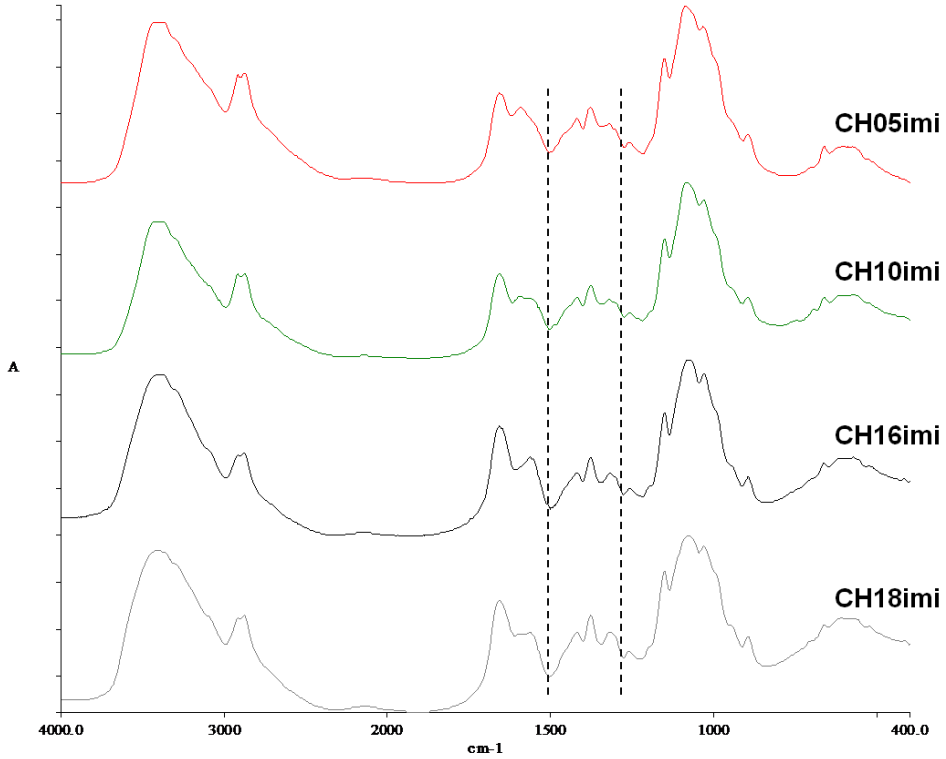

Figure S5. FT-IR spectra of imidazole-grafted chitosan obtained from chitosan with different degree of acetylation.

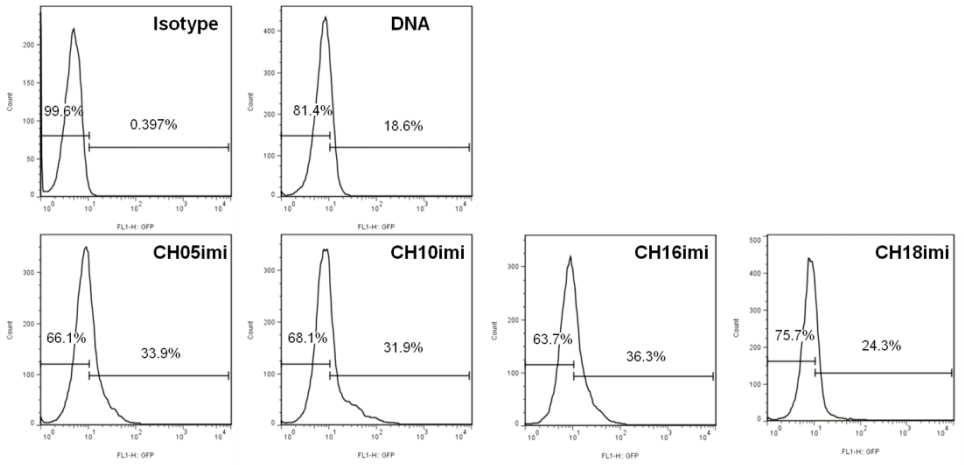

Figure S6.: Representative histogram plot of the extent of internalization in 293T cells of DNA or complexes prepared with CHimi with different degree of acetylation.

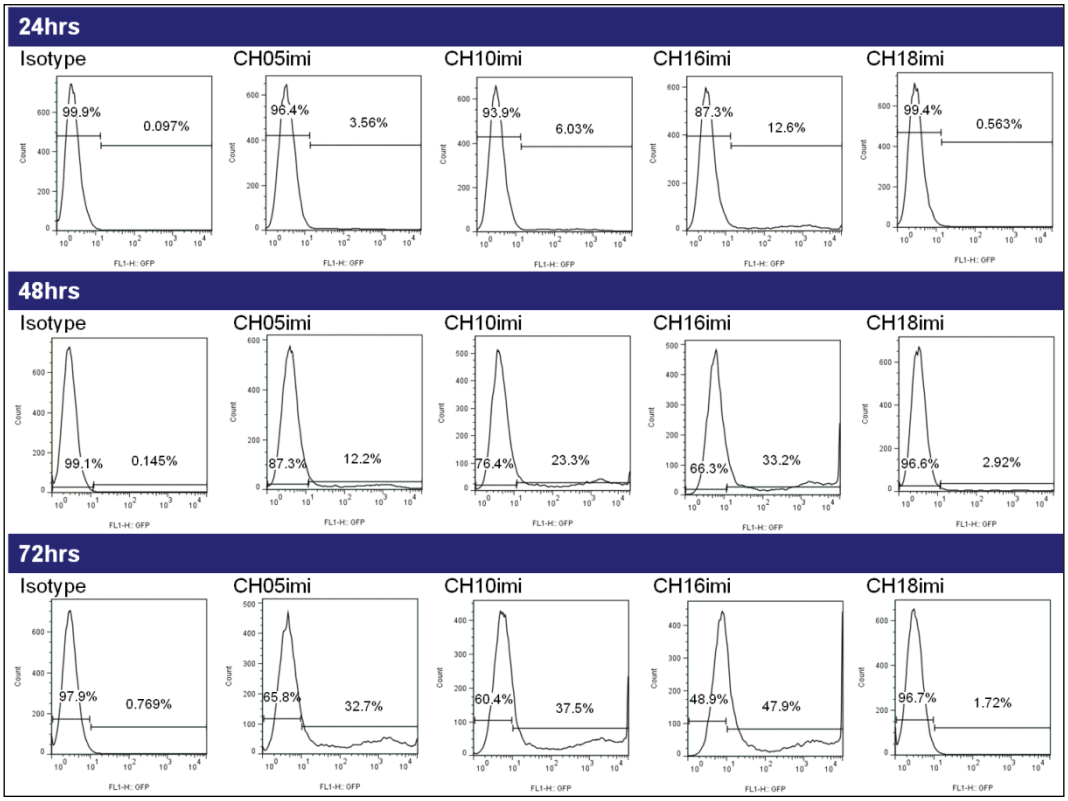

Figure S7. Representative histogram plot of GFP expression by 293T cells 24, 48 and 72 hrs after being transfected with CHimi-based complexes with variable degree of acetylation.

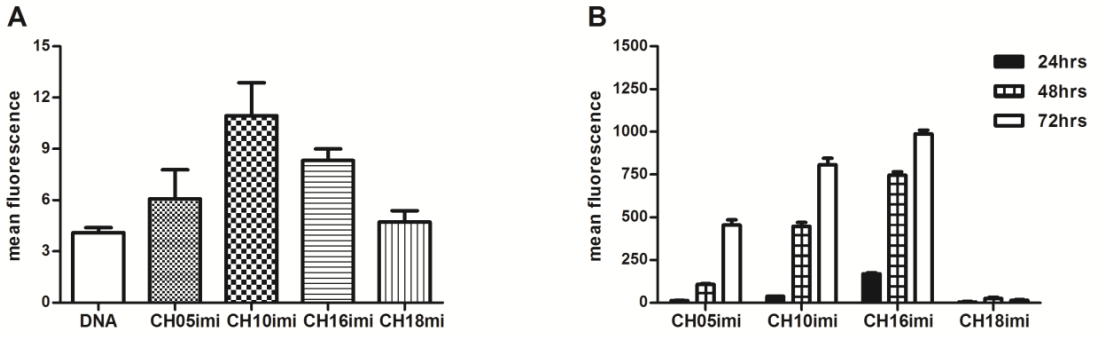

Figure S8. Mean fluorescence intensity of 293T cells that incorporated YoYo-1 (A) or express GFP (B) as determined by FACS.

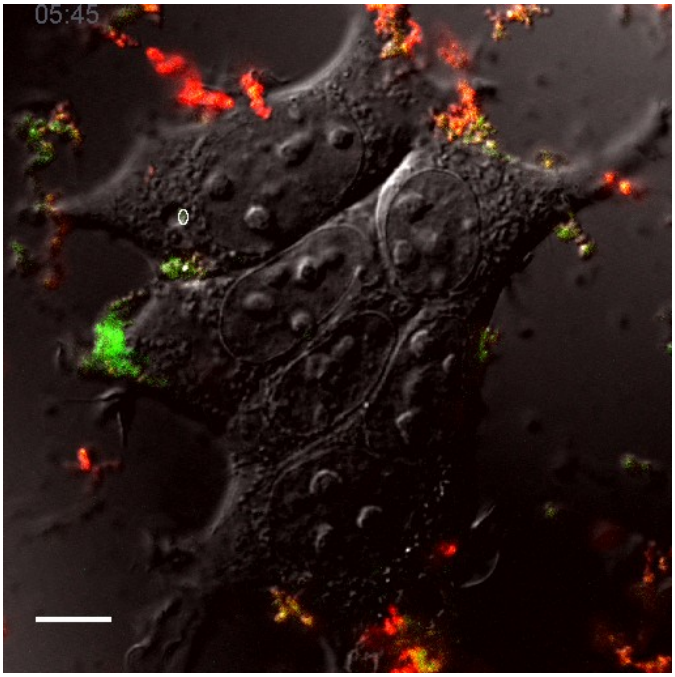

Figure S9. Time-lapse images obtained by CLSM. The experiment started at 2h30min and finished at 5h45min post-transfection. Acquisitions were performed each 15 min. The video can be found in http://www.futuremedicine.com/loi/nnm. It shows the degradation of a $CHimi_{ROX}$-DNA_{Cy5} complex inside a vesicle in the cell cytoplasm. The vesicle (region of interest – ROI) is delimited by a white circle in the video. Complexes were entrapped in the vesicle during the all course of the experiment. $CHimi_{ROX}$ signal is shown in red and DNA_{Cy5} in green. Scale bar: 10μm. Changes in the gamma settings were performed in order to allow the better visualization of $CHimi_{ROX}$.

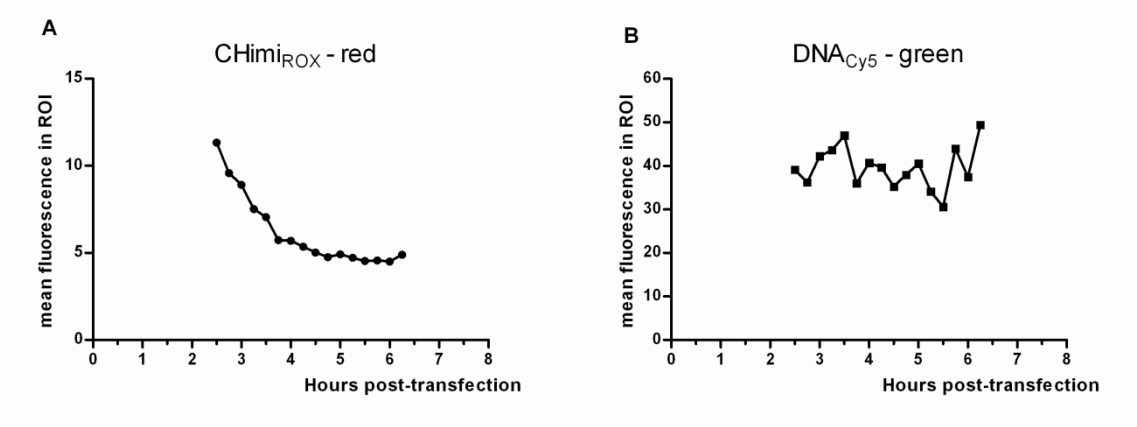

Figure S10.: Mean fluorescence of CHimi$_{ROX}$ (A) and DNA$_{Cy5}$ (B) measured in the region of interest (ROI) depicted in the Figure S4. It can be noticed that DNA$_{Cy5}$ mean fluorescence values are higher than the ones for CHimi$_{ROX}$. This occurs because Cy5 is a much brighter fluorophore than rhodamine.

APPENDIX I

Preliminary results on the incorporation of chitosan-based nanoparticles in poly(trimethylene carbonate-co-ε-caprolactone) electrospun fibres

1. Introduction

The combination of gene therapy-based strategies with tissue engineering scaffolds holds the promise of providing both physical support for cell adhesion and growth, and genetic material to tune specific cellular processes [1]. Nucleic acids have been directly incorporated into the matrices [2-5], or vectorized through virus [6, 7] or nanoparticles formed by interaction with lipids [3] or cationic polymers, such as poly(ethylene imine) (PEI) [8] and chitosan [9].

In the context of spinal cord injury, the use of this combined strategy has already showed promising results *in vivo*. The implantation of a multiple channel bridge loaded with lipid-DNA nanoparticles promoted the expression of a reporter gene during at least 3 weeks [3]. More recently, Yao and co-workers reported the sustained expression of a growth factor - neurotrophin-3 (NT-3) - at the lesion site after implantation of a collagen conduit loaded with polymeric particles containing the NT-3 gene. While a statistically significant functional improvement was not achieved in the time frame of the study (4 weeks), an increased number of axons was found crossing the conduit at the time of evaluation [10].

Currently, electrospinning is being actively investigated for the preparation of tissue engineering scaffolds since it allows the formation of fibres at the nano/micrometer scale, mimicking the extracellular matrix [11, 12]. Furthermore, alignment of these fibrous structures can be achieved, by applying a rotating target. The use of aligned fibres is very promising in the field of nerve regeneration as these can provide physical guidance for axonal regrowth [13, 14]. Although the scientific publications concerning the incorporation of genetic material into electrospun fibres in the context of nerve regeneration is still in its infancy, this combined strategy was already investigated *in vitro* using DNA [15, 16], siRNA [17, 18] or nanocomplexes with nucleic acids [16, 18-20]. Furthermore, positive results were already reported *in vivo* [16, 21], namely in a diabetic ulcer model [16].

The application of electrospun-based scaffolds for the delivery of genetic material into a SCI can combine topographic guidance with the delivery of gene vectors that mediate the sustained expression of therapeutic molecules (such as growth factors) or that can block the expression of specific inhibitory factors, leading, ultimately, to an enhancement on the process of nerve regeneration. In this study, we aim at incorporating chitosan-based nanoparticles in poly(trimethylene carbonate-co-ε-caprolactone) [P(TMC-CL)] electrospun fibres, in order to create

a device for the delivery of genes to the SCI site. P(TMC-CL) is a synthetic polymer that has previously showed interesting properties to assist nerve regeneration both in the peripheral [22, 23] and the central nervous system [24]. Our group has recently described the preparation of P(TMC-CL) fibres by electrospinning and its application *in vitro* as drug delivery platform [25]. Additionally, we have previously studied chitosan chemical modification [26, 27] and its intracellular trafficking [28] getting hold of relevant cues for the optimization of gene delivery mediated by chitosan-based nanoparticles. Taking advantage of this previously obtained know-how, the present communication reports preliminary results on the efforts made to combine nanoparticles with electrospun fibres, foreseeing the development of a combinatorial strategy to promote nerve regeneration.

Results and Discussion

Electrospinning of nanoparticle containing solutions: solvent screening

In order to incorporate chitosan-based nanoparticles within P(TMC-CL) fibres during the electrospinning process, it was firstly necessary to find a solvent mixture compatible with both the chitosan-based nanoparticles and the P(TMC-CL) copolymer. P(TMC-CL) and chitosan (CH) differ significantly on their nature and solubility. P(TMC-CL) is a synthetic polyester, mainly soluble in organic solvents; whereas CH is a natural polycation, soluble in slight acidic solutions. Considering that to assure the fibre formation by electrospinning from this mixture the major component - P(TMC-CL) - needs to be well solubilised, the compatibility of CH or CH-DNA nanoparticles with solvents commonly used to dissolve P(TMC-CL) was tested (see Table 1).

CH solutions prepared in sodium acetate buffer (pH 5.5) [26, 28] were found to be immiscible with the organic solvents tested, namely chloroform or dichloromethane. CH-DNA nanoparticles (in suspension in acetate buffer pH 5.5 [26]) when added to these solvents tend to precipitate. If added to dimethylformamide (DMF), nanoparticles tend to aggregate, but do not precipitate. However, when formed it was not possible to re-disperse these aggregates.

Table 1. Solvent mixtures tested.

Solvent	P(TMC-CL)	CH	CH-DNA nanoparticles
Chloroform	Soluble	Immiscible	–
Dichloromethane	Soluble	Immiscible	–
Dimethylformamide	Soluble	–	Aggregate
Acetone	Soluble	–	Precipitate
Dioxane	Soluble	–	Precipitate

CH-chitosan (Mw: 121000, DDA:84.6%);P(TMC-CL): poly(trimethylene carbonate-co-ε-caprolactone)

In view of the results summarized in Table 1, it was considered that to efficiently suspend CH-based nanoparticles in a polymeric organic solution required the stabilization of the nanoparticles.

Electrospinning of P(TMC-CL) fibres containing TriM-CH based nanoparticles

Our group is currently investigating the use of the CH derivative trimethyl chitosan (TriM-CH). The quaternization of the primary amine groups of CH with methyl groups has been found to considerably improve CH solubility, rendering it soluble in a wider range of pHs, including at physiological pH. The group has tested TriM-CH of different molecular weights and degrees of quaternization, as these parameters can significantly affect the polymer properties, and, ultimately, transfection. In general, in comparison to CH, TriM-CH forms by electrostatic interaction with plasmid DNA nanoparticles with smaller diameter and with an improved complexation stability in different dispersants [29]. In particular, it was found that TriM-CH-based nanoparticles have an improved stability, comparing to CH-based ones, after freezing or freeze-drying process [29].

In the present work, we tested two modified CHs with similar degree of quaternization (< 30%), but different molecular weights - high (110,000, TriM-CH(H)) and low molecular weight (30,000, TriM-CH(L)). The detailed description of polymer characterization is supplied in the experimental section (Table 3). Taking advantage of the described stability to the freeze-drying process, we explored the possibility of resuspending these nanoparticles in an organic solvent – DMF – to, subsequently, mix it with P(TMC-CL) solution. DMF has been commonly applied in electrospinning solutions as a mean to increase solution conductivity [30]. Particularly, it showed to improve P(TMC-CL) fibre morphology and homogeneity, decreasing mean fibre diameter [25].

In the preparation of the TriM-CH-DNA complexes for transfection, we have been employing TriM-CH polymer solutions in glucose 5% (w/v), pH 7.4 (Aida Moreira, unpublished data). In order to avoid interference of glucose in the electrospinning process, the stability of the TriM-CH based nanoparticles to the freeze-drying process when in a water solution (MilliQ grade) was firstly investigated.

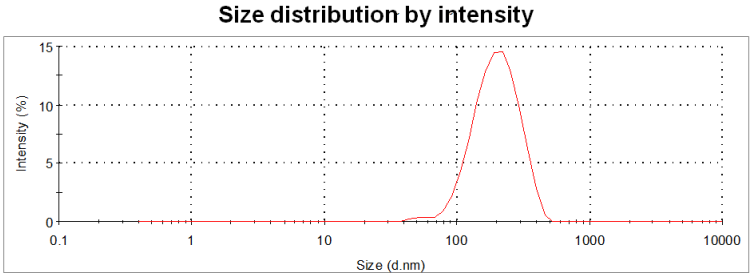

	Z-average (nm)	PDI
TriM-CH(H)–DNA	198 ± 13	0.230 ± 0.034

Figure 1. Size distribution graph for TriM-CH(H)-DNA nanoparticles (N/P molar ratio = 4) prepared in water (MilliQ grade). The table shows the z-average and polydispersity index (PDI) of the prepared nanoparticles (n=3).

TriM-CH(H) prepared in glucose solution (5% (w/v)) yielded nanoparticles with a mean diameter around 320 nm. However, when TriM-CH(H) nanoparticles are prepared in water, mean diameter decreases to 200 nm, suggesting that polymer-DNA condensation is affected by the presence of glucose. Nevertheless, when the TriM-CH(H) particles were freeze-dried and subsequently resuspended in water, the formation of large aggregates is denoted. This process hindered a valid characterization of nanoparticle in terms of mean diameter and suggests that the presence of glucose in solution is critical for nanoparticle stability to the freeze-drying process. The tendency to form aggregates was also observed when the nanoparticles were resuspended in DMF. Nonetheless, the mixture was added to a P(TMC-CL) solution in dichloromethane (DCM) and stirred overnight to be subsequently, electrospun. The final solvent mixture was 3:1 DCM:DMF and DNA concentration was set to 0.02% (w/w of polymer). After overnight mixing, TriM-CH(H)–DNA nanoparticles and P(TMC-CL) yield an apparently homogeneous suspension. As shown in Figure 2, homogeneous fibres were formed, being the fibre mean diameter 0.37 ± 0.11 μm. The mean fibre diameter was found to be significantly decreased comparing to the diameter of P(TMC-CL) fibres obtained using a similar electrospinning setup found to be 0.67 ± 0.12 μm [25].

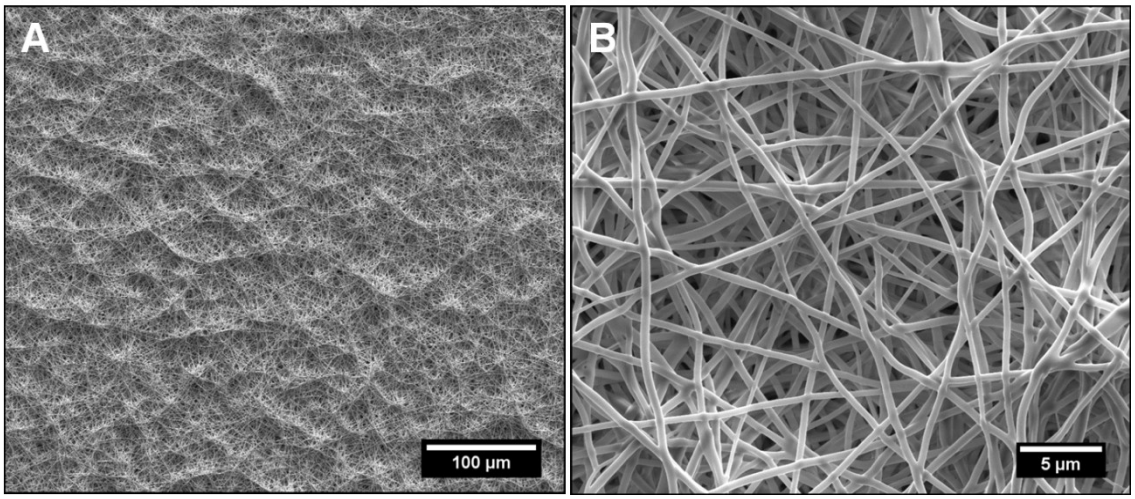

Figure 2. SEM micrographs of the fibres obtained after electrospinning of a P(TMC-CL) solution containing TriM-CH(H)–DNA nanoparticles using a 3:1 DCM:DMF solution.**(A)** Low and **(B)** high magnification images are presented.

The differences found in terms of fibre mean diameter suggest that the presence of nanoparticles alter the conductivity of the electrospun solution and, therefore, fibre diameter. To obtain evidence on the presence of DNA incorporated in the fibres, an electrophoresis was performed, after dissolving the obtained fibrous mesh. Results are presented in Figure 3.

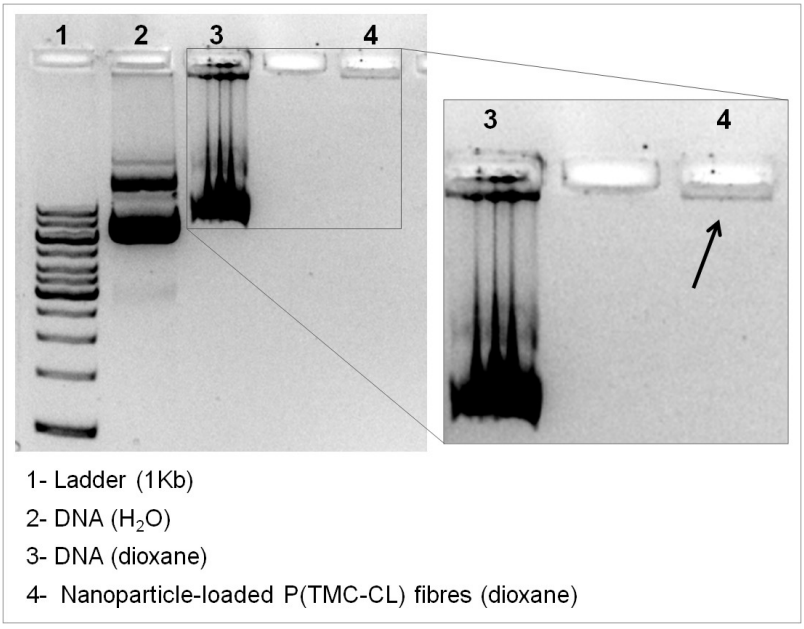

Figure 3. Gel electrophoresis of P(TMC-CL) fibres containing TriM-CH(H)-DNA nanoparticles after dissolution in dioxane (lane 4). Plasmid DNA solutions in H_2O and dioxane were used as control (lanes 2 and 3, respectively).

Gel electrophoresis of the fibrous mesh solution was performed along with a DNA solution in water or in the same solvent used to dissolve the fibrous mesh. Figure 3 shows that dioxane interferes with the plasmid DNA run, but does not hamper its detection (Figure 3, lane 3). When analysing the run of the fibrous mesh solution (lane 4), one should take into account that P(TMC-CL) fibres were prepared with a DNA loading of 0.02% (w/w of polymer). Consequently, in this particular experiment, the maximum amount of DNA present in the fibres and therefore, loaded in the gel, was 70 ng, corresponding to approximately 15 times less than the control (1 µg, lane 3). Figure 3 (lane 4) shows a band that although significantly smaller in comparison to control, suggests the presence of DNA that has been retained near the loading well. This result points to the presence of TriM-CH and that the positive charge from the polymer is hindering the DNA to move electrophoretically. Although suggesting that both DNA and polymer are present, the result obtained in this assay cannot assure that in the fibre both are still complexed in the form of nanoparticles.

To prove the presence of the nanoparticles in the fibres we prepared fluorescently-labelled nanoparticles, by labelling TriM-CH(L) with rhodamine (TriM-CH(L)$_{ROX}$) as previously described for chitosan [28]. We proceeded these studies with TriM-CH(L) with a lower molecular weight (see Table 3) as in the course of this work this polymer was found to be more efficient in terms of stability to storage and transfection efficiency than TriM-CH(H) (Aida Moreira, unpublished data).

The nanoparticles prepared using TriM-CH(L)$_{ROX}$ dissolved in water (MilliQ grade) were characterized in terms of size as prepared and after freeze-drying and resuspension (Table 2).

Table 2. Characterization in terms of Z-average diameter (nm) and polydispersity index (PDI) of nanoparticles prepared with TriM-CH(L)$_{ROX}$ (n=3) at an N/P molar ratio of 2.

Nanoparticles	Z-average (nm)	PDI
TriM-CH(L)$_{ROX}$–DNA	136 ± 31	0.248 ± 0.02
TriM-CH(L)$_{ROX}$–DNA (freeze dryed)	349 ± 29	0.349 ± 0.02

Z-ave (nm): Z-average nanoparticle diameter; PDI: polydispersity index.

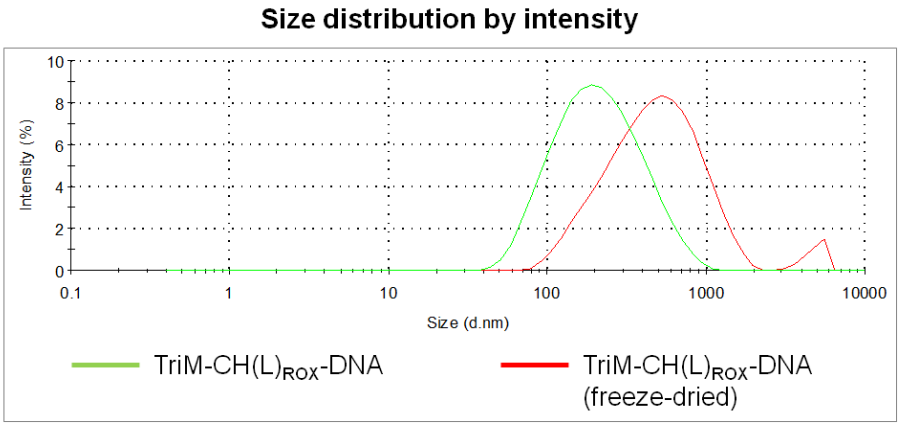

Figure 4. Size distribution graph of fluorescently-labelled TriM-CH(L)R_{OX}-DNA nanoparticles (N/P molar ratio= 2) prepared in water, before and after freeze-drying process.

Nanoparticles prepared using the fluorescently-labelled TriM-CH(L)$_{ROX}$ show a mean diameter around 136 nm. After freeze-drying and resuspension, particle diameter increases above 300 nm, being observed the formation of a small population of particles of larger diameter. These effects may be caused by the use of water as solvent, as mentioned above for TriM-CH(H). The use of water as dispersant for nanoparticles does not favour stability to the freeze-drying process, comparing to glucose solutions. Indeed, glucose and other sugars have been previously applied as cryopreservatives [31]. Nonetheless, it was observed that nanoparticles based on TriM-CH(L)$_{ROX}$ can be easily suspended after freeze-drying without forming aggregates.

To prepare nanoparticle-loaded P(TMC-CL) fibres, TriM-CH(L)$_{ROX}$–DNA nanoparticles were resuspended in DMF and added to a P(TMC-CL) solution. The mixture showed a light pink colour, indicating the presence of the fluorochrome. The fibres obtained after electrospinning of this mixture are presented in Figure 5.

The fibre formation was found not to be homogeneous and two distinct regions of deposition were obtained. In the main region, fibres are formed (Figure 5, A-B), being the fibre mean diameter found to be 1.04 ± 0.38 µm. In the second region some fibres are deposited, as well as drops of the suspension (Figure 5, C). Since the two deposition areas were independent, fibres collected in the first area were considered for the posterior analyses.

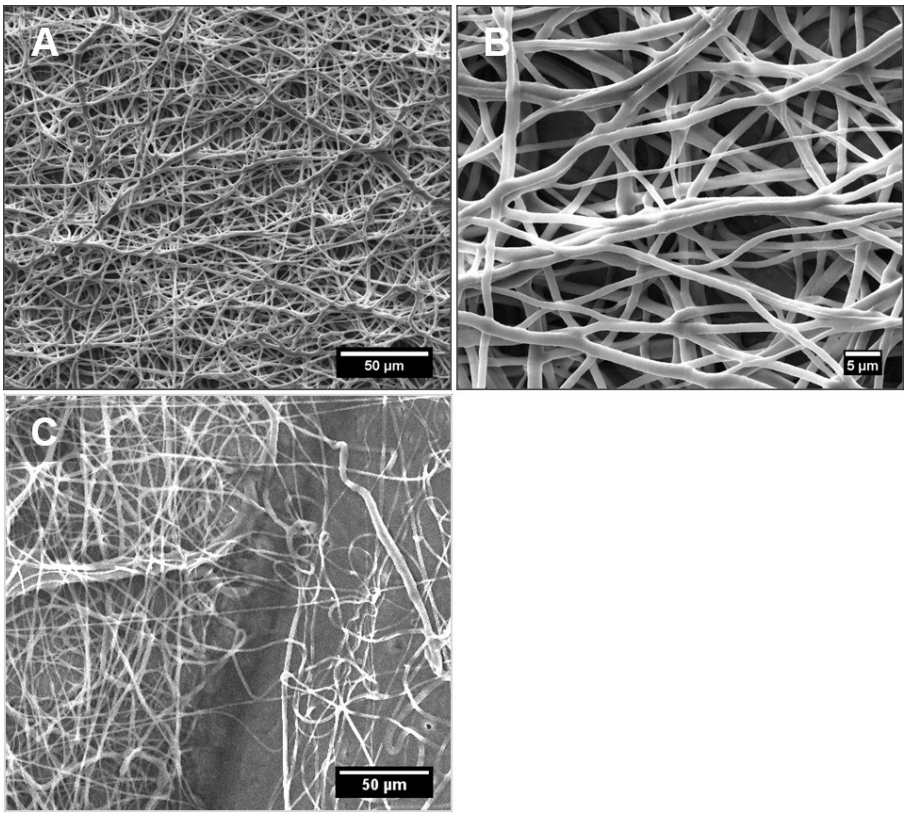

Figure 5. SEM micrographs of the fibres obtained after electrospinning of a P(TMC-CL) solution containing TriM-CH(L)$_{ROX}$–DNA nanoparticles using a 3:1 DCM:DMF solution. **(A)** Low and **(B)** high magnification images are presented. **(C)** Secondary region of deposition where both fibres and polymer drops were deposited . Images presented are representative from three independent experiments.

Since fluorescently-labelled TriM-CH was applied for the preparation of these fibres, the fluorescence of the prepared mesh was analysed by fluorescence microscopy (Figure 6). The images suggest that a large amount of nanoparticles is present in the fibres, due to high intensity signal in the rhodamine fluorescence channel (Figure 6, A). When combining fluorescence and bright field, the image (Figure 6, B) suggests the presence of fluorescently-labelled polymer within the fibres.

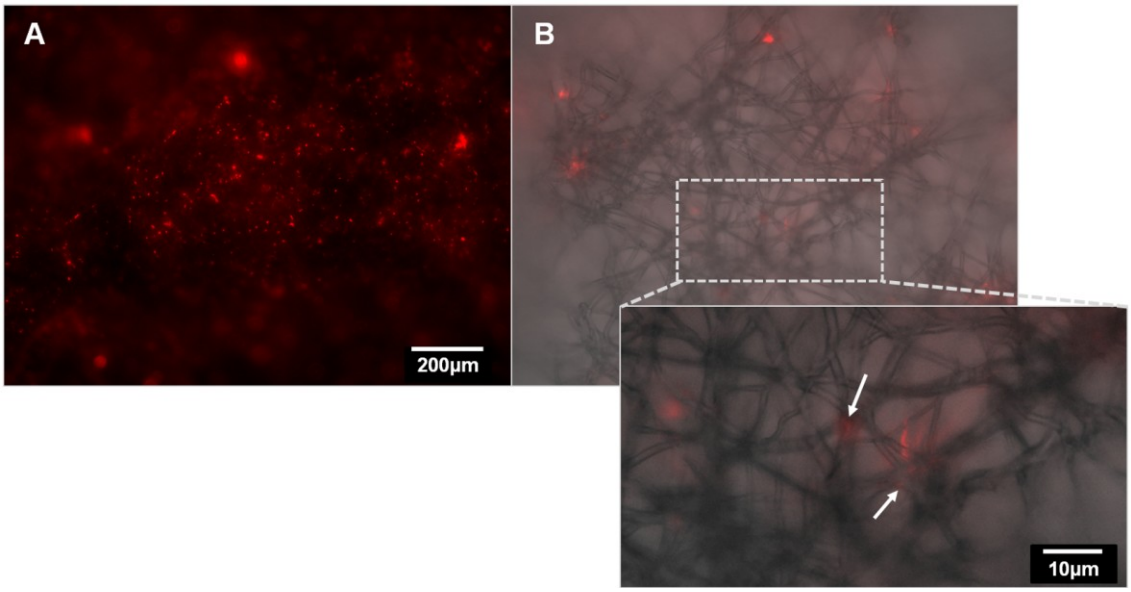

Figure 6. **(A)** Fluorescence images **(B)** combined with bright field image of the P(TMC-CL) fibres containing TriM-CH(L)R_{OX} nanoparticles. Amplification image suggests that fluorescence from TriM-CH$(L)_{ROX}$ co-localize with the fibre as indicated by the arrows.

To investigate if the TriM-CH$(L)_{ROX}$ were present in the P(TMC-CL) fibres and can be released when incubated in phosphate buffered saline (PBS), the fluorescence of the releasing medium was followed during 23 days (Figure 7).

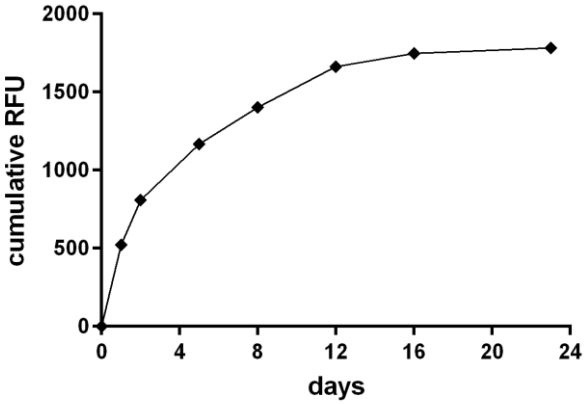

Figure 7. Cumulative release of fluorescent particles (λ_{ex}=575nm, λ_{ex}=605nm) to the releasing medium when P(TMC-CL) fibres containing TriM-CH$(L)_{ROX}$ nanoparticles were incubated with PBS at 37°C. RFU: relative fluorescence units.

The results presented in Figure 7 show that there is a gradual release of fluorescent particles to the medium (PBS) over time, suggesting that TriM-CH$(L)_{ROX}$ based nanoparticles are being released from P(TMC-CL) fibres. The fluorescence intensity of the prepared fibres was mapped using the area scan functionality of the fluorometer before and after incubation in PBS.

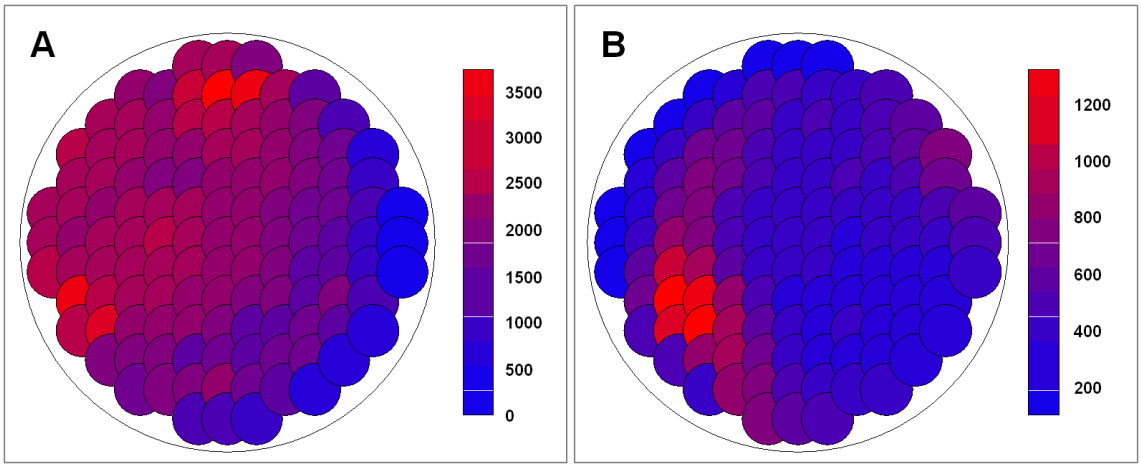

Figure 8. Area scan of fluorescence (λ_{ex}=575 nm, λ_{ex}=605 nm) found in P(TMC-CL) fibres containing TriM-CH(L)$_{ROX}$–DNA nanoparticles before (A) and after (B) incubation in PBS during 23 days.

The mapping of the fluorescence of P(TMC-CL) fibres demonstrates that fluorescence intensity decreases after incubation with PBS in all the sample. Since some fluorescence can still be found, this suggests that the majority of the nanoparticles were released from the P(TMC-CL) fibres during the 23 days of incubation, but some can still be entrapped within the polymer mesh.

In a very preliminary experiment, ND7/23 cells were seeded on top of P(TMC-CL) fibres loaded with TriM-CH(L)$_{ROX}$ nanoparticles. As shown in Figure 9 a significant amount of cells are found adhered to the fibres, suggesting that these can be a good substrate for cell growth. Additionally, the presence of fluorescence signal in the rhodamine channel (shown in red) suggests that the fluorescent polymer is present in the fibrous mesh. In this experiment a plasmid DNA encoding for green fluorescence protein (GFP) was applied, in order to identify transfected cells by their green fluorescence. However, no GFP signal was observed, indicating that transfection was not efficient in the time frame of the experiment (72 hrs). This result could be caused by the limited period of incubation with the fibres. The sustained/delayed release of the nanoparticles from the fibrous mesh may limit the amount of nanoparticles available to be internalized by the cells, and consequently can limit transfection. Previous reports using polymeric nanoparticles based on PEI incorporated on electrospun fibres showed that transfection efficiency increases up to day 7 after seeding [16, 19]. Alternatively, we hypothesize that the amount of plasmid DNA available to be delivered in this experiment can be insufficient. since the prepared fibres were loaded with 0.02% (w/w of polymer) DNA whereas others report the use of 0.1% (w/w of polymer) DNA loading [19]. A quantification of the actual amount of DNA that is released over time is necessary to adjust DNA loading in the P(TMC-CL) fibres and also to establish appropriate cell culture time-points.

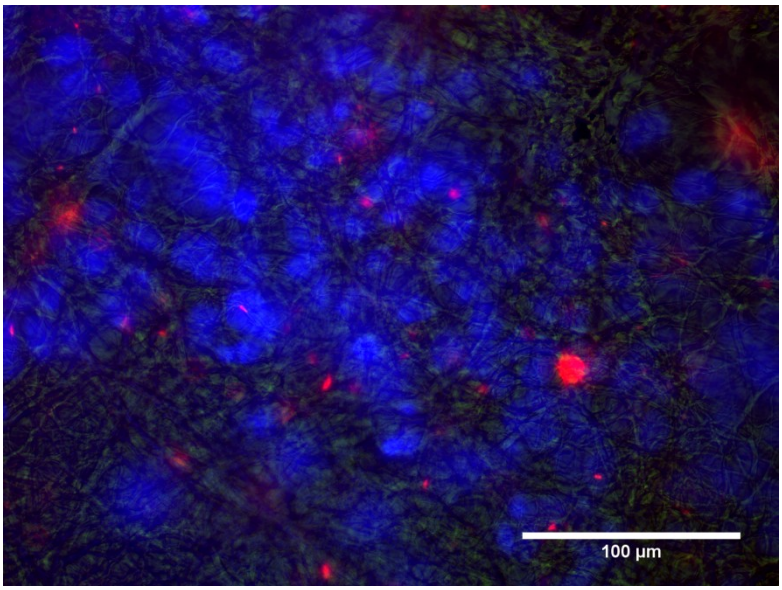

Figure 9. Fluorescence image of ND7/23 cells seeded on top of P(TMC-CL) electrospun fibre loaded with TriM-CH(L)$_{ROX}$-DNA nanoparticles. The nanoparticles are shown in red and cell nucleus is shown in blue. The auto-fluorescence of the P(TMC-CL) fibres allows its identification below the cells.

4. Conclusion and future directions

The results presented in this section, although preliminary, provide important insights for a successful preparation of electrospun fibres containing chitosan-based nanoparticles.

We found that nanoparticles based on TriM-CH are appropriate to combine with P(TMC-CL) electrospun fibres. Their stability to freeze-drying process allowed resuspension in a organic solvent, favouring fibre formation process. Our preliminary results suggest that nanoparticles prepared with TriM-CH(H), though tending to form aggregates after freeze-drying, can be homogeneously dispersed in the P(TMC-CL) solution, yielding more homogeneous electrospun fibres. Conversely, TriM-CH(L)$_{ROX}$ based nanoparticles dispersed in P(TMC-CL) solution fibres yield higher diameter fibres and a less homogeneous mesh. The higher molecular weight of TriM-CH(H) can better fit in the electrospinning requirements. Future efforts will be focused on the preparation of homogeneous solutions in order to avoid the formation of droplets during electrospinning, effect that we were not able to circumvent when using TriM-CH(L)$_{ROX}$, so far.

The presented results also highlight the importance of using labelled nanoparticles to allow its identification within the fibrous mesh. The fluorescent labelling was explored in this study but, although the presence of fluorescence signal in the fibres suggests the presence of particles, one cannot exclude that some unbound fluorochrome exists. Furthermore, it is important to figure out if the fluorescence signal corresponds to nanoparticles (polymer and DNA) or only to TriM-CH entrapped in the P(TMC-CL) mesh. Double fluorescent-labelling of DNA and TriM-CH can address this issue. Alternative labelling methods using quantum dots or gold nanoparticles can improve sensibility of detection. The use of chemical characterization techniques, like confocal-Raman

should be taken into consideration, as it can also provide information on the nanoparticle distribution within the mesh.

Future work on this project will certainly include the investigation of DNA bioactivity in transfection experiments in order to clarify if electrospinning process alters DNA or if CH-based nanoparticles maintain their ability to deliver DNA. The quantitative evaluation of the amount of DNA released over time will be paramount for establishing appropriate time-points for cell culture studies on transfection efficiency.

Experimental section

Materials

Poly(trimethylene carbonate-co-ε-caprolactone) [P(TMC-CL)] was synthesized as previously described [25, 32] using trimethylene carbonate as received (Boehringer Ingelheim, Germany) and ε-caprolactone (Merck, Germany) distilled before co-polymerization reaction. The synthesized polymer was purified by precipitation into a tenfold volume of ethanol (96%, v/v; AGA, Portugal). The purified polymer contains 11% mol of TMC; the number weight molecular weight was found to be $8.2x10^4$ and the polydispersity index was 1.61 [25].

Technical grade chitosan (CH) (Chimarin™, degree of deacetylation (DDA) 87%, apparent viscosity 8 mPa.s, supplied by Medicarb, Sweden) was purified as previously described [26]. The average weight molecular weight ($\overline{M}w$), polydispersity index and DDA of the purified polymer were found to be $1.2x10^5$, 2.1 and 84.6%, respectively [26] (Table 3). Chitosan stock solutions (0.1% (w/v)) were prepared in acetate buffer solution (5 mM, pH 5.5) and stored at 4°C till further use.

Trimethylchitosan (TriM-CH) of fungal origin was obtained from Kitozyme (Belgium). Two TriM-CH of different molecular weight were tested in these experiments. The characterization of the polymers under investigation is presented in Table 3. TriM-CH solutions were prepared by dissolving the polymer overnight in water (MilliQ grade) at a final concentration of 0.1% (w/v).

Table 3. Characterization of the polymers tested in this study.

	Mw x 10^3	DQ (%)	DDA (%)
CH	121	–	84.6
TriM-CH(L)	30	22	88.8
TriM-CH(H)	110	29	77.7

Mw: average weight molecular weight; DQ: degree of quaternization; DDA: degree of deacetylation;

Plasmid DNA encoding for GFP (pCMV-GFP, 7.4 kbp) was used in this study to prepare nanoparticles with CH or TriM-CH. Plasmid was amplified in DH5α Escherichia coli (*E. coli*) and

isolated using GENELUTE™ high performance endotoxin-free plasmid Gigaprep kit according to the manufacturer instructions (Sigma-Aldrich). Plasmid concentration and purity were determined spectrophotometrically (NanoDrop, Thermo Scientific). The ratio between optical density at 260 nm and 280 nm was found to be higher than 1.7.

Preparation of nanoparticles

To prepare nanoparticles, equal volumes of pre-heated (55°C, 10 minutes) CH or TriM-CH and DNA (in MilliQ-grade water) solutions were mixed by adding the DNA solution dropwise to the polymer solution, under vortex. Nanoparticles were allowed to form and stabilize for 15 minutes at RT before further use.

Taking into consideration the transfection activity results previously obtained [26, 28], CH-DNA complexes were prepared at a molar ratio of chitosan primary amines to DNA phosphate groups (N/P) of 18. For TriM-CH-based complexes, N/P molar ratio is expressed in terms of moles of quaternized amine groups of the polymer (-N-$(CH_3)_3$), to moles of phosphate groups of DNA. The N/P molar ratios applied in this study were 4 and 2, respectively for TriM-CH(H) and Tri-CH(L).

For electrospinning experiments, TriM-CH-based nanoparticles were prepared containing 20 µg of plasmid DNA, freeze-dried (-80ºC, 0.008 mBar, 48 hrs, Labconco, USA) and stored at room temperature till further use.

Solvent screening

The compatibility of P(TMC-CL) and CH or CH-DNA nanoparticles with different solvents was investigated. Solvents tested include dichloromethane (DCM), dimethylformamide (DMF), chloroform, acetone, and dioxane. Visual analysis was performed.

Chitosan-based nanoparticle characterization

Nanoparticles prepared as previously mentioned were characterized in terms of size using a Zetasizer Nano Zs (Malvern, UK). Cumulant analysis was used for mean particle size determination. All measurements were performed in triplicate, at 25°C.

Trimethyl chitosan fluorescent labelling

Fluorescent labelling of TriM-CH was performed based on the previous described procedure [28] with minor modifications. In brief, TriM-CH(L) was dissolved overnight in MilliQ water (1% (w/v)). 5(6)-Carboxy-X-rhodamine N-succinimidyl ester (ROX, Fluka) was dissolved in dimethylsulfoxide (7.5 $mg.ml^{-1}$) and added dropwise to the polymer solution, under stirring. The reaction occurred during 3 hrs at room temperature, under constant agitation. The labelled polymer was washed with distilled water using Amicon® ultra centrifugal filters (3,000 kDa, Millipore), till no significant fluorescence was detected in the supernatant (λ_{ex} 575 nm, λ_{em} 605 nm). The polymer solution was collected and freeze dried. Stock solutions of the fluorescently-labelled polymer (TriM-CH$(L)_{ROX}$) were prepared in water (MilliQ grade) at a final concentration of 0.1% (w/v).

Preparation of electrospun P(TMC-CL) fibres loaded with nanoparticles

To prepare P(TMC-CL) fibres loaded with TriM-CH nanoparticles, P(TMC-CL) was dissolved overnight in DCM. Lyophilized TriM-CH-based nanoparticles were resuspended in DMF and stirred at 1,400 rpm overnight (Thermomixer, Eppendorf Iberica, Spain). Nanoparticle suspension was added dropwise to the P(TMC-CL) solution and the mixture was under magnetic agitation for additional 4 hrs. The final concentration of P(TMC-CL) was 10% (w/v) and the solvent mixture corresponds to a 3:1 DCM:DMF ratio. DNA loading tested was 0.02% (w/w of polymer), corresponding to 20 µg of DNA per each 100 mg of P(TMC-CL).

Although variations in the electrospinning parameters were tested, the prepared solution was electrospun using similar electrospinning setup as described in previous work [25]. In brief, using a vertical configuration of electrospinning, solutions were dispensed at a controlled flow rate of 1 $ml.h^{-1}$ using a syringe pump (Ugo Basille, Italy). An electric field of 1 $kV.cm^{-1}$ was created (Gamma High Voltage source, USA) between the spinneret (inner diameter 0.8 mm) and the flat collector (15x15 cm) covered with aluminium foil. Fibres were collected during 30-40 minutes and subsequently, vacuum dried during 24 hrs.

Fibre morphology analysis

The morphology of the P(TMC-CL) fibres was observed by scanning electron microscopy (SEM, FEI Quanta 400FEG, FEI, the Netherlands) after being sputter-coated with gold-palladium for 90 seconds (SPI Supplies, USA). Fibre diameter was quantified from SEM micrographs using an image analysis software (Image J, version 1.39).

Gel electrophoresis

P(TMC-CL) fibres containing TriM-CH–DNA nanoparticles were dissolved in dioxane (18 $mg.ml^{-1}$) overnight at room temperature. 20 µl of this solution were loaded along with 5 µl of loading buffer (Fermentas) in a 1% (w/v) agarose gel containing 0.05 $\mu g.ml^{-1}$ of ethidium bromide (Q-BioGene, USA). 1 µg of plasmid DNA was used as control. The electrophoresis was run at 100 V for 45 minutes. The gel was visualized using a Gel Doc™ system (Bio-Rad, Portugal).

Evaluation of nanoparticle release from P(TMC-CL) electrospun fibres

To investigate the release of fluorescently-labelled nanoparticles the prepared fibres were incubated in PBS at 37ºC and at day 1, 2, 5, 8, 12, 16 and 23 of incubation, the releasing medium was completely refreshed. Fluorescence (λ_{ex}=575nm, λ_{ex}=605nm) of the collected medium was analyzed using a SynergyMax (Biotek, Portugal) fluorometer. The fluorescence of P(TMC-CL) fibres was mapped using the functionality of area scan of this equipment.

Preliminary transfection experiment using ND7/23 cell line

ND7/23 cell line (mouse neuroblastoma (N18 tg 2) x rat dorsal root ganglion neuron hybrid) was obtained from ECACC (UK) and routinely cultured in Dulbecco's Modified Eagle Medium (DMEM) with Glutamax, supplemented with 10% (w/v) foetal bovine serum (FBS) (heat-inactivated at 56ºC for 30 minutes) and 1% penicillin/streptomycin (PS, 10,000 $units.ml^{-1}$ penicillin and 10,000 $\mu g.ml^{-1}$

streptomycin), all supplied by Gibco (Life Technologies S.A., Spain). The cells were seeded ($4x10^4$ viable cells.cm^{-2}) on top of P(TMC-CL) fibres loaded with TriM-CH$(L)_{ROX}$–DNA nanoparticles. After 72 hrs of incubation, the cells were fixed in 4% (w/v) paraformaldehyde and incubated with 4',6-diamidino-2-phenylindole (DAPI, Vector Laboratories) for 10 minutes, to allow nucleus fluorescent labelling. The cells were observed under an inverted fluorescence microscope (Axiovert 200, Zeiss, Germany).

References

1. Jang JH, Houchin TL, and Shea LD (2004). "Gene delivery from polymer scaffolds for tissue engineering". *Expert Review of Medical Devices*, 1 (1): 127-138.

2. Guo T, Zhao J, Chang J, Ding Z, Hong H, Chen J, and Zhang J (2006). "Porous chitosan-gelatin scaffold containing plasmid DNA encoding transforming growth factor-beta1 for chondrocytes proliferation". *Biomaterials*, 27 (7): 1095-1103.

3. De Laporte L, Lei Yan A, and Shea LD (2009). "Local gene delivery from ECM-coated poly(lactide-co-glycolide) multiple channel bridges after spinal cord injury". *Biomaterials*, 30 (12): 2361-2368.

4. Hosseinkhani H, Hosseinkhani M, Gabrielson NP, Pack DW, Khademhosseini A, and Kobayashi H (2008). "DNA nanoparticles encapsulated in 3D tissue-engineered scaffolds enhance osteogenic differentiation of mesenchymal stem cells". *Journal of Biomedical Materials Research - Part A*, 85 (1): 47-60.

5. Shea LD, Smiley E, Bonadio J, and Mooney DJ (1999). "DNA delivery from polymer matrices for tissue engineering". *Nature Biotechnology*, 17 (6): 551-554.

6. Liao IC, Chen SL, Liu JB, and Leong KW (2009). "Sustained viral gene delivery through core-shell fibers". *Journal of Controlled Release*, 139 (1): 48-55.

7. Wu HF, Cen JS, Zhong Q, Chen L, Wang J, Deng DYB, and Wan Y (2013). "The promotion of functional recovery and nerve regeneration after spinal cord injury by lentiviral vectors encoding Lingo-1 shRNA delivered by Pluronic F-127". *Biomaterials*, 34 (6): 1686-1700.

8. Saul JM, Linnes MP, Ratner BD, Giachelli CM, and Pun SH (2007). "Delivery of non-viral gene carriers from sphere-templated fibrin scaffolds for sustained transgene expression". *Biomaterials*, 28 (31): 4705-4716.

9. Nie H and Wang CH (2007). "Fabrication and characterization of PLGA/HAp composite scaffolds for delivery of BMP-2 plasmid DNA". *Journal of Controlled Release*, 120 (1-2): 111-121.

10. Yao L, Daly W, Newland B, Yao S, Wang W, Chen BKK, Madigan N, Windebank A, and Pandit A (2013). "Improved axonal regeneration of transected spinal cord mediated by multichannel collagen conduits functionalized with neurotrophin-3 gene". *Gene Therapy*, 20 (12): 1149-1157.

11. Agarwal S, Wendorff JH, and Greiner A (2009). "Progress in the Field of Electrospinning for Tissue Engineering Applications". *Advanced Materials*, 21 (32-33): 3343-3351.

12. Sill TJ and von Recum HA (2008). "Electrospinning: Applications in drug delivery and tissue engineering". *Biomaterials*, 29 (13): 1989-2006.

13. Hurtado A, Cregg JM, Wang HB, Wendell DF, Oudega M, Gilbert RJ, and McDonald JW (2011). "Robust CNS regeneration after complete spinal cord transection using aligned poly-l-lactic acid microfibers". *Biomaterials*, 32 (26): 6068-6079.

14. Patel S, Kurpinski K, Quigley R, Gao H, Hsiao BS, Poo MM, and Li S (2007). "Bioactive nanofibers: Synergistic effects of nanotopography and chemical signaling on cell guidance". *Nano Letters*, 7 (7): 2122-2128.

15. Luu YK, Kim K, Hsiao BS, Chu B, and Hadjiargyrou M (2003). "Development of a nanostructured DNA delivery scaffold via electrospinning of PLGA and PLA-PEG block copolymers". *Journal of Controlled Release*, 89 (2): 341-353.

16. Yang Y, Xia T, Chen F, Wei W, Liu C, He S, and Li X (2012). "Electrospun fibers with plasmid bFGF polyplex loadings promote skin wound healing in diabetic rats". *Molecular Pharmaceutics*, 9 (1): 48-58.

17. Cao H, Jiang X, Chai C, and Chew SY (2010). "RNA interference by nanofiber-based siRNA delivery system". *Journal of Controlled Release*, 144 (2): 203-212.

18. Rujitanaroj PO, Wang YC, Wang J, and Chew SY (2011). "Nanofiber-mediated controlled release of siRNA complexes for long term gene-silencing applications". *Biomaterials*, 32 (25): 5915-5923.

19. He S, Xia T, Wang H, Wei L, Luo X, and Li X (2012). "Multiple release of polyplexes of plasmids VEGF and bFGF from electrospun fibrous scaffolds towards regeneration of mature blood vessels". *Acta Biomaterialia*, 8 (7): 2659-2669.

20. Mittnacht U, Hartmann H, Hein S, Oliveira H, Dong M, Pêgo AP, Kjems J, Howard KA, and Schlosshauer B (2010). "Chitosan/siRNA nanoparticles biofunctionalize nerve implants and enable neurite outgrowth". *Nano Letters*, 10 (10): 3933-3939.

21. Rujitanaroj PO, Jao B, Yang J, Wang F, Anderson JM, Wang J, and Chew SY (2013). "Controlling fibrous capsule formation through long-term down-regulation of collagen type I (COL1A1) expression by nanofiber-mediated siRNA gene silencing". *Acta Biomaterialia*, 9 (1): 4513-4524.

22. Pêgo AP, Poot AA, Grijpma DW, and Feijen J (2003). "Biodegradable elastomeric scaffolds for soft tissue engineering". *Journal of Controlled Release*, 87 (1-3): 69-79.

23. Vleggeert-Lankamp CLAM, Wolfs J, Pêgo AP, Van Den Berg R, Feirabend H, and Lakke E (2008). "Effect of nerve graft porosity on the refractory period of regenerating nerve fibers: Laboratory investigation". *Journal of Neurosurgery*, 109 (2): 294-305.

24. Rocha DN, Brites P, Fonseca C, and Pêgo AP (2014). "Poly(Trimethylene Carbonate-co-ε-Caprolactone) Promotes Axonal Growth". *Plos One*, 9(2): e88593.

25. Pires LR, Guarino V, Oliveira MJ, Ribeiro CC, Barbosa MA, Ambrosio L, and Pêgo AP (2013). "Ibuprofen-loaded poly(trimethylene carbonate-co-ε-caprolactone) electrospun fibers for nerve regeneration". *Journal of Tissue Engineering and Regenerative Medicine*: *Accepted for publication*.

26. Moreira C, Oliveira H, Pires LR, Simões S, Barbosa MA, and Pêgo AP (2009). "Improving chitosan-mediated gene transfer by the introduction of intracellular buffering moieties into the chitosan backbone". *Acta Biomaterialia*, 5 (8): 2995-3006.

27. Oliveira H, Pires LR, Fernandez R, Martins MCL, Simões S, and Pêgo AP (2010). "Chitosan-based gene delivery vectors targeted to the peripheral nervous system". *Journal of Biomedical Materials Research - Part A*, 95 (3 A): 801-810.

28. Pires LR, Oliveira H, Barrias CC, Sampaio P, Pereira AJ, Maiato H, Simões S, and Pêgo AP (2011). "Imidazole-grafted chitosan-mediated gene delivery: *In vitro* study on transfection, intracellular trafficking and degradation". *Nanomedicine*, 6 (9): 1499-1512.

29. Gomes CP, Varela-Moreira A, Moreno PDM, and Pêgo AP. *Trimethylchitosan as a gene carrier to the peripheral nervous system*. in *25th European Conference on Biomaterials*. Madrid, 2013.

30. Hsu CM and Shivkumar S (2004). "N,N-dimethylformamide additions to the solution for the electrospinning of poly(ε-caprolactone) nanofibers". *Macromolecular Materials and Engineering*, 289 (4): 334-340.

31. Abdelwahed W, Degobert G, Stainmesse S, and Fessi H (2006). "Freeze-drying of nanoparticles: Formulation, process and storage considerations". *Advanced Drug Delivery Reviews*, 58 (15): 1688-1713.

32. Pêgo AP, Poot AA, Grijpma DW, and Feijen J (2001). "Copolymers of trimethylene carbonate and epsilon-caprolactone for porous nerve guides: Synthesis and properties". *Journal of Biomaterials Science, Polymer Edition*, 12 (1): 35-53.

CHAPTER VII

Concluding Remarks and Future Perspectives

After the primary insult that leads to the interruption of the axonal pathways, a lesion to the spinal cord is followed by the activation of a number of inhibitory mechanisms and a protracted period of tissue destruction. Axonal regeneration fails in this hostile environment and the process ends up with the formation of a cavity surrounded by scar tissue [1]. In order to promote regeneration in such inhibitory scenery, it is well accepted that a multi-targeted approach is required [2]. In this context, the ultimate goal of the work described in this thesis is to propose a scaffold to be implanted in the spinal cord after a lesion, that provides physical support, guidance and biochemical cues, constituting, utterly, a permissive substrate for axonal regrowth. Each of the presented experimental chapters were sought to contribute to the design of such a structure.

Poly(trimethylene carbonate-co-ε-caprolactone) [P(TMC-CL)] was chosen as starting material for the development of this scaffold, based on previous reports showing the interesting properties of the polymer in the context of peripheral [3, 4], and central nervous system regeneration [5].

The use of electrospinning for the preparation of scaffolds for tissue engineering has been largely investigated due to the characteristics of the resulting fibrous structure that emulates the features of the extracellular matrix [6, 7]. Herein we report the preparation of P(TMC-CL) fibres by electrospinning. Taking into consideration the importance of microglia, the resident immune cells on the central nervous system (CNS), in triggering the response to injury, we described for the first time the effect of electrospun fibres on primary microglia cells in comparison to flat solvent cast films. In line with what is described in the open literature for other cell types, we showed that microglia morphology is remarkably affected by the topography of the surface. It was shown that the fibrous structure favours microglia cytoplasm elongation, and, surprisingly, the release of the pro-inflammatory cytokine - TNFα. The classical classification of microglia ascribes a pro-inflammatory phenotype to cells with an amoeboid morphology [8]. Moreover, in macrophages, an elongated cell shape has been associated with an anti-inflammatory phenotype [9]. Our study highlights the importance of specifically addressing the response of microglia in the context of CNS regeneration. Indeed, although sharing important lineage features with macrophages, microglia can respond differently to stimuli. This study also showed that the P(TMC-CL) surfaces under investigation do not significantly activate microglia, as astrogliosis markers were not exacerbated when astrocytes were in contact with microglia conditioned media. Furthermore, it was demonstrated that microglia seeded on P(TMC-CL) fibres or solvent cast films was able to actively contribute in myelin phagocytosis, a critical step on the progress of regeneration as myelin debris accumulation after injury leads to the release/exposure of molecules inhibitory to axonal regrowth. These results put forward the P(TMC-CL) surfaces as contributors for the CNS regeneration process, modulating microglia towards a pro-regenerative activity.

Another contribute to the design of a multi-target strategy to promote axonal regeneration in the aftermath of a spinal cord injury (SCI) is to convert these three-dimensional (3D) structures into

drug delivery devices. By adding a drug to the electrospinning solution, drug-loaded fibres can be obtained. To tame the inflammatory response at the spinal cord lesion site, we explored the incorporation of a non-steroidal anti-inflammatory drug – ibuprofen – in P(TMC-CL) fibres. Ibuprofen-loaded P(TMC-CL) fibres were successfully prepared. The fibre formation process was optimized and by adjusting solvent mixture applied in the electrospun solution, it was demonstrated that fibre mean diameter can be tuned. The release of ibuprofen *in vitro* in sink conditions occurred in the first 24 hrs, being the released drug able to reduce the secretion of prostaglandin E_2 by human-derived macrophages, pointing out that the drug bioactivity is maintained after the process. Furthermore, this study shows that ibuprofen-loaded P(TMC-CL) fibres can be applied as structures with anti-inflammatory properties.

The use of ibuprofen in scaffolds to implant after a SCI enclosed, however, a double target strategy. If on the one hand, ibuprofen can reduce cyclooxygenase activity at the lesion site and consequently, might contribute to tame the inflammatory response [10]; on the other hand, ibuprofen has been described to limit RhoA-mediated axonal growth inhibition, improving functional recovery after SCI [11-13]. Consequently, we explored the effect of ibuprofen released from drug loaded P(TMC-CL) fibre on the RhoA pathway in neuronal cells. Foreseeing an application *in vivo*, we firstly created an ibuprofen-loaded bilayer scaffold composed by an outer layer based on a P(TMC-CL) solvent cast film and an inner layer made of preferentially aligned electrospun fibres to provide physical guidance cues for axonal regrowth. Here we report the preparation of the scaffold and its assessment both *in vitro* and *in vivo*. It was demonstrated that ibuprofen released from these bilayer P(TMC-CL) scaffolds is able to limit RhoA activation in neuronal cells when these are stimulated with lysophosphatidic acid. This result encouraged the *in vivo* testing of the prepared scaffolds. As proof-of-concept of the effect of ibuprofen released from the implanted scaffold on the RhoA pathway, a preliminary study using a dorsal hemisection SCI model was conducted. The ibuprofen-loaded P(TMC-CL) scaffolds were implanted immediately after the lesion and maintained during five days. So far, it was observed that the scaffold is suitable for implantation at the lesion site, wrapping the spinal cord tissue. No harmful effects were detected; particularly, the implantation of ibuprofen-loaded scaffolds showed to have no impact on animal survival rate. The analysis of the results of this study is currently in progress and will be paramount to determine whether this strategy can move forward to an extended study in order to understand if the early effects can have a consequence in axonal growth and functional outcome and to assess the contribution of P(TMC-CL) and fibre alignment in the process.

An alternative to load scaffolds with biochemical cues is to use gene therapy-based strategies. The premise is that the release of nanoparticles containing genetic material can guarantee the long-term expression of proteins of interest in the spinal cord lesion site. Chitosan-based vectors were previously proposed as gene delivery vectors [14, 15]. In this regard, we firstly performed an extensive *in vitro* work on the characterization of chitosan-based vectors gene delivery, namely its

intracellular trafficking, degradation and time window of gene expression. We showed that these vectors mediate a long-term gene expression that can be modulated by adjusting chitosan degradation rate.

In order to translate these knowledge into a 3D scaffold, we tested the incorporation of chitosan-based nanoparticles in P(TMC-CL) fibres during the electrospinning process. However, it was not possible to obtain a homogeneous polymer solution that could allow the formation of fibres. As alternative, we proposed the use of trimethylated-chitosan based nanoparticles. This polymer has higher solubility and nanoparticle stability is improved. In preliminary tests we showed that P(TMC-CL) fibres containing nanoparticles can be obtained. The nanoparticle release profile and the bioactivity of the delivered gene wait for a more detailed study. Still, the preliminary tests presented in this thesis are encouraging indicating the feasibility of incorporating such nanoparticles as vectors for nucleic acid delivery within electrospun polymeric fibres.

Overall, the work described in this thesis provides relevant knowledge that contributes to the design of a multi-target scaffold to be used as a therapeutic strategy in the context of a SCI. Engineering a permissive substrate for axonal regrowth by means of combining topography, ibuprofen and trimethyl-chitosan-based nanoparticles for gene delivery might constitute a successful approach towards nerve regeneration in the CNS.

While this thesis reports major findings, some questions remain to be answered as well as additional ones can be raised. The more relevant points that remain to be addressed are described below.

The detailed analysis of the tissues collected in the preliminary *in vivo* study performed is critical to determine the significance of the proposed strategy in a SCI scenario. The evaluation of RhoA activity in the tissues, and the characterization of the cellular populations at the lesion site can also provide new insights for future improvements on scaffold design. In particular, the drug loading or the drug release profile can be adjusted accordingly. The short-term study (5 days) performed only addresses the early effect of the released drug. To assess the contribution of P(TMC-CL) or fibre alignment on axonal growth and, ultimately, on functional recovery, the implantation of ibuprofen-loaded scaffolds for a longer period will be of remarkable importance.

The second question that comes up from the reported work is whether one can prepare a scaffold that combines chitosan-based nanoparticles (vectorizing a therapeutic gene) with P(TMC-CL) fibres already loaded with ibuprofen. The combination of both gene and drug delivery strategies

would be a major achievement, and to tune timely the release of each, would certainly constitute the major challenge.

Additionally, of remarkable interest in the context of this thesis is to investigate the effect of ibuprofen loaded P(TMC-CL) fibres on microglia, and to figure out how microglia response can be altered when using surfaces based on aligned fibres.

References

1. Schwab JM, Brechtel K, Mueller CA, Failli V, Kaps HP, Tuli SK, and Schluesener HJ (2006). "Experimental strategies to promote spinal cord regeneration - An integrative perspective". *Progress in Neurobiology*, 78 (2): 91-116.

2. McCreedy DA and Sakiyama-Elbert SE (2012). "Combination therapies in the CNS: Engineering the environment". *Neuroscience Letters*, 519 (2): 115-121.

3. Pêgo AP, Poot AA, Grijpma DW, and Feijen J (2001). "Copolymers of trimethylene carbonate and epsilon-caprolactone for porous nerve guides: Synthesis and properties". *Journal of Biomaterials Science, Polymer Edition*, 12 (1): 35-53.

4. Vleggeert-Lankamp CLAM, Wolfs J, Pêgo AP, Van Den Berg R, Feirabend H, and Lakke E (2008). "Effect of nerve graft porosity on the refractory period of regenerating nerve fibers: Laboratory investigation". *Journal of Neurosurgery*, 109 (2): 294-305.

5. Rocha DN, Brites P, Fonseca C, and Pêgo AP (2014). "Poly(Trimethylene Carbonate-co-ε-Caprolactone) Promotes Axonal Growth". *Plos One*, 9(2): e88593**.**

6. Agarwal S, Wendorff JH, and Greiner A (2009). "Progress in the Field of Electrospinning for Tissue Engineering Applications". *Advanced Materials*, 21 (32-33): 3343-3351.

7. Sill TJ and von Recum HA (2008). "Electrospinning: Applications in drug delivery and tissue engineering". *Biomaterials*, 29 (13): 1989-2006.

8. Streit WJ, Walter SA, and Pennell NA (1999). "Reactive microgliosis". *Progress in Neurobiology*, 57 (6): 563-581.

9. McWhorter FY, Wang T, Nguyen P, Chung T, and Liu WF (2013). "Modulation of macrophage phenotype by cell shape". *Proceedings of the National Academy of Sciences of the United States of America*, 110 (43): 17253-17258.

10. Kopp MA, Liebscher T, Niedeggen A, Laufer S, Brommer B, Jungehulsing GJ, Strittmatter SM, Dirnagl U, and Schwab JM (2012). "Small-molecule-induced Rho-inhibition: NSAIDs after spinal cord injury". *Cell and Tissue Research*, 349 (1): 119-132.

11. Fu Q, Hue J, and Li S (2007). "Nonsteroidal anti-inflammatory drugs promote axon regeneration via RhoA inhibition". *Journal of Neuroscience*, 27 (15): 4154-4164.

12. Wang X, Budel S, Baughman K, Gould G, Song KH, and Strittmatter SM (2009). "Ibuprofen enhances recovery from spinal cord injury by limiting tissue loss and stimulating axonal growth". *Journal of Neurotrauma*, 26 (1): 81-95.

13. Zhou Y, Su Y, Li BL, Liu F, Ryder JW, Wu X, Gonzalez-DeWhitt PA, Gelfanova V, Hale JE, May PC, Paul SM, and Ni BH (2003). "Nonsteroidal anti-inflammatory drugs can lower amyloidogenic A beta(42) by inhibiting Rho". *Science*, 302 (5648): 1215-1217.

14. Mao HQ, Roy K, Troung-Le VL, Janes KA, Lin KY, Wang Y, August JT, and Leong KW (2001). "Chitosan-DNA nanoparticles as gene carriers: synthesis, characterization and transfection efficiency". *Journal of Controlled Release*, 70 (3): 399-421.

15. Moreira C, Oliveira H, Pires LR, Simões S, Barbosa MA, and Pêgo AP (2009). "Improving chitosan-mediated gene transfer by the introduction of intracellular buffering moieties into the chitosan backbone". *Acta Biomaterialia*, 5 (8): 2995-3006.